Aortic Stenosis – a Myocardial Disease

Insights from Myocardial Tissue Characterisation

PhD Thesis

Dr Thomas Alexander Treibel

UCL

Cardiovascular Sciences

2017

Declaration

I, Thomas Alexander Treibel, confirm that the work presented in this thesis is my own. Where information has been derived from other sources, I confirm that this has been indicated in the thesis.

Signature.....

Name: Thomas A. Treibel Date .....

For Elouisa

Abstract

Aortic stenosis (AS) is a disease of not just the valve, but also of the myocardium. Patient symptoms and outcome are determined by the myocardial response; a crucial but poorly understood process. Diffuse and focal myocardial fibrosis play a key role. Until recently, both could only be assessed using invasive histology, but now cardiovascular magnetic resonance (CMR) offers late gadolinium enhancement (LGE) and extracellular volume fraction (ECV) techniques. In this thesis, I developed new methods to quantify ECV by synthetic ECV and cardiac CT. I then explored myocardial remodelling and fibrosis in patients with severe AS undergoing aortic valve replacement (AVR) using myocardial biopsy, CMR, biomarkers and a wide range of clinical parameters.

Prior to AVR, CMR in patients with severe AS revealed important differences in myocardial remodelling between sexes, otherwise missed on echocardiography alone. Given apparently equal valve severity, the myocardial response to AS appeared unexpectedly maladaptive in men compared to women.

Intra-operative myocardial biopsy revealed three pattern of fibrosis: endocardial fibrosis, microscars (mainly in the subendomyocardium), and diffuse interstitial fibrosis. Biopsy best captured the transmural gradient of fibrosis and microscars, while on CMR, LGE captured mainly microscars and ECV captured mid-myocardial related functional changes beyond LGE. Combining LGE and ECV allowed better stratification of AS patients. Incidentally, I found that 6% of AS patients older then 65 years had wild-type transthyretin amyloid deposits on cardiac biopsy, which was associated with poor outcome. This is now the basis of a BHF research fellowship.

Following AVR, I demonstrated for the first time non-invasively that diffuse fibrosis regresses (focal fibrosis did not), which is accompanied by structural and functional improvements suggesting that human diffuse fibrosis is plastic, measurable by CMR and a potential therapeutic target.

Funding

This work was funded by a doctoral research fellowship from the National Institute for Health Research (DRF-2013-06-102) to whom I am extremely grateful.

Acknowledgments

I would like to thank the subjects and patients who took part in the studies that constitute this thesis. Without their generous cooperation and help I would not have been able to successfully progress through the different stages of this project.

I would like to acknowledge and thank the following people:

In particular I would like to thank my supervisor Prof James Moon for his expert guidance, constructive criticism, enthusiasm and encouragement over the last 4 years. The unique environment he set up at the Heart Hospital Imaging Centre was crucial for the success of my project.

I would also like to thank my secondary supervisor Prof Stuart Taylor for his input into the CT aspects of my project and for his support during my upgrade. The collaboration with his team, in particular Dr Steve Bandula, was key for the development of the CT ECV methodology at UCL.

Importantly, I would like to thank the fellows at the Heart Hospital, colleagues and friends – the team work and joint ideas have enable our joint achievements: Marianna Fontana, Steve White, Dan Sado, Rebecca Kozor, Rebecca Schofield, Katia Menacho, Stefania Rosmini, Silvia Castelletti, Anish Bhuva, Paul Scully, Sanjay Banypersad, Andy Flett, Viviana Maestrini, Amna Abdel-Gadir, Arthur Nasis, Maria Espinoza, Patrizia Reant, Sabrina Nordin, Camilla Torlasco, Guilia Benedetti. I would also like to thank Dr Anna Herrey, Dr Charlotte Manisty, Sarah Anderson, Jodee Cooper, Louise McGrath and especially our never-stopping Sandy Gardner.

I would like to acknowledge the contributions of the, theatre, nursing and administrative staff, physiologists, radiographers and biomedical scientists at the Barts Heart Centre and the University College London Hospitals. I grateful to the cardiothoracic team at the Heart Hospital for their support of my project and for obtaining the myocardial biopsy, in particular the cardiothoracic surgeons Martin Hayward, John Yap, Shyam Kolvekar, David Lawrence, Carmelo diSalvo, Amir Sheikh, Neil Roberts and Prof Christopher McGregor. I would also like to thank Dr Petros Syris, UCL, for helping me in biopsy and biomarker logistics.

I would like to thank the team at the department at Histopathology, Great Ormond Street Hospital for their technical expertise and high quality input into my project, in particular Dr Michael Ashworth and Tobias Hunt.

I would like to thank the team a the National Amyloidosis Centre for their support, knowledge and patience, in particular Prof Philip Hawkins, Janet Gilbertson, Thirusha Lane, Dr Julian Gillmore, Dr Helen Lachmann, Dr Carol Whelan and Dr Ashutosh Wechalekar, as well as the clinical and administrative staff.

I would like to thank Drs. Stefan Piechnik, Peter Kellman, Matt Robson, and Vivek Muthurangu for physics support and advice during technical development, and Prof Alun Hughes, Dr Guy Lloyd, Dr Francesca Pugliese and Dr Erik Schelbert for guidance and advice in the preparation of manuscripts.

I would also like to thank my collaborators in Pamplona, Prof Javier Díez, Dr Arantxa Gonzales and Dr Begoña Lopes, as well as the whole team at CIMA.

Lastly and most importantly, I would like to thank my wife Lucy for her support, patience and tolerance during these last 4 years.

Abbreviations

6MWT	=	6-minute-walk test
ACE-I	=	angiotensin-converting-enzyme inhibitor
AF	=	atrial fibrillation
AL	=	immunoglobulin light-chain amyloid
ARB	=	angiotensin-receptor blocker
AS	=	aortic stenosis
ATTR	=	transthyretin amyloid
AVAi	=	aortic valve area index
AVR	=	aortic valve replacement
BMI	=	body mass index;
BSA	=	body surface area
CABG	=	coronary artery bypass graft
CAD	=	coronary arterial disease
CMR	=	cardiovascular magnetic resonance
CCT	=	cardiac computed tomography
CVF	=	collagen volume fraction
DBP	=	diastolic blood pressure
ECV	=	extracellular volume fraction
eGFR	=	estimated glomerular filtration rate
ECM	=	extracellular matrix
EDVi	=	end-diastolic volume index
ESVi	=	end-systolic volume index
EuroScoreII	=	European System for Cardiac Operative Risk Evaluation II
Gd-DTPA	=	Gadolinium-diethylenetriamine penta-acetic acid
HCM	=	hypertrophic cardiomyopathy
HCT	=	haematocrit
HFpEF	=	heart failure with preserved ejection fraction
HHF	=	hospitalisation for heart failure
hs-TnT	=	high sensitivity troponin T
HTN	=	hypertension
HU	=	Hounsfield units
IQR	=	interquartile range
LAAi	=	left atrial area index
LGE	=	late gadolinium enhancement
LVEF	=	left ventricular ejection fraction
LVH	=	left ventricular hypertrophy
LVMi	=	left ventricular mass index
LVEF	=	left ventricular ejection fraction
MAPSE	=	mitral annular plane systolic excursion
MOLLI	=	MOdified Look-Locker Inversion recovery
MOCO	=	motion correction
NT-proBNP	=	N-terminal pro-brain natriuretic peptide
NYHA	=	New York Heart Association
SBP	=	systolic blood pressure
ShMOLLI	=	Shortened MOdified Look-Locker Inversion recovery
STS	=	Society of Thoracic Surgeons' risk model score
TAVI	=	transcatheter aortic valve implantation
TTR	=	transthyretin

Table of Contents

Table of Tables

Table of Figures

Figure 1: Aortic Stenosis – A Disease of the Myocardium.

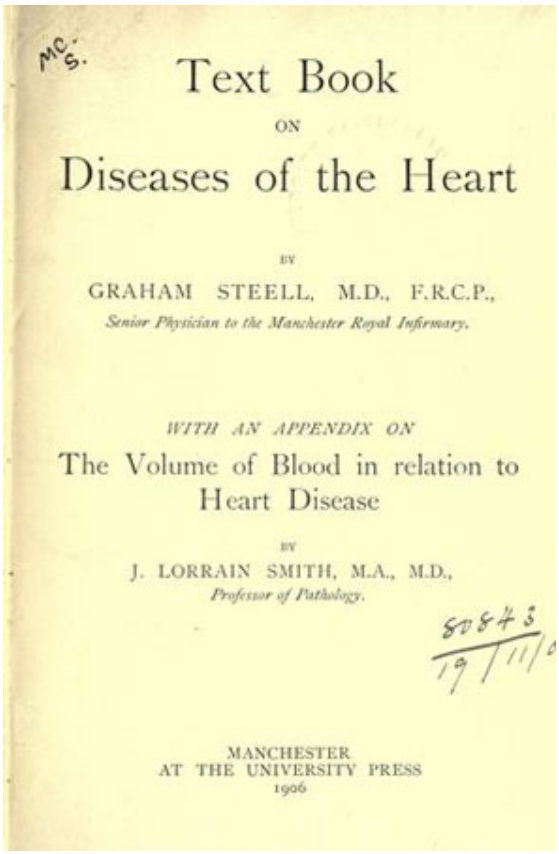

MC'S.

Text Book

ON

Diseases of the Heart

BY

GRAHAM STEELL, M.D., F.R.C.P.,

Senior Physician to the Manchester Royal Infirmary.

WITH AN APPENDIX ON

The Volume of Blood in relation to Heart Disease

BY

J. LORRAIN SMITH, M.A., M.D.,

Professor of Pathology.

80843

19/11/0

MANCHESTER
AT THE UNIVERSITY PRESS
1906

[In aortic Stenosis], dilatation of the ventricle is thus an unmixed evil, and hypertrophy of its walls is all that is necessary to compensate for obstructive lesion at the aortic orifice.

Graham Steell, MD, FRCP, Professor of Medicine, Manchester Royal Infirmary. Text-Book on Diseases of the Heart, Manchester University Press, 1906.

Chapter 1 Introduction

1.1 Aortic stenosis

Aortic valve stenosis (AS) is defined as aortic valve thickening and calcification that causes a significant gradient across the aortic valve (usually with an aortic jet velocity of at least 2 m/sec). As is the most common valvular heart condition in the Western world. Its prevalence increases with age [1], with around 3% of people aged over 75 having severe AS [2]. In 2008/9, nearly 6000 patients underwent aortic valve replacement (AVR) for AS in England and this is predicted to double in the next decade [3]. The cost to the NHS for AVR surgery alone is over £200 million per year, not accounting for additional costs of medical management of AS.

1.1.1 Natural history

AS occurs when the aortic valve progressively fails to open fully. The most common aetiology in the elderly is calcific degeneration; congenital bicuspid or rheumatic (now rare) aortic valve disease present earlier. During a period of progressive valve narrowing, the LV adapts to the increased pressure with increasing concentric muscle hypertrophy. However, eventually this remodelling becomes maladaptive and the LV less compliant, leading to symptoms (breathlessness, chest pain, and syncope). This heralds a significant increase in morbidity and mortality. Untreated, most will die within five years [4] (Figure 1).

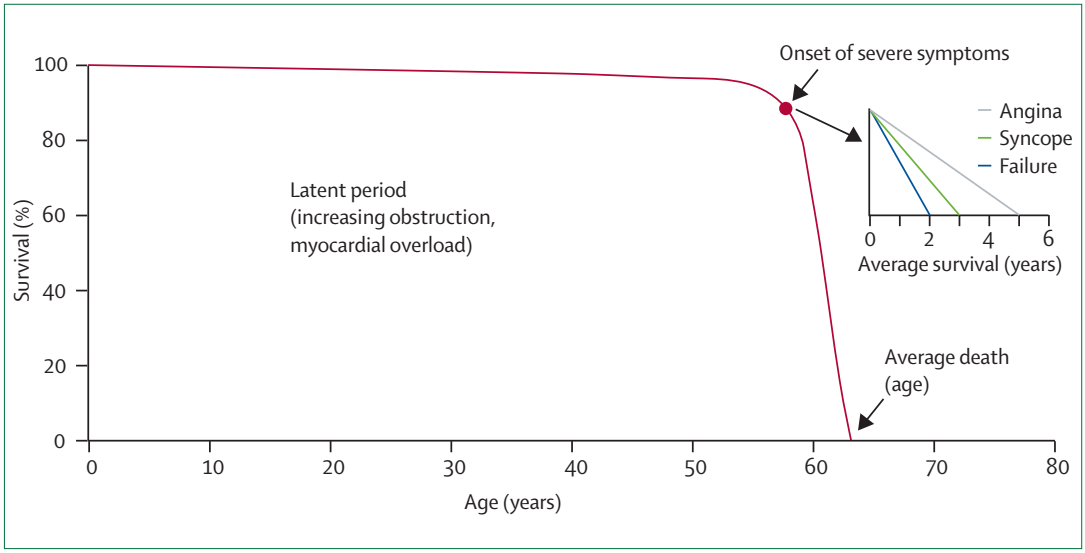

Figure 2: The natural history of aortic stenosis

Onset of symptoms is preceded by a long latent period of increasing obstruction, leading to myocardial pressure overload. Adapted from Ross and Braunwald 1983.

1.1.2 Indications for intervention

AVR is the definitive therapy for severe AS and improves symptoms and survival [5]. For the majority of patients, this is performed by open surgery. Current guidelines for AS have evolved from clinical assessment to using transthoracic echocardiography as the primary diagnostic modality for evaluating aortic valve anatomy (leaflets, calcification, orifice area), AS severity (peak velocity, mean gradient and velocity ratio; Figure 3) as well as the LV response to chronic pressure overload [6, 7].

When asymptomatic, surgery offers no obvious benefit in quality of life and the risk of sudden cardiac death is <1% per year [8, 9], however equally it is not zero, and once symptoms occur the death rate rises to 2% per month [10]. Uncovering latent symptoms and haemodynamic instability with exercise testing is a key new addition to current guidelines. For truly asymptomatic patients, current indicators poorly predict progression to symptoms – putting the 20% who develop symptoms within 1 year at high risk, while waiting for their 6-monthly follow-up and eventual surgery (most patients will require an AVR within 2 years) [11].

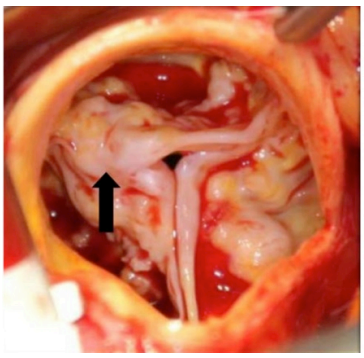

Grading aortic stenosis

	Mild	Moderate	Severe
Peak velocity (m/s)	2.5–3.0	3.0–4.0	>4.0
Peak gradient (mm Hg)	<40	40–65	>65
Mean gradient (mm Hg)	<20	20–40 (50)*	>40 (50)*
EOA (cont eq.) (cm^2)	>1.5	1.0–1.5	<1.0
EOAi (cm^2/m^2)	>0.85	0.60–0.85	<0.60
Velocity ratio	>0.50	0.25–0.50	<0.25

*Denotes European Association of Echocardiography (EAE) only.[1] All other parameters are according to both the EAE and American Society of Echocardiography.[2]
EOA, effective orifice area; EOAi, indexed effective orifice area.

Figure 3: Grading of aortic stenosis

Severely stenosed aortic valve with leaflet fusion (black arrow) at time of surgery (left). Grading of aortic stenosis by echocardiography (right) according to European and American Guidelines (Vahanian 2012, Nishimura 2014). Adapted from Walter et al 2012 [12].

There is no randomized controlled trial data to guide management in these particular patients [13]. There are indicators predicting adverse outcome in seemingly asymptomatic patients with severe AS, who should be considered for pre-emptive valve replacement: abnormal resting ECG with strain, critical AS (velocity >4.5-5m/s), inappropriate LVH, reduced longitudinal strain, abnormal impedance, abnormal exercise test (serious arrhythmia, ischaemic response, abnormal blood pressure response), and elevated or rising brain natriuretic peptide [14-16]. The evidence base however is limited and derived from a small number of patients with a high likelihood of selection bias. Ultimately, better risk stratification is necessary to identify patients that would benefit from early surgery.

1.1.3 Assessment of Aortic Stenosis beyond the Valve

Unfortunately, these echocardiography parameters poorly predict symptom development and/or optimal timing of surgery [17]. The literature acknowledges this, and new concepts in the assessment of the severity of AS are appearing – highlighting the importance of the intricate interplay of the vasculature (aortic stiffness and hypertension), valve stenosis and responses of the ventricle to the global load (valvular-arterial impedance); see Figure 3.

This concept was first highlighted by Professor Graham Steell in 1906 (Figure 1), who described LV decompensation an “unmixed evil”. Patients may tolerate severe AS for many years, but after the onset of symptoms and LV dysfunction, prognosis is poor [18, 19]. Consequently, AVR in symptomatic patients is a Class I indication [20]. In most asymptomatic patients however, prophylactic surgery is controversial [21, 22].

Operative mortality is low at 1-3% (registry data), even <1.5% in Heart Valve Centres of Excellence [23].

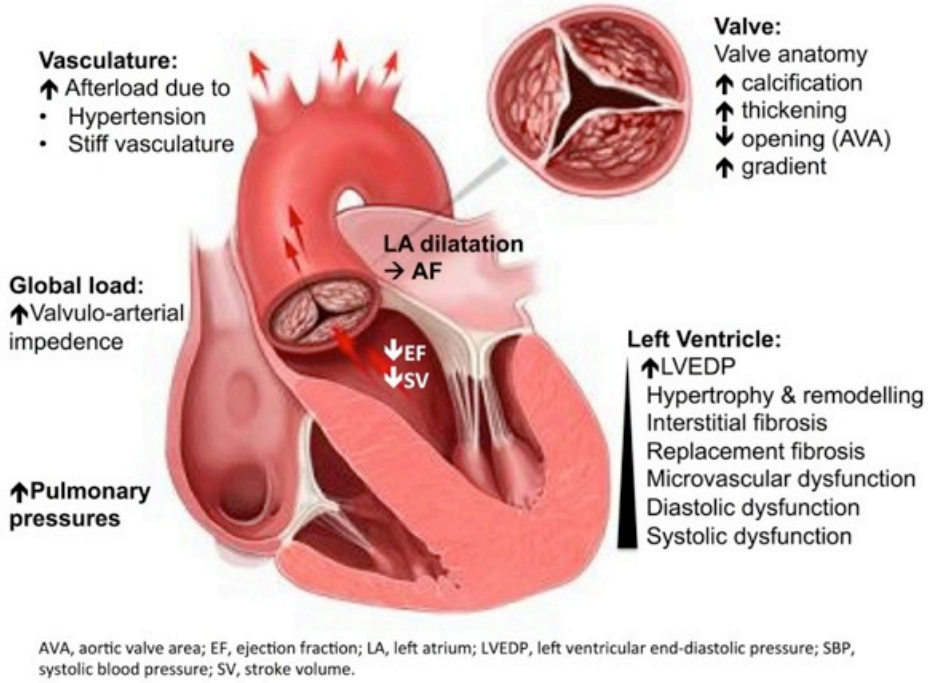

Figure 4: Complex physiology in aortic stenosis

Aortic stenosis is not just a disease of the valve – the intricate interplay of valve, vasculature and ventricle eventually resulting in symptom development.

1.1.4 The myocardium in Aortic Stenosis

1.1.4.1 Left Ventricular Remodelling

Left ventricular hypertrophy (LVH) occurs in response to increasing afterload and LV intra-cavity pressure in order to maintain normal wall stress. The adaptive changes result in alteration of the LV geometry (radius and wall thickness, or mass volume ratio) [24]. Four pattern of ventricular remodelling in AS have been described using imaging (based on wall thickness, LV volume and mass), which are (Figure 5): normal geometry, concentric remodelling, concentric hypertrophy and eccentric hypertrophy (LV decompensation) [25]. This response however is heterogeneous (10-20% of patients with severe AS display no LVH) and only weakly correlates with the degree of apparent AS. Importantly, other factors affecting the magnitude of hypertrophic response are age, sex, metabolic syndrome, obesity, angiotensin enzyme polymorphism and concomitant hypertension (see section 1.1.7).

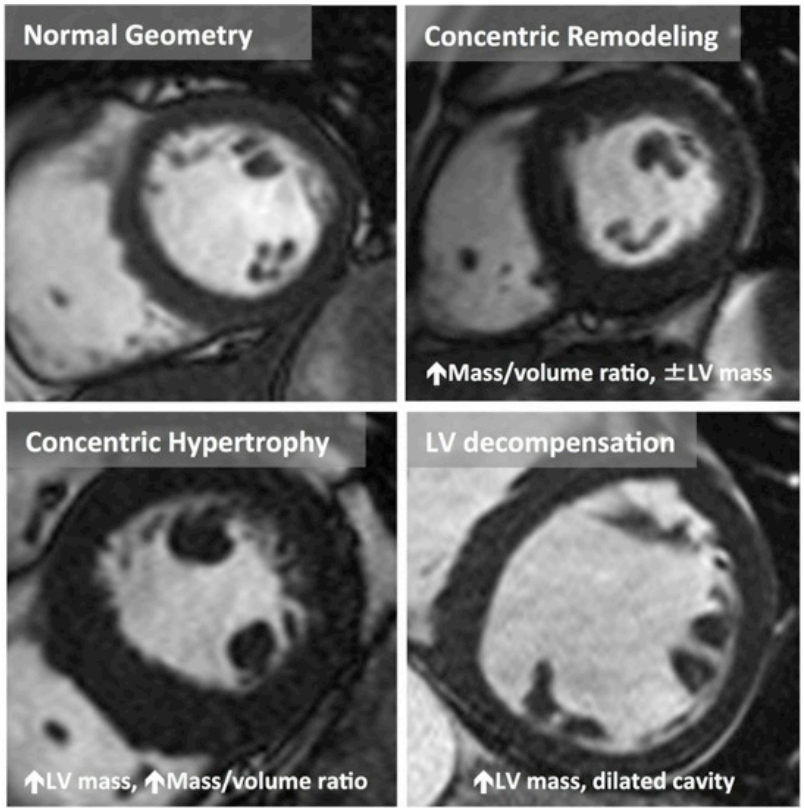

Figure 5: Pattern of myocardial remodelling by CMR

The four patterns of LVH and remodelling in AS demonstrated on CMR.

Cioffe et al found that patients with inappropriately high LV mass index on echocardiography (LV mass exceeding 10% of the expected value predicted from height, sex and stroke work) had a 4.5-fold higher risk of adverse events compared to counterparts with appropriate LVH [26]. Electrocardiographic evidence of significant LVH with strain was also associated with cardiovascular events in the SEAS study [27]. Presence of severe LV hypertrophy has been shown to be a major determinant of late death [28], while conversely LV mass regression of more than 150g is an independent predictor of improved long-term survival on multivariate analysis after AVR at 10 year [29]. Focus has recently turned on patients with preserved EF and paradoxical low-flow, low-gradient severe AS because they appear to have a worse prognosis [30]. As a population, they are characterized by severe concentric remodelling, high wall thickness, and small LV volumes and resulting low indexed stroke volume and mean gradients [30]. CMR as the reference standard for quantifying LV mass, volume and function allows a more accurate assessment of geometric changes, particularly in patients with challenging transthoracic echo windows (which are not uncommon in this population).

1.1.4.2 Impaired left ventricular function in AS

Impaired systolic function (LVEF<50%) in severe AS is even in asymptomatic patients a class I indication for AVR (even in asymptomatic patients), but is a poor and late indicator of LV contractile deterioration. Prior to deterioration in systolic function, LVH and fibrosis result in impaired LV relaxation and diastolic dysfunction. Left atrial size, Doppler mitral inflow and myocardial tissue velocities assessed by echocardiography in AS are associated with worse patient symptoms and increased cardiovascular events [31]. Left atrial size is also associated with the development of atrial fibrillation, which in turn increases the risk of heart failure and cerebrovascular events [32]. Mitral annular plane systolic excursion (MAPSE) [33], and mid-wall fractional shorting [34] as well as myocardial deformation/strain [35] imaging by echocardiography allow detection of more subtle deterioration in myocardial contractility. In particular, strain imaging, which accounts for the different myofibril orientation within the myocardium, shows subendocardial dysfunction in mild AS (reduced longitudinal strain), mid-wall dysfunction in moderate AS (reduced circumferential strain), and transmural dysfunction in severe AS (reduced radial strain), and has been shown to be prognostic [36].

1.1.4.3 Left ventricular remodelling after valve replacement

Myocardial changes are also important for the recovery after surgery, and have been studied by echocardiography and CMR. Following valve replacement (surgical or transcatheter), LV mass (LVM) regresses fastest in the first 6 to 12 months with 20% to 30% LVM reduction at 1 year, which is associated with significant improvement in LV systolic function [37-44]. Diastolic dysfunction (relaxation) only improves later with further regression of both LVH and diffuse fibrosis [45]. Patients with mild to moderate diffuse fibrosis at baseline show improvement in symptoms, LV function and a marked reduction in LVH after surgery [46, 47]. Patients, however, with severe fibrosis show only a slight clinical improvement, without a significant change in LV size or function [46]. As many patients develop diffuse fibrosis without symptoms or detectable reduced LV function [48], quantifying fibrosis directly has the potential to dramatically improve the management of these patients.

1.1.4.4 Myocardial changes in AS

Myocardial changes are thought to play a key role in functional deterioration, symptoms and outcome in AS [49].

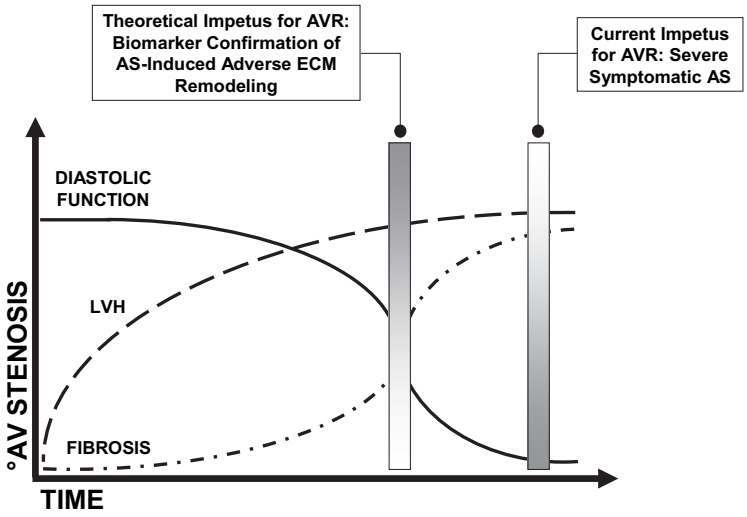

Figure 6: Theoretical impetus for early aortic valve replacement.

This is based on irreversible changes due to maladaptive ECM remodelling. AS, Aortic stenosis; AV, aortic valve; AVR, aortic valve replacement; ECM, extracellular matrix; LVH, left ventricular hypertrophy (Yarbrough 2011).

The theoretical impetus for early AVR is therefore based on irreversible changes due to extracellular matrix (ECM) remodelling. Identification of a biomarker capable of heralding the transition from adaptive to maladaptive ECM remodelling would certainly have therapeutic value. Specifically, such a biomarker may be used to direct more timely elimination of the pressure overload state, thus optimizing the chances for normalisation within the ECM and improved postoperative outcomes [50] (Figure 6).

1.1.5 The Myocardial Interstitium in AS

The cardiac interstitium plays a key role in the myocardial remodelling processes, acting as the stage for an intricate interplay between fibroblasts, myocytes, the neuro-hormonal system and mechanical stresses. In health, the complex three-dimensional extracellular matrix is composed of type I (80%) and type III (11%) collagen fibres (a ratio that changes in disease), which self-assemble into fibrils and large fibres after being secreted as procollagens and cleaved by proteinases. Fibrils are further strengthened by cross-links catalysed by lysyl oxidase (LOX)[51].

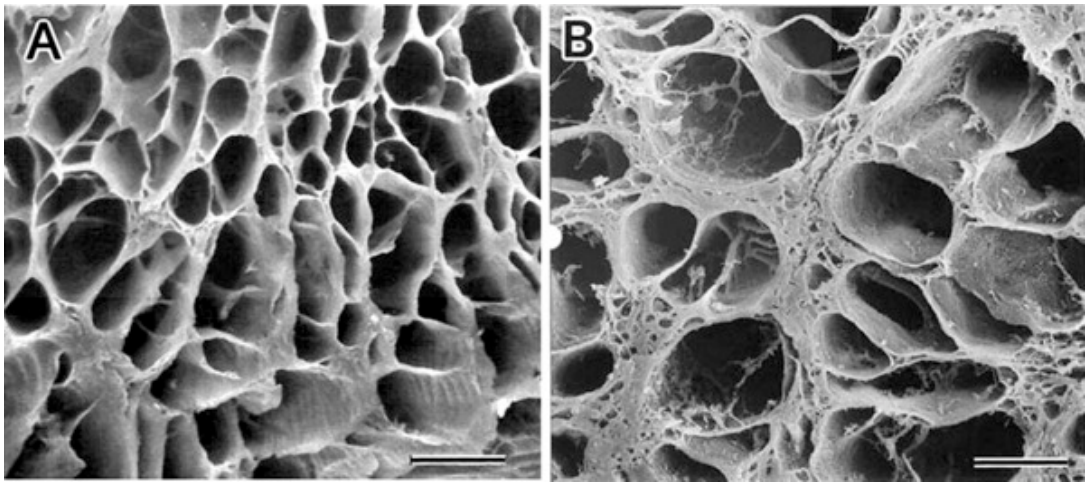

Figure 7: Myocardial fibrosis by scanning electron microscopy

Scanning electron microscope image showing the extracellular skeleton made up of collagen microfibrils in a normal subject (A) and a patient with severe aortic stenosis, where there is significant expansion of the extracellular space by collagen fibrils (adapted from Kanzaki Circulation 2009), Bar=30 µm, magnification ×600 [52].

Collagen degradation is regulated by a family of proteolytic enzymes, the matrix metalloproteinases (MMPs), which are themselves regulated by their tissue inhibitors (TIMPs). The key intracellular components are actin and titin filaments, which during diastole serve as tensiometers and passive force generators [53]. In disease, this environment changes due to fibroblast metaplasia into myofibroblasts, an increase in larger diameter higher-tensile type I collagen relative to type III collagen and increased LOX activity leading to amplified fibre cross-linking. On an intracellular level, myofibroblast smooth muscle actin increases and titin filament phosphorylation occurs, causing passive stiffness.

1.1.6 Interstitial versus Replacement fibrosis

Myocardial fibrosis can be described by different, partly disease-specific patterns, described as compact or 'focal,' perimyseal, perivascular, plexiform or patchy [54]: in AS, interfibre and perivascular fibrosis increase disproportionally [54]. Alternatively, one can distinguish between replacement fibrosis and diffuse interstitial fibrosis (due to a change in quantity and quality of collagen I and III – phosphorylation and crosslinking). Replacement fibrosis can occur due to apoptosis (pathway leading to cell death that features the activation of caspases to cleave cellular substrates), autophagy (degradation of cellular components within the intact dying cell in

autophagic vacuoles) or oncosis (cell death accompanied by cellular and organelle swelling and membrane breakdown).

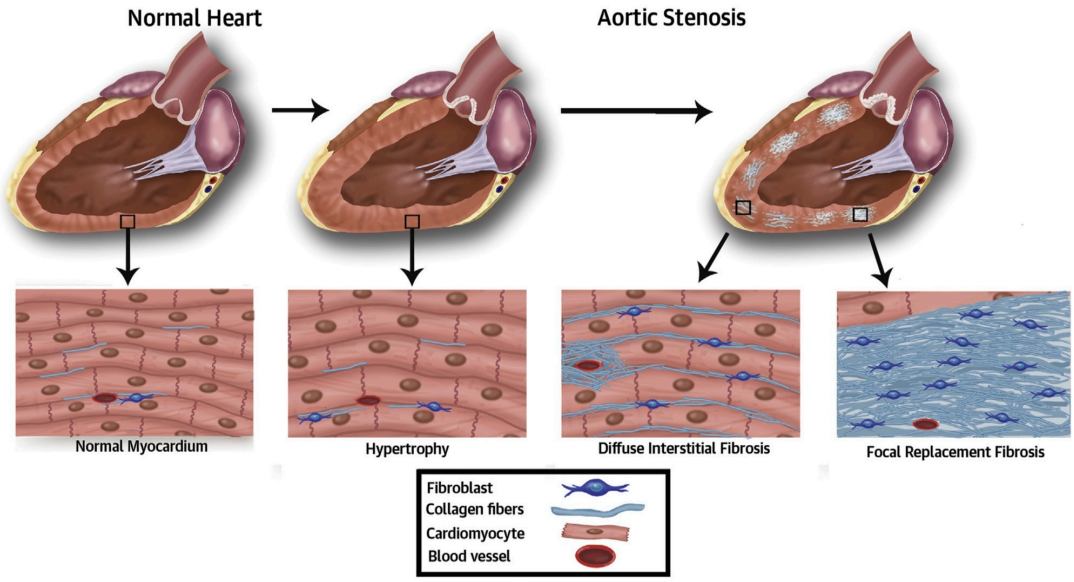

Figure 8: Pathophysiology of myocardial fibrosis in Aortic Stenosis

Chronic pressure overload of severe aortic stenosis results in compensatory concentric left ventricular hypertrophy, which is associated with not only increased myocyte volume but also coordinated remodelling and increased extracellular matrix, with development of both diffuse interstitial and focal replacement fibrosis. Adapted from Barone-Rochette 2014 [55].

Interestingly, replacement fibrosis in AS is predominantly due to ubiquitin mediated autophagy and oncosis rather than apoptosis, without any evidence of myocyte proliferation [56]. Furthermore, fibrosis in AS follows an endo- to epicardial gradient, with the increased fibrosis in the subendocardial portion (see section 1.4.5.2) likely due to a combination of increased cavity pressure, increased LVH-induced metabolic demand and reduced perfusion [57]. In histological practice, these subtypes of fibrosis are often captured together by staining procedures targeting the interstitium (picrosirus red/van Giessen/ Masson's trichrome) and described as collagen volume fraction (CVF). Myocardial fibrosis quantified using CVF at the time of AVR is highly variable and only poorly correlates with haemodynamic markers of AS severity, nevertheless patients with severe fibrosis have a significantly worse 5-year survival than those with only mild fibrosis (Figure 9 [58]). The current gold standard investigation for quantifiying fibrosis is endomyocardial biopsy, which is unfortunately prone to sampling error and is an invasive procedure associated with significant morbidity and mortality [59].

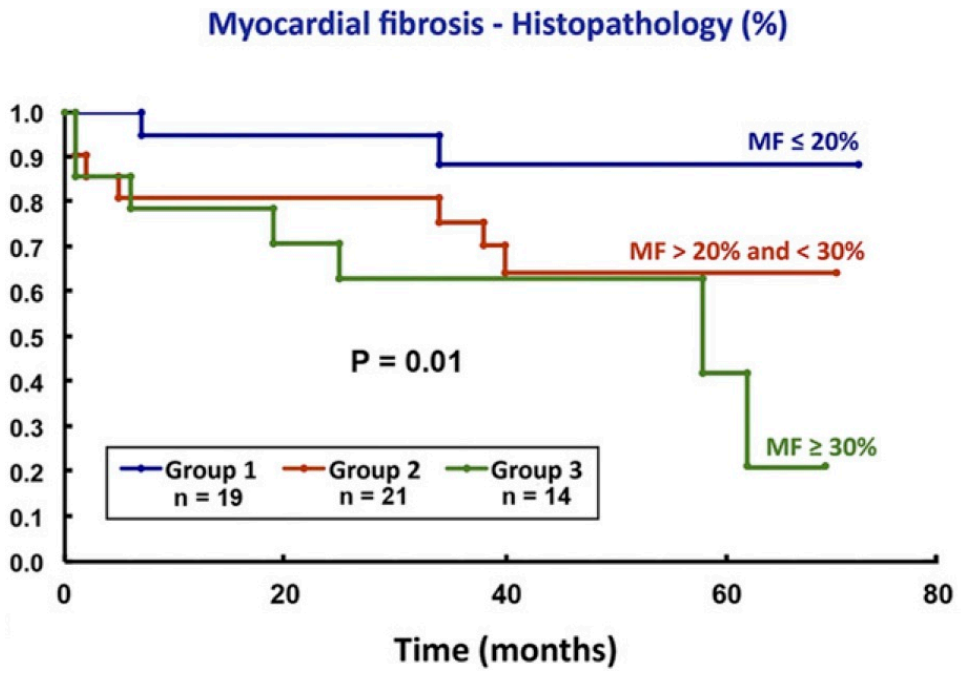

Figure 9: Myocardial fibrosis and outcome

Myocardial fibrosis quantified by histology during valve replacement predicts outcome. Adapted from Azevedo et al 2010 [58].

1.1.7 Influences of myocardial remodelling in Aortic Stenosis

The magnitude of the hypertrophic response to AS is also affected, among others, by age, sex, hypertension and occult disease (e.g. cardiac amyloid).

1.1.7.1 Sex

Sex appears to exert an important influence on LV remodelling [60-62]. Previous work has shown that men are more likely to have higher indexed LV mass, lower LVEF, and increased diastolic myocardial stiffness [42, 63], whereas women have more concentric remodelling with higher relative wall thickness and LVEF. To date however most studies have relied on echocardiography alone, with only limited combined echocardiography and CMR data available[42].

1.1.7.2 Hypertension

Hypertension is very common in calcific AS, depending on the age of the study population, e.g. affecting 72% of patients in the SEAS trial (Statin usE in Aortic Stenosis) [64]. The under-appreciation of hypertension and reluctance to treat it in this population results in increased vascular afterload and LV load (valvular-arterial impedance; Zva) leading to increased hypertrophic remodelling, interstitial fibrosis

and LV dysfunction [65], which in turn herald worse outcome. Uncontrolled hypertension may mask severity of AS, and should be treated aggressively, with re-evaluation of AS severity after adequate control. In addition to the favourable effect on LV remodelling, the potential anti-fibrotic effect of ACE-inhibitors and angiotensin receptor blockers medications may be beneficial [66-68].

1.1.7.3 Cardiac Amyloidosis

Amyloidosis is a rare multisystem disease characterised by the extracellular deposition of abnormally folded protein [69, 70]. Cardiac involvement is the leading cause of morbidity and mortality in these patients, and is characterised by a progressive infiltrative cardiomyopathy. Deposits of amyloid accumulate in the ventricular myocardium, almost always of either immunoglobulin light-chain (AL) or transthyretin (ATTR) type [69, 70]. ATTR cardiac amyloid deposition is present in up to a 25% of individuals aged over 85 at autopsy [71]. To date, this has been no more than an academic observation, but technology is changing this: cardiac imaging, particularly CMR and ^{99m}Tc-3,3-diphosphono-1,2-propanodicarboxylic acid (DPD) scintigraphy can now detect the disease antemortem, often without the need for invasive endomyocardial biopsy [72], which is generating a major increase in national awareness. Prognosis is often poor, and treatments are substantially influenced by cardiac involvement. Given the prevalence of both AS and ATTR in octogenarians, the two are likely to co-exist and the literature has early evidence for this. In a cohort of 20 patients with AS, who had undergone TAVI and subsequently valve explantation at autopsy (n=17) or surgery (n=3), cardiac amyloid was found in a third of these patients and was thought to contribute to death in the majority [73]. There are two separate aspects of ATTR in AS. First, ATTR in patients with moderate AS may mimic severe AS, (particularly low-flow, low-gradient) causing misdiagnosis. Second, ATTR may itself be a disease modifier, leading to a more severe phenotype with more heart failure, arrhythmia, and higher mortality.

1.2 Current dilemmas in the management of AS

Judicious timing of aortic valve intervention (surgical AVR or transcatheter aortic valve implantation [TAVI]) is crucial. Unnecessary morbidity and mortality associated with early intervention needs to be balanced against irreversible changes in the heart muscle due late intervention, because these can lead to increased post-

operative complications, the development of heart failure and an adverse long-term prognosis.

Current guidelines using the onset of symptoms and reduced LVEF as primary indications for intervention have significant limitations for the timing of surgery, because symptoms are often difficult to interpret, especially in the elderly, and reduction in LVEF occurs late and is associated with irreversible LV scarring. There is therefore a major need for:

1. A better understanding pathophysiological changes in the LV myocardium during the transition from physiological adaptation to pathophysiological maladaptation in severe AS.

2. More objective and specific markers of LV decompensation that influence outcome and therefore can be used to more accurately define the optimum timing of surgical AVR or TAVI.

CMR may deliver these more specific markers, as it offers a large array of techniques that allow accurate quantification of LV volumes, geometry and function (bSSFP cine imaging), stress perfusion imaging for quantification of the myocardial perfusion reserve, quantification of focal fibrosis (late gadolinium enhancement) and diffuse fibrosis (T1 mapping and ECV).

1.3 Myocardial Tissue Characterisation by CMR

This chapter is based on the following publications: ***Treibel TA****, Moon JC. T1 mapping in Cardiomyopathy (book chapter) in Cardiovascular Magnetic Resonance, 3rd Edition by Warren J. Manning and Dudley J. Pennell, Elsevier 2017.*

CMR exploits the inherent difference between tissues in their configuration of atoms by generating differing signals – the fundamental tissue properties T1, T2 and T2*. Whereas differences in T1 and T2 had to be previously visualised by weighted sequences, they can now be measured in a single breath-hold with T1, T2 or T2* displayed as pixel maps where each colour coded pixel carries the absolute value. Furthermore, if T1 is measured before and after contrast, the myocardial extracellular volume (ECV) is mapped, representing the percentage of tissue that is extracellular water, a surrogate for the process holding water - fibrosis, amyloid or

oedema. In turn, T2 mapping is a highly attractive technique for characterisation of myocardial tissue in disease state accompanied by inflammation. T1, T2 and ECV change in disease, each being differentially sensitive to pathological processes. The potential of these techniques is best appreciated in rare (infiltrations), common (oedema) and ubiquitous (diffuse fibrosis) disease processes.

1.3.1 Cardiovascular Magnetic Resonance for Scar Imaging

Tissue characterisation and measurement of fibrosis is a mainstay of clinical care in Respiratory medicine, Nephrology and Hepatology, but in Cardiology this has been limited to the few patients who receive cardiac biopsies. The emergence of CMR is changing this. Myocardial fibrosis is inherently an important clinical parameter, as it represents one of the hallmarks of pathological remodelling of the myocardium [54, 74-76]. CMR has established itself over the last decade not only as the gold standard for cardiac chamber volume and function quantification, but also for non-invasive myocardial tissue characterisation. Its strengths lie in the use of multiple parameters to characterise the myocardium. The development of imaging parameters for the quantification of oedema, infarction and scar has been followed by their adoption by the CMR community of non-invasive tissue characterisation, in particular in acute and chronic myocardial infarction (MI). During an acute MI, occlusion of a coronary artery territory leads to myocyte necrosis, which typically spreads from the subendocardial to the subepicardial layers. Without reperfusion, or a collateral blood supply, complete necrosis of the territory distal to the occluded coronary artery ensues. The majority of animal models are based on myocardial ischaemia and infarction, therefore large amounts of histological and pathophysiological evidence arise from the exemplar conditions of acute and chronic myocardial infarction.

Magnetic resonance characteristics of protons vary between tissues, depending on the configuration of atoms in the tissues. These inherent differences can be exploited to generate differing signal from particular tissues: T1 relaxation time (longitudinal relaxation time) is determined by how rapidly protons re-equilibrate their spins with their environment following a radiofrequency (RF) pulse. The native (non-contrast) myocardial T1 varies with water content and increases in cases of oedema, fibrosis or infiltration of the extracellular space (e.g. in cardiac amyloid). Inherently, it embodies composite signal from both cells and interstitium, and varies

with measurement technique and MRI field strength. Regional difference in T1 can be visualised by T1-weighted MR sequences or directly estimated by T1 mapping. T2 relaxation time (spin-spin relaxation time) is determined by how rapidly the refocused transverse signal decays after a RF pulse (in contrast to the rate of spin dephasing, which is called T2*). T2 is shorter when water is tightly bound to large molecules like collagen, but longer when water is free. T2-weighted images emphasize tissues with long T2 or in conditions like where myocardial oedema is present; new T2 mapping sequences are able to quantify T2 directly. Technical advances in T1- and T2-weighted imaging have allowed in-vivo visualisation and accurate quantification of myocardial oedema, a substantial feature of MI with ischaemic and reperfusion injury. Preliminary work by Higgins et al in a dog infarct model showed T1 and T2 elevation in infarction [77]. The observed changes were theoretically consistent with myocardial oedema and correlated with the measurements of myocardial water content estimated by wet-weight to dry-weight ratios. This early work aimed to develop non-contrast methods for diagnosing MI but overestimated infarct size.

1.3.2 Gadolinium contrast agents

*This chapter is based on the following publications: **Treibel TA**, White SK, Moon JC. Myocardial Tissue Characterization: Histological and Pathophysiological Correlation (Review). Current Cardiovascular Imaging Reports, 7 (3), 1-9, 2014.*

Historically, myocardial scar has been visualised and measured directly on histological sections using stains specific for the connective tissue in the extracellular space [54]. However, to allow non-invasive measurement, tracers were needed that are confined to the extracellular space. These tracers needed to distribute homogeneously through the extracellular space but not enter cells; be highly water but not fat soluble; not be adsorbed, actively transported, protein-bound or metabolized; be non-toxic, stable and be cleared freely from the body; and finally be easily measured. Gadolinium-diethylenetriamine penta-acetic acid (Gd-DTPA) fulfils these requirements as a tracer; it diffuses rapidly from the vascular space into most extracellular tissue fluid, but not to the intracellular space, leading to the term ‘extracellular contrast agent’. Gadolinium is a paramagnetic metal and because it has the most unpaired electrons [78], is the most efficient T1 relaxing agent, and also shortens T2 and T2*. In the presence of gadolinium, T1 of tissues is potently

shortened, resulting in increased signal on T1-weighted images and appearing bright on a T1 inversion recovery image. The relaxation rate (R1 or 1/T1) is directly proportional to the concentration of gadolinium. Gadolinium-based contrast agents are safe, with serious adverse events being extremely rare when appropriately used, with an incidence less than 1 in 100,000. Its safety profile and effect on the fundamental properties of T1 make it an ideal MR contrast agent.

1.3.3 Gadolinium contrast kinetics

To understand the pathophysiological basis of gadolinium contrast imaging, the pharmacokinetics of Gd-DTPA need to be considered. Following an intravenous bolus, gadolinium enters the myocardium down a concentration gradient ("wash-in phase"), and later, as the gadolinium has been cleared from the blood pool, it returns to the blood pool down the reversed concentration gradient ("wash-out phase"). This occurs over seconds to minutes in healthy myocardium, where cells are tightly packed and cell membranes are intact. In acute infarction, these kinetic effects are delayed due to changes in coronary flow rates, capillary permeability, and functional capillary density [79]. As importantly, the volume of distribution is larger due to ruptured cell membranes allowing Gd-DTPA to passively diffuse into the cellular compartment [80]. In combination with this the Gd-DTPA accumulates and lingers in the infarcted tissue shortening the T1. In chronic infarct (i.e. established scar), the volume of distribution is larger because of a significant reduction in living myocytes, which are replaced by a dense, hydrated collagen matrix, resulting in a higher accumulation of Gd-DTPA.

In practical terms, following administration of a bolus of Gd-DTPA, an inversion recovery sequence is performed, with the inversion time (TI) set manually by the operator. The TI is set in order to null "normal" remote myocardium which then appears black, resulting in the greatest image intensity difference between normal and infarcted tissue [81]. This late gadolinium enhancement (LGE) enables direct quantification of the spatial extent of focal scar, but the ability for absolute quantification of either diffuse, background fibrosis or density of focal scar is lost. Despite the extremely high resolution and correlation between histology and LGE in ex-vivo rat hearts at high field strength [82], it remains unknown what the clinical minimum "critical mass" of collagen is for LGE detection by. LGE imaging and analysis relies on thresholding techniques for quantification. Depending on the

disease and technique, there can be a two-fold difference [83]. New T1 mapping sequences, which will be discussed later, allow objective quantification of signal magnitude, which is potentially directly comparable between studies and patients.

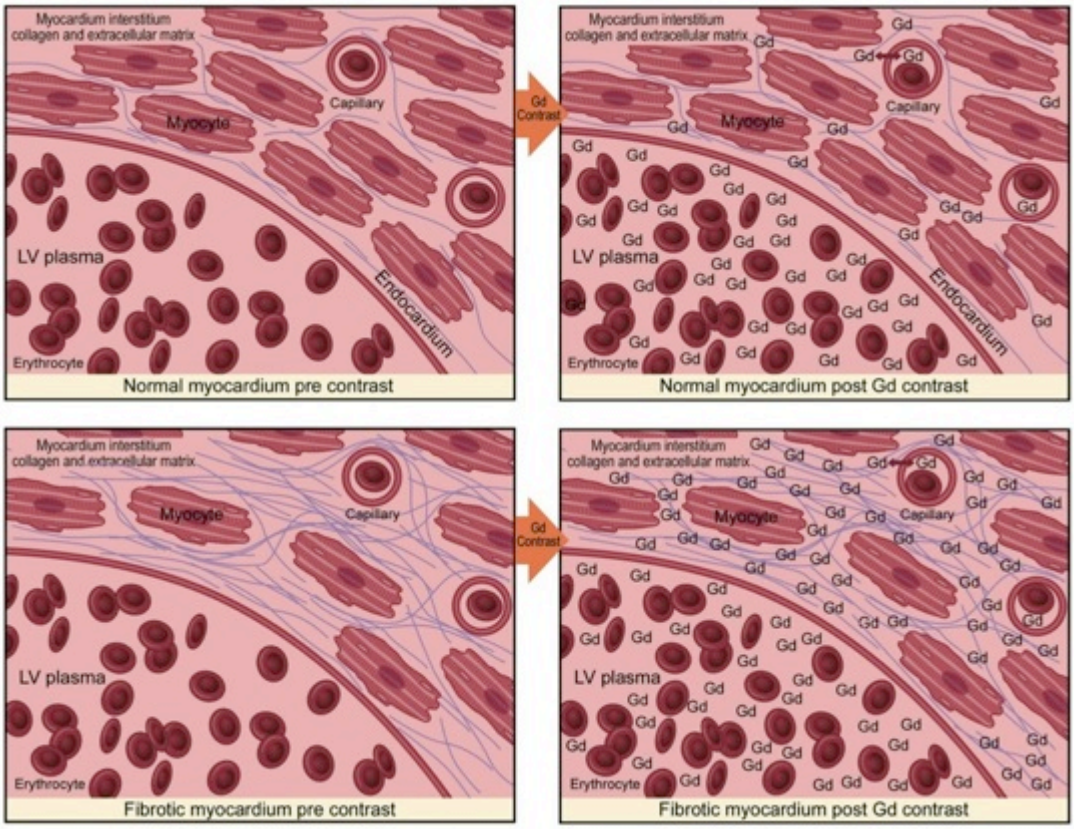

Figure 10: Gadolinium kinetics

Pre- and post-gadolinium (Gd) contrast dispersion in normal versus fibrotic myocardium. Adapted from Jellis Cardiovascular diagnosis and therapy 2014 [84].

Initial animal work in the 1980s was performed with manganese chloride [85] and later gadolinium chelates in canine models of myocardial infarction showing differential and time-varying effects on relaxation times of normal and infarcted myocardium [86, 87]. The development of inversion recovery LGE MRI [88] and extensive preclinical and clinical validation studies established MRI as a reference standard method for imaging myocardial infarction and viability. Kim et al published a seminal canine infarct study that documented that LGE MRI depicted infarcted myocardium with remarkable fidelity [89]. That work was supported by extensive validations of gadolinium concentrations in acute infarction [90]. The histological

validation of LGE has been taken close to a cellular level by Schelbert et al, who performed extremely high resolution ex-vivo LGE imaging on rats at 7 Tesla and compared with histological sections showing a remarkable correlation (R^2=0.96; p<0.001) [82]. Clinical validation studies established that gadolinium differentiated viable myocardium from infarcted myocardium in patients. Kim et al showed that the transmural extent of infarction predicted the recovery of contractile function after revascularisation [91], a study confirmed by Selvanayagam et al [92], provided revascularisation did not induce infarction.

LGE-CMR has now become the gold standard for non-invasive quantification of focal fibrosis, in particular infarct size, with the spatial resolution needed to determine the transmural extent of infarction. The burden of LGE predicts function recovery after MI [93] and revascularization [92], as well as mortality and MACE [94-96]. Single-photon emission tomography (SPECT) and positron-emission tomography (PET) validation studies confirmed that CMR LGE had equal or better sensitivity for infarction [97], in particular in small subendocardial infarctions seen on histology [98].

The LGE method has proved to be reproducible [99], and performed with high sensitivity and specificity in a multicentre clinical trial [100]. LGE has therefore established itself as the gold standard method for assessment of focal scar in both ischaemic and non-ischaemic heart diseases including cardiomyopathy [101], myocarditis [102], pressure-overload hypertrophy [103] and infiltrative diseases [104].

1.3.4 Late gadolinium enhancement in Aortic Stenosis

Various pattern of LGE have been reported in AS ranging from no fibrosis, subendocardial infarction-pattern, patchy focal, and linear mid-wall LGE Figure 11. Several groups have investigated the role of LGE in AS (see Table 1: LGE papers in aortic stenosis): Debl et al showed in 44 patient with severe symptomatic AS that 27% of patients had LGE and that LGE presence was associated with more severe valvular stenosis [105]. Weidemann et al investigated 58 consecutive patients with severe AS at baseline and 9 months after AVR (also obtaining intra-operative myocardial biopsies), and found that the degree of LGE did not change; they concluded that AVR failed to reduce the degree of replacement fibrosis [33]. Azevedo et al. showed in a combined biopsy and LGE study of 54 patients with

severe aortic stenosis or incompetence undergoing AVR that both histological and imaging fibrosis (LGE) was associated with all-cause mortality late (>2 years) after AVR. Lee et al investigated 118 patients with moderate to severe AS, and found that LGE was associated with parameters of systolic and diastolic function [106].

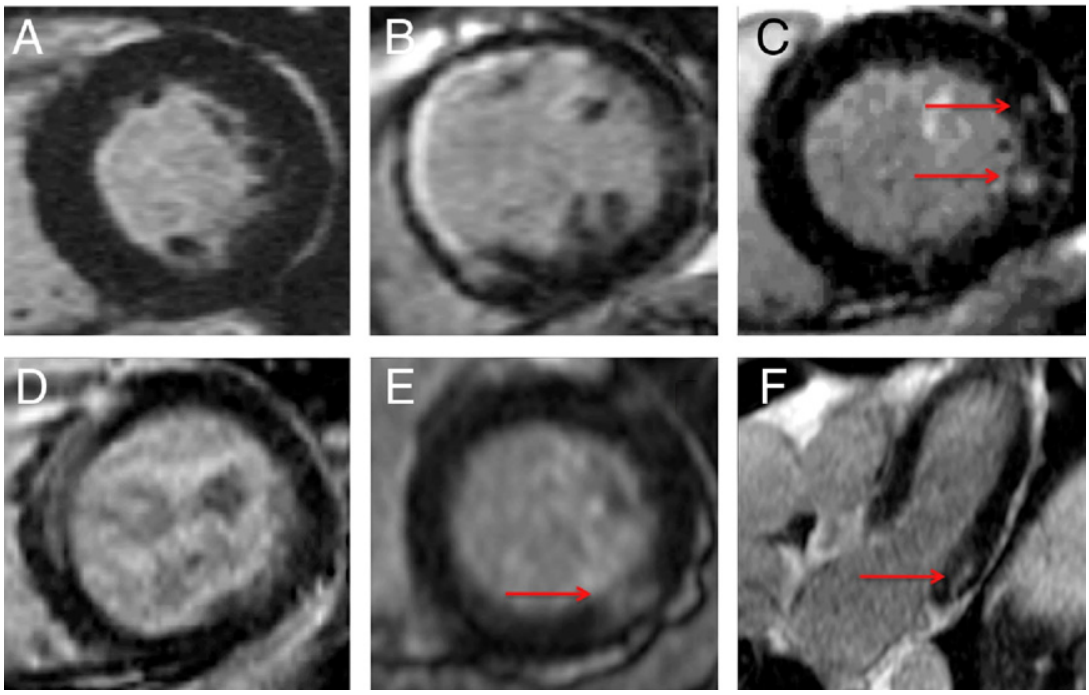

Figure 11: Late gadolinium enhancement in aortic stenosis.

(A) No late gadolinium enhancement (LGE). (B) Infarct LGE with a subendocardial pattern observed in the septum and anterior wall. (C) Two focal areas of midwall LGE in the lateral wall of the left ventricle (red arrows); (D) Midwall LGE in a more linear pattern affecting the septum. (E) Short- and (F) long-axis views of midwall LGE (red arrows) of the inferolateral wall in the same patient. *From Dweck et al JACC 2011.*

Dweck et al showed in a study consisting of 143 patients with moderate-to-severe AS that the presence of replacement fibrosis was an independent predictor of mortality providing incremental prognostic value over and above that of LVEF, with non-ischaemic LGE being a stronger predictor of mortality than infarct-pattern fibrosis [103]. Barone-Rochette et al investigated 154 consecutive patients undergoing AVR for severe AS, found LGE in 29%, and showed that LGE (non-ischaemic or infarct-pattern) was an independent predictor of mortality [55].

Author, Year of Publication	Inclusion Criteria	Outcome	Findings	Mean Follow-up	Comments
Debl et al, 2006	Moderate to severe AS n=22	LGE more common in severe than moderate AS	LGE found in 4.5 of 12 segments	Cross-section-al	LGE volume was larger in HCM control patients
Azevedo et al, 2010	AS referred for AVR n=28	Age & LGE were independent predictors of all-cause mortality	higher degrees of LGE associated with worse long-term survival	52 ± 17 months	LGE and histological fibrosis measured. Also 26 patients with AR followed.
Lee et al, 2013	Moderate to severe AS n=118	LGE associated with more advanced LV remodelling and decreased LV function and LV compliance	Midwall LGE was more common in patients with reduced LVEF	Cross-section-al	Potential usefulness of LGE to detect LV deterioration in AS
Steadman et al, 2012	Severe AS n=46	Myocardial perfusion reserve by MRI associated with peak VO2	LGE negatively associated with myocardial perfusion reserve	Cross-section-al	Links reduced myocardial blood flow with increased fibrosis
Quarto et al, 2012	AS referred for AVR n=63	Midwall LGE associated with greatest MACCE risk (P = .01)	No LGE (n = 25) had no 1- or 2-year mortality	30 d, up to 2 y	Postoperative AV block more common with midwall LGE
Dweck et al, 2011	Moderate and severe AS n=143	Midwall LGE increased mortality by 8-fold	Midwall LGE and LVEF predicted mortality	2 ± 1.4 years	Midwall LGE associated with increased LVMI
Fairbairn et al, 2013	Severe AS n=50	LGE reduced post-TAVI but not post-SAVR	LGE major predictors of remodelling.	6 months	FWHM quantification used.
Barone-Rochette et al, 2014	AS referred to AVR (n = 154) or TAVR (n = 40)	Presence of LGE increased all-cause mortality after AVR (HR, 2.8), but not after TAVR	Postoperative mortality was also greater with LGE	2.9 years	Low statistical power for events in TAVR group

Table 1: LGE papers in aortic stenosis

Significance of Late Gadolinium Enhancement by Cardiac Magnetic Resonance Imaging in Aortic Stenosis (adapted from Rader et al AJM 2015[107]).

1.3.5 Tissue Characterization – Moving Beyond Late Enhancement

The LGE technique has become the gold standard technique for assessing the presence of scar on CMR in both ischemic and non-ischemic heart diseases including cardiomyopathy [101], myocarditis [102], AS-induced pressure-overload hypertrophy [103] and infiltrative diseases [104]. LGE is, however, a difference test between normal and abnormal myocardium, and therefore is not able to accurately quantify diffuse myocardial disease, provide information the adaptation on non-scarred areas to the increased workload or indeed if they are at risk of generating new scar. There are many pathways active in normal myocardium, and these vary with different pathological processes. Each parameter may be differently sensitive to these. Multi-parametric tissue characterization is therefore an attractive strategy for non-invasive “biopsy” and “whole heart” sampling, avoiding potential morbidity and mortality of biopsy [59].

1.4 T1 Mapping and Diffuse Myocardial Fibrosis

Early in-vitro CMR work by Kehr et al. on human myocardium obtained post-mortem compared T1 values, calculated from the inversion recovery signal curves, with collagen volume fraction, determined by the picrosirus red method, and showed a significant correlation between the two methods [108]. Flett et al then developed an extracellular volume technique and showed strong correlation in patients with severe aortic stenosis and hypertrophic cardiomyopathy [109]: by calculating pre- and post-contrast T1 values from inversion recovery signal curves, the ECV was derived by incorporating the blood volume of distribution (1-haematocrit). The ECV showed a strong correlation with the collagen volume fraction of biopsies obtained intra-operatively in this cohort. This work has been replicated with shorter protocols and with newer, faster T1 mapping sequences (Figure 14; Table 2) in a variety of disease processes [110, 111]. After administration of gadolinium, T1 is dominated by and inversely proportional to the amount of gadolinium present in a tissue. Measuring T1 after contrast provides a value linked to the interstitium and has been applied to patients with heart failure [112].

Reference (et al)	Year	Population	n	Parameter	Sequence	Correlation
Iles [113]	2008	DCM	25	Post contrast T1	1.5T; IR VAST	r=-0.7 p=0.03
Flett [114]	2010	AS/HCM	26	ECV	1.5T; EQ-CMR; Multi-breath-hold FLASH IR	r2=0.8 p<0.001
Sibley [115]	2012	DCM/IHD/ HCM/Amyloid	47	Post contrast T1	1.5T, IR Look Locker	r=-0.57 p<0.001
Mascherbauer [116]	2013	HFpEF	9	Post contrast T1	1.5T, IR FLASH	r=0.98 p<0.01
White [117]	2013	AS	18	ECV	1.5T; EQ-CMR ShMOLLI	r=0.83 p<0.01
Miller [118]	2013	DCM/IHD (Transplant)	6	ECV	1.5T, MOLLI	r=0.94 p<0.01
Bull [119]	2013	AS	19	Native T1	1.5T; ShMOLLI	r=0.66 p<0.01
Lee [120]	2015	AS	20	Native T1	3T, MOLLI	r=0.77 p<0.01
De Meester [121]	2015	AS/AR/MR	31	T1 & ECV	3T, MOLLI	r=0.78 p<0.01

Table 2: Correlation of histology with T1 mapping parameters

AS, aortic stenosis; AR, aortic regurgitation; DCM, dilated cardiomyopathy; HCM, hypertrophic cardiomyopathy; IHD, ischaemic heart disease; IR, inversion recovery.

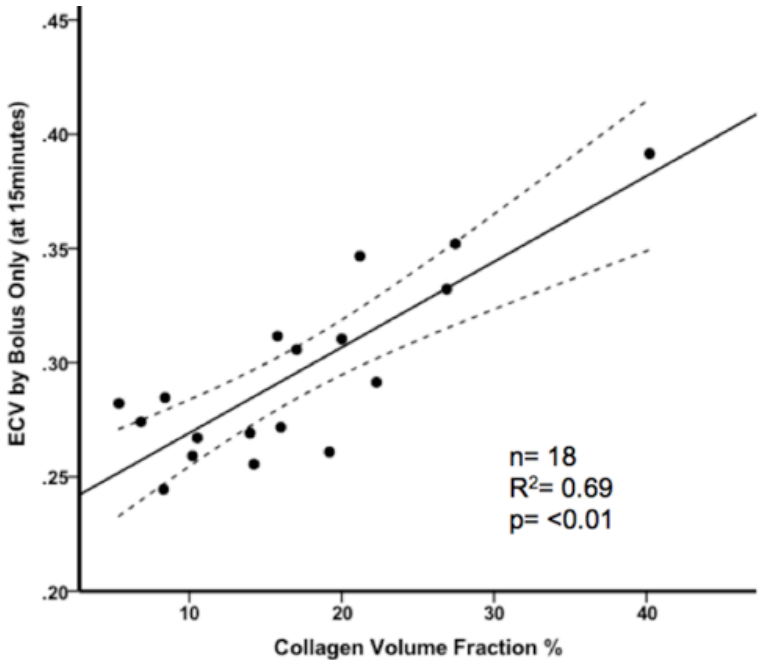

Figure 12: Histological validation of diffuse fibrosis in severe AS

Graph showing the correlation of extracellular volume (ECV) measured by CMR with histological collagen volume fraction in patients with severe aortic stenosis. The dashed lines represent 95% confidence intervals. Adapted from White et al. JACC CVI 2013 [117].

1.4.1 Native T1, post-contrast T1 and ECV

Native T1. Native T1 measures the intrinsic signal from the combined cellular and interstitial compartments of the myocardium [122]. The advantages are that it does not require an exogenous gadolinium based contrast agent. Native T1 relaxation time is prolonged with collagen (fibrosis) [109], oedema [123] and amyloid [124]. It is shortened with low fibrosis (i.e. cellular hypertrophy) [125], iron [126], fat [127] and haemorrhage [128] (Figure 13). Given that native T1 measures both interstitium and myocyte T1 – a signal from the interstitium alone is somewhat diluted by the myocyte signal so subtle differences (diffuse fibrosis) are harder to detect. Moreover, capillary density, capillary vasodilatation and "partial voluming" between blood pool and myocardium are also measured – introducing potential bias if the signal sought is the matrix or myocyte compartments alone. Native T1 time is different with field strength, sequence [129] and scanner type - making comparison of native and post-contrast values between centres challenging. Several groups have developed T1 phantoms to facilitate multicentre trials (HCMR [130]) or develop reference standards (T1MES [131]).

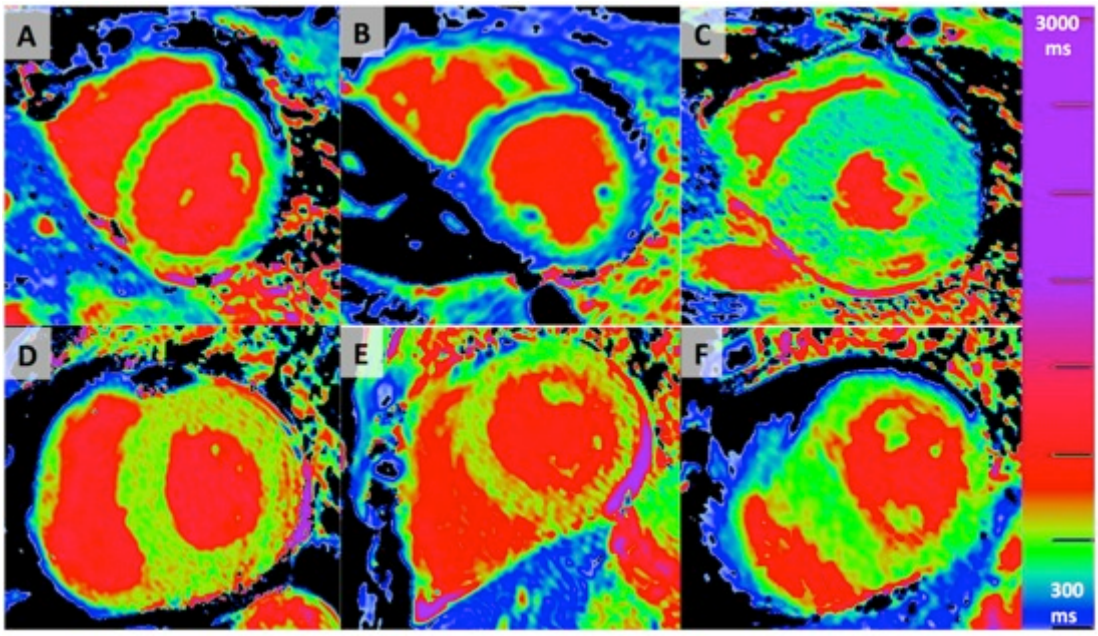

Figure 13: Native T1 across health and disease

Native T1 maps (ShMOLLI) in the basal short axis of healthy volunteer (A): the normal myocardium appears homogenously green and the blood is red; Severe iron overload (B): the myocardium appears blue as the T1 is low from iron; Fabry disease (C): the myocardium has a lower T1 (blue) due to intracellular lipid accumulation, except in the inferolateral wall which is red due to fibrosis; ATTR amyloid (D): the myocardium has a higher T1 (red); AL amyloid (E): the myocardium has a very high T1 with less hypertrophy then ATTR; and hypertrophic cardiomyopathy (F): there is asymmetrical septal hypertrophy with right ventricular insertion point scar (red). Adapted from Treibel TA, Moon JC. T1 mapping in Cardiomyopathy (book chapter) in Cardiovascular Magnetic Resonance, 3rd Edition by Warren J. Manning and Dudley J. Pennell, Elsevier 2017.

Post-contrast T1. After administration of gadolinium, T1 is dominated by and inversely proportional to the concentration of tissue gadolinium. Measuring T1 after contrast provides a value linked to the interstitium and has been applied to patients with heart failure [112]. Post-contrast T1 also varies with gadolinium dose, time post bolus, and importantly with patient specific factors such as heart rate, clearance rate, body composition and haematocrit.

Extracellular volume fraction. If the change in T1 pre- and post-contrast is measured in both blood and myocardium after equilibration of the contrast distribution, the partition coefficient can be calculated. By correcting for the haematocrit, the myocardial extracellular volume (ECV) is derived and can be calculated by:

$$\mathbf{ECV = (1 - haematocrit) \times \Delta(1/T1_{myo}) / \Delta(1/T1_{blood})}$$

Emerging evidence suggests that this ECV measurement is the more robust parameter then native or post contrast T1 [132] and early papers on prognosis show that, in unselected patients, it predicts outcomes at least as strongly as left ventricular ejection fraction ([133, 134].

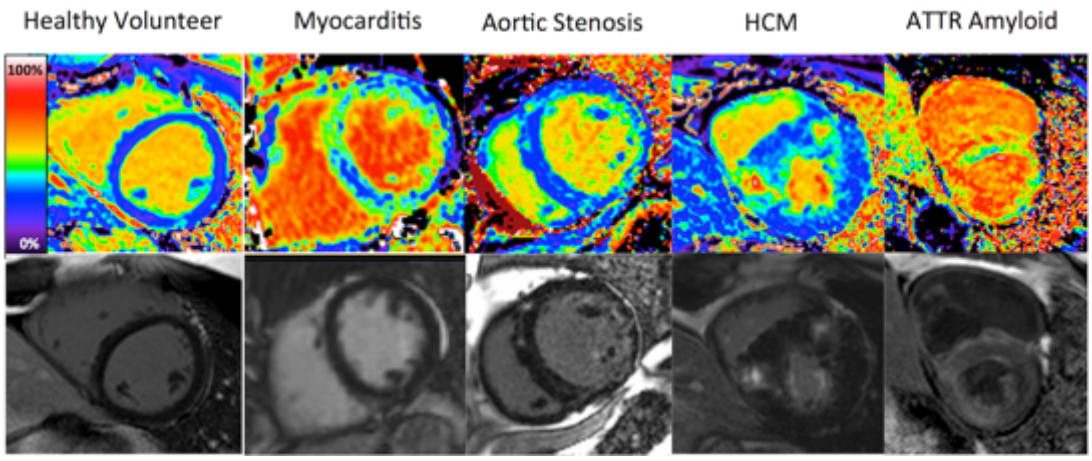

Figure 14: ECV and LGE across health and disease

ECV maps (top row) and corresponding late gadolinium image (LGE - bottom row) in the short axis of healthy volunteer: the myocardium appears homogenously blue; global myocarditis: note, due to the homogenous oedema, there is no focal LGE, but the ECV map shows diffusely elevated ECV; Aortic Stenosis: the ECV maps depicts ECV elevation corresponding to scar in the LGE image; Hypertrophic Cardiomyopathy (HCM): the ECV maps shows ECV elevation corresponding to scar in the right ventricular insertion points in the LGE image; ATTR amyloid; the blood:myocardial interface is lost in the ECV map, because the ECV is as high as in the blood pool (i.e.~60%) – the LGE images show classical global enhancement. Adapted from Treibel TA, Moon JC. T1 mapping in Cardiomyopathy (book chapter) in Cardiovascular Magnetic Resonance, 3rd Edition by Warren J. Manning and Dudley J. Pennell, Elsevier 2017.

1.4.2 ECV dichotomizing the myocardium into cell and matrix components

ECV divides the myocardium into two compartments (extracellular and cellular), and allows therefore non-invasive quantification of the myocardial *matrix volume* and its counter-part, *cell volume* (Figure 15). The cell volume represents the intact myocardial cellular component – providing a way to measure myocyte volume (N.B. this also includes fibroblasts, blood cells, macrophages, etc.). How these vary in disease (e.g. LVH) is important. For example, in transthyretin-related hereditary amyloidosis and light-chain amyloidosis, both have a massive matrix increase – but TTR has more matrix *and* 20% higher cell volume suggesting compensatory hypertrophy may permit more tolerance of the amyloid burden [135]. By modelling water exchange, there is also some evidence that the contrast kinetics could be

used to obtain cell size-dependent parameters particularly if very high doses of contrast are used [122].

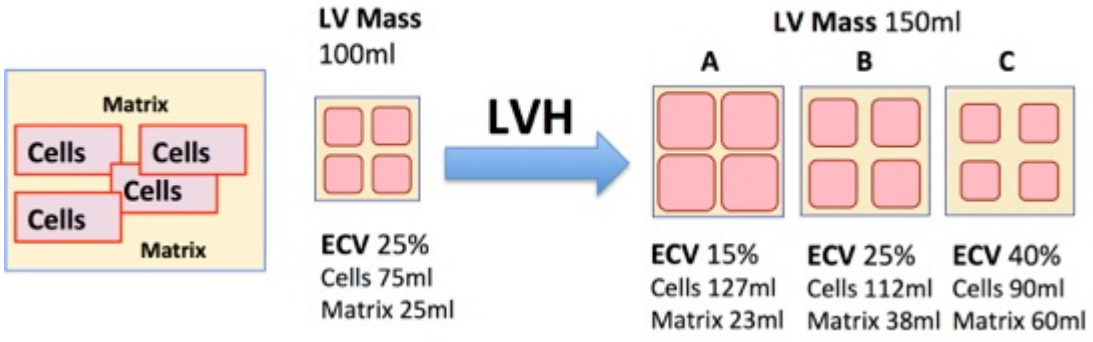

Figure 15: Cell and matrix volume by ECV

ECV dichotomizes the myocardium into matrix and cell compartments; these can be calculated by multiplying the volume of the LV myocardium by ECV or 1 – ECV, respectively.

1.4.3 Technical advances in T1 mapping and ECV

1.4.3.1 T1 Mapping Evolution

The T1 mapping field is rapidly advancing to the point of widespread clinical utility. The first to use T1 measurements was Messroghli in 2004 with a pulse-sampling scheme known as Modified Look-Locker Inversion Recovery (MOLLI) [136], which replaced previous multi breath-hold approaches. This was refined over time including new MOLLI variants, ShMOLLI (a shortened variation with long T1 advantages [136-138]), saturation recovery variants such as SASHA (offering complete heart rate insensitivity [138]) or hybrid approaches (ANGIE, QALAS, SAPPHIRE [139-141]); see Table 3. Incremental developments such as respiratory motion correction [142] gradually increased accuracy and precision [139, 143]. For ECV, contrast regimes were simplified from bolus followed by infusion or multi-timepoint sampling to a single pre and post-contrast T1 map [144, 145]. Split contrast dose protocols suitable for stress perfusion imaging have also been validated [146]. ECV maps are now routine in some centres [147]. ECV quantification is less field and sequence sensitive than native T1 mapping but ECV standardization is on-going. Finally, MR finger printing may offer more rapid multi-parametric tissue characterization in the future by providing myocardial T1, T2, and Proton Spin Density in a single breath-hold [148].

Sequence	T1 preparation (sampling)	Imaging readout	Respiratory motion correction	Dura-tion	Advantage	Disadvantage
MOLLI	Inversion 3(3)3(3)5	Single-shot bSSFP	Single breath-hold	17s	Good image quality, high precision, wide availability, inter-centre reproducibility	T1 dependence in T2, MT, sequence parameters, heart rate.
MOLLI variants	Inversion 5s(3s)3s; 4s(1s)3s(1s)2s	Single-shot bSSFP	Single breath-hold	11s	Short breath-hold, little heart rate variability, optimal precision for pre and post contrast	Different pre-and post-contrast sequence
ShMOLLI	Inversion 5(1)1(1)1	Single-shot bSSFP	Single breath-hold	9s	Very short breath-hold, unified sequence for pre/post, little heart rate variability	Low number of fitted images
SASHA	Saturation	Single-shot bSSFP	Single breath-hold	10s	Excellent accuracy, invarient to T2, MT and inversion efficiency	Low precision, prone to artifact, low image contrast for registration
SAPPHIRE	Hybrid Saturation / Inversion	Single-shot bSSFP	Single breath-hold	10s	Good accuracy, improved precision (greater than SASHA)	Lower precision than MOLLI, prone to artifacts
STONE	Inversion	Single-shot bSSFP	Free-breathing; registration / tracking	55s	Improved accuracy, free breathing, no rest periods	Potential susceptibility to heavy breathing, perturbation of blood T1
ANGIE	Inversion	Seg-mented bSSFP	Navigator-gated, free breathing	41s	Enables high-resolution scans, motion compensation robust to deep breathing	Accuracy as in MOLLI, elaborated CS reconstruction required

Table 3: T1 mapping Techniques - an overview

Overview of current T1 mapping techniques and sampling schemes (adapted from Sebastian Weingaertner, SCMR 2016). MOLLI, Modified Look-Locker Inversion; ShMOLLI, Shortened MOLLI; MT, magnetisation transfer; bSSFP, balanced steady-state free precession; SASHA, Saturation-recovery Single-SHot Acquisition; SAPPHIRE, Saturation-Pulse Prepared Heart-rate independent Inversion-REcovery; STONE, slice-interleaved T1 mapping; ANGIE, accelerated and navigator-gated Look-Locker imaging [139-141].

For clinical utilization, these developments need to transition to standardized methodologies to diagnose disease, define mechanistic pathways of disease affecting the interstitium, the myocyte or both, change therapy and employ ECV as a surrogate endpoint in trials of drug development. This is the aim underpinning the first T1 mapping consensus statement [149]. The conceptual models are simple, but there is more going on: effects such as magnetization transfer, diffusion distance and time, contrast mechanisms, trans-cytolemmal water exchange rate, flow, T2 or T2* relaxation will all require further investigation [150, 151]. This will require global support and involvement. Quality control systems, commercial sequences, mega-registries (e.g. Global CMR Registry, HCM Registry, UK Biobank) are in progress,

and will provide high volumes of new insights in what is now the most active CMR research area [130, 152].

1.4.3.2 Original MOLLI

T1 Mapping using an ECG triggered MOLLI allows the acquisition of single shot bSSFP (balanced steady-state free precession) images acquired at different inversion times after a single inversion pulse, all gated to the same cardiac phase, thereby enabling a pixel-based T1 quantification in the myocardium.

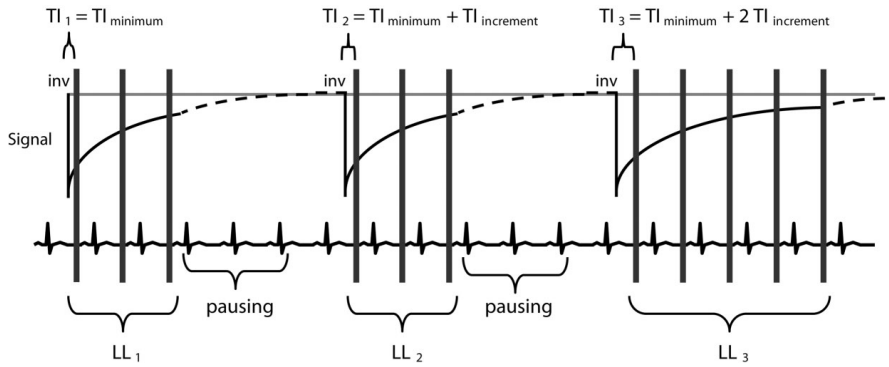

Figure 16: MOLLI Sampling scheme

After the inversion, the magnetization following the T1 relaxation curve is repetitively sampled in several heartbeats for a small duration until the longitudinal magnetization has fully recovered. By combining several (up to 3) inversions with slightly shifted TI times within one protocol, the relaxation curve is sampled in an interleaved manner, resulting in a sufficient number of points for accurate T1 quantification acquired within a single breath-hold (adapted from Messroghli et al 2007).

1.4.3.3 ShMOLLI

ShMOLLI was developed as a shortened alternative to MOLLI (hence the name), which can generate rapid and high-resolution myocardial T1-maps in a single short breath-hold of only 9 heartbeats. It uses a conditional data-fit to ensure recovery. The same sequence is used for pre and post contrast, and it has minimal heart rate variability.

1.4.3.4 MOLLI variants

The most advanced MOLLI variant proposed by Dr Peter Kellman is a combination of separate pre-contrast (sampling scheme: 5s(3s)3s)) and post-contrast (sampling scheme: *4s(1s)3s(1s)2s*). Furthermore, these sequences offer motion correction (MOCO), a better inversion pulse, standard deviation maps (error maps) and phase

sensitive inversion recovery (PSIR) fitting (using a 3-parameter model). Finally, this sequence is also compatible with an offline ECV map prototype.

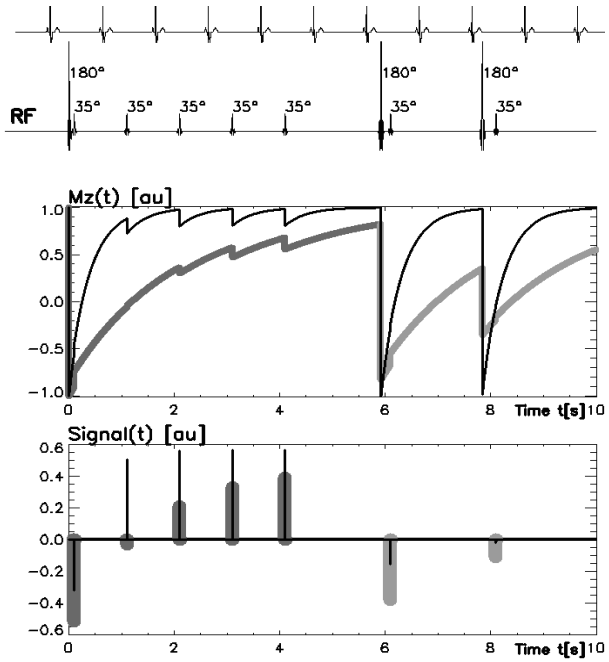

Figure 17: ShMOLLI Sampling scheme

ECG-gated pulse sequence schemes for simulation of ShMOLLI at a heart rate of 60 beats per minute (adapted from Piechnik et al 2010).

1.4.3.5 ECV by Bolus versus Infusion

The ECV technique has been taken a step closer to routine clinical applicability by work removing the requirement for a logistically cumbersome and time consuming primed infusion technique for the calculation of ECV. Schelbert et al showed no apparent detriment to the relationship with collagen volume fraction in low ECV states; White et al confirmed this, but highlighted that in high ECV (>40%) subjects, the bolus only approach consistently and increasingly overestimated the ECV [110, 153].

1.4.4 T1 and ECV in Aortic Stenosis

T1 quantification and mapping was applied early on to aortic stenosis, because of the relative ease of obtaining myocardial biopsies during AVR for histological validation of the technique. As mentioned above, the first histological validation was by Flett et al [109], who used a multi-breath-hold FLASH inversion recovery technique in 18 patients with severe AS. He then applied this technique to track clinical progression prior to and 6 months post AVR. This showed that diffuse

fibrosis was higher in AS patients compared to controls and correlated with functional capacity at baseline, but was underpowered to detect an increased mortality in those patients with severe fibrosis . Native T1 has also been validated against histology and has been shown to track AS severity [154]. ECV using new T1 mapping techniques shows great promise due to a stronger biological signal and higher reproducibility [155]. T1 mapping data in aortic stenosis is summarized in Table 4. Prospective outcome data is currently not available, but T1 mapping has been incorporated as a secondary end-point to the PRIMID-AS study investigating myocardial fibrosis and perfusion reserve in asymptomatic moderate to severe AS (n=170) [156].

Author	n	AS group	Type	Sequence	Parameter	Comment
Flett et al, 2010[114]	18	Severe	Histology	FLASH IR	ECV	R^2=0.86
Flett et al, 2012[48]	63	Severe	Outcome	FLASH IR	ECV	ECV predicts 6MWT improvement post op
Bull et al, 2013[157]	109	Moderate to severe	Histology & mechanistic	ShMOLLI	Native T1	R^2=0.43
White et al, 2013[117]	18	Severe	Histology & technical	ShMOLLI	ECV	R^2=0.69; bolus as good as infusion protocol
Chin et al, 2014[158]	20	Mild to severe	Technical	MOLLI (3T)	ECV + T1	ECV better reproducibility then T1
Chin et al, 2014[159]	122	Mild to severe	Mechanistic	MOLLI	ECV	ECV not independent predictor of Troponin
Dusenbery et al, 2015[160]	29	Congenital	Mechanistic	MOLLI	ECV	ECV elevation associated with diastolic dysfunction
Mahmod et al, 2014[161]	26	Severe	Mechanistic	ShMOLLI (3T)	T1	Hyperemia substantially alter T1 values
Singh et al, 2015[162]	40	Moderate to severe	Technical	MOLLI (3T)	ECV + T1	No difference in T1 or ECV between AS & controls
Lee et al, 2015[120]	80	Moderate to severe	Mechanistic	MOLLI (3T)	T1	R^2=0.60
de Meester et al, 2015[121]	12	Severe	Histology	MOLLI (3T)	ECV + T1	R^2=0.61
Kockova et al, 2016[163]	31	Severe	Histology	MOLLI	ECV + T1	R^2=0.15 T1; R^2=0.10 ECV
Nadjiri et al, 2016[164]	94	Severe (TAVI)	Mechanistic	MOLLI	ECV	ECV: predictor of heart failure post TAVI (p=0.06)

Table 4: Overview of T1 mapping publications in AS

1.4.5 Challenges for T1 mapping in Aortic Stenosis

1.4.5.1 Capillary density.

Rakusan et al reported reduced capillary and arteriolar density with increasing LVH on histological examination of myocardial samples [165]. Compensatory vasodilatation has been proposed by Mahmod et al as a potential confounder for

elevated native myocardial T1 and ECV in severe AS. They showed that during adenosine hyperaemia, patients with severe AS had a blunted stress response, however 7 months following AVR, native myocardial T1 and response to adenosine stress returned to normal [161].

1.4.5.2 Fibrosis gradient from endocardium to epicardium.

Weber [166] showed that in patients with AS the fibrosis percentage was higher in the subendocardium than in the subepicardium (19 versus 13%, $p<0.05$). Cheitlin et al then demonstrated a gradient of myocardial fibrosis from the inner to the outer third of the myocardium in patients with congenital aortic stenosis (Figure 18)[167].

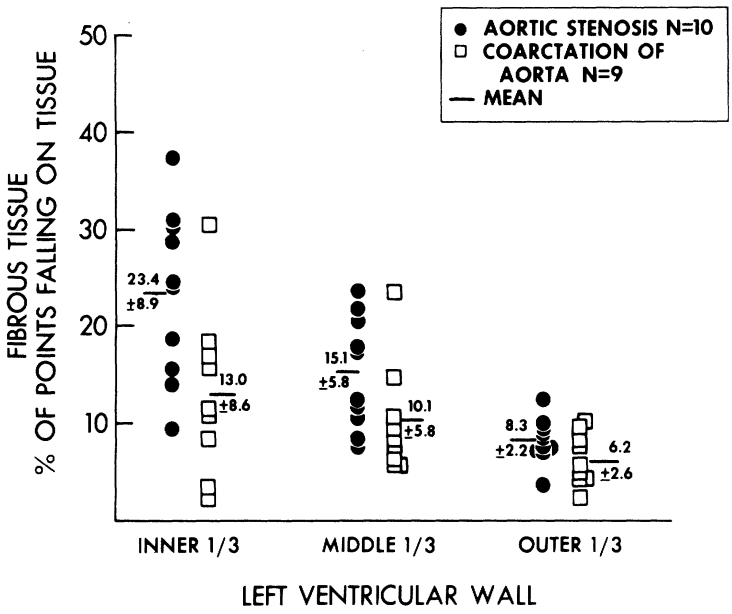

Figure 18: Gradient of myocardial fibrosis

A gradient of myocardial fibrosis from the inner to the outer third of the myocardium in patients with congenital aortic stenosis (adapted from Cheitlin et al Circulation 1980) [167].

1.5 Myocardial tissue characterisation by Computed Tomography

Computed Tomography (CT) can also quantify the ECV (CT_{ECV}) from pre and post contrast measurements of attenuation, and shows good correlation with ECV measured by CMR (ECV_{CMR}), as well as histological measures of myocardial fibrosis [168-170].

1.5.1 Previous CT ECV work

Previous ECV_{CT} work is limited to two studies by Nacif and colleagues comparing heart failure patients with controls and a single histological validation study by Bandula and colleagues. In the first study by Nacif, subjects underwent ECV_{CMR} and ECV_{CT} demonstrating results in line with the ECV_{CMR} literature (28.6±4.4% vs 31.6±5.1%, *p = 0.03*) [169]. In the second study, whole heart 3D ECV was quantified; ECV was significantly higher than in the previous CT study by the same group and in CMR_{ECV} studies (41±6%, 33±2%; *p = 0.02*) [170], raising the concern that partial voluming of the blood pool may have occurred. Bandula et al. measured ECV by using equilibrium CT in patients with aortic stenosis and showed that it correlated with histological quantification of myocardial fibrosis and with ECV derived by using CMR imaging (r = 0.71, *p<0.001* and r = 0.84, *p<0.0001*, respectively) [168].

1.5.2 Reasons to pursue ECV by CCT

CT has advantages over CMR: although ECV quantification by CMR is accurate and feasible, it is not suitable for patients with claustrophobia or commonly implanted devices like pacemakers. Furthermore, its widespread implementation into the NHS may be limited by cost, lack of widespread scanner access and time constraints (demands on NHS MRI resources is high and scans involving ECV quantification can take up to 60 minutes, reducing patient throughput). CT is faster and more ubiquitously available, with higher spatial resolution and a simple linear relationship between attenuation measurement (Hounsfield units, HU) and iodine concentration (compared to the non-linear effect on relaxivity of hydrogen following administration of gadolinium). Therefore, translation and validation of ECV by CT will aid dissemination of the technique throughout the NHS.

Chapter 2 Research Aims

2.1 The RELIEF-AS Study

REgression in **L**eft ventricular **I**nterstitial **E**xpansion and **F**ibrosis after **A**ortic stenosis **S**urgery Study. ClinicalTrials.org Identifier: NCT02174471

The RELIEF-AS Study was the main project of my PHD and the focus of my original funding application, which was granted by both the British Heart Foundation and National Institute for Health Research (I accepted the NIHR Doctoral Research Fellowship). The majority of my research time was dedicated to this work and the data originating from this is the basis for multiple submitted papers.

2.1.1 Overview and Study Design

RELIEF-AS was a large single centre, 180 patient observational outcome study of aortic stenosis patients undergoing valve replacement with comprehensive baseline assessment, including CMR and biopsy in all and 1-year follow-up for cardiac, functional and mortality endpoints.

2.1.2 Hypotheses

We hypothesized using clinical invasive and non-invasive quantification that

I. Extracellular matrix expansion predicts surgical outcome in AS after AVR.

II. Recovery after AVR is associated with diffuse fibrosis regression at 1 year.

2.1.3 Aims

To use dynamic CMR to measure ECV as a marker of extracellular matrix expansion in patients with severe AS before and after valve replacement to establish if ECV, is predictive of outcome after surgery, and regresses parallel to LVH with reduction of afterload at 12 months (post AVR). Furthermore, our aim was to gain pathophysiological insights into extracellular matrix expansion in AS by invasive myocardial biopsy obtained during surgery.

2.1.4 Study design

This was a single centre, prospective observational cohort study of patients with severe AS undergoing AVR in a tertiary referral cardiac centre (Figure 18 for Study Flow Chart proposed at study begin). The study was approved by the ethical committee of UK National Research Ethics Service (07/H0715/101) and registered on ClinicalTrials.gov (NCT02174471). The study conformed to the principles of the Helsinki Declaration, and all subjects gave written consent to participate.

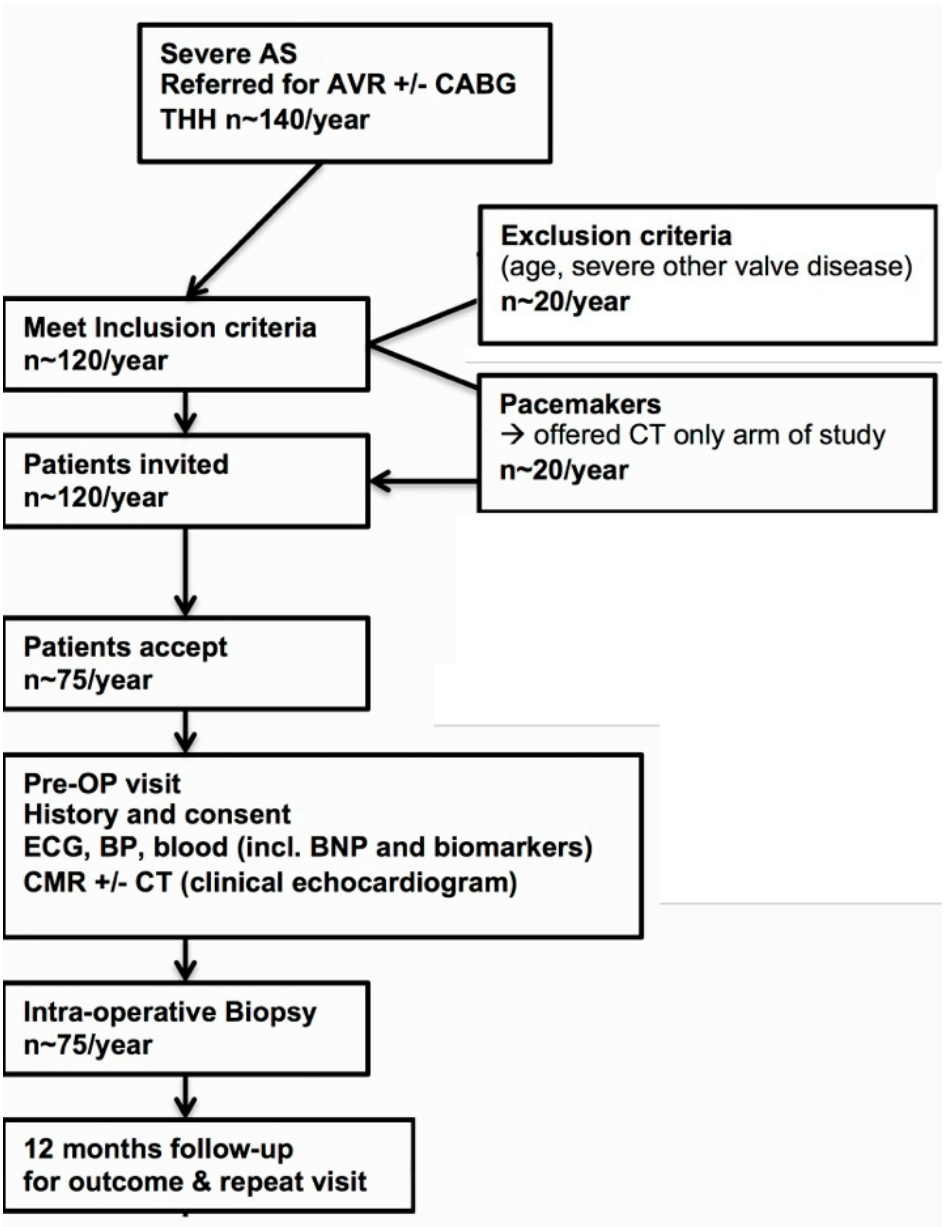

Figure 19: Planned study flow chart of RELIEF-AS Study.

2.1.5 Patient selection:

- Inclusion criteria: patients with severe aortic stenosis (2 or more of: AVA<1cm^2, peak pressure gradient 64mmHg, mean pressure gradient 40mmHg, velocity ratio < 0.25; or reclassification of discordant echocardiographic data to severe by alternate modality) undergoing AVR+/-CABG at Heart Hospital, consenting for study protocol; age 18-90 years, ability to undergo CMR scan.
- Exclusion criteria: pregnancy/breastfeeding, GFR <30mls/minute, CMR incompatible devices, inability to complete the protocol, previous valve surgery, severe valve disease other than AS.

2.1.6 Primary outcome measures:

- Death post AVR.
- Regression of diffuse myocardial fibrosis at 1-year post AVR.

2.1.7 Secondary outcome measures:

Secondary outcome measures were post-operative changes in diffuse fibrosis (measured by ECV), LV remodelling, symptoms (NYHA functional class, CCS class and quality of live measured by EQ-5DL) functional recovery (measured by 6 minute walk test) at 12 months.

2.1.8 Recruitment

Patients were recruited from cardiology, cardiothoracic, echocardiography or Heart Team meeting reports, were approached in the in- or outpatient setting and given a patient information sheet (PIS) if interested. Baseline assessment was co-localised with the surgical pre-operative assessment clinics to minimize travel for patients.

2.1.9 Justification of sample size / Power calculations:

The study with 150 subjects was calculated to have 80% power (binomial test) to show that patients with severe fibrosis (high ECV) have a higher event rate than patients with mild to moderate fibrosis (low ECV) at 1 year. The power calculations were reviewed by Paul Bassett (Senior Research Associate, UCL Biostatistics

Group). We based our sample size calculation on a previous cohort in our institution (Flett *et al* 2012), which was followed up at 6 months with a sample size of 63 patients, and showed a trend of higher mortality with severe DMF.

- Patients were to be divided into tertiles of diffuse fibrosis: group 1 comprising of patients with mild and moderate fibrosis, group 2 comprising of patients with severe fibrosis; Group 1 and 2 represented in a 2:1 ratio (based on a similar cohort).
- Flett *et al.* described the following mortality figures at 6 months:
  - Group 1: Mild/moderate fibrosis = 2.4% (P1)
  - Group 2: Severe fibrosis = 19% (P2)
- Power of the test = 80%; Type 1 error = 0.05 (K); ratio p1 : p2 = 2:1

Adequate power was calculated to be achieved with a group size of 44, equalling a total sample size of 132. Furthermore, we decided to extend the follow-up to one year, and adjusting the sample size to allow for dropout (or implantation of non-MR compatible PPMs) of 10%. Therefore, a sample size of **150 patients** was calculated to give adequate power our study, and to be a realistic recruitment target for our institution (140 AVR/year, 50-60% participation).

2.2 Sub-studies

2.2.1 Left Ventricular Remodelling in Severe Aortic Stenosis

Background: Four main geometric patterns have been defined: normal geometry, concentric remodelling, concentric hypertrophy, and eccentric hypertrophy – based on left ventricular mass, cavity size and the ratio of these two.

Aim: To understand the influences on AS remodelling using all available modalities to investigate patterns of remodelling at macroscopic and tissue level.

2.2.2 Occult amyloidosis in Aortic Stenosis

Background: Coexistence of AS and cardiac amyloidosis has been reported but this has not been studied systematically and the prognostic significance is unknown.

Hypothesis: We hypothesized that unrecognized ATTR amyloid deposits may act as a disease modifier in aortic stenosis. We aimed to: 1 – assess the prevalence of

occult cardiac amyloid in AS; 2 - identify the amyloid subtype; 3 – determine the role of comprehensive imaging; and 4 - elucidate its clinical and prognostic significance.

2.2.3 Combining multimodality phenotyping with advanced histology

Background: Although new insights are being generated by imaging tissue characterisation, the histological basis of LGE and ECV in AS and their association with fibrosis subtypes are only partly understood.

Aims: To investigate myocardial fibrosis in a large series of severe aortic stenosis patients using invasive biopsy and non-invasive imaging, assessing simultaneously and at scale cardiac status, structure and function and by performing non-invasive (ECV and LGE) and histological tissue characterisation.

2.3 Technical Development

The following technical developments arose through observations and collaborations while setting up the RELIEF-AS study.

2.3.1 Synthetic ECV

Background: ECV quantification requires blood haematocrit measurement. This is cumbersome, involves blood sampling and delay. However, there is a linear relationship between the longitudinal relaxivity (R1=1/T1) of blood and haematocrit.

Hypothesis: We hypothesized that a CMR native T1 blood could estimate *synthetic* Hct, permitting immediate *synthetic* ECV calculation and an instantaneous synthetic ECV map without blood sampling.

2.3.2 ECV by Cardiac Computed Tomography

Background: ECV can be quantified by computed tomography (CT), which has advantages over CMR: ubiquitously available equipment, higher spatial resolution and a simple linear relationship between attenuation and iodine concentration. We developed the ECV_{CT} methodology requiring a complex primed-infusion.

Aim: This study was designed to simplify the progenitor equilibrium methods by using a bolus-only, dynamic equilibrium approach in order to develop a simple alternative ECV method to CMR.

Chapter 3 Material and Methods

3.1 Ethical Approval

All ethics were approved by the UCL/UCLH Joint Committees on the Ethics of Human Research Committee; the CMR work-streams were recruited under UK National Research Ethics Service 07/H0715/101 (original ethics obtained by Dr Andrew Flett, which I amended for the RELIEF-AS Study), whereas the CT work-streams were recruited under UK National Research Ethics Service 09/H0716/75. Both conformed to the principles of the Helsinki Declaration, and all subjects gave written consent to participate in the study. The RELIEF-AS Study was registered on ClinicalTrials.gov (NCT02174471).

3.2 Patients

3.2.1 Aortic stenosis patients

Patients were recruited prior to pre-operative assessment, which included a comprehensive clinical assessment with clinical history, blood pressure, 6-minute-walk test [171], blood sampling (for haematocrit, renal function, NT-pro-BNP and hs-Tn T, electrocardiogram, transthoracic echocardiogram and CMR. Inclusion criteria were patients with severe AS (2 or more of: AVA<1cm^2, peak pressure gradient 64mmHg, mean pressure gradient 40mmHg, velocity ratio < 0.25; or reclassification of discordant echocardiographic data to severe by alternate modality) undergoing AVR+/-CABG at Heart Hospital, consenting for study protocol; age >18 years, ability to undergo CMR scan. Exclusion criteria were pregnancy/breastfeeding, GFR <30mls/minute (<45mls/min for CT), CMR incompatible devices, inability to complete the protocol, previous valve surgery, or severe valve disease other than AS.

3.2.2 *Amyloidosis Patients*

Patients with systemic amyloidosis were recruited during their visit to the National Amyloidosis Centre or to the CMR Department at the Heart Hospital. For ATTR, cardiac amyloidosis was defined by presence of ATTR amyloid in a myocardial biopsy (Congo red and immunohistochemical staining) or positive DPD scintigraphy [172]. Definite cardiac involvement by DPD was defined as DPD grade 2 or 3; possible cardiac involvement was defined as grade 1 (i.e. minimal cardiac DPD uptake) in the absence of LVH; in practice, none of these patients had LVH. All TTR

patients also underwent sequencing of exons 2, 3, and 4 of the TTR gene. For AL, systemic AL amyloidosis was proven with biopsies from non-cardiac tissues. Cardiac categorization was based on international consensus criteria [173] but with an additional "possible involvement" category, as previously described [174].

3.2.3 *Other cohorts*

For the technical development sections, other patient cohorts were utilized to cover a wider spectrum of aetiologies of left ventricular hypertrophy. These are further described in the specific sections.

3.3 Cardiovascular Magnetic Resonance Protocol

All patients also underwent CMR at 1.5 Tesla (Magnetom Avanto, Siemens Medical Solutions, Germany) with 32 channel cardiac coil arrays (Figure 20). All images were acquired during breath-hold at end expiration, apart from late gadolinium imaging which was performed during breath-hold or free-breathing.

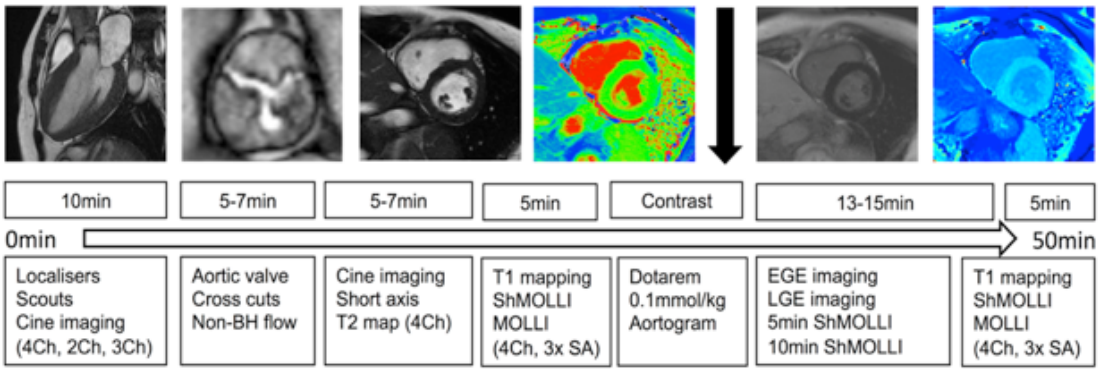

Figure 20: CMR protocol for RELIEF-AS

4/2/3Ch, 4/2/3 chamber long axis; EGE, early gadolinium enhancement; LGE, late gadolinium enhancement; LV, left ventricular.

3.3.1 Pilot images

All studies started with single shot pilot images with the following settings: repeat time (TR): 3.39ms, echo time (TE): 1.7ms, slice thickness, 5mm, field of view (FOV) 360 x 360mm, read matrix 256 and flip angle 60^{o}.

3.3.2 SSFP Cine Images

After piloting, steady state free precession (SSFP) cine imaging was undertaken, firstly in the long axis planes with a short axis cut through the aortic valve. A standard LV short axis stack was then acquired using a slice thickness of 7mm with a gap of 3mm. Retrospective ECG gating was used with 25 phases. Typical fast imaging with steady state precession (FISP) imaging parameters were TE: 1.6ms, TR: 3.2 ms, in plane pixel size 2.3 x 1.4mm, slice thickness 7mm, flip angle 60°. These settings were optimised in cases of arrhythmia or difficulties with breath-holding.

3.3.3 Flow quantification

Aortic flow for calculation of the regurgitant volume was measured (echocardiography was however the primary modality scrutinizing the valve severity) using cross sectional through-plane velocity encoded phase contrast (VENC) images obtained perpendicular to the aortic jet just above the aortic valve tips.

3.3.4 LGE imaging

Intravenous Gadoterate meglumine (gadolinium-DOTA, marketed as Dotarem® Guerbet, S.A., France) was then administered as a 0.1mmol/kg dose via a pressure injector at a rate of 3ml/sec, with a 25ml normal saline flush. LGE assessment was then undertaken using a FLASH IR sequence. Magnitude reconstruction was available in all patients (MAG-IR) phase sensitive inversion recovery sequences (PSIR) reconstructions in all but the first twenty patients. Slice thickness 8 mm, TR: 9.8 ms, TE: 4.6ms, α: 21o, FOV 340 x 220 mm (transverse plane), sampled matrix size 256 x 115-135, 21 k–space lines acquired every other RR interval (21 segments with linear reordered phase encoding), spatial resolution 1.3 x 2.1 x 8 mm, no parallel imaging, pre-saturation bands over CSF and any pleural effusions.

These parameters were optimised according to individual patient characteristics. The TI was manually set to achieve nulling of the myocardium between 300 and 440 ms. When LGE was observed, images were acquired in phase swap and cross cut to ensure artefact elimination. Where the LGE distribution appeared particularly diffuse, a TI scout was used to ascertain the specific parts of myocardium with the highest concentration of gadolinium. If the participant was struggling with the breath-

hold, FISP imaging or IR-SSFP imaging (single shot or segmented) was used as an alternative sequence.

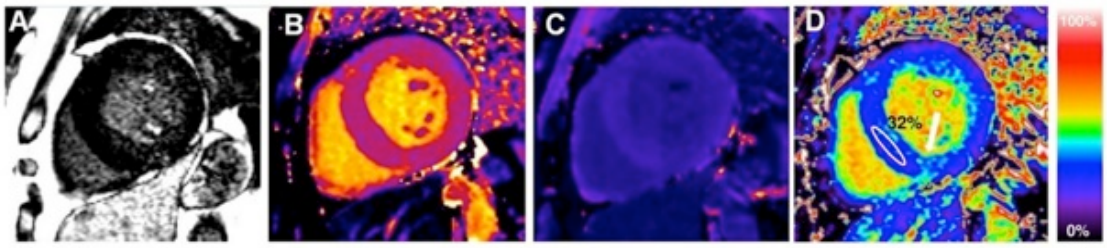

Figure 21: Non-invasive quantification of fibrosis in AS by CMR

A severe aortic stenosis patient with moderate concentric LVH and modest scar on LGE imaging (A). Pre-contrast (B) and post-contrast T1 maps (C) and derived ECV map (D) add information: RV insertion point native T1 elevation is seen (B) and there is diffuse extracellular expansion, with an ECV of 32%. Adapted from Maestrini et al 2013 [175].

3.3.5 T1 mapping

T1 mapping prior to and after bolus gadolinium contrast (0.1mmol/kg of Gadoterate meglumine [gadolinium-DOTA, marketed as Dotarem, Guerbet S.A., Paris, France]). Post contrast imaging was performed at 15 minutes. The T1 mapping sequences used were balanced-SSFP-based MOdified Look-Locker Inversion Recovery (MOLLI)[136] variants (investigational prototypes), both a Shortened MOdified Look-Locker Inversion recovery (ShMOLLI) sequence and a MOLLI variant with motion-correction (MOCO) were used [176, 177]. The same ShMOLLI sequence was used pre- and post-contrast, and has been described in detail in section 1.4.3.3. The MOLLI, we used separate pre- and post-contrast sequences, optimised for the differences in T1 range before and after contrast administration. The pre-contrast MOLLI was a 5s(3s)3s variant, indicating 2 inversions with acquisition of images for at least 5 seconds, followed by a recovery of at least 3 s, and a second inversion with images acquired for at least 3 s. The post-contrast MOLLI was a 4s(1s)3s(1s)2s variant, indicating 3 inversions with acquisition of images for at least 4 seconds, followed by a recovery of at least 1 second, a second inversion with images acquired for at least 3 s, followed by a recovery of at least 1 second, and a final acquisition of at least 2 seconds.

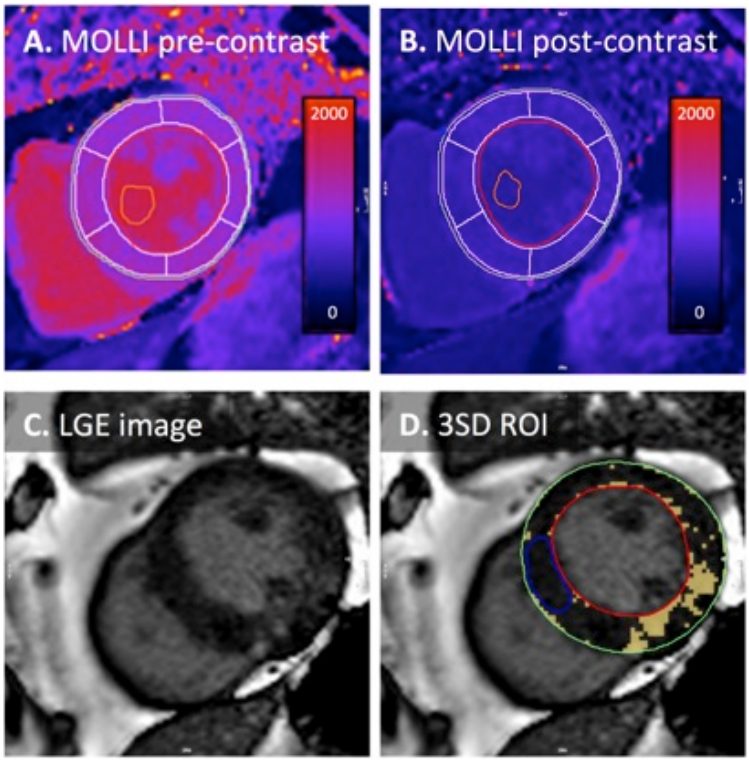

Figure 22: Analysis of T1 mapping and LGE images

Examples of pre-contrast (Panel A) and post-contrast (Panel B) T1 mapping analysis are shown. For the regions of interests (ROI), endocardial (red) and epicardial (green) borders as well as a blood pool ROI (orange) were manually drawn. Partial voluming of blood was minimized by setting an automatic offset of 10% from the endo- and epicardial border. A short axis late gadolinium enhancement images is shown in Panel C with exemplar ROIs drawn in Panel D. The blue ROI identifies the mean signal intensity of remote myocardium; pixels with a signal intensity >3 standard deviations were highlighted and measured.

3.3.6 Image analysis

Imaging analysis was performed using CVI42 software (Version 5.1.2[303], Calgary, Canada). All analysis was performed by operators blinded to clinical parameters. LV volume and mass analysis was performed by manual contouring of the endo- and epicardial borders at end-diastole and end-systole with papillary muscle and trabeculations included in the LV mass (40); wall and cavity dimensions were measured on mid-ventricular (”high basal”) short axis slices at end diastole. Left atrial area and length at end-systole were measured in the horizontal long axis (4-chamber) and vertical long axis (2-chamber) cine views for calculation of LA volumes by the biplane area length method and indexed (40). Aortic flow for aortic regurgitant fraction and mitral regurgitant fraction were calculated as previously described (41). Late gadolinium enhancement was quantified in grams (mls x 1.05 g/ml) and as a percentage of the LV using signal intensity threshold of 5, 3 and 2

standard deviations (SD)(42) above the mean remote myocardium. For T1 mapping, three short axis T1 maps (base, mid and apex) were manual contoured at the endo- and epicardial border, segmented into an AHA 16 segment model using the RV insertion points. Partial voluming of blood was minimized by setting an automatic offset of 10% from the endo- and epicardial border (see Figure 22). Segments with myocardial infarction (endocardial LGE) on LGE imaging were excluded.

ECV was then calculated from the global native and post contrast myocardial T1 values. ECV was defined as: ECV = (1-Hct) * [ΔR1myocardium] / [ΔR1bloodpool] (43). Total LV Matrix and cell volumes were calculated from the product of LV mass and ECV or (1 minus ECV), respectively.

3.4 Cardiac Computed Tomography

CT examinations were performed on a 64–detector row CT scanner (Somatom Sensation 64; Siemens Medical Solutions, Erlangen, Germany). A topogram was used to plan CT volumes from the level of the aortic valve to the inferior aspect of the heart, typically a 10cm slab. Cardiac scans (tube voltage, 120 kV; tube current–time product, 160 mAs; section collimation, 64 detector rows, 1.2-mm section thickness; gantry rotation time, 330 msec) were acquired with prospective gating (65%–75% of R-R interval), and reconstructed into 3-mm-thick axial sections with a B20f kernel.

CT image analysis was performed using a free and open-source Digital Imaging and Communications in Medicine viewer (OsiriX v4.1.2; Pixmeo, Bernex, Switzerland) independently by two experienced readers blinded to all other study data; this was repeated by the second reader to establish inter- and intra-observer agreement. Regions of interest (ROIs) were in axial sections in all acquisitions. For myocardium, polygonal ROIs were drawn an axial slice containing the greatest area of myocardial septum; for the blood pool, circular ROIs were drawn in the LV blood pool away from papillary muscles and the myocardial septum to avoid the endocardial edge and therefore partial voluming. Myocardial and blood attenuation values were used to calculate the ECV fraction following three steps: first, a CT scan to obtain baseline pre-contrast blood and myocardial attenuation in Hounsfield units (HU); second, contrast administration and delay so the contrast distributes into a blood:myocardial dynamic equilibration; third, a repeat scan to re-measure blood and myocardial

attenuation. The ratio of the change in blood and myocardial attenuation (ΔHU) represents the contrast agent partition coefficient. If the blood volume of distribution is substituted in (1 minus venous haematocrit; obtained prior to imaging), the myocardial extracellular volume, ECV_{CT}, is obtained, reflecting the myocardial interstitium:

$$ECV_{CT} = (1\text{-Haematocrit}) \times (\Delta HU_{tissue} / \Delta HU_{blood})$$

Signal-to-noise ratios (SNR) were measured in five myocardial ROIs per time point from the ratio of the average HU attenuation value to the standard deviation of the HU attenuation. Radiation exposure was quantified using the dose-length product multiplied by a chest conversion coefficient (κ=0.014mSv/mGy.cm)[178].

3.5 Echocardiography Protocol

Echocardiography was performed using a GE Vivid E9 system (GE Healthcare, Wauwatosa, USA) with a 4-MHz transducer, following the guidelines for AS assessment as recommended by the European and American Societies of Echocardiography [17, 30]. Doppler assessment of AS included measurement of peak and mean transvalvular velocities and gradients; aortic valve area by the continuity equation, indexed for body surface area; pressure recovery adjusted aortic valve area (i.e., energy loss index (ELI)); global hemodynamic load by the valvulo-arterial impedance index (Zva); stroke work loss; systemic vascular resistance and systemic arterial compliance.

3.6 Definition Of The Patterns Of Remodelling And Hypertrophy

AS patients were categorized into four pattern of LV geometric adaption by echocardiography and CMR: “normal geometry”, “concentric remodelling”, “concentric hypertrophy” and “eccentric hypertrophy”; no distinction was made between symmetrical or asymmetric pattern (Figure 5 and Figure 37). For echocardiography, categories were defined by BSA-indexed LV mass (LVMi), end-diastolic cavity dimension (EDD) and relative-wall thickness (RWT)[179]. For CMR, categories were defined by BSA-indexed LV mass (LVMi), indexed LV end-diastolic volume (LVEDVi) and mass-volume ratio (MVR) [25, 180]. Echocardiographic and CMR analysis were performed by separate operators, blinded to the other results.

3.7 Other investigations

3.7.1 Six minute walking test (6MWT)

6MWT was performed at the Heart Hospital (where the test was originally developed) along a flat corridor in accordance with current guidelines. Patients were asked to walk a 30-metre length of the corridor at their own pace while attempting to cover as much ground as possible in the 6-minute period.

3.7.2 Blood Test

All participants had blood tests taken prior to the CMR scan. This included a renal profile, full blood count, NT-proBNP, high senstitivity troponin T (hsTnT) and serum/plasma storage for collagen biomarkers. NT-proBNP and hsTnT were measured by ELISA (Roche Diagnostics). The inter-assay coefficients of variation were less than 7% for both of them. The lower limit of detection was 5 pg/mL for NT-proBNP and 3 ng/L for hsTnT. NT-pro-BNP ratio was calculated as the ratio between absolute NT-proBNP concentration divided by the upper limit of normal for patient's gender and age [181].

3.8 Statistical Analysis

Statistical analyses were carried out using SPSS 22 and 24 (IBM, Armonk, NY). All continuous variables are expressed as mean ± standard deviation. Categorical variables are expressed as percentages. Normality was checked using the Shapiro-Wilk test. Groups were compared using independent-samples t-test for normally distributed continuous variables, the Mann-Whitney U test for non-normally distributed variables, and the Chi-squared test for binomial variables. Correlations were estimated by using the Pearson correlation coefficient once normality was demonstrated; otherwise, the Spearman correlation coefficient was used. Log transformation was applied to normalize the distribution of NT-proBNP and hs-TnT. The influence of potential confounding factors (i.e. age, gender and history of coronary artery disease) was evaluated by multivariate linear regression analysis. The unstandardized coefficient B and its 95% confidence interval were recorded. A two-sided p-value of <0.05 was considered significant.

Agreement between conventional and synthetic ECV was analysed using the Bland-Altman method. The significance of the difference between two correlation coefficients was tested using the Fisher r-to-z transformation.

Survival was evaluated using Cox proportional hazards regression analysis, providing estimated hazard ratios (HR) with 95% confidence intervals (CI) and Kaplan Meier curves.

In the synthetic ECV section, survival analyses examined: time to the first HHF after CMR, time to death, and time to either HHF or death. First HHF included any HHF event after CMR, and required physician documentation of: 1) symptoms and physical signs consistent with HF; 2) supporting clinical findings; or 3) therapy for HF. Vital status was ascertained by Social Security Death Index queries and medical record review (confirmed by two blinded investigators). Mortality was right censored for the first HHF after CMR analysis. The log-rank test with ECV (categorized arbitrarily in 5% increments) and Cox regression (ECV expressed as a continuous variable) examined associations between ECV and outcomes.

Chapter 4 Technical Development

4.1 Synthetic ECV by CMR

4.1.1 Preface

This chapter is based on the publication below:

Treibel TA, *Fontana M, Maestrini V, Castelletti S, Rosmini S Simpson J, Nasis A, Bulluck H, Abdel-Gadir A, White SK, Manisty C, Spottiswoode BS, Robson MD, Wong TC, Piechnik SK, Kellman P, Schelbert EB, Moon JC. Automatic Measurement Of The Myocardial Interstitium: Synthetic Extracellular Volume Quantification without Haematocrit Sampling. JACC: Cardiovascular Imaging. 2016 Jan;9(1):54-63.*

My contribution was recruiting, consenting and performing the scans of all the AS patients. I analysed all the data as first operator, did the statistical analysis and wrote the paper. In order to derive and validate this new methodology, this work draws upon my own data and data collected by several other researchers. Contributors (by disease) include: Normal subjects – Stefania Rosmini; AS – Myself; Amyloidosis – Marianna Fontana; Anthracycline toxicity patients – Viviana Maestrini; Hypertrophic Cardiomyopathy – Silvia Castelletti; Histology cohort - Steven White; Outcome cohort – Erik Schelbert.

4.1.2 Introduction

ECV measurement is useful in CMR as it provides insights into health and disease, measuring the interstitial and cell volume (see Introduction). The method relies on the administration of an extracellular contrast agent. After sufficient time, the ratio of signal change with the contrast agent between blood and myocardium is the partition coefficient. If this is multiplied by the blood volume of distributions (1-haematocrit), the myocardial ECV is derived. Practically however, this is cumbersome. It involves blood sampling and delay. Uncertain errors are introduced (eg by the blood settling during transit to the lab), and the ECV is not easy to visualise – there is no immediacy of the results [136, 137, 143].

We knew however that the longitudinal relaxivity (R1=1/T1) of blood has been studied since the 1980s and was found to be in a linear relationship with blood Hct. It is determined by the water fractions of plasma and the erythrocyte cytoplasm,

which undergo fast water exchange [182-189]. This means that native blood T1 increases with anaemia.

4.1.3 Hypothesis and aims

We hypothesize that native T1 blood could estimate *synthetic* Hct, permitting immediate *synthetic* ECV calculation and an instantaneous synthetic ECV map without blood sampling. We formed a network of collaboration with existing key patient cohorts to investigate if *synthetic* ECV (a) was valid compared to conventional ECV, (b) correlated with the gold standard collagen volume fraction, (c) predicted outcome, and (d) could be automated for in-line point-of-care use.

4.1.4 Methods

Patient Populations

Research was carried out at two centres (Table 5): University College London Hospital NHS Trust, UK (proof-of-concept and histology cohorts); and UPMC CMR Center, Pittsburgh, USA (outcome cohort). Study approval was granted by local ethics committees. The study conformed to the principles of the Helsinki Declaration. ECV data of two previously published cohorts was used to validate the synthetic ECV methodology (histology and outcome cohorts).

	Subjects	***Location***	***Characteristics***
Proof-of-concept	n=427	London, UK	Health and Disease, split into derivation and validation cohorts.
Histology	n=18	London, UK	Severe aortic stenosis patients undergoing aortic valve replacement (with intraoperative myocardial biopsy)
Outcome	n=1172	Pittsburgh, USA	Clinical cohort referred for CMR

Table 5: Overview of synthetic ECV study cohorts

Proof-of-concept of synthetic ECV – cohorts 1 (derivation) and 2 (validation).

A total of n = 427 subjects gave written informed consent and were scanned between January 2012 and October 2014. They were then randomly split into derivation and validation sub-groups (Table 6) with equal health and disease representation.

- Normal healthy subjects (n = 66, median age 45±14 [range 24 to 74 years], 59% male), with no history or symptoms of cardiovascular disease or diabetes. All had normal blood pressure (defined as <140/90 mmHg), 12-lead electrocardiogram and clinical CMR results.
- Hypertrophic cardiomyopathy (HCM) patients (n = 68, median age 52±14 [range 23 to 77 years], 81% male). All met previously described diagnostic criteria [190]. Hypertrophy was 81% asymmetrical, 9% concentric and 10% apical predominant.
- Severe aortic stenosis (AS) patients (n = 123, median age 70±10 [range 34 to 84 years], 55% male). All had undergone clinical evaluation and echocardiography for diagnosis of severe AS and were listed for surgical valve replacement.
- Cardiac amyloidosis patients (n = 74, median age 72±11 [range 38 to 85 years], 82% male). Cardiac amyloid was only ATTR amyloid. This was defined by either a myocardial biopsy, or positive bone scintigraphy. Patients underwent sequencing of exons 2, 3, and 4 of the *TTR* gene. Consensus criteria for definite cardiac involvement are pending but not published: definite cardiac ATTR amyloid was defined as previously described [172, 191].
- Patients post-anthracycline chemotherapy for histologically proven breast carcinoma at a median follow-up of 6.4 years (n = 96, median age 54 [range 28 to 71 years], 100% female, 100% Caucasian), with no previous chemo- or radiotherapy or any pre-existing cardiovascular disease or drug history.

Histological validation of synthetic ECV – Histology cohort

Consenting (same centre) severe AS patients (n = 18, median age 71±10 years [range 47 to 84 years], 78% male) were scanned between May 2011 and February 2012. All had undergone clinical evaluation and echocardiography for diagnosis prior to surgical aortic valve replacement, and intra-operative biopsies were obtained for histological measurement of collagen volume fraction (CVF) as previously described [110].

	Derivation	Validation	*p-value*
Total	214	213	
Male	107	104	*0.8*
Age (years)	60±15	60±15	*0.6*
BSA (m^2)	1.87±0.23	1.87±0.23	*0.8*
Healthy Volunteer	33	33	
Aortic Stenosis	62	61	
Cardiac Amyloidosis	37	37	
Hypertrophic Cardiomyopathy	34	34	
Anthracycline	48	48	
Cardiac			
EDVi (ml/m^2)	71±21	70±20	*0.9*
ESVi (ml/m^2)	25±14	24±13	*0.5*
LV mass index (g/m^2)	90±35	92±35	*0.5*
Stroke Volume index (ml/m^2)	47±12	47±13	*0.7*
LVEF (%)	66±12	67±12	*0.7*
LAAi (cm^2/m^2)	14±3	14±5	*0.5*
Clinical			
Haematocrit	0.40±0.04	0.40±0.04	*0.4*
Creatinine	79±24	78±21	*0.9*
eGFR	80±23	78±22	*0.4*
SBP (mmHg)	110±44	108±49	*0.7*
DBP (mmHg)	65±28	62±31	*0.5*
T1 Mapping			
ShMOLLI ECV (%)	33±10	33±11	*0.9*
MOLLI ECV (%)	33±11	33±11	*0.8*

Table 6: Patient Characteristics for Derivation / Validation of Synthetic Hct

Values are mean ± SD or %. BSA = body surface area; ECV = extracellular volume fraction; EDVi = indexed end-diastolic volume; ESVi = indexed end-systolic volume; eGFR = estimated glomerular filtration rate; DBP = diastolic blood pressure; LAAi = indexed left atrial area; LVEF = left ventricular ejection fraction; MOLLI = MOdified Look-Locker Inversion recovery; ShMOLLI = Shortened MOdified Look-Locker Inversion recovery; SBP = systolic blood pressure.

Correlation of synthetic ECV with Outcome – Outcome cohort

For external validation of synthetic ECV and comparison with outcome data, we applied the method to a large ECV outcome cohort [192]: 1765 consecutive adult patients referred for clinical CMR at UPMC CMR Center, Pittsburgh, USA (enrolled December 2009 to May 2013; follow-up until July 2013). Inclusion criteria were

written informed consent and completion of contrast CMR. Exclusion criteria were cardiac amyloidosis (n=27), HCM (n=133), stress-induced cardiomyopathy (n=10), adult congenital heart disease (n=195), inadequate image quality (n=4), and missing follow-up (n=224). Patients with myocardial infarction were included to maximize generalizability (ECV measured in remote non-infarcted myocardium). The final cohort included 1172 patients.

Automated inline ECV – synthetic ECV maps "on-the-fly".

An investigational prototype ECV tool, previously developed by Kellman et al [147, 193], was adapted to measure $T1_{blood}$, calculate synthetic Hct and generate inline synthetic ECV maps as a DICOM images on the CMR scanner; fully automated using co-registration and blood pool segmentation.

CMR scanning

All subjects underwent CMR at 1.5 Tesla (Magnetom Avanto, Espree and Aera, Siemens Medical Solutions) with 32 channel cardiac coil arrays. Exclusion criteria were uncontrolled arrhythmia, impaired renal function (estimated glomerular filtration rate <30mL/min), or contraindications to MR imaging (e.g. implanted devices). Specific details are listed in the individual cohort descriptions. All patients underwent standard clinical scan with late gadolinium imaging [194] with T1 mapping prior to and after bolus gadolinium contrast: for the proof-of-concept and histology cohorts, 0.1mmol/kg of Gadoterate meglumine, (gadolinium-DOTA, marketed as Dotarem, Guerbet S.A., Paris, France); for the outcome cohort, 0.2 mmol/kg intravenous gadoteridol bolus (Prohance, Bracco Diagnostics, Princeton, NJ). Post contrast imaging was performed at 15-20 minutes apart from amyloid patients, where we acquired equilibrium-contrast T1 maps [110, 195]. The T1 mapping sequences used were MOLLI [136] variants (investigational prototypes): in the proof-of-concept cohort, both a ShMOLLI sequence and a MOLLI variant with motion-correction (MOCO) were used [176, 177]. The histological validation was performed with ShMOLLI, whereas the outcome cohort was performed with a MOLLI with MOCO.

T1 analysis and ECV quantification

A region of interest (ROI) was drawn in myocardium (septum on SA slice) and blood (same slice) on the pre-contrast images and transposed to the post-contrast

images. All analysis was performed blinded. We quantified ECM expansion with ECV defined as:

ECV = (1-haematocrit) * [$\Delta R1_{myocardium}$] / [$\Delta R1_{bloodpool}$]

(where, $\Delta R1_{myocardium} = R1_{myocardium}^{post-contrast} - R1_{myocardium}^{pre-contrast}$, $\Delta R1_{blood} = R1_{blood}^{post-contrast} - R1_{blood}^{pre-contrast}$, and R1=1/T1) [196].

Laboratory haematocrit variability

Whole blood for venous Hct was drawn in all subjects by venepuncture and analysed as routine clinical samples using a Sysmex XE2100 haematology analyser [197]. Repeat sampling variability was tested in 44 patients who underwent two samples a median of 4 hours apart.

Synthetic haematocrit derivation

The longitudinal relaxivity (R1=1/T1) of blood has a linear relationship with blood Hct, and is determined by the relaxivity of the water fractions of plasma ($R1_P$) and the erythrocyte cytoplasm ($R1_{RBC}$): $R1_{Blood} = R1_P * (1 - Hct) + R1_{RBC} * Hct$

Rearranging gives: $Hct = - R1_P / (R1_{RBC} - R1_P) + R1_{Blood} * (1 / (R1_{RBC} - R1_P))$

Simplified as: $Hct = Constant\#1 + (Constant\#2 * R1_{blood})$

Therefore, synthetic Hct was derived from the linear relationship between Hct and $R1_{blood}$, in turn used to estimate a synthetic ECV and was then compared to the conventional ECV.

Histological analysis of collagen volume fraction

Histological quantification of the extracellular space was performed by measuring the collagen volume fraction (CVF) as previously described.[110] In summary, an intra-operative deep myocardial biopsy (Tru-Cut type biopsy) was taken from the basal LV septum, stained with picrosirius red, photographed at high-power magnification (200µm) and CVF (%) automatically quantified over an average of 12 high-power fields with a purpose-written macro in ImageJ. All samples were analysed blinded to other findings.

Statistical analysis

Analyses were performed using SAS (Cary, NC) and SPSS (Chicago, IL, USA, version 22). Details have been previously described.

4.1.5 RESULTS

Proof-of-Concept – Derivation and Validation cohorts

The proof-of-concept cohort was divided randomly into a derivation (n=214) and a validation (n=213) cohort (Table 6). In the derivation cohort, there was a broad range of Hct (40.3±3.7%; range 32-51%) and native $T1_{blood}$ (ShMOLLI $T1_{blood}$ 1549±80ms; range 1261-1823ms; MOLLI $T1_{blood}$ 1649±83ms; range 1441-1898ms). The regression line between haematocrit and $R1_{blood}$ ($1/T1_{blood}$) was linear with R^2=0.51, *p<0.001*; and 0.45, *p<0.001*; for MOLLI and ShMOLLI, respectively (Figure 23). The regression equations were:

Synthetic Hct_{MOLLI} = (866.0 * $[1/T1_{blood}]$) – 0.1232

Synthetic $Hct_{ShMOLLI}$ = (727.1 * $[1/T1_{blood}]$) – 0.0675

where Hct is haematocrit (0 to 1) and $R1_{blood}$ = $[1/T1_{blood}]$ in milliseconds

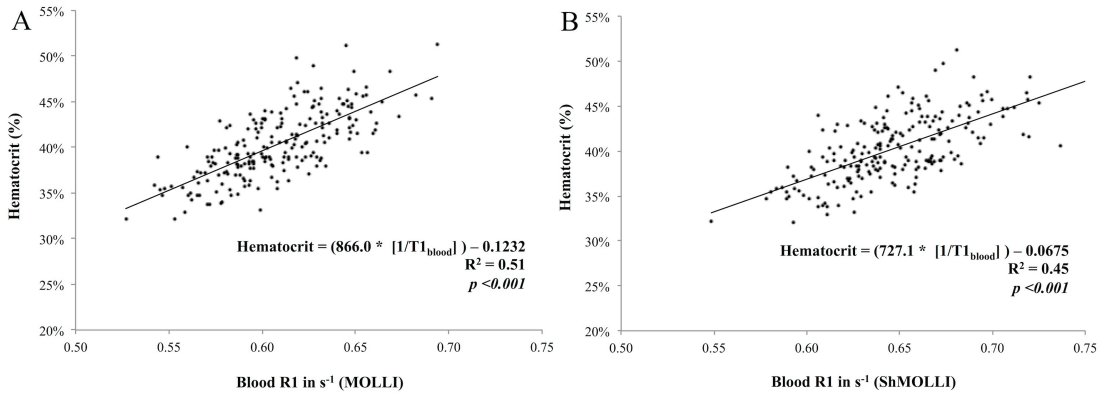

Figure 23: Derivation cohort - Correlation $R1_{blood}$ versus Haematocrit

The proof-of-concept cohort was divided randomly into a derivation (n=214) and a validation (n=213) cohort. The regression line between haematocrit and pre-contrast $R1_{blood}$ was linear with R^2=0.51, p<0.001, and R^2=0.45, p<0.001, for MOLLI (A) and ShMOLLI (B) with regression equations as given in the graphs.

Using these curve-fits in the validation cohort, *synthetic* and conventional ECV were highly correlated (R^2=0.97; *p<0.001,* both mapping techniques) with a 2.8% SD of differences and minimal bias on Bland-Altman analysis for fibrosis quantification and a slightly higher SD in difference of 5% in extracellular expansion due to amyloidosis (Figure 23). Synthetic and conventional ECV correlated equally with clinical markers of disease severity (Table 7).

ECV Method	**Conventional**	***Synthetic***	**Conventional**	***Synthetic***
Sequence	**ShMOLLI**		**MOLLI**	
NT-pro-BNP	0.6	0.6	0.62	0.63
Systolic blood pressure	-0.64	-0.64	-0.62	-0.63
LV ejection fraction	-0.57	-0.61	-0.56	-0.6
Stroke volume indexed	-0.36	-0.38	-0.31	-0.34
Left atrial area indexed	0.39	0.41	0.44	0.44
LV mass index	0.49	0.49	0.52	0.52

Table 7: Synthetic and Conventional ECV versus Clinical Parameters

Correlation coefficient R, all values significant with a p-value <0.001; ShMOLLI = Shortened MOdified Look-Locker Inversion recovery; MOLLI = Modified Look-Locker Inversion recovery.

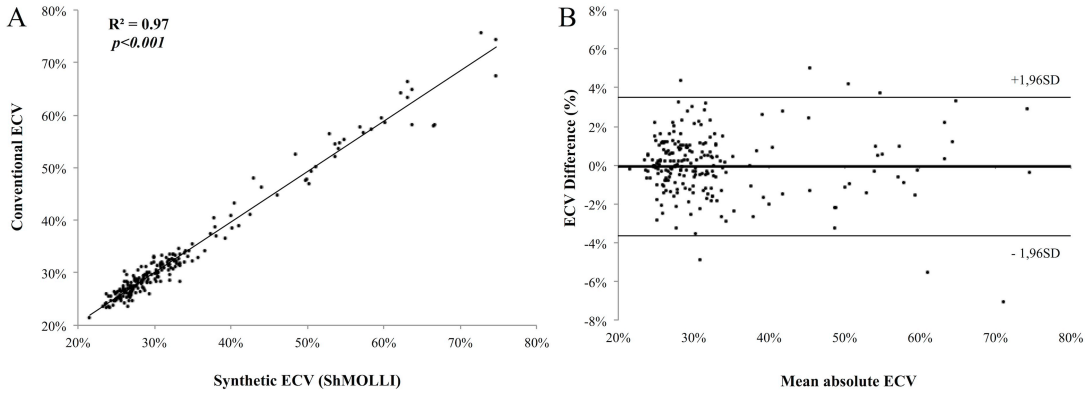

Figure 24: Validation Cohort – conventional versus synthetic ECV.

Using these curve-fits in the validation cohort, synthetic and conventional ECV were highly correlated (R^2=0.97; p<0.001, both mapping techniques) with a 2.8% SD of differences and minimal bias on Bland-Altman analysis for fibrosis quantification and a slightly higher SD in difference of 5% in extracellular expansion due to amyloidosis.

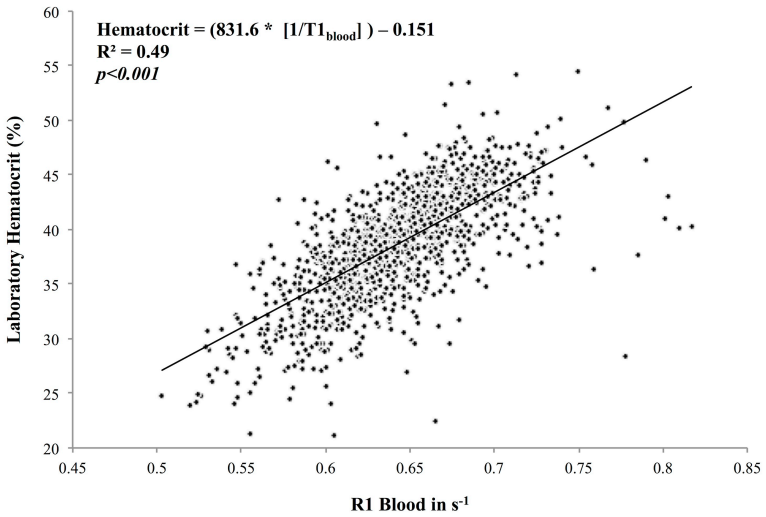

Figure 25: Outcome cohort

Measured vs synthetic Hct correlation and Bland-Altman comparison.

Test-retest variability

Bland-Altman comparison of laboratory Hct vs *synthetic* Hct in the validation cohort revealed a variability of 14%, R^2=0.44. To understand the sources of variability attributable to laboratory Hct and synthetic Hct (i.e. $T1_{blood}$), test-retest was performed. Test:retest variability of laboratory haematocrit was higher than expected (n=44, variability 10% with hct:hct R^2=0.86; Figure 26), where test-retest for $T1_{blood}$ (and by inference *synthetic* Hct) in healthy volunteers was low for MOLLI (n=20, variability 0.02%, R^2=0.95) and ShMOLLI (n=20, variability 0.012%, R^2=0.94). Inter-observer reproducibility for $T1_{blood}$ was also excellent (ICC 0.994, 95% CI 0.984-0.998).

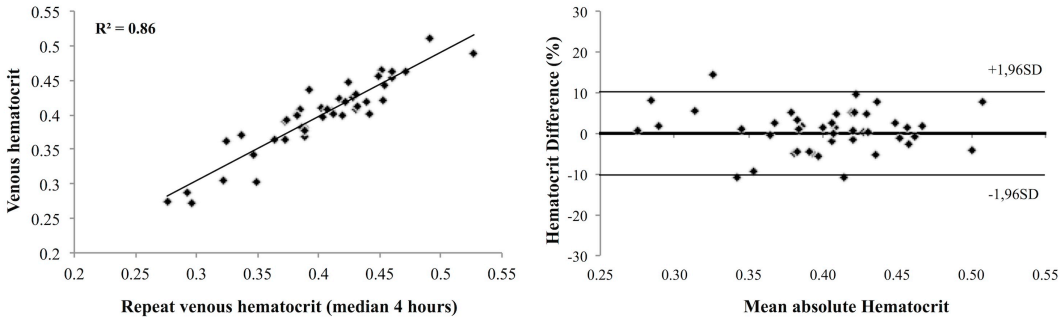

Figure 26: Variability In Repeated Haematocrit Samples.

Repeat sampling variability was tested in 44 patients who underwent two samples a median of 4 hours apart. Test:retest variability of haematocrit was higher than expected (n=44, variability 10% with hct:hct R^2=0.86, p<0.001).

Histology Cohort

The mean histological CVF of the 18 biopsies was 17 ± 8% (range 5% to 40%). *Synthetic* and conventional ECV both correlated well with collagen volume fraction (R^2 = 0.61, *p < 0.001* vs. R^2 = 0.69, *p < 0.001*; Figure 27) and did not differ statistically (*p=0.70*).

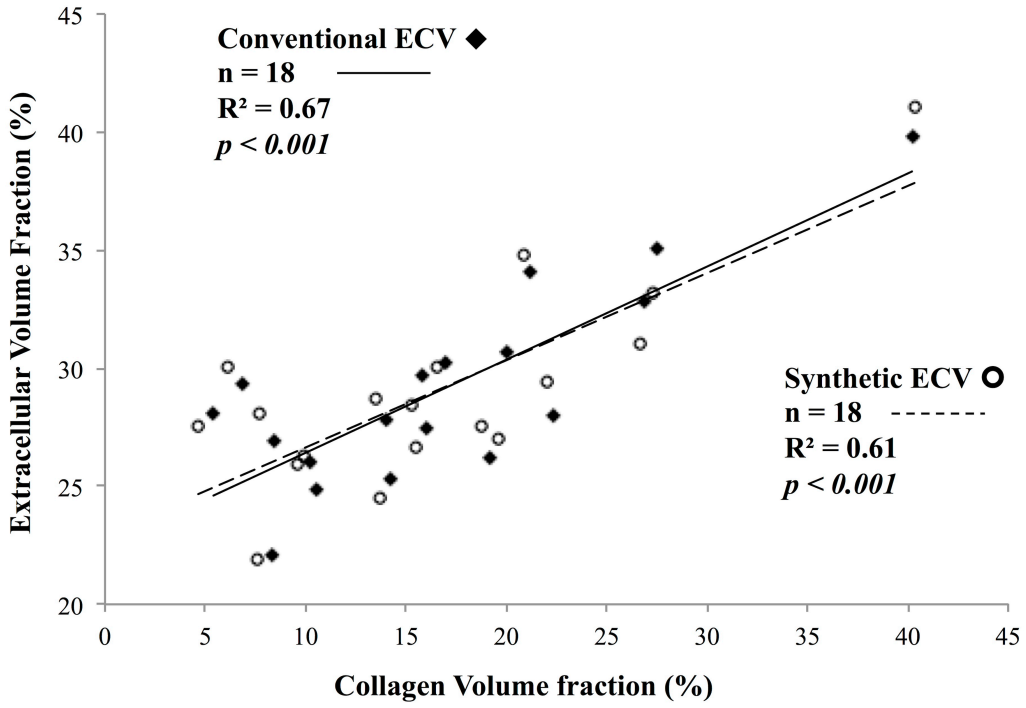

Figure 27: Histology Cohort.

Conventional ECV and synthetic ECV versus CVF. The mean histological collagen volume fraction (CVF) of the 18 biopsies was 17 ± 8% (range 5% to 40%). The correlation with histology for synthetic extracellular volume fraction (ECV) was slightly lower than the conventional ECV (R^2 = 0.61, p < 0.0.01 vs. R^2 = 0.69, p < 0.001) and did not differ statistically (p=0.70).

Outcome Cohort

Baseline characteristics are presented in Table 8. The UK derivation resulted in a 2% bias in synthetic ECV, therefore a local synthetic Hct calibration was obtained. In the outcome cohort, conventional and synthetic ECV had similar ranges (16.6-47.8% and 16.2-50.9%, respectively) with excellent correlation (R2 = 0.82, p<0.001) and no significant bias.

Demographics	**n = 1172**	
Age, median (Q1-Q3), y	56	*(43-66)*
Female, No. (%)	484	*48%*
White race, No. (%)	1033	*88%*
Black race, No. (%)	112	*10%*
Comorbidity		
Diabetes, No. (%)	239	*20%*
Hypertension, No. (%)	585	*50%*
Dyslipidemia, No. (%)	448	*38%*
Atrial fibrillation or flutter, No. (%)	121	*10%*
Prior coronary revascularization, No. (%)	217	*19%*
Body mass index, median (Q1-Q3), kg/m^2	28	*(25-33)*
Laboratory and CMR characteristics		
Creatinine, median (Q1-Q3), mg/dL	0.9	*(0.8-1.1)*
Glomerular filtration rate, median (Q1-Q3), $mL/min/1.73m^2$	89	*(70-94)*
Ejection fraction, median (Q1-Q3), %	57	*(45-64)*
Left ventricular mass index, median (Q1-Q3), g/m^2	57	*(46-71)*
End diastolic volume index, median (Q1-Q3), mL/m^2	82	*(67-101)*
End systolic volume index, median (Q1-Q3), mL/m^2	34	*(25-51)*
Myocardial infarction, No. (%)	238	*20%*
Non-ischemic fibrosis evident on LGE images, No. (%)	236	*20%*
Extracellular volume fraction, median (Q1-Q3), %	28	*(26-31)*

Table 8: Baseline characteristics of Outcome cohort

Over a median of 1.7 years (Q1-Q3, 1.0-2.4 years), there were 55 HHF events and 74 deaths after the baseline CMR scan among 111 individuals experiencing adverse events in the n=1172 cohort (18 individuals experiencing HHF subsequently died). *Synthetic* and conventional ECV were associated with adverse events with a graded response, where higher ECV was associated with higher event rates (Figure 27). Conventional and *synthetic* ECV were comparable to EF in their univariable association with HHF but ECV (conventional and *synthetic*) was better than EF for mortality (Table 9). A post-hoc samples size calculation (based on n=1172 and 111 events) showed 80% power to detect a HR of 1.346 by increasing one SD of a covariate (based on a Cox proportional hazards regression and a type I error rate of 0.05).

Outcome	Univariable Cox regression model covariate	Hazard ratio (CI 95%)	x2	*p-value*
HHF (n=55)	Conventional ECV (5% increase)	**2.41** (1.93-3.02)	59.6	*<0.001*
	Synthetic ECV (5% increase)	**2.30** (1.87-2.81)	64.5	*<0.001*
	LVEF (5% decrease)	**1.33** (1.23-1.43)	54.3	*<0.001*
Death (n=74)	Conventional ECV (5% increase)	**2.13** (1.74-2.61)	53.4	*<0.001*
	Synthetic ECV (5% increase)	**1.90** (1.55-2.31)	39.8	*<0.001*
	LVEF (5% decrease)	**1.21** (1.16-1.29)	32	*<0.001*
HHF or Death (n=111)	Conventional ECV (5% increase)	**2.25** (1.91-2.64)	96	*<0.001*
	Synthetic ECV (5% increase)	**2.06** (1.77-2.40)	89.2	*<0.001*
	LVEF (5% decrease)	**1.26** (1.19-1.33)	71.7	*<0.001*

Table 9: Outcome variables

Conventional and synthetic ECV and LVEF were comparable in their univariable association with (HHF), mortality or combined. ECV = extracellular volume fraction; HHF = hospitalization for heart failure; LVEF = left ventricular ejection fraction.

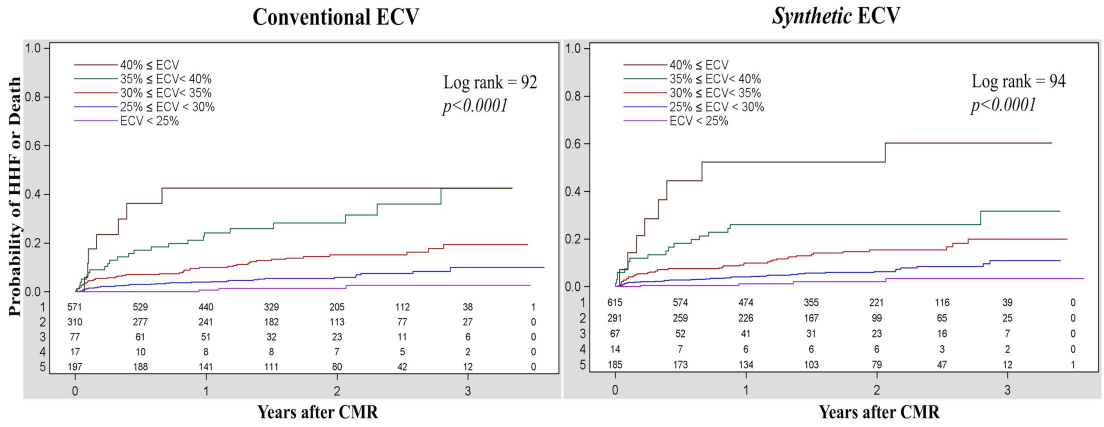

Figure 28: Outcome Cohort – Kaplan-Meier Plot (Death And HHF) for ECV.

Among 1172 individuals, both conventional and synthetic myocardial extracellular volume fraction (ECV) were significantly associated with increased risks of hospitalization for heart failure (HHF) or death (n=111) following CMR scanning.

Outcome	Cox regression model covariate ECV (5% increase)	Hazard ratio (CI 95%)	χ^2	*p-value*
HHF (n=55)	Conventional – univariable	**2.41** (1.93-3.02)	59.6	*<0.001*
	Synthetic – univariable	**2.30** (1.87-2.81)	64.5	*<0.001*
	Conventional – multivariable model	**1.77** (1.32-2.36)	14.9	*<0.001*
	Synthetic – multivariable model	**1.74** (1.32-2.30)	15.2	*<0.001*
Death (n=74)	Conventional – univariable	**2.13** (1.74-2.61)	53.4	*<0.001*
	Synthetic – univariable	**1.90** (1.55-2.31)	39.8	*<0.001*
	Conventional – multivariable model	**1.87** (1.45-2.40)	23.9	*<0.001*
	Synthetic – multivariable model	**1.70** (1.34-2.16)	18.9	*<0.001*
HHF or Death (n=111)	Conventional – univariable	**2.25** (1.91-2.64)	96	*<0.001*
	Synthetic – univariable	**2.06** (1.77-2.40)	89.2	*<0.001*
	Conventional – multivariable model	**1.85** (1.50-2.27)	33.9	*<0.001*
	Synthetic – multivariable model	**1.69** (1.38-2.75)	24.9	*<0.001*

Table 10: Multivariable Cox Regression models.

In multivariable modelling, conventional and synthetic ECV remained associated with HHF, death, or the combined endpoint of HHF/death. Hazard ratios and Chi-Square ($\chi 2$) for conventional and synthetic ECV are shown unadjusted (univariable) and in a multivariable model. The multivariable model stratified by heart failure stage and hospitalization status, and adjusted for LVEF, age, glomerular filtration rate, myocardial infarction size, and gender. ECV = extracellular volume fraction; HHF = hospitalization for heart failure; LVEF = left ventricular ejection fraction.

Automated inline *synthetic* ECV cohort – real-world application

A module was created to generate automatic *synthetic* ECV maps inline ("on-the-fly") as post-contrast T1 maps are acquired (Figure 29; online video [http://jaccimage.acc.org/video/2016/1001_VID1.mp4]). The additional processing time is less than 1 second per slice for finding paired pre-contrast T1 mapping data, performing image co-registration, and generating the blood mask and *synthetic* ECV map. The user is able to analyse images immediately by drawing regions of interest on the scanner console, where pixel values represent percentage ECV.

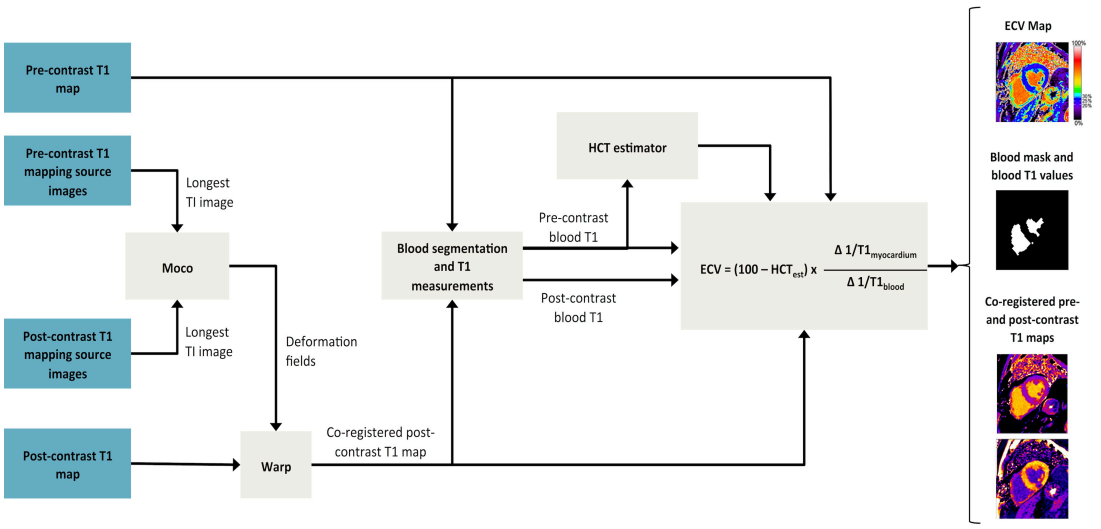

Figure 29: Automatic synthetic ECV tool

ECV mapping "on-the-fly". An automated inline synthetic ECV tool was implemented as an investigational prototype to produce a fast and fully automated approach for generating pixel-wise synthetic ECV maps.

4.1.6 Discussion

CMR extracellular volume quantification is a promising imaging biomarker [198-200], but development and clinical uptake have been slowed by the necessity of venous blood sampling, analysis and then offline calculation. I created a team who implemented a simpler, *synthetic* ECV measured using haematocrit estimated from pre-contrast blood T1. *Synthetic* ECV performed well – it is highly correlated to conventional ECV, and has a similar relationship to the histologic gold standard collagen volume fraction, other cardiac parameters and predicts outcome similarly – even at a different centre. The implementation here as an inline tool on a clinical CMR scanner would be an aid to clinical workflow, providing automated immediate point-of-care results.

The technique arose out of need and the observation that pre-contrast blood T1 is considerably determined by haematocrit (pre-contrast blood T1 increases with anaemia). Indeed, the linear relationship between Hct and $R1_{blood}$ ($1/T1_{blood}$) has been abundantly been described [182-187, 189, 201], and therefore $R1_{blood}$ was used for curve fitting. Beyond mathematical derivation, we describe $1/T1_{blood}$ as it is more intuitive for the CMR clinicians and easier to sell to the CMR community. This is analogous to the T2* field that uses T2* rather than the R2*. Although the correlation of peripheral haematocrit and ventricular cavity pre-contrast $R1_{blood}$ is

only moderate (other influences are discussed below), *synthetic* ECV performance is good, which we believe is in part due to considerable error in standard laboratory haematocrit when taken as a routine clinical test, and also as the ECV has other dependencies which make it robust [132-134, 202, 203]. It may be that an overlooked weakness has been the variability of Hct measurement [204]. Here the correlation of two Hct samples on the same day to a clinical service (located in a different building so with potential settling and re-suspension of red cells during transport) was only a R^2 of 0.86 – potentially a greater source of inaccuracy than the differences contested between T1 mapping approaches [139, 176].

ECV is gaining recognition as a potentially key biomarker of ECM expansion and has been called “non-invasive” or “virtual biopsy” [205]. The near exponential increase of evidence for the role of T1 mapping and ECV quantification for myocardial tissue characterization calls for the routine clinical use beyond late gadolinium enhancement [*HCMR Study; NCT01915615].* Separate analysis of pre- and post-contrast images is cumbersome. Although implementation of automated ECV map tools is simplifying this [206], haematocrit measure is burdensome in busy departments, is a source of user error and introduces reporting delay. An inline *synthetic* ECV tool would reduce the barriers to clinical use of ECV and potentially increase quality as review is immediate.

The study has limitations: Although this study was not a multicentre study, following validation and derivation in a single centre, we then tested outcome in a separate centre. The T1 mapping methods varied across parts of experiments (in line with rapid developments within the T1 mapping field) and further comparisons are required. As for any other non-contrast mapping parameter, *synthetic* haematocrit requires local calibration, unless T1 mapping sequence, CMR scanner and Hct machine are identical. Other sources that affect the relaxation rate of blood like flow, oxygen content, body temperature and contributions from other biological variables need further investigation (e.g. red cell shape and size, other macromolecules, and even added substances e.g. intravenous iron or other paramagnetic substances)[182, 183, 186, 187, 207-209]. In iron overload, particular in thalassemia patients, the R1:Hct relationship breaks down (unpublished data), which may to be due to iron-chelator complexes. Finally, there are additional influences on measured $T1_{blood}$ (e.g. residual heart rate dependence with some sequences, where measured $T1_{blood}$ decreases with increasing HR). The range of diseases studied was not

exhaustive and extreme patients (e.g. very anaemic) are not well represented. Variability of repeat *synthetic* ECV was not tested due to the requirement to give gadolinium contrast to assess this, but variability of $T1_{blood}$ and thereby *synthetic* Hct was low across repeated scans, making it a suitable tool for clinical trials [210]. The *synthetic* ECV approach highlights Hct measurement issues that may be easily solved without resorting to new approaches, improving the conventional ECV method.

4.1.7 Conclusion

The CMR biomarker ECV is promising as a measure of the myocardial interstitial space and can be simplified and automated by using a *synthetic* haematocrit. *Synthetic* ECV is validated in health and disease, against histology, across centres and predicts outcome as well as the conventional ECV. Automated synthetic ECV measures can be implemented inline on the CMR scanner with test performances approaching that of conventional ECV measurement – a significant workflow improvement bringing ECV closer to routine clinical practice.

4.2 Dynamic Equilibrium Cardiac CT

4.2.1 **Preface:**

This chapter is based on the publication below:

***Treibel TA**, Bandula S, Fontana M, White SK, Gilbertson JA, Gillmore JD, Punwani S, Hawkins PN, Taylor SA, Moon JC. Quantification and diagnosis of cardiac amyloid by cardiac computed tomography: Clinical Development And Application Of Extracellular Volume Quantification By Dynamic Equilibrium Computed Tomography (DynEQ-CT). J Cardiovasc Comput Tomogr. 2015 Jul 10.*

My contribution was recruiting, consenting and performing the scans. I have analysed all the data as first operator, did the statistical analysis and wrote the paper. Development of the pseudo-equilibrium technique and collection of the data in AS and amyloid was performed equally by myself and Dr Steven Bandula.

4.2.2 Introduction

Extracellular volume fraction (ECV) quantified by Equilibrium Contrast CMR (EQ-CMR) tracks amyloid burden[211]. Equilibrium Computed Tomography can also quantify the ECV from pre and post contrast measurements of attenuation, and shows good correlation with ECV measured by EQ-CMR as well as histological measures of myocardial fibrosis [168-170]. CT has advantages over CMR: ubiquitously available equipment, higher spatial resolution and a simple linear relationship between attenuation (Hounsfield units) and iodine concentration as opposed to the nonlinear effect on relaxivity of hydrogen following administration of gadolinium.

4.2.3 Aims and Objectives

This study was designed to simplify the progenitor equilibrium methods by using a bolus-only, dynamic equilibrium approach (DynEQ-CT). Our objective was to evaluate optimal post bolus contrast timing for DynEQ-CT.

4.2.4 Methods

All research was carried out at University College London Hospital and the Royal Free NHS Trusts, London, UK, between January 2013 and December 2013. The

study was approved by the ethical committee of U.K. National Research Ethics Service (REC reference 09/H0716/75) and conformed to the principles of the Helsinki Declaration.

Amyloid patients. 26 patients with systemic amyloidosis were recruited. Eighteen patients had ATTR amyloidosis (16 male, age 68±8 years), and eight patients (5 male, age 56±12 years) had systemic AL amyloidosis.

Comparator group. Twenty-seven age- and sex-matched patients with severe aortic stenosis (19 male, age 68±8 years) underwent DynEQ-CT and CMR (n=22 with 5 exclusions due to claustrophobia or pacemaker). AS was chosen as a comparator for having LV remodelling and hypertrophy, and allowing for cardiac amyloid to be excluded histologically on myocardial biopsy (Congo red staining) taken during aortic valve surgery as part of a separate study. Baseline characteristics shown in Table 11.

DynEQ-CT Protocol.

The DynEQ-CT protocol consisted of three steps (Figure 30 for flow chart): first, a CT scan to obtain baseline pre-contrast blood and myocardial attenuation in Hounsfield units (HU); second, contrast administration and delay so the contrast distributes into a blood:myocardial dynamic equilibration; third, a repeat scan to re-measure blood and myocardial attenuation. The ratio of the change in blood and myocardial attenuation (ΔHU) represents the contrast agent partition coefficient. If the blood volume of distribution is substituted in (1 minus venous haematocrit; obtained prior to imaging), the myocardial extracellular volume, ECV_{CT}, is obtained, reflecting the myocardial interstitium:

$$ECV_{CT} = (1\text{-Haematocrit}) \times (\Delta HU_{tissue} / \Delta HU_{blood})$$

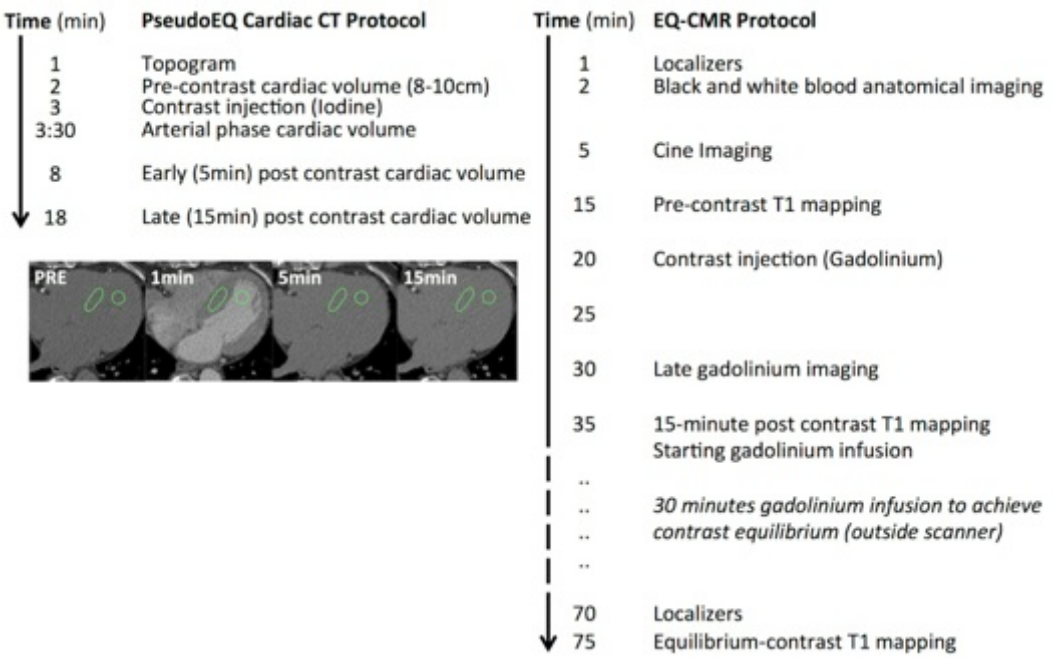

Figure 30: PseudoEQ Cardiac CT and EQ-CMR Protocols

EQ-CMR was performed either after or at least 24 hours prior to the CT to avoid residual gadolinium causing an increase in measured attenuation. The CMR protocol for amyloidosis is 3.5x longer than the CT protocol.

CT examinations were performed on a 64–detector row CT scanner (Somatom Sensation 64; Siemens Medical Solutions, Erlangen, Germany). A topogram was used to plan CT volumes from the level of the aortic valve to the inferior aspect of the heart, typically a 10cm slab. Cardiac scans (tube voltage, 120 kV; tube current–time product, 160 mAs; section collimation, 64 detector rows, 1.2-mm section thickness; gantry rotation time, 330 msec) were acquired with prospective gating (65%–75% of R-R interval), and reconstructed into 3-mm-thick axial sections with a B20f kernel.

To establish the best timing, post contrast imaging was performed at both 5- and 15-minutes following a bolus of Iodixanol (652mg/mL) at a standard dose of 1mL/kg and injection rate of 3ml/sec without a saline chaser. An additional single 3mm slice acquisition at 1-minute (other parameters as previously described) was introduced in the amyloid cohort to aid blood:myocardial boundary detection for segmentation of the myocardium during analysis.

	Systemic Amyloidosis	Comparator with Aortic Stenosis	*p-value*
N	26	27	
Men/women	21 / 5	19 / 8	
Age, yrs	64±14	68±8	*0.2*
eGFR, ml/min/1.73 m^2	71±11	78±19	*0.1*
LV structure by CMR			
Indexed LV mass, g/m^2	116±40	103±27	*0.05*
Indexed LA area,cm^2/m^2	15.3±3.4	13.2±3.7	*0.05*
LV systolic function by CMR			
LVEF, %	59±15	69±13	*0.02*
Indexed SV,ml/m^2	42±10	50±13	*0.02*
Echocardiography			
E-wave	0.86±0.20	0.73±0.32	*0.08*
E/A	1.46±0.94	0.93±0.55	*0.02*
E/E'	14.7±7.2	13±8	*0.1*
E-deceleration time, ms	178±54	246±76	*0.001*
Aortic Valve Peak Gradient	7±1	68±21	*0.001*
Clinical Parameters			
6 minutes walking test, meters	356±130	469±168	*0.01*
SBP (mmHg)	129±22	131±18	*0.5*
DBP (mmHg)	76±12	74±11	*0.3*
Atrial Fibrillation	3 (11.5%)	2 (8%)	
Biomarkers			
NT-proBNP, pmol/L	356 (24-1426)	155 (8-568)	*0.04*
Troponin T, pmol/L	0.080 (0.01-0.24)	NA	

Table 11: Baseline characteristics of amyloidosis and AS patients.

Values are mean +/- SD or %. Patients with systemic amyloidosis encompassing light-chain and transthyretin amyloidosis and aortic stenosis patients with severe stenosis awaiting valve replacement. eGFR, estimated glomerular filtration rate; NT-proBNP, N-terminal pro-brain natriuretic peptide; CMR, cardiovascular magnetic resonance; EDV, end diastolic volume; ESV end systolic volume; LVEF, left ventricular ejection fraction; SV, stroke volume; LV, left ventricular; LAA left atrial area.

CT image analysis was performed using a free and open-source Digital Imaging and Communications in Medicine viewer (OsiriX v4.1.2; Pixmeo, Bernex, Switzerland) independently by two experienced readers blinded to all other study data; this was repeated by the second reader to establish inter- and intra-observer agreement. Regions of interest (ROIs) were drawn in the contrast-enhanced 1-minute acquisition in axial sections and propagated to the pre-contrast, 5-minute and 15-minute acquisitions. For myocardium, polygonal ROIs were drawn an axial slice

containing the greatest area of myocardial septum; for the blood pool, circular ROIs were drawn in the LV blood pool away from papillary muscles and the myocardial septum to avoid the endocardial edge and therefore partial voluming (Figure 2). Myocardial and blood attenuation values were used to calculate the ECV fraction as described.

Signal-to-noise ratios (SNR) were measured in five myocardial ROIs per time point from the ratio of the average HU attenuation value to the standard deviation of the HU attenuation. Radiation exposure was quantified using the dose-length product multiplied by a chest conversion coefficient (κ=0.014mSv/mGy.cm)[178].

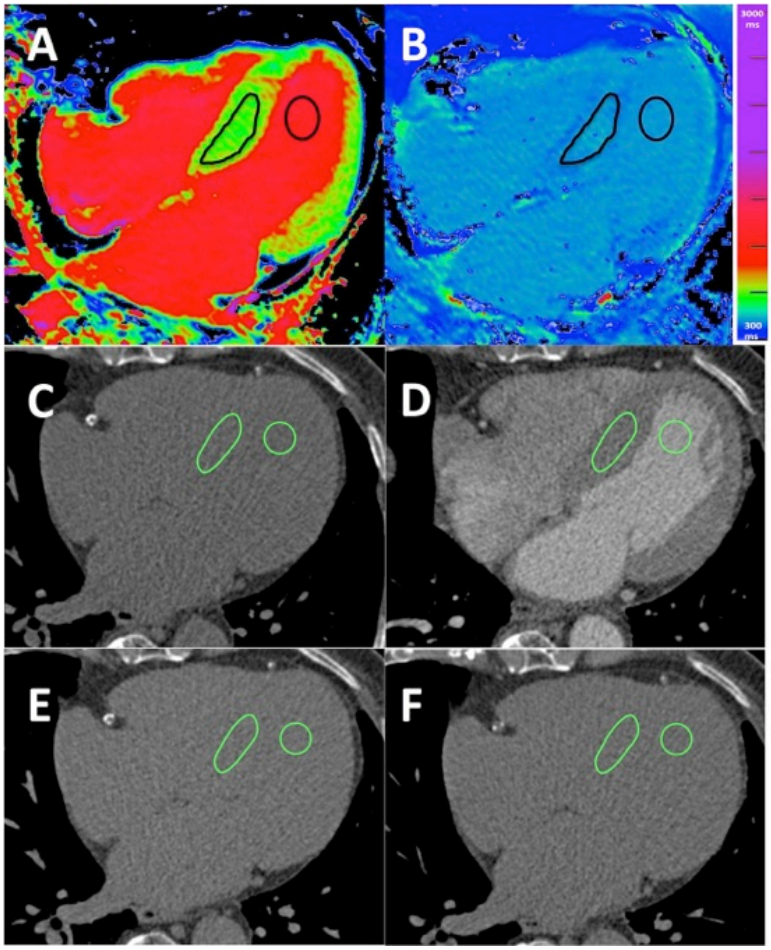

Figure 31: Examples of typical CMR and CT analysis

Top row displays regions of interest (ROIs) in CMR T1 maps images acquired before (A) and after gadolinium contrast (B). Middle and bottom rows show ROIs in gated cardiac CT images acquired pre-contrast (C), 1 minute (D), 5 and 15 minutes post iodine contrast (E+F). ROIs were drawn in the myocardial septum and blood pool.

EQ-CMR protocol. EQ-CMR was performed either after or at least 24 hours prior to the CT to avoid residual gadolinium causing an increase in measured attenuation. In addition to the standard CMR protocol (Figure 30 for flow chart), T1 mapping used ShMOLLI (Shortened Modified Look-Locker Inversion recovery)[137], providing single-section T1 map in one breath-hold [109]. For CMR image analysis, a large ROI was drawn manually by a reader blinded to the clinical data on each image to define the septum and blood pool; source data and error maps were used for quality control (Figure 31)[196].

Statistical Analysis. Analyses were performed using SPSS (Chicago, IL, USA, version 22). Details have been previously described.

4.2.5 Results

DynEQ-CT ECV performance at 5 and 15 minutes

Comparison of the signal to noise ratios showed that the SNR was significantly higher in the 5 minute rather than 15 minute scan (4.7±0.9 vs 3.9±0.9, *p<0.001*). ECV_{CT} at 5 minutes was strongly correlated with ECV_{CMR} (r^2 = 0.85, *p<0.001*) but correlation was weaker at 15 minutes (r^2 = 0.74 *p<0.001*; Figure 32). Bland-Altman comparisons of ECV_{CT} and ECV_{CMR} demonstrated no bias at 5 minutes post contrast, with slight bias at 15 minutes (4%, no slope), Compared to the 5 minute time point, the 95% confidence limits were nearly twice as wide at 15 minutes (95% confidence limits: -18%, 22% vs -11%, 11%).

The mean total calculated effective radiation dose for the whole DynEQ-CT protocol (including both post contrast time points) was 1.56mSv±0.58mSv, with a mean administered total Iodixanol (Visipaque) volume of 78 mL±11mL.

For DynEQ-CT, inter- and intra-observer agreement was excellent for myocardial (ICC=0.92 and ICC=0.94, respectively) and blood pool (ICC=0.96 and ICC=0.99, respectively) attenuation measurements. Similarly for ECV excellent agreement was found (ICC=0.95 and ICC=0.98, respectively).

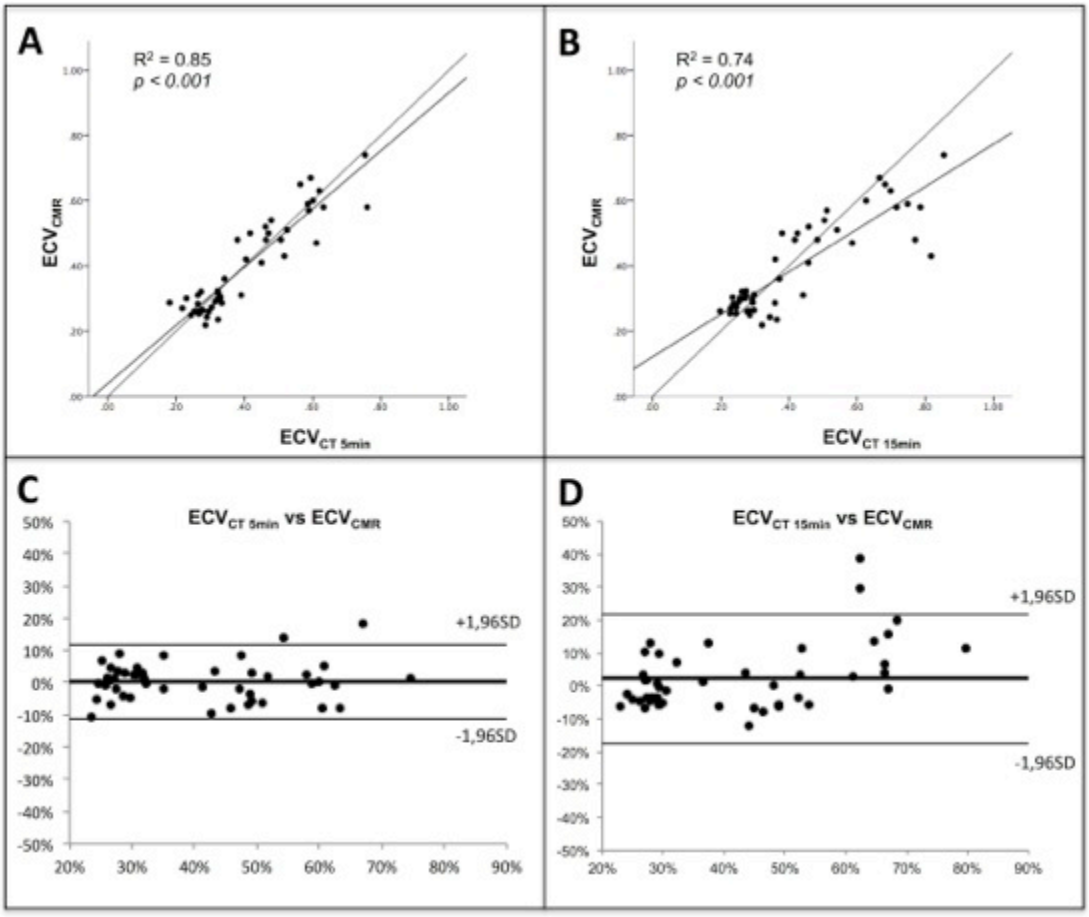

Figure 32: Correlation and agreement of ECV derived by CT and CMR

Top row show ECV_{CMR} and ECV_{CT} correlations; the 5 minute CT (A) correlates better than at 15 minutes (B) (r^2 = 0.85 vs r^2 = 0.74; p<0.001). Bottom row shows Bland-Altman comparisons of the ECV measurement by CMR versus CT at 5 minutes (C) and 15 minutes (D). ECV differences are expressed as a percentage, calculated by subtracting ECV_{CT} from ECV_{CMR}) against mean ECV (solid thick line), with lower (bottom thin line) and upper (top thin line) 95% limits of agreement.

4.2.6 Discussion

This study showed that the myocardial extracellular volume, ECV_{CT}, can be measured using a simple 5-minute, gated cardiac CT protocol, DynEQ-CT. This protocol can simply be added to routine CT coronary angiography protocols with only a small increase in radiation dose. It has the potential to offer a unique insight into the myocardial interstitium. Our previous protocol using a primed infusion to reach contrast equilibrium was logistically cumbersome and time consuming, therefore development of a bolus-only approach brings ECV, this promising novel biomarker, a step closer to routine clinical applicability. Furthermore, we unequivocally demonstrated that imaging at 5 minutes post bolus was superior to

acquisition at 15 minutes, with superior SNR. The theoretical advantage of allowing equilibration of the iodine concentration in myocardium and blood between the 5 minute and 15 minute scan is out-weighed by the loss in signal due to overall lower iodine concentrations. The addition of a low dose, early arterial phase scan facilitated blood myocardial segmentation overall. The resulting triple phase scan using a 64-slice scanner had an overall radiation dose of (1.5 mSv) – significantly lower than conventionally used bone tracer scintigraphy (4 mSv).

The ECV_{CT} technique carries some advantages in clinical practice; CMR is not suitable in around 10% of patients (due to claustrophobia or many cardiac pacemakers). Furthermore, there are concerns that the CMR signal is affected by limits to the fast exchange of protons (this does not apply to CT)[196]. The CT approach is cheaper, completed in 5 minutes, and widely available, providing high-resolution 3D ECV volumes with two single breath-hold acquisitions, and the scanner design can accommodate patients with obesity and claustrophobia. Although it has a lower signal to noise ratio, and probably more dependency on a reasonable eGFR, ECV_{CT} therefore has several advantages over ECV_{CMR}.

4.2.7 Conclusion

DynEQ-CT is a simple 5-minute, gated, easily implementable contrast-enhanced cardiac CT scan that has advantages over cardiovascular MR including scanner availability and cost, reduced examination time and applicability to those with CMR contraindications.

4.3 Synthetic ECV by Cardiac CT

4.3.1 **Preface:**

This chapter is based on the publication below:

***Treibel TA**, Fontana M, Steeden JA, Nasis A, Yeung J, White SK, Sivarajan S, Punwani S, Pugliese F, Taylor SA, Moon JC, Bandula S. Automatic Quantification of the Myocardial Extracellular Volume by Cardiac Computed Tomography: Synthetic ECV by CT. Journal of Cardiovascascular Computed Tomography. 2017 Feb 22.*

My contribution was conceiving the idea for the study analysing all the data as first operator, performing the statistical analysis and writing the paper. I also recruited, consented and performed the scans of the clinical validation cohort. Dr Jennifer Steeden, UCL, developed the OsiriX plug-in.

4.3.2 Introduction

I have demonstrated the transition of ECV from CMR to CT, and the creation of a synthetic ECV approach via CMR – where the haematocrit is estimated from native blood T1. Using CCT, a relationship between anaemia and unenhanced blood attenuation has been observed [212-217]. For example the “aortic ring sign” and “dense intra-ventricular septum“ on unenhanced thoracic CTs suggest underlying anaemia [217-219]. Here, I explored creating a synthetic ECV approach by CT.

4.3.3 Hypothesis and Aims

We hypothesized that the relationship between haematocrit (Hct) and unenhanced blood attenuation (HU_{blood}) could be used to estimate a *synthetic* Hct, permitting immediate *synthetic* ECV calculation without blood sampling. We used existing patient cohorts [168, 220] to investigate how *synthetic* ECV (a) compares to conventional ECV, and (b) correlates with the reference standard collagen volume fraction. We also tested implementation of an automated *synthetic* ECV measurement plug-in within the open-source DICOM viewer *OsiriX* [221].

4.3.4 Methods

This study is a retrospective analysis of prospectively acquired data, received local ethical approval and conformed to the principles of the Helsinki Declaration. The

study received no industry support. All participants provided informed and written consent. Exclusion criteria were uncontrolled arrhythmia or impaired renal function (estimated glomerular filtration rate <45mL/min). Prior to the scan, following insertion of an intravenous cannula, a 2-mL blood sample was collected and sent for complete blood cell count analysis.

4.3.4.1 ECV CCT Protocols.

CCT protocol and imaging analysis have been described above.

4.3.4.2 Synthetic Haematocrit and ECV Methodology

1. Derivation of synthetic Haematocrit

To derive a regression model predicting haematocrit from pre-contrast HU_{blood}, clinical unenhanced CT scans of the thorax were retrospectively analysed (120 kV; reconstructed at 5mm slice thickness and B70F soft tissue kernel). These were consecutive clinical CT scans of the thorax for investigation of malignancy, fibrosis or infection. Datasets were included if the patients had a contemporaneous paired laboratory measured Hct (within 20 days, median 8 days). HU_{blood} was analysed in a single axial slice through the centre of the right atrium. This was chosen to minimize beam-hardening artifact from the spine (compared to aortic blood pool) and partial voluming of papillary muscles in the left or right ventricular blood pool. *Synthetic* Hct was obtained from the equation describing the linear regression line between laboratory HU_{blood} and Hct.

2. Creation of a synthetic ECV Equation

Blood haematocrit was substituted by the derived *synthetic* Hct to derive a *synthetic* ECV: $\textbf{\textit{Synthetic} ECV} = \textbf{(1 – \textit{synthetic} Hct)} \times \textbf{(}\Delta HU_{tissue} / \Delta HU_{blood}\textbf{)}$

3. Validation of synthetic ECV

For validation, we used existing patient cohorts to investigate how *synthetic* ECV (a) compares to conventional ECV with laboratory blood haematocrit [220], and (b) correlates with the reference standard collagen volume fraction [168].

3a. Clinical Validation Cohort

In order to test *synthetic* ECV across a range of ECV values, the cohort used by our group to validate ECV by CT in amyloidosis was chosen; this comprised of two sub-groups with differing degrees of extracellular volume expansion: I. patients with cardiac amyloidosis (typically high ECV), comprising of 26 patients with systemic amyloidosis (21 males, age 55±10 years; 18 with transthyretin amyloidosis; 8 with systemic AL amyloidosis) with varying degrees of cardiac involvement; II. A comparator group of 27 age- and sex-matched patients with severe aortic stenosis (19 male, age 68±8 years) who typically exhibit only mild ECV elevation. Scans were performed between January and December 2013. In the clinical cohort, contrast administration was performed using a bolus only approach with a 1 mL/kg bolus of iohexol, which had been validated by our group previously [220].

3b. Histological Validation Cohort

For histological validation, the performance of *synthetic* ECV against a histological measure of fibrosis, the collagen volume fraction (CVF), was tested in a second smaller cohort of patients with severe AS, who underwent intra-operative biopsy (no overlap with clinical cohort). This cohort had been used by our group to validate ECV by CT again histology [168]: Consenting severe AS patients (n = 17, median age 71±10 years, 76% male) underwent CCT between July 2010 and February 2012. Biopsies were obtained and stained with picrosirius red for histological measurement of collagen volume fraction (CVF) as previously described [114]. In the histology cohort, contrast administration followed primed iodinated contrast material infusion (bolus plus maintenance infusion) with a 1 mL/kg bolus of iohexol followed by a maintenance infusion of at a rate of 1.88 mL/kg per hour for 25 minutes, when the post contrast imaging was performed [168].

4.3.4.3 OsiriX Plugin

To facilitate offline analysis and to exemplify future inline automation by scanner manufacturers, an automatic *synthetic* ECV plug-in was developed for OsiriX.

4.3.4.4 Statistical analysis

Analyses were performed using SPSS (Chicago, IL, USA, version 22). Details have been previously described.

4.3.5 Results

Step 1. Derivation cohort

40 thoracic CT scans with contemporaneous Hct samples within 20 days (mean 8.8±7.3 days) of the scan were included (n=40, 53% male, age 60±20 years) with a broad range of Hct (mean 38.2±6.0%; range 24.7-50.7%) and HU_{blood} (mean 40.7±8.0; range 19.5-55.2). The linear regression equation was: (*sHct* = [0.51 * HU_{blood}] + 17.4) with R^2=0.47 *p<0.001* (Figure 33).

	Systemic Amyloidosis	**Aortic Stenosis**	***p-value***
N	26	27	
Men/women	21-May	19-Aug	
Age, yrs	64±14	68±8	*0.2*
eGFR, ml/min/1.73 m^2	71±11	78±19	*0.1*
Echocardiography			
E-wave	0.86±0.20	0.73±0.32	*0.08*
E/A	1.46±0.94	0.93±0.55	*0.02*
E/E'	14.7±7.2	13±8	*0.1*
E-deceleration time, ms	178±54	246±76	*0.001*
Aortic Valve Peak Gradient	7±1	68±21	*0.001*
Clinical Parameters			
6 minutes walking test, meters	356±130	469±168	*0.01*
SBP (mmHg)	129±22	131±18	*0.5*
DBP (mmHg)	76±12	74±11	*0.3*
Atrial Fibrillation	3 (11.5%)	2 (8%)	

Table 12: Validation Cohort.

Values are mean +/- SD or %. Patients with systemic amyloidosis encompassing light-chain and transthyretin amyloidosis and aortic stenosis patients with severe stenosis awaiting valve replacement. eGFR, estimated glomerular filtration rate.

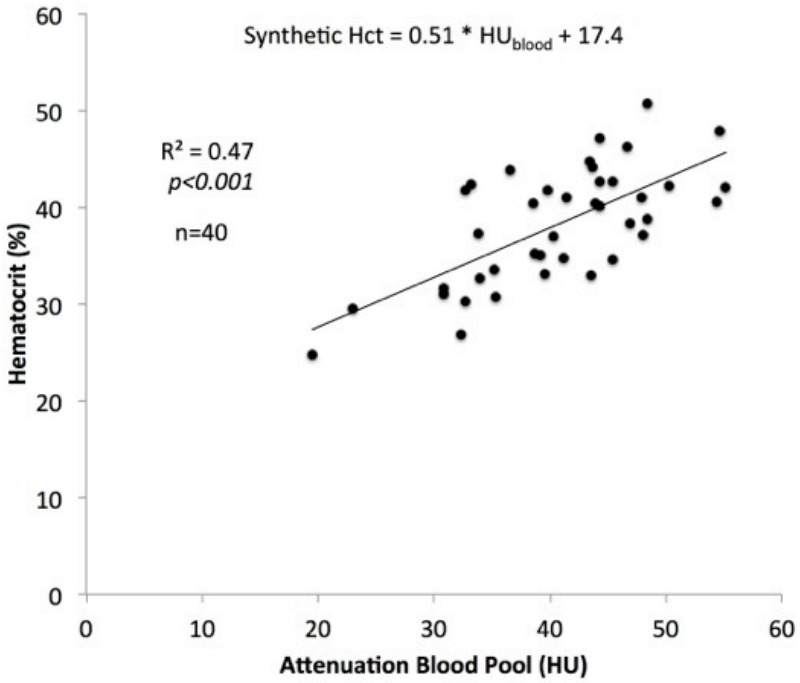

Figure 33: Derivation of synthetic haematocrit from the attenuation of blood.

*Thoracic CT scans (n=40, 53% male, age 60±20 years) with contemporaneous haematocrit samples (mean interval 8.8±7.3 days) of the scan were used to create a regression line between haematocrit (Hct; 38.2±6.0%; range 24.7-50.7%) and blood attenuation (HU_{blood}; 40.7±8.0; range 19.5-55.2). The regression line between Hct and HU_{blood} was linear (R^2=0.47 p<0.001) with a regression equation for synthetic Hct = [0.51 * HU_{blood}] + 17.4).*

<u>Step 2.</u> Creation of the *synthetic* ECV Equation

Blood haematocrit was substituted by the derived *synthetic* Hct to derive a *synthetic* ECV: *Synthetic* ECV = (1 – **([0.51 * HU_{blood}] + 17.4)** x (ΔHU_{tissue} / ΔHU_{blood})

<u>Step 3.</u> Validation

<u>Step 3a.</u> Clinical cohort

Baseline characteristics of twenty-six systemic amyloidosis and twenty-seven AS patients are shown in Table 12. In this cohort, Hct were mean 41.4±3.8% (range 29.3-47.4%) and HU_{blood} mean 40.2±3.9 (range 29.3-50.1). *Synthetic* ECV, calculated using the regression model to derive HCT, and conventional ECV were highly correlated (R^2=0.96; *p<0.001*) with a 5.7% SD of differences and minimal bias (2.4%) on Bland-Altman analysis (Figure 34).

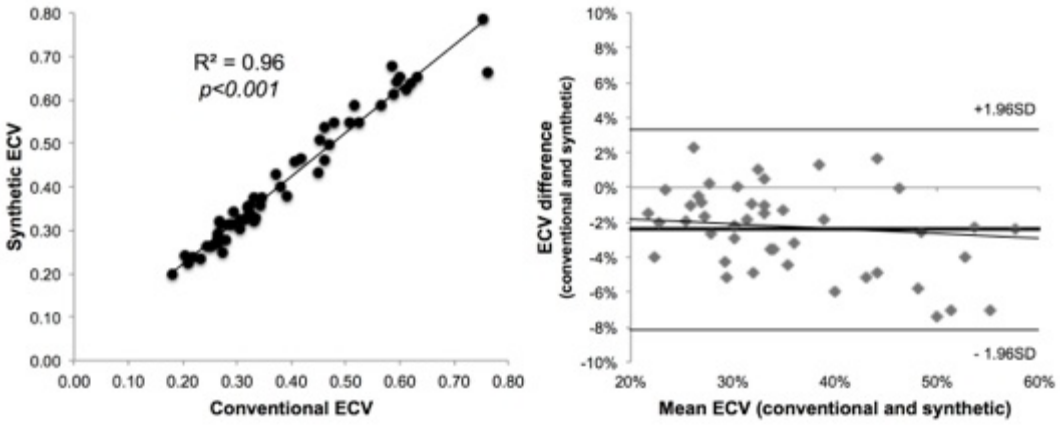

Figure 34: Validation of synthetic ECV vs conventional ECV in AS and Amyloid

Synthetic ECV, calculated using the regression model, and conventional ECV were highly correlated (R^2=0.96; p<0.001; left image) with a 5.7% SD of differences and minimal bias (2.4%) on Bland-Altman analysis (right image).

Step 3b. Histology cohort

Baseline characteristics of the histology cohort are described in Table 13. The mean histological CVF of the 17 biopsies was 18 ± 8% (range 5% to 40%), Hct were 40.2±4.6% (range 29.4-46.4%) and HU_{blood} 37.7±4.2 (range 29.5-45.1). *Synthetic* and conventional ECV both correlated well with collagen volume fraction (R^2 = 0.50, *p < 0.001* vs. R^2 = 0.50, *p < 0.001*; Figure 35) and did not differ statistically on Fisher r-to-z transformation (p = 0.8).

	Aortic Stenosis Histology Cohort
N	17
Men/women (% male)	13/4 (76%)
Age, yrs	71±10
eGFR, ml/min/1.73 m^2	88±28
Aortic Valve Peak Gradient (mmHg)	81±15
Atrial Fibrillation	0

Table 13: Histology Cohort.

Values are mean +/- SD or %. Patients with aortic stenosis patients with severe stenosis awaiting valve replacement. eGFR, estimated glomerular filtration rate.

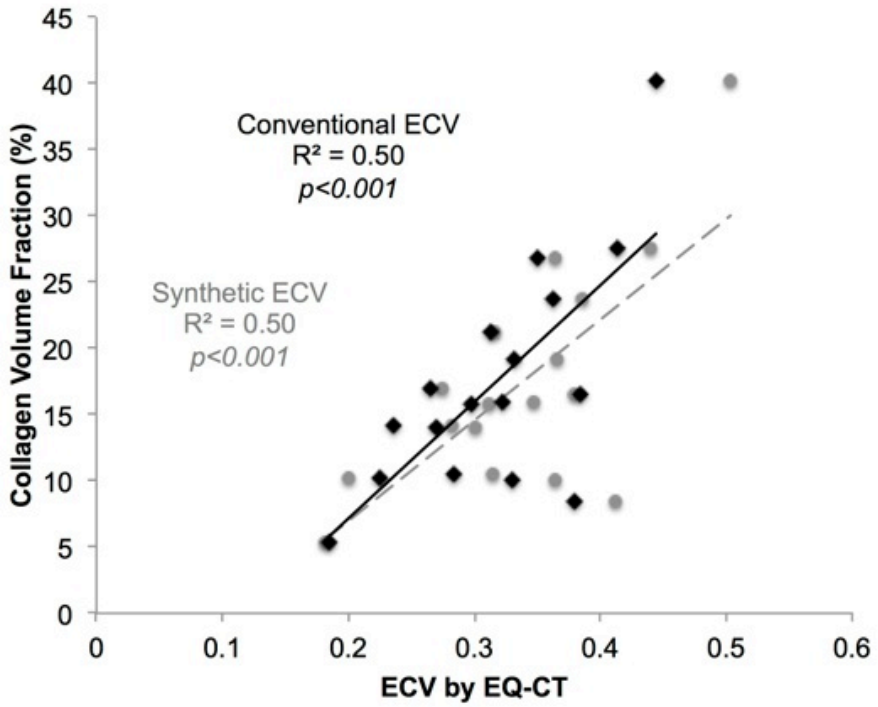

Figure 35: Histological Validation of Synthetic ECV

Synthetic and conventional ECV both correlated well with collagen volume fraction (R^2 = 0.50, $p < 0.001$ vs. R^2 = 0.50, $p < 0.001$) and did not differ statistically.

Step 4. Automatic *synthetic* ECV plug-in in OsiriX

Example output of the OsiriX plugin are shown in Figure 36. This plugin involves three simple steps: I. Manual segmentation of the blood pool in the pre- and post-contrast images; II. The plug-in automatically estimates blood haematocrit using the attenuation relationship defined above; III. The plug-in produces a three-dimensional myocardial ECV volume, where each image voxel represents an ECV value.

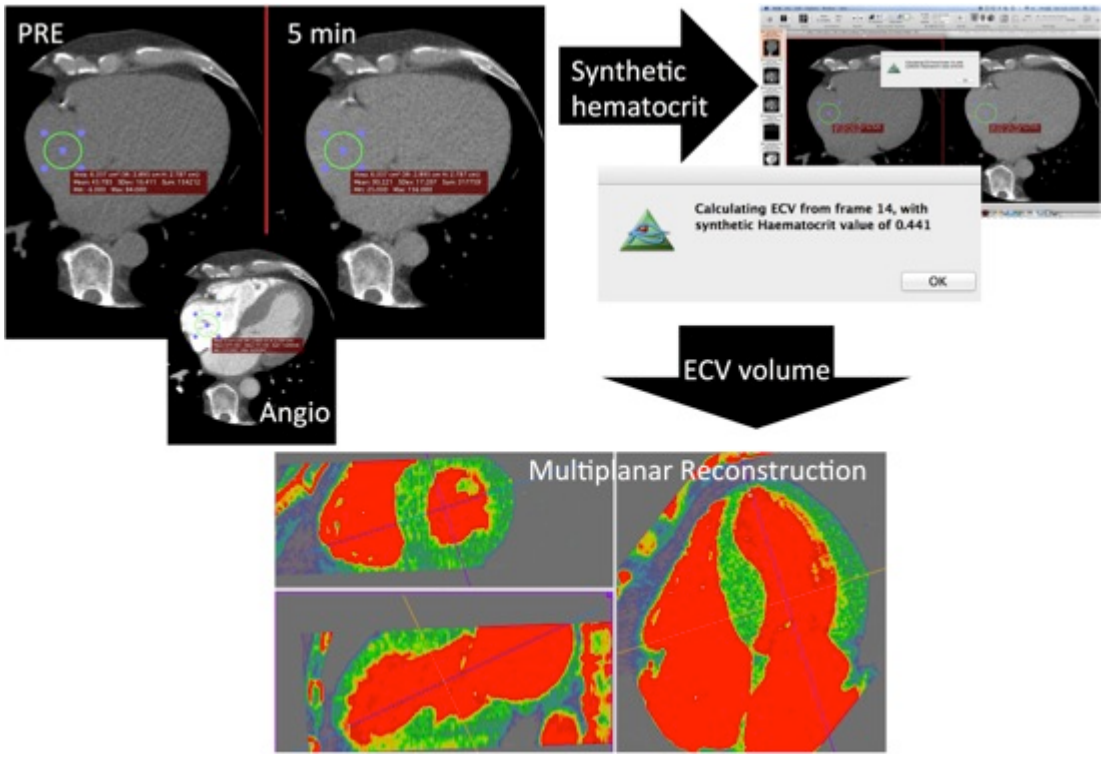

Figure 36: OsiriX Plugin workflow.

To facilitate offline analysis and allow future inline automation, an automatic synthetic ECV plug-in was developed for Osirix by Dr Jennifer Steeden, UCL. Following manual segmentation of the blood pool in the pre- and post-contrast images, the plug-in automatically estimates blood haematocrit using the attenuation relationship defined above, and produces a three-dimensional myocardial ECV volume from pre- and post-contrast CCT data.

4.3.6 Discussion

Identifying interstitial heart disease is important for diagnosis and prognosis, and myocardial extracellular volume fraction (ECV) can be measured non-invasively by CCT [168, 169, 220, 222]. However, its measurement is complicated by the necessity for venous blood sampling, image analysis and then offline ECV calculation. This process is cumbersome and a major obstacle for implementing this technique into routine clinical practice. In this manuscript, we simplify the technique by calculating ECV without blood haematocrit. This development arose out of a need to simplify ECV measurement to make it more clinically applicable. We utilize the relationship between haematocrit and blood attenuation (the attenuation of blood decreases with anaemia)[212-214, 217-219] to derive a *synthetic* haematocrit for immediate *synthetic* ECV calculation without blood sampling.

I showed that *synthetic* ECV was highly correlated to conventional ECV, and had a similar association to the histologic reference standard of CVF. The implementation of an offline automated processing tool provides a significant aid to workflow, allowing for ECV measurement in routine clinical practice. Automated *synthetic* ECV can be implemented inline on CT scanners with test performances approaching that of conventional ECV measurement. ECV by CCT carries some advantages in clinical practice; CMR is not suitable in around 10% of patients (due to claustrophobia or many cardiac pacemakers) [223]. Furthermore, CMR measures water that is influenced by the tracer, gadolinium – the tracer is not directly quantified, and there are complex water behaviours (fast exchange) and assumptions that could introduce errors. CT is more direct – the tracer is directly measured as the iodine concentration and Hounsfield units are proportional [196].

The CT approach is cheaper, can be completed in 5 minutes, and scanners are widely available. ECV by CCT can provide high-resolution 3D ECV volumes, and the scanner design can accommodate patients with obesity and claustrophobia.

4.3.7 Limitations

The study has limitations. The control cohort used in this study comprised of patients with AS rather then healthy volunteers, but, given the exposure to ionizing radiation and contrast, patients with AS were deemed as adequate control cohort, avoiding exposure of healthy volunteers. For the same reasons, variability of repeat *synthetic* ECV was not tested.

Development and validation were performed using a single scanner platform, therefore this regression model is only valid for 120 kV and an X-ray tube used in a specific CT vendor. Spectrum of the X-rays emitted by a CT X-ray tube substantially varies among CT vendors. In addition, low KV scans are increasingly used to reduce radiation exposure to the patients. Consequently, multiple regression models for different KV settings as well as for different CT vendors should be carefully prepared for synthetic ECV by CCT.

Other factors that may affect the attenuation of blood such as temperature[224] and other blood constituents such as macromolecules, fat and iron require further investigation. The 64-slice-CT-system employed here reflects commonly available systems, but did not offer iterative reconstruction algorithms, dual energy acquisition

and larger detector arrays that allow acquisition of whole heart, isotropic volumes of in one heart beat and at low radiation dose.

In single-source 64 detector rows CT, myocardial CT attenuation is not homogenous due to artifacts, especially in the inferior wall and lateral wall. In the current study, we only included data from ROIs in the left ventricular septum. The accuracy of synthetic ECV should be validated in other segments in LV myocardium, if synthetic ECV by CT is more widely available and used in patients. Furthermore, 3D image registration and processing, reduces the errors of whole heart ECV maps [170].

4.3.8 Conclusion

Synthetic haematocrit derived from the relationship between blood haematocrit and blood attenuation allows quantification of the myocardial extracellular volume fraction by cardiac computed tomography without the need for blood sampling. ECV shows great potential, allowing myocardial tissue characterization with negligible effect on workflow and radiation dose. However wider adoption requires simplification and automation of the established technique – *synthetic* ECV offers this.

Chapter 5 Results 1: Sex Dimorphism in Myocardial Remodelling

5.1.1 Preface

This chapter is based on the publication below:

***Thomas A Treibel**, Rebecca Kozor, Marianna Fontana, Camilla Tolasco, Patricia Reant, Sveeta Badiani, Maria Espinoza, John Yap, Javier Diez, Alun Hughes, Guy Lloyd, James C Moon. Sexual Dimorphism in Myocardial Remodelling. JACC: Cardiovascular Imaging. 2017 (in press at the time of thesis printing).*

My contribution was recruiting, consenting and performing the scans of all patients. I performed the T1 mapping analysis as first operator, performed quality control on LV volume and function as well as LGE analysis, I performed the statistical analysis and wrote the paper. Rebecca Kozor performed the LV volume and function analysis.

5.1.2 Introduction

In aortic stenosis (AS), Four main geometric patterns have been defined: normal geometry, concentric remodelling, concentric hypertrophy, and eccentric hypertrophy – based on left ventricular mass, cavity size and the ratio of these two [25, 179, 225]. Sex appears to exert an important influence on this [60-62]. Previous work has shown that men are more likely to have higher indexed LV mass, lower LVEF, and increased diastolic myocardial stiffness [42, 63], whereas women have more concentric remodelling with higher relative wall thickness and LVEF. But to date, most studies have relied on echocardiography alone, with only limited combined echocardiography and CMR data available . [42]

5.1.3 Aims

This study aimed to understand the sex influence on AS remodelling using all available modalities to investigate patterns of remodelling at macroscopic and tissue level.

5.1.4 Methods

This is the baseline assessment of the RELIEF-AS cohort. Recruitment was between January 2012 and January 2015. Inclusion and exclusion criteria were as planned. Overall 48% of patients undergoing surgical AVR for severe AS at Heart hospital in 3 years were recruited.

5.1.4.1 Cardiac Imaging

Echocardiography: Clinical transthoracic echocardiography was performed using a GE Vivid E9 system (GE Healthcare, Wauwatosa, USA) with a 4-MHz transducer, following the guidelines for assessment of AS severity and diastolic function as recommended by the American and European Societies of Echocardiography [226]. Assessment of AS included measurement of peak and mean transvalvular velocities and gradients; aortic valve area by the continuity equation, indexed for body surface area; pressure recovery adjusted aortic valve area (i.e., energy loss index (ELI), [227, 228]; global hemodynamic load by the valvulo-arterial impedance index (Zva, [229]; stroke work loss [230]; systemic vascular resistance and systemic arterial compliance [65]. Left ventricular wall thickness and internal dimensions were measured in the parasternal long axis view. Left ventricular mass was calculated using the Devereux formula as recommended by the American Society of Echocardiography [231]:

$$\text{LV mass} = 0.8 \times (1.04\,[(\text{LVEDd} + \text{PWTd} + \text{SWTd})^3 - (\text{LVEDd})^3]) + 0.6\text{g}.$$

Relative wall thickness was calculated using the formula: (2 x PWTd) ÷ LVEDd

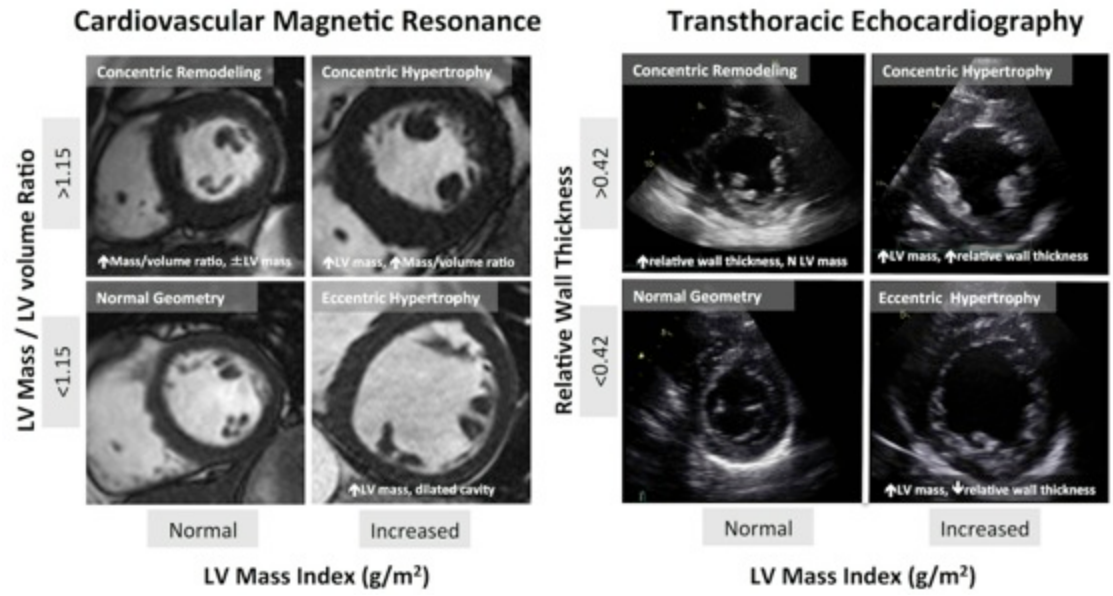

Figure 37: Remodelling by CMR and Echocardiography.

Patients were categorized into four pattern of LV geometric adaption: "normal geometry", "concentric remodelling", "concentric hypertrophy" and "eccentric hypertrophy". For cardiovascular magnetic resonance, categories were defined by BSA-indexed LV mass, indexed LV end-diastolic volume and mass-volume ratio. For 2D-echocardiography, categories were defined by BSA-indexed LV mass, end-diastolic cavity dimension and relative wall thickness.

CMR: as described earlier. This main project used MOLLI as the T1 mapping method. LGE was quantified in grams and as a percentage of the LV using signal intensity threshold of three standard deviations (SD) above the mean remote myocardium [232]. ECV was calculated and total LV matrix and cell volumes were calculated from the product of LV myocardial volume and ECV or (1 minus ECV).

5.1.4.2 Patterns of Left Ventricular Remodelling

AS patients were categorized into four patterns of LV geometric adaption (see Figure 37): "normal geometry", "concentric remodelling", "concentric hypertrophy" and "eccentric hypertrophy".

For CMR, categories were defined by BSA-indexed LV mass (LVMi), indexed LV end-diastolic volume (LVEDVi) and mass-volume ratio (MVR) [25]: Left ventricular hypertrophy was defined as an indexed left ventricular mass >95th percentile of the widely-used normal range, corrected for age and gender [233]. LV concentric remodelling, when a normal LVMi was combined with MVR ≥1.15; eccentric LVH, when increased LVMi was associated with MVR <1.15; and concentric LVH, when increased LVMi occurred with MVR ≥1.15.

For 2D-echocardiography, categories were defined by BSA-indexed LV mass (LVMi), end-diastolic cavity dimension (EDD) and relative wall thickness (RWT) [179]: Left ventricular hypertrophy was defined as LVMi ≥125 g/m^2 in men and ≥110 g/m^2 in women. LV concentric remodelling, when a normal LVMI was combined with RWT ≥0.42; eccentric LVH, when increased LVMI was associated with RWT <0.42; and concentric LVH, when increased LVMI occurred with RWT ≥0.42.

5.1.4.3 Statistical Analysis

As described before.

5.1.5 Results

5.1.5.1 Study population

There were 181 patients with severe, symptomatic AS recruited (age 69±10, 56% male) representing 48% of all surgical AVRs at the study institution. Thirteen patients were excluded: claustrophobia (n=2), hemodynamic instability (n=1), pseudo-severe AS (n=1), severe mitral regurgitation (n=2), significant myocardial bystander disease (cardiac amyloidosis n=6; Fabry Disease n=1)[234].

	Total	Men	Women	p-value
n	168	92 (55%)	76 (45%)	
Age	70±10	70±10	70±10	0.9
Trileaflet*	118	61 (66%)	57 (76%)	0.2
Bicuspid*	49	31 (34%)	18 (24%)	0.2
BSA	1.88±0.21	1.98±0.19	1.76±0.17	***<0.001***
Co-morbidities				
Hypertension	77%	81%	73%	0.4
SBP, mmHg	133±18	130±18	137±18	***0.01***
DBP, mmHg	75±11	74±10	77±13	0.1
Diabetes	26%	22%	29%	0.5
Coronary artery disease	30%	37%	21%	***0.03***
Atrial Fibrillation, %	14%	16%	14%	0.7
Smoker, current/ex/never	50/21/97	28/17/46	22/04/1951	0.2
Risk Scores				
STS, %	1.43 (0.98-2.37)	1.31 (0.88-2.32)	1.62 (1.04-2.39)	0.3
EuroScore II, %	1.49 (1.01-2.44)	1.42 (0.98-2.47)	1.54 (1.02-2.40)	0.6
Drug History				
ACE-I / ARB	43%	53%	31%	***0.006***
Beta-blocker	34%	32%	56%	0.5
Statin	61%	63%	59%	0.8
Aspirin	44%	47%	41%	0.4
Symptomatic (yes/no)	161/7	87/5	74/2	0.3
NYHA functional class	2.3±0.7	2.2±0.8	2.4±0.6	0.1
I	30	23	10	
II	79	40	39	
III	54	26	28	
IV	5	4	1	
Chest pain by CCS 0	115	60	55	0.9
1	14	12	2	
2	29	9	20	
3	10	8	2	
Syncope	14 (8%)	7 (8%)	7 (9%)	0.7
Six minute walk test	480 (338-600)	510 (360-630)	420 (300-510)	***0.02***
ECG				
LVH by Cornell criteria	43 (26%)	25 (27%)	18 (24%)	0.3
ECG Strain	29 (17%)	17 (19%)	12 (16%)	0.5
Blood				
NT-pro-BNP, ng/L	71 (29-238)	94 (36-304)	50 (28-143)	***0.04***
NT-pro-BNP ratio	0.18 (0.08-0.69)	0.33 (0.09-1.12)	0.11 (0.05-0.35)	***0.04***
hs-Troponin T, pmol/L;	14 (9-20)	15 (11-25)	12 (7-16)	***0.02***
Creatinine, micromol/l	85±25	94±26	74±18	***<0.001***
eGFR, mls/min/1.73m^2	77±22	79±23	74±18	0.3
Haematocrit, %	40±4	41±5	39±4	***0.01***

Table 14: Baseline characteristics.

**one patient had unicupid AS (female). Values are given as mean ± SD or n (and percentage), unless stated. BSA means body surface area; SBP, systolic blood pressure; DBP, diastolic blood pressure; NYHA, New York Heart Association; IQR, interquartile range; STS, Society of Thoracic Surgeons' risk model score; EuroScoreII, European System for Cardiac Operative Risk Evaluation II score; ACE-I, angiotensin-converting-enzyme inhibitor; ARB, angiotensin-receptor blocker; LVH, left ventricular hypertrophy; NT-proBNP, N-terminal pro-brain natriuretic peptide; hs-TnT, high sensitivity troponin T; eGFR, estimated glomerular filtration rate.*

Characteristics of the remaining 168 patients (age 70±10 years, 55% male; 70% trileaflet AS) are summarized in Table 14 and Table 15. All but seven patients were symptomatic (96%) with dyspnoea (82%), chest pain (32%) and/or syncope (8%). CMR was suggestive of LV decompensation in 55 patients with pericardial effusions (>5mm) in 47 patients and pleural effusions (>1cm) in 36 patients (22 with both).

There were no sex differences in the aortic valve regurgitant fraction (14% vs 10%, *p=0.1*), or mitral valve regurgitant fraction (3% vs 6%, *p=0.4*). Furthermore, there were no sex differences in age, smoking status, diabetes or hypertension prevalence, although office systolic blood pressure (130±18 vs 137±18, *p=0.01*) and glycosylated hemoglobin (HbA1c; 38±9% vs 44±20%, *p=0.003*) were higher in women. Coronary artery disease (stenosis >50%) was more prevalent in men (37% vs 21%, *p=0.03*).

5.1.5.2 Aortic Stenosis Severity and Sex

There were no sex differences in standard echocardiographic parameters of AS severity (valve area, gradient or velocity ratios; Table 15). Advanced echocardiographic parameters revealed subtle sex differences in AS severity and vascular load: men had a trend towards lower energy recovery measured by the energy loss index (0.46±0.17 vs 0.53±0.30cm^2/m^2, *p=0.06*)[227] with larger aortic dimensions (6.4±1.7cm^2 vs 4.6±1.6cm^2, *p<0.001*). Furthermore, men had lower mean arterial pressure (93±11 vs 97±12mmHg, *p=0.02*) and systemic vascular resistance (1252±376 vs 1419±361 dyne*s*cm^{-5}, *p=0.005*), though global afterload assessed by valvulo-arterial impedance (*p=0.2*) was not different.

5.1.5.3 Pattern of Remodelling and Sex

The geometry and function by CMR (Table 15) differed by sex: Men had larger LV dimensions, even when indexed (EDVi: 73±23ml vs 61±19ml vs, *p<0.001*; ESVi: 27±22g vs 18±16g, *p=0.004*), and greater LVMi (98±23 vs 75±20g/m^2, *p<0.001*; also when indexed to height^2.7)[235], and mass-volume ratio (MVR; 1.44±0.39 vs 1.30±0.28, *p<0.001*). There were also marked sex differences in remodelling (χ^2 = 34, *p<0.001*): normal geometry (82% female) and concentric remodelling (60% female) were predominantly seen in women, whereas concentric hypertrophy (71% male) and eccentric hypertrophy (76% male) in men; this was not apparent by echocardiography (p=0.4; female: normal geometry 56%, concentric remodelling 51%, concentric hypertrophy 38%, eccentric hypertrophy 39%; Figure 38).

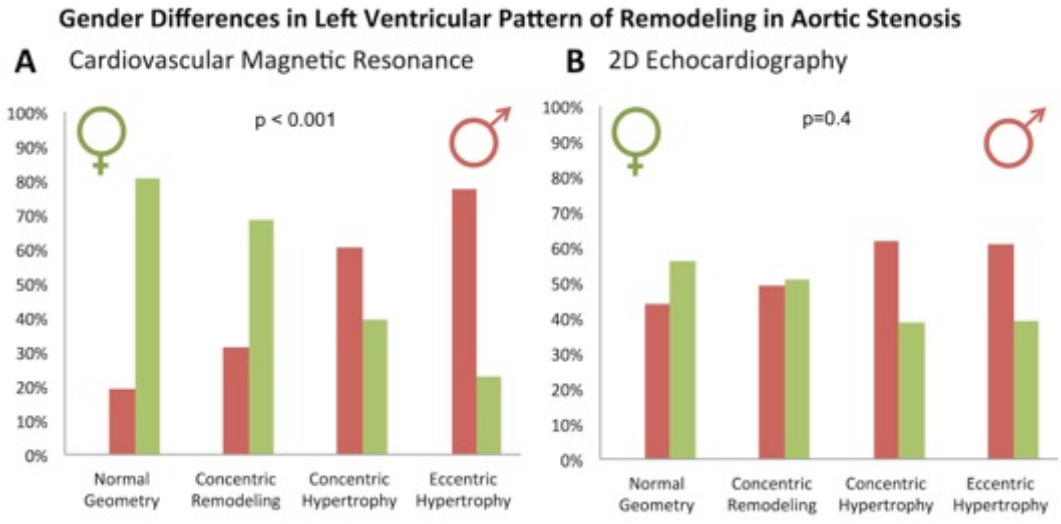

Figure 38: Sex Differences In Left Ventricular Pattern of Remodelling

Cardiovascular Magnetic Resonance (A) found marked sex *differences in left ventricular remodelling (χ^2 = 34, p<0.001): Normal geometry (82% female) and concentric remodelling (60% female) were predominantly seen in women, whereas concentric hypertrophy (71% male) and eccentric hypertrophy (76% male) in men. This was not apparent by 2D-echocardiography (B; female: normal geometry 56%, concentric remodelling 51%, concentric hypertrophy 38%, eccentric hypertrophy 39%; χ^2 = 2.7, p=0.4*).

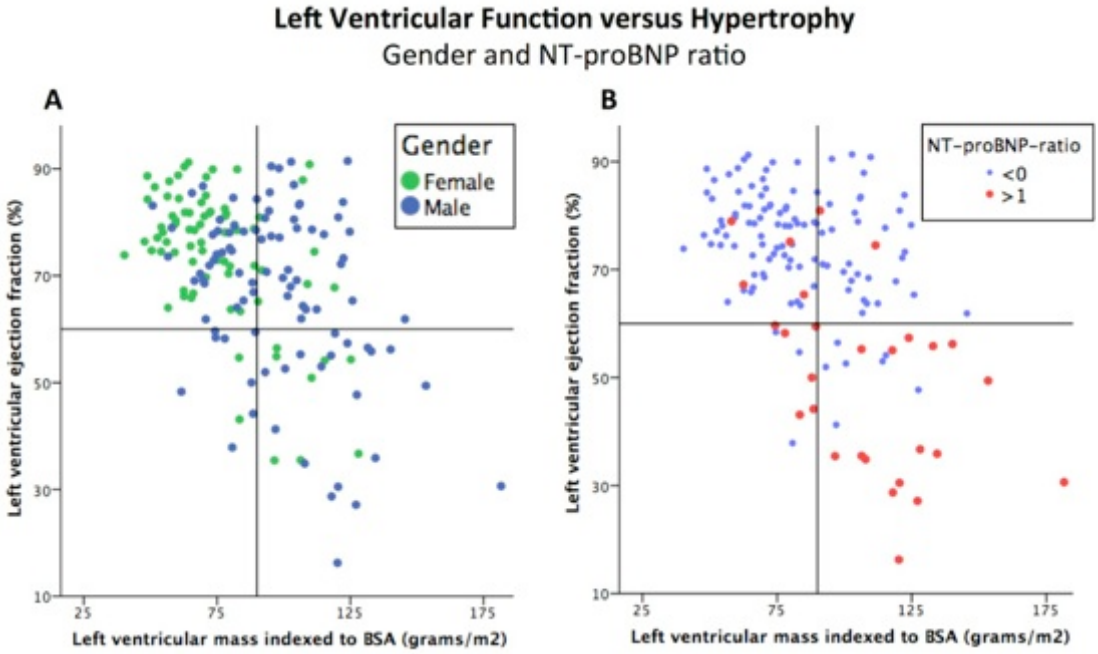

Figure 39: Sex, Left Ventricular Hypertrophy And Decompensation.

Panel A shows indexed left ventricular mass (LVMi) and left ventricular ejection fraction (LVEF) by sex: Men had greater LVMi (98±23 vs 75±20g/m^2, p<0.001) and lower LVEF than women (67±16% vs 74±13%, p<0.001). Panel B *shows LVMi and LVEF by NT-pro-BNP ratio greater or less then 1, which were higher in men than women (0.33 [IQR 0.09-1.12] vs 0.11 [0.05-0.35];* p=0.04).

Echocardiography	**Total**	**Men**	**Women**	**p-value**
Vmax (m/s)	4.33±0.59	4.38±0.59	4.27±0.59	0.3
Peak gradient (mmHg)	76±20	78±21	75±19	0.4
Mean gradient (mmHg)	47±14	49±15	46±13	0.3
AVAi (cm^2/m^2)	0.40±0.13	0.39±0.13	0.41±0.13	0.3
VTI ratio	0.23±0.08	0.22±0.07	0.24±0.08	0.1
Energy loss index (cm^2/m^2)	0.48±0.19	0.46±0.17	0.53±0.30	0.06
Systemic vascular resistance (dyne*s/cm^5)	1326±379	1252±376	1419±361	***0.005***
Systemic arterial compliance (ml/mmHg*m^2)	1.35±0.47	1.28±0.49	1.42±0.43	0.06
Zva (mmHg/ml*m^2)	4.2±1.2	4.1±1.3	4.4±1.0	0.2
E-wave	0.85±0.30	0.83±0.30	0.87±0.29	0.4
E/A ratio	0.97±0.49	1.03±0.59	0.89±0.32	0.1
E deceleration time (ms)	237±75	236±82	238±66	0.9
E/e' ratio	13.6±5.9	13.5±6.2	13.8±5.6	0.8
PASP (mmHg)	31±8	31±9	31±8	0.8
CMR parameters				
EDVi (ml/m^2)	67±22	73±23	61±19	***0.001***
ESVi (ml/m^2)	23±20	27±22	18±16	***0.001***
LVMi (g/m^2)	88±25	98±23	75±20	***0.001***
Septal wall thickness (mm)	14±3	15±2	13±2	***<0.001***
Left ventricular diameter (mm)	50±7	52±7	47±6	***<0.001***
Mass:Volume Ratio	1.37±0.35	1.44±0.39	1.30±0.28	***0.001***
LAAi_preop (cm^2/m^2)	13.5±3.7	13.6±3.3	13.4±4.1	0.8
LVEF (%)	70±15	67±16	74±13	***0.001***
SVi (ml/m^2)	45±10	46±12	43±8	0.3
Myocardial Contraction Fraction (%)	0.53±0.15	0.48±0.13	0.59±0.14	***0.001***
Wall Stress index (kPa)	1.40±0.29	1.35±0.29	1.46±0.27	***0.008***
Pattern of Remodelling by CMR				
Normal Geometry	28 (17%)	5 (18%)	23 (82%)	$\chi^2 = 34$ ***p<0.001***
Concentric Remodelling	45 (27%)	18 (40%)	27 (60%)	
Concentric Hypertrophy	70 (41%)	50 (71%)	20 (29%)	
Eccentric Hypertrophy	25 (15%)	19 (76%)	6 (24%)	
CMR flow				
Aortic regurgitant fraction % (IQR)	12 (4-35)	14 (6-47)	10 (3-24)	0.1
Mitral regurgitant fraction % (IQR)	5 (1-23)	3 (0-24)	6 (1-22)	0.4
Late gadolinium enhancement				
3SD method (g)	11.0±17.1	14.3±19.5	7.2±12.8	*0.007*
T1 mapping (ShMOLLI)				
T1 myocardium (native, in ms)	978±31	977±33	979±28	0.7
ECV (%)	28.7±2.9	28.7±3.1	28.6±2.5	0.8
Cell volume, indexed (ml/m^2)		73±17	55±13	***<0.001***
Matrix Volume, indexed (ml/m^2)		29±9	21±6	***<0.001***

Table 15: Imaging Parameters (Echocardiography and CMR).

Values are given as mean ± SD or n (and percentage), unless stated. Vmax, peak velocity through the aortic valve; AVAi, aortic valve area index; VTI ratio, velocity-time-integral ratio; Zva, valvulo-arterial impedance; E, peak early velocity of the transmitral flow; DT, deceleration time; E´, peak early diastolic velocity of the mitral annulus displacement; PASP, pulmonary artery systolic pressure measured by echocardiography; EDVi, end-diastolic volume index; ESVi, end-systolic volume index; LVMi, left ventricular mass index; LVEF, left ventricular ejection fraction; SVi, stroke volume index, LAAi, left atrial area index; IQR, interquartile range; 3SD, three standard deviations; ECV, extracellular volume.

5.1.5.4 Symptoms and Myocardial Response

No sex differences in NYHA functional class were found (p=0.2). Although men were able to walk further than women on 6MWT assessment (510 [IQR 360-630] m vs 420 [IQR 300-510] m, *p=0.02*), the percentage-predicted 6MWT distance [236] was not significantly different between men and women (97±34% vs 96±40%, *p=0.6*). LVEF was lower in men then in women (67±16% vs 74±13%, *p<0.001*, see Table 15). Men had lower minute work (15.6±4.7 vs 17.7±4.5ml*mmHg/min, *p=0.005*) and myocardial contraction fraction (48±13% vs 59±14%, *p<0.001*). Furthermore, both NT-pro-BNP and hsTnT were higher in men (NT-pro-BNP: 94 [IQR 36-304] vs 50 [IQR 28-143] pmol/L, *p=0.04*; hsTnT: 15 [IQR 11-25] vs 12 [7-16] pg/L, *p=0.01*). Figure 3 displays the distribution of LVEF vs indexed LV mass by gender and by BNP clinical activation, defined as a NT-pro-BNP ratio >1 (absolute NT-proBNP concentration indexed for the 95th centile of normal range for age and sex [181]).

5.1.5.5 Myocardial Fibrosis and Sex

Examples of LGE pattern are shown in Figure 40. There was more LGE in men by both prevalence (71% vs 46%, *p<0.01*) and extent (16.5±11.2 vs 10.5±8.9g, *p<0.001)*, although these differences were not statistically significant when expressed as a percentage of the LV mass (8.6±5.6 vs 7.7±5.9%, p=0.1). No sex differences in native myocardial T1 or ECV (T1: 1041±42ms vs 1051±47ms, p=0.2; ECV: 28.6±3.1% vs 28.2±2.7%, p=0.2) were observed. However, using the ECV to dichotomize the LVMi into matrix and cell compartments, both indexed matrix (28.5±8.8 vs 21.4±6.3ml/m^2, *p<0.001*) and cell volumes (72.7±16.7 vs 54.7±13.0ml/m^2, *p<0.001*) were higher in men.

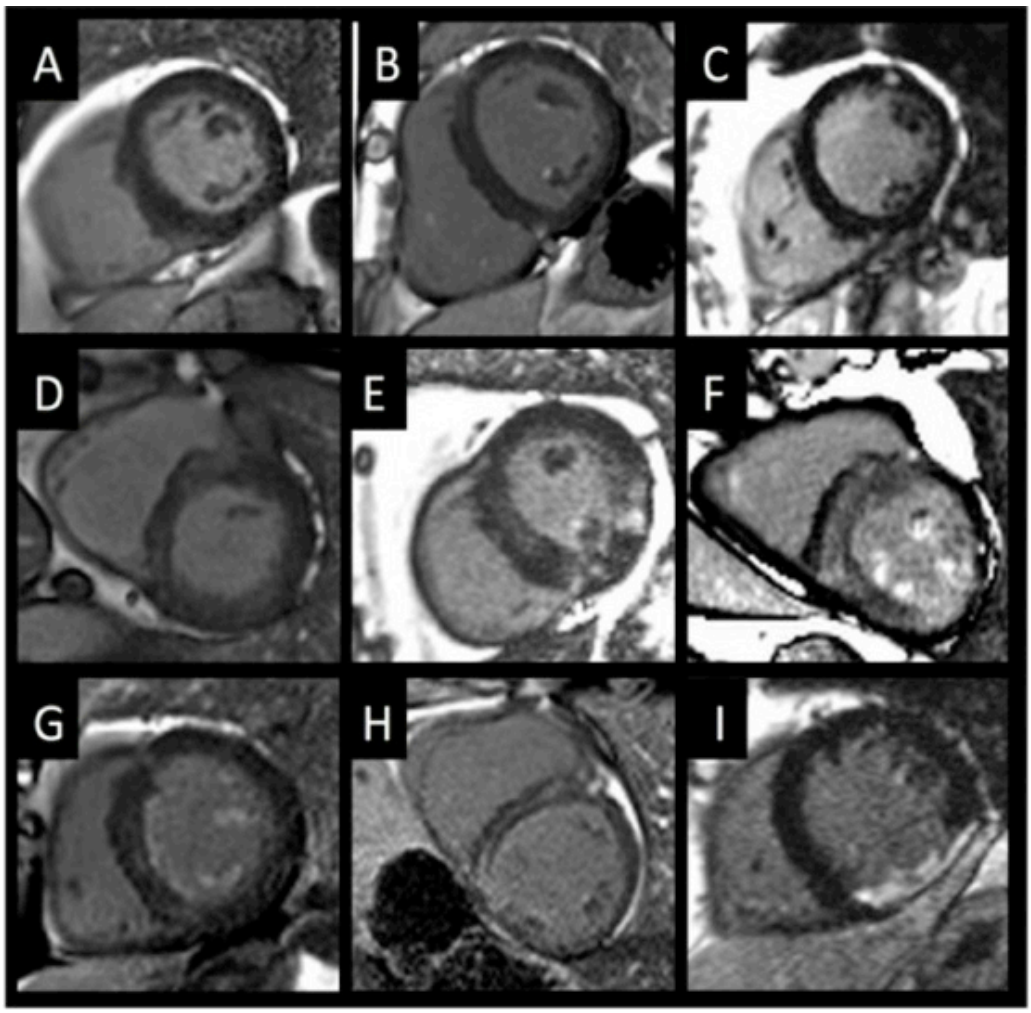

Figure 40: Late gadolinium enhancement in aortic stenosis.

A – No late gadolinium enhancement (LGE). B – Focal Papillary muscle and RV insertion point LGE. C – Focal mid-wall LGE in the anterolateral wall. D-F – diffuse, patchy myocardial LGE ranging from mild (D) to moderate (E) to severe LGE burden (F), associated with papillary muscle RV insertion and RV free wall LGE. G – Non-infarct, subendocardial and papillary muscle LGE. H – dilated cardiomyopathy-pattern LGE. I – Full thickness infarct in the thinned inferior wall.

5.1.6 Discussion

In this prospective multimodality study of 168 patients with symptomatic severe AS at baseline referred for surgical AVR, despite the same referral age, valve severity and functional status, there were major sex differences in myocardial remodelling, fibrosis and resultant left ventricular function. Our data highlights the importance of the myocardial response in AS encompassing a wide geometric and functional range (Figure 41), which is neither associated with the hemodynamic severity of the aortic valve stenosis nor observed by conventional echocardiography: Men predominantly had concentric or eccentric LVH as well as a less favourable,

maladaptive ventricular phenotype (lower LVEF, higher NT-pro-BNP and hs-TnT, more myocardial fibrosis). In contrast, women exhibited a possibly more favourable phenotype with less hypertrophy, less fibrosis, and a higher prevalence of normal geometry or concentric remodelling with higher LVEF.

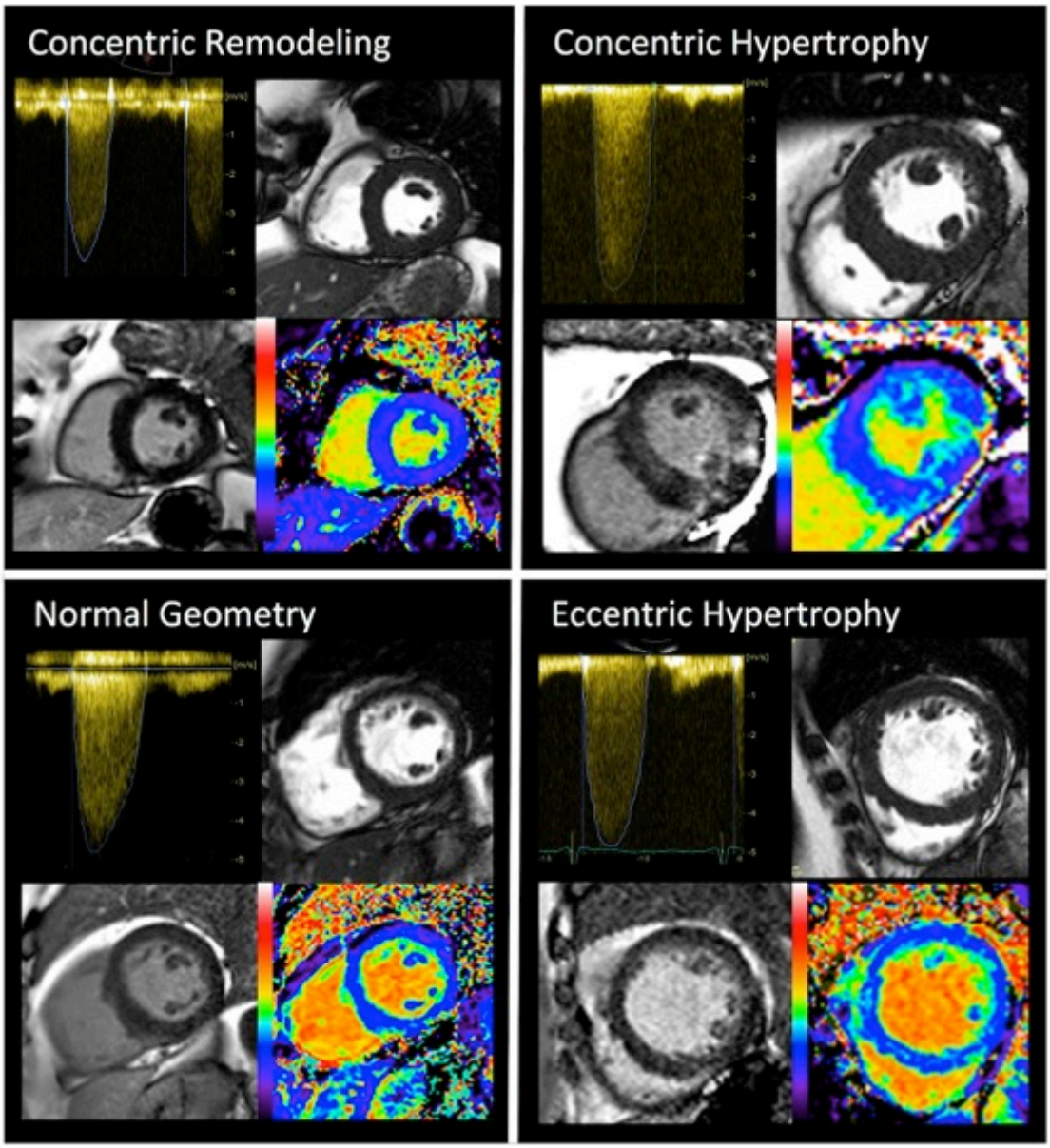

Figure 41: Left Ventricular Remodelling in AS by Multimodality Imaging.

This panel shows four images each for all four patterns of remodelling: continuous wave Doppler assessment of aortic stenosis severity (top left); SSFP short axis cine clip demonstrating the pattern of remodelling (as described in Figure 1; top right); phase-sensitive inversion recovery late gadolinium enhancement image for focal fibrosis (bottom left); extracellular volume fraction map for diffuse fibrosis (bottom right).

These findings raise a few key issues: Firstly, given the stark differences in myocardial remodelling, how do these affect the interpretation of the hemodynamic

severity of the valve stenosis? Secondly, these changes may be adaptive or maladaptive – can LVEF, NT-pro-BNP and hs-Troponin adequately highlight the transition into maladaptation, or are other biomarkers needed? And are blood biomarkers more informative than imaging? Finally, what are the mechanisms driving the sex differences in remodelling?

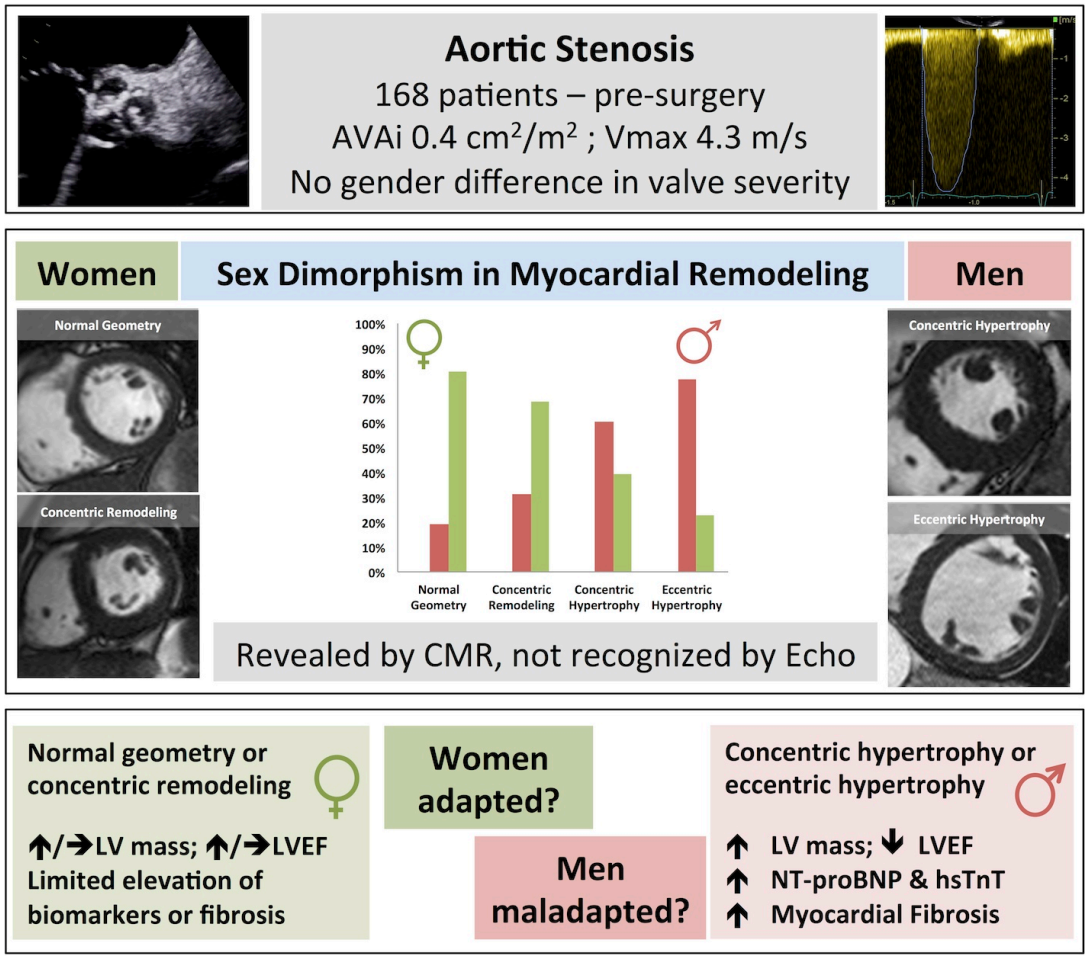

Figure 42: Sex Dimorphism in Myocardial Response to Aortic Stenosis.

Aortic stenosis (AS) is a disease of both valve and left ventricle (LV). Sex difference may play a role in disease phenotyping. This study investigated 168 patients with severe symptomatic AS by echocardiography, cardiovascular magnetic resonance (CMR) and biomarkers. There were no sex differences in AS severity or functional capacity, but CMR captured a sex dimorphism in LV remodelling pattern; missed by 2D-echocardiography and more adverse in men with more LV dysfunction (by LVEF, NT-pro-BNP, hsTnT) and myocardial fibrosis (focal and diffuse). Given equal valve severity, LV associations with AS appear more maladaptive in men, with more extreme sex differences then previously reported. AVAi, indexed aortic valve area; CMR, cardiovascular magnetic resonance; ECV, extracellular volume fraction; hsTnT, high-sensitivity troponin T; LGE, late gadolinium enhancement; LV, left ventricular; LVEF, left ventricular ejection fraction; NT-proBNP, N-terminal pro-brain natriuretic peptide; Vmax, peak velocity.

5.1.6.1 Sex dimorphism in myocardial response

In our study, women appeared to tolerate a similar level of valve-related afterload better (women even had higher blood pressures and fewer cardioprotective drugs), with better-preserved wall stress and better systolic pump performance (LVEF and myocardial contraction fraction) then men. Sex-related differences in myocardial remodelling have been reported in the elderly with or without AS [60, 61, 237-239]. In animal models, sex dimorphism exists in the baseline findings of the heart (difference in size, physiology, gene profiles, contractile properties), response to pressure or volume overload (more hypertrophy and dilatation, respectively), and cardiomyocyte response to aging and modification of cardiac gene expression [240]. Cellular, molecular and neurohormonal mechanisms for the differential response in men have been proposed, including increased interstitial fibrosis, greater activation of profibrotic and inflammatory pathways, and differential expression of androgen and oestrogen receptors [63, 241-243]. Although the interplay of protective effects of oestrogens and deleterious effects of androgens may play a key role in the sex dimorphism, the majority of female patients in our study were post menopausal and none were on hormone replacement therapy. Sex differences in the renin-angiotensin system, nitric oxide activity and norepinephrine release may contribute to differences in LV remodelling [244]; similar differences in cardiac function and arterial haemodynamics to those observed here have also been seen in community based samples of older men and women [245]. A less explored possibility is that the myocardium could have been sex-patterned during cardiac foetal formation to adapt differently during adult life.

5.1.6.2 Discordance with previous echocardiographic data

Sex dimorphism in cardiac remodelling in AS is present in the literature, but has not been emphasized; for example in an echocardiographic study of 2017 patients (36% female) awaiting AVR [246], LV impairment had a 3.5 to 1 male to female ratio and LVEF >70% had a 1:1 male to female ratio. Given the study entry gender ratios, if there had been no sex dimorphism, both of these ratios should have been 1.7 to 1. However, the sex dimorphism of cardiac remodelling found by CMR here was much more extreme than by echocardiography (Figure 2). Modality specific ascertainment differences that could explain this: cross-sectional echocardiography uses derived wall thickness to cavity width ratios whilst CMR uses a 3D derived mass to volume ratio [25]. Each technique also has indexed gender specific reference ranges and

cut-points, which could be inaccurate and magnify differences. These may be differently sensitive to gender influenced confounders (such as a basal septal bulge). Such explanations appear however inadequate and the impression is that an echocardiography-based approach to cardiac remodelling has induced an underestimation of biological sex dimorphism in cardiac remodelling in AS.

5.1.6.3 Perspective – do we need sex-specific thresholds for AVR?

Timing of aortic valve intervention is one of the greatest challenges in AS, in particular in asymptomatic patients. Recent focus has turned towards the complex interplay between AoV stenosis, vascular load and myocardial response (inappropriate hypertrophy, myocardial stress [NT-proBNP], fibrosis [troponin, LGE, ECV], myocardial perfusion reserve). Our data supports the notion that we may need to treat men and women differently as they experience a different cardiac "milieu", different combined (valve and vasculature) afterload and display a different myocardial response. Crucially, data showing reverse remodelling after valve replacement and its impact on outcome is required and pending.

5.1.7 Limitations

This study has several limitations. Only patients with severe disease referred for surgery at a specialist centre were included and the study is therefore not representative of patients treated medically or by transcatheter aortic valve intervention. CMR inclusion criteria excluded patients with pacemakers and eGFR<30; this only excluded 7% of patients and is unlikely to have biased our findings. No invasive LV pressure data was obtained; due to stroke risk associated with crossing the AoV [247], this is not routinely performed in our institution.

5.1.8 Conclusion

CMR reveals sex differences in associations between AS and myocardial remodelling that are not evident from conventional echocardiography and that we had been missing. Given equal valve severity, the myocardial response to AS appears more maladaptive in men then previously reported. This data suggests that more detailed phenotyping of patients with AS is required – resultant uncovering of a maladaptive ventricular response may be influential in the current debate regarding immediate or deferred intervention for severe AS.

Chapter 6 Results 2: Occult Cardiac Amyloid in Aortic Stenosis

6.1.1 Preface

This chapter is based on the publication below:

***Treibel TA**, Fontana M, Gilbertson JA, Castelletti S, White SK, Scully PR, Roberts N, Hutt DF, Rowczenio DM, Whelan CJ, Ashworth MA, Gillmore JD, Hawkins PN, Moon JC. Occult Transthyretin Cardiac Amyloid in Severe Calcific Aortic Stenosis: Prevalence and Prognosis in Patients Undergoing Surgical Aortic Valve Replacement. Circulation Cardiovascular Imaging. 2016 Aug;9(8).*

My contribution was recruiting, consenting and performing the scans of all patients, as well as collecting the myocardial biopsies at time of surgery. I analysed all data as first operator, did the statistical analysis and wrote the paper. Histological processing and analysis was performed at Great Ormond Street Hospital and the National Amyloidosis Centre, Royal Free Hospital, UCL. This work has also led to the granting of a BHF research fellowship to Dr Paul Scully (FS/16/31/32185) to continue to explore occult amyloid in the elderly with AS.

6.1.2 Introduction

In RELIEF-AS, there was a likelihood of occult amyloid. Coexistence of AS and cardiac amyloidosis has been reported but this has not been studied systematically and the prognostic significance is unknown [248, 249]. It has been suggested that occult amyloid might account for the frequent need for pacemakers among TAVI patients, and the high prevalence of CMR LGE [250], but this has not been studied systematically. It has not hitherto been possible to reliably detect the presence of cardiac amyloidosis without recourse to biopsy, but this is now possible in most patients using a combination of multiparametric CMR incorporating native T1 mapping [251], estimation of ECV [135], and the Phase Sensitive Inversion Recovery (PSIR) LGE technique [252], coupled with bone scintigraphy [253]. This is all the more important given that several specific drug therapies for ATTR amyloidosis are now in clinical trial [254, 255].

6.1.3 Hypotheses and Aims

We hypothesized that unrecognized ATTR amyloid deposits may act as a disease modifier in aortic stenosis. We aimed to: 1 – assess the prevalence of occult cardiac

amyloid in AS; 2 - identify the amyloid subtype; 3 – determine the role of comprehensive imaging; and 4 - elucidate its clinical and prognostic significance.

6.1.4 Methods

In the RELIEF-AS Study 146 patients (81%) underwent intra-operative myocardial biopsies. CMR and echo were performed as previously described. DPD bone scintigraphy was conducted during subsequent specialist clinical evaluation of subjects found to have amyloid on biopsy (see later). Prior to AVR, all patient underwent a clinical transthoracic echocardiogram (TTE), primarily to assess aortic valve mean gradient, peak jet velocity and effective orifice area, i.e. assessment of AS severity, as well as systolic and diastolic function [226]. Global longitudinal strain was not performed routinely as and was therefore not available prior to AVR. Analysis was performed retrospectively in patients with adequate endocardial border definitions as previously described [256].

6.1.4.1 CMR scanning

As described before in section 3.3. In addition, two amyloid specific indices, myocardial contraction fraction (the ratio of stroke to myocardial volume) and ECG-voltage/LV mass ratio, were calculated [257, 258].

6.1.4.2 Histological analysis

An intra-operative septal biopsy (typically tubular, measuring 1.6x1.6x10mm) was harvested from the basal left ventricular septum under direct vision by the surgical team using a 14-gauge coaxial needle, formalin fixed and paraffin embedded (FFPE). Histological analysis was performed by Congo red staining on 6μm FFPE sections and viewed in brightfield and cross polarized light [259]. When amyloid was confirmed by displaying apple green birefringence under cross polars, immunohistochemistry (IHC) was carried out on the Shandon Sequenza™ system using a panel of monospecific antibodies against known amyloid-forming proteins, in an attempt to identify the amyloid fibril. Antigen retrieval was not performed with the exception for TTR antibodies which uses oxidation with 1% aqueous Na-m-periodate (10 min) and 0.1% di-NA borohydride (10 min) followed by 6 M guanidine (4h). Sections were blocked for endogenous peroxidases and with normal serum, incubated overnight at 4°C with the primary antibodies. Antibodies were detected with the appropriate species-specific IMMPRESS (Vector Laboratories) polymer

detection kit and labelled using metal-enhanced 3,30-diaminobenzidine chromagen (Thermo Scientific). Interpretation was carried out initially without any clinical information by two people independently using a Leica DMLB with and without crossed polars. Diagnosis was confirmed by laser microdissection and mass spectroscopy (LDMS) [260, 261].

6.1.4.3 Clinical assessment of patients with amyloid on myocardial biopsy

Patients found to have amyloid were referred for full clinical assessment at the National Amyloidosis Centre, London, UK. A particular emphasis was to exclude AL amyloid, which can be treated with chemotherapy. Clinical work-up included: serum and urine immunofixation, serum free light chain analysis, comprehensive transthoracic echocardiogram, ^{123}I-labeled serum amyloid P component scintigraphy, sequencing of the transthyretin gene, and cardiac scintigraphy using the ^{99m}Tc-labelled DPD bone tracer. This was graded on the Perugini scale: Grade 0 - no myocardial uptake; Grade 1 - minor cardiac uptake of less intensity than uptake in the bony skeleton; Grade 2 - moderate cardiac uptake with greater signal intensity than the bone; Grade 3 - strong cardiac uptake with little or no bone uptake visible [172, 253].

6.1.4.4 Statistical Analysis

As described in the main methods section 3.8. Survival was evaluated using Cox proportional hazards analysis, providing estimated hazard ratios (HR) with 95% confidence intervals (CI) and Kaplan Meier curves. Due to the low number of events (deaths) multivariable Cox regression models were not tested.

6.1.5 Results

146 patients with severe AS awaiting aortic valve replacement (AVR) were recruited. All patients had echocardiography, CMR with LGE and T1/ECV mapping as well as intra-operative myocardial biopsy. 112 patients had calcific AS (cAS) [75±6years; 58% male]; 32 patients had bicuspid AS (bAS) [59±6years; 66% male], one patient each rheumatic (65, female) and unicuspid AS (35, female). The treatment received was tissue or mechanical valve in 71% and 29%, respectively, with additional bypass grafting in 23%, aortic intervention in 6% (interposition graft, reduction aortoplasty, replacement of the ascending aorta) and mitral valve replacement in 1.4%. Baseline characteristics are shown in Table 16.

	Calcific AS	Other Etiologies*	*p-value*
N	112	34	
Men	64 (58%)	21 (58%)	0.9
Age, years	75±6	59±7	***<0.001***
BMI, kg/m^2	28±5	27±7	0.2
Cardiovascular MR			
Indexed EDV, ml/m^2	64±21	74±21	***0.02***
Indexed ESV, ml/m^2	21±17	25±20	0.6
Indexed LV mass, g/m^2	85±24	94±24	0.2
LVEF, %	69±15	70±15	0.5
Myocardial contraction fraction, %	0.53±0.16	0.55±0.14	0.5
Voltage-mass ratio	0.13±0.06	0.11±0.04	0.3
Indexed LA area, cm^2/m^2	14±4	13±3	0.08
Echocardiography			
Aortic Valve Peak Velocity	4.3±0.6	4.4±0.5	0.8
Aortic Valve Mean Gradient	46±15	47±15	0.8
Aortic Valve Area, indexed	0.41±0.17	0.42±0.15	0.2
E-wave	0.84±0.29	0.89±0.29	0.4
E-deceleration time (ms)	240±79	224±63	0.3
E/A	0.92±0.42	1.18±0.65	*0.06*
E/E'	13±6	15±7	0.3
Clinical Parameters			
Hypertension (%)	87 (78%)	31(90%)	0.1
Diabetes (%)	26 (23%)	6 (18%)	0.5
Coronary Artery Disease (%)	37 (33%)	9 (27%)	0.6
STS score	1.9±1.4	1.6±0.9	0.3
EUROscore II	2.3±2.1	1.6±0.9	***0.02***
Bloods			
NT-proBNP, pmol/L	186 (5-1307)	177 (8-1400)	0.7
eGFR, ml/min/1.73 m^2	72±18	88±20	***0.03***
Surgery			
Tissue AVR	82 (73%)	21 (62%)	
Mechanical AVR	30 (27%)	13 (38%)	
CABG	29 (26%)	5 (17%)	
Aortic intervention	4 (3.6%)	4 (11.8%)	

Table 16: Baseline Characteristics.

**Bicuspid AS n=32; unicuspid AS n=1; rheumatic AS n=1. Values are mean +/- SD or %. AS, aortic stenosis; eGFR, estimated glomerular filtration rate; NT-proBNP, N-terminal pro-brain natriuretic peptide; CMR, cardiovascular magnetic resonance; EDV, end diastolic volume; ESV end systolic volume; LVEF, left ventricular ejection fraction; SV, stroke volume; LV, left ventricular; LAA left atrial area.*

6.1.5.1 Histological and Genetic Analysis

Of the 146 biopsies, six contained amyloid (prevalence 4.1% all-comers). All six were cAS aged >65 (prevalence 5.4% for cAS and 5.6% for >65). Typing by IHC, supported by LDMS, confirmed ATTR amyloid type in all six cases (Figure 43 and Figure 44). Genetic sequencing confirmed non-hereditary wild-type transthyretin sequence in each case.

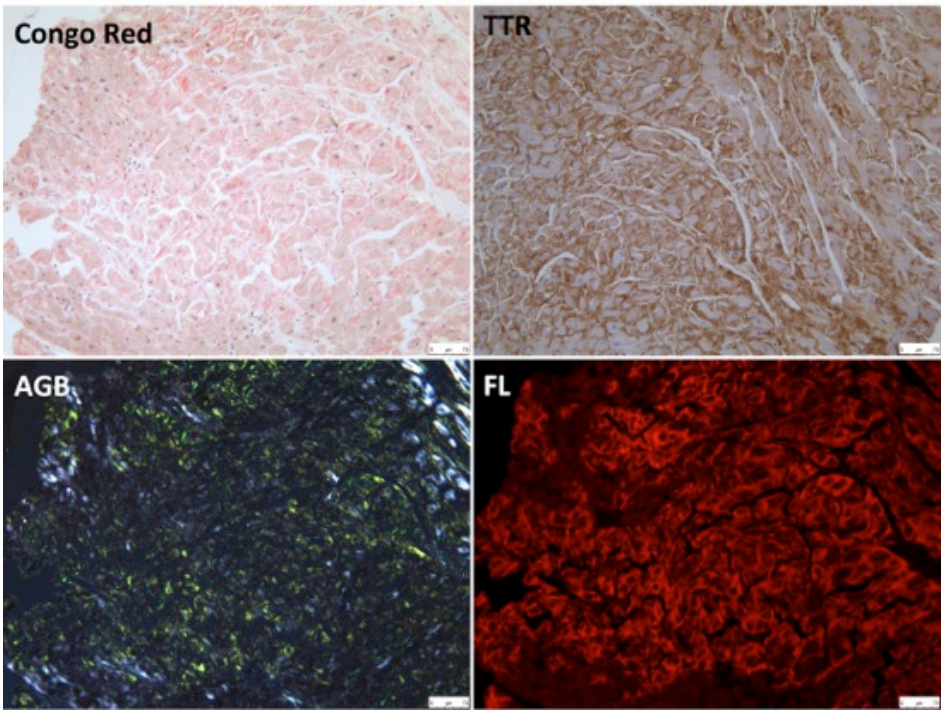

Figure 43: Myocardial biopsy in severe AS and overt ATTR amyloid deposits.

Histological slides stained with Congo red under brightfield light (Congo Red), under cross polars with typical apple green birefringence (AGB) and under fluorescent (FL) microscopy. Separate slide prepared by transthyretin-specific immunohistochemistry (TTR) showing widespread ATTR amyloid staining (brown).

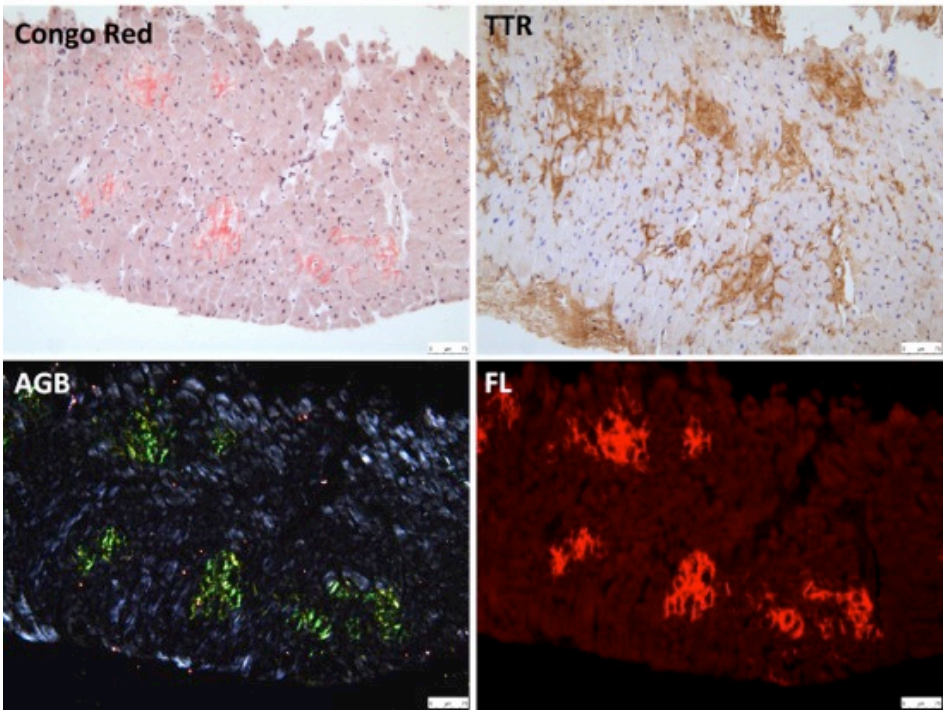

Figure 44: Myocardial biopsy in patient without clinical evidence of amyloid

Histological slides stained with Congo red under brightfield light (Congo Red), under cross polars with typical apple green birefringence (AGB) and under fluorescent (FL) microscopy. Separate slide by TTR immunohistochemistry. All showing patchy ATTR amyloid deposits.

	Patient 1	Patient 2	Patient 3	Patient 4	Patient 5	Patient 6
Age/Gender	73 female	69 male	80 female	85 male	84 male	71 male
Status	Alive	Dead	Dead	Alive	Dead	Alive
Biopsy/Genotype	TTR/wild type	TTR/wild type	TTR/wild type	TTR/wild type	TTR/wild type	TTR/wild type
DPD Scintigraphy*	Grade 2	Grade 2	Not attended	Grade 1	Not attended	Grade 1
SAP scan†	negative	negative	Not attended	negative	Not attended	negative
Red flags	Carpel tunnel	No neuropathy	No neuropathy	No neuropathy	No neuropathy	No neuropathy
NT-pro-BNP, pmol/L	431	458	510	51	188	201
Light chains	negative	negative	NA	negative	NA	negative
6-minute-walk test, m	432	244	510	276	150	264
EKG voltage	LVH criteria	LVH criteria	Normal	Normal	Normal	Normal
Voltage-mass-ratio	0.13	0.12	0.14	0.18	0.16	0.07
AVAi (cm^2/m^2)‡	0.36	0.52	0.6	0.34	0.35	0.24
AoV Peak Gradient (mmHg)§	74	45	70	110	61	116
Global longitudinal strain	-6.40%	-11.60%	NA	-19.60%	-12.70%	NA
LGE patternǁ	Amyloidosis	Amyloidosis	AS	AS	AS	AS
LV Ejection Fraction (%)#	61	68	67	77	67	64
LV mass index (g/m^2)#	137	150	117	101	93	132
Myocardial contraction fraction	25%	33%	44%	64%	50%	43%
Maximal wall thickness (mm)	18	21	15	12	15	19
Extracellular Volume Fraction	60%	52%	31%	25%	32%	32%

Table 17: Summary of findings in patients with severe AS and wtATTR

**DPD scintigraphy = Tc-99m-3,3-diphosphono-1,2-propanodicarboxylicacid (DPD) scintigraphy; †SAP scan = serum amyloid-P scan; ‡AVAi = indexed aortic valve area; §AoV = Aortic Valve; ǁLGE pattern = late gadolinium enhancement pattern; #LV = left ventricular.*

6.1.5.2 Clinical Assessment of patients with amyloid

Clinical evaluation of the six patients with amyloid was scheduled at the National Amyloidosis Centre, UK, but two patients died prior to their appointment. Assessment revealed carpal tunnel syndrome in one patient but no other extra-cardiac manifestations, which is typically the case. AL amyloidosis was excluded in all cases. Summary findings are shown in Table 17.

6.1.5.3 Multimodality Imaging

Figure 45 and Figure 46 summarize the findings of multimodality imaging.

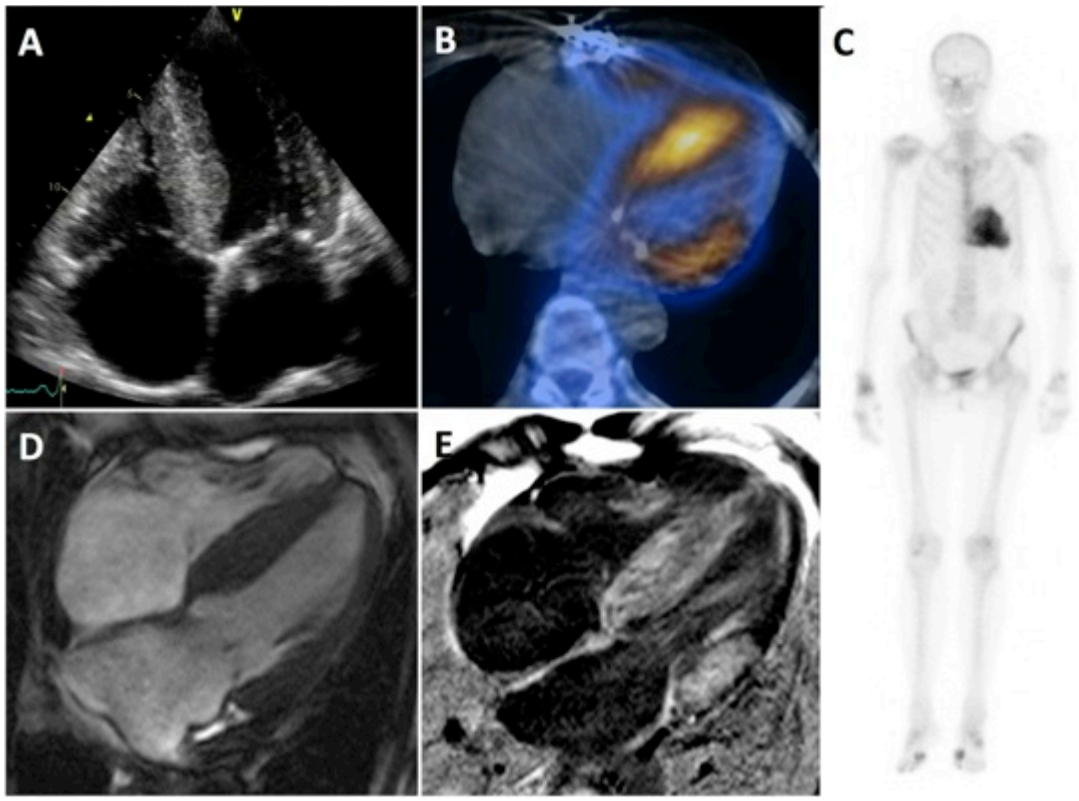

Figure 45: Patient with clinical features of cardiac amyloidosis.

Although the echocardiogram showed LVH (B), this was attributed to the myocardial response to severe AS. DPD scintigraphy showed Perugini Grade 2 cardiac uptake on bone scan (C) and SPECT (B). CMR showed overt LVH and impaired systolic function (D), and transmural LGE with higher signal from the myocardium then the blood pool (E).

Echocardiography. Pre-operative routine transthoracic echocardiography did not raise any suspicion of amyloid among the 6 patients in whom amyloid was identified histologically, and were consistent with severe AS by indexed valve area (mean AVAi 0.41±0.17cm^2/m^2) and/or transvalvular peak velocity (4.3±0.6 m/s). Clinical reporting identified significant concentric left ventricular hypertrophy (LVH) with

impaired longitudinal shortening and diastolic dysfunction in 3 out of 6 patients but this was attributed to AS afterload. No suspicion of a dual pathology was raised. Retrospective analysis of global longitudinal strain (GLS; not performed routinely in our clinical AS work-up) was markedly reduced GLS in patient 1 and 2 (-6.4% and -11.6%, respectively), but could only be obtained in a minority of patients in our cohort due to poor endocardial wall definition in many patients (Table 17).

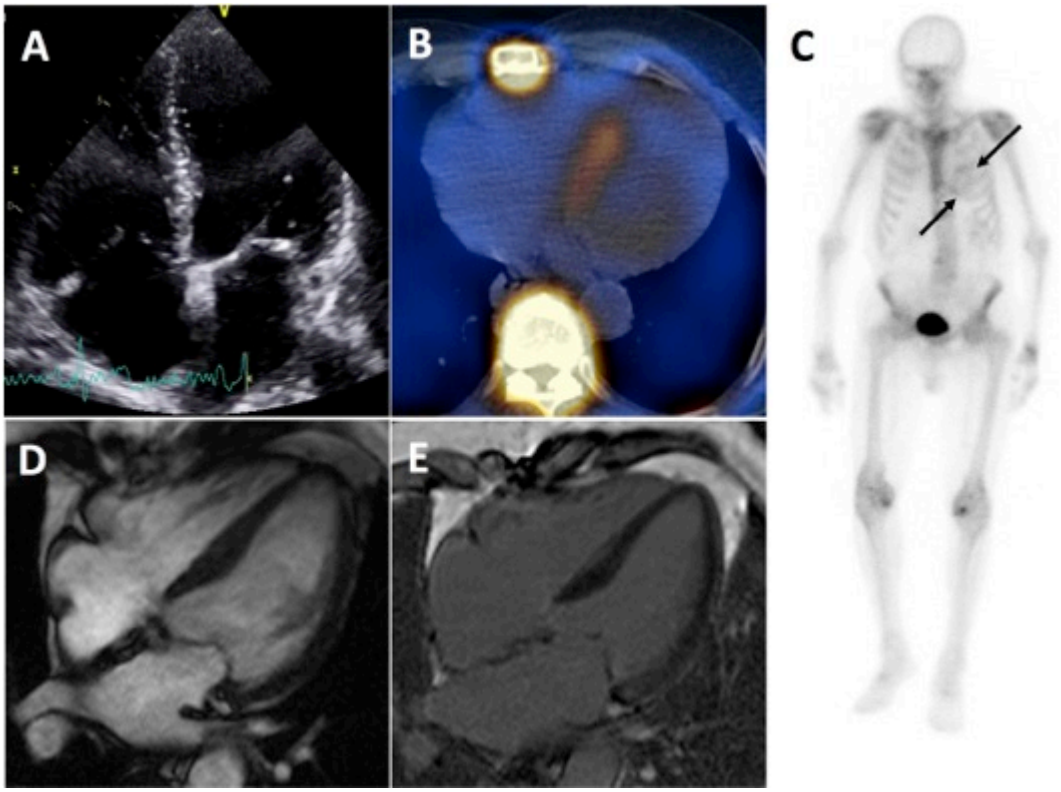

Figure 46: Patient with amyloid deposits on biopsy but no clinical features.

Neither pre-operative echocardiogram nor CMR highlighted any features consistent with cardiac amyloidosis. DPD scintigraphy showed Perugini Grade 1 cardiac uptake on bone scan (C – there is subtle uptake in the basal third of the left ventricle [see arrows]), which is more obvious on SPECT (B). There was no LVH and good LV systolic function on CMR cine imaging (D), and only subtle patchy, non-ischemic LGE in the basal lateral wall (E).

CMR. In two patients, the pre-operative research multiparametric CMR study identified the dual pathology of AS and cardiac amyloidosis. This was based on the combination of severe LV hypertrophy out of proportion for the degree of AS, and (more definitively) tissue characterization findings of cardiac amyloid (global transmural late gadolinium enhancement with blood pool nulling after the myocardium on the TI scout, elevated native myocardial T1 (here >5SD above normal) and ECV >50%). These research findings were communicated to the

surgical team but a multidisciplinary decision was made to proceed with AVR and to conduct further evaluation of amyloidosis afterwards (patients 1 and 2, table 2). The myocardial contraction fraction (MCF) was also markedly reduced in both these patients (25% and 33%, respective) despite preserved LVEF; in the other four patients, MCF fell within one SD of the overall AS cohort (53±13%; see Table 17).

DPD Scintigraphy. DPD bone scintigraphy was performed in the four surviving patients during the post-operative amyloid evaluation and was positive in all cases, with Perugini Grade 2 uptake in both patients with features of amyloidosis on CMR, and Perugini Grade 1 uptake in the two without.

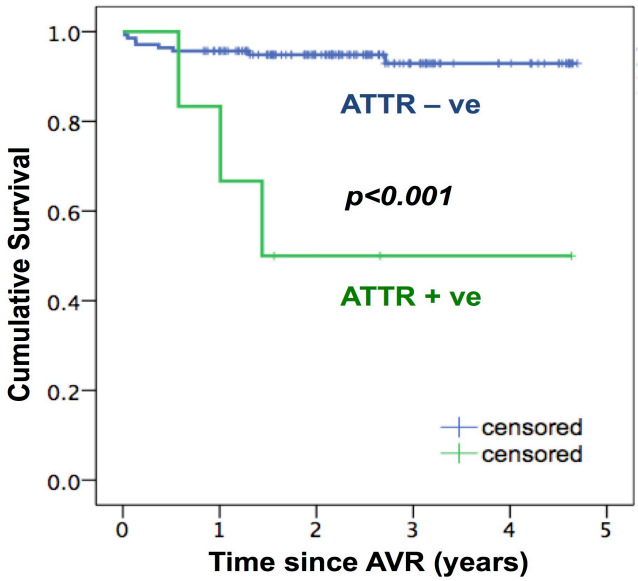

Figure 47: Outcome with occult amyloid

Kaplan-Meier plot of cumulative survival comparing aortic stenosis patients (n=146) with ATTR amyloid on myocardial biopsy and those without. At median follow-up of 2.3 years (0.02-4.7 years), 11 patients with calcific aortic stenosis (AS) had died whereas all patients with bicuspid AS were alive. Three out of six cAS with wild-type ATTR amyloid (50%) died compared to 8 out of 106 (7.5%) in the remaining calcific AS cohort.

6.1.5.4 Outcome

As of 31st of December 2015, at median follow-up of 2.3 years (0.02-4.7 years), 11 cAS patients had died whereas all of the bAS patients were alive. Three out of six cAS with wtATTR (50%) died compared to 8 out of 106 (7.5%) in the remaining cAS cohort, 7 out of 101 (6.9%) in those over the age of 65, and 8 out of 140 (5.7%) in overall cohort (Figure 51). Of all parameters assessed, the presence of ATTR amyloid had the highest hazard ratio for death (HR 9.5 [2.5-35.8], p=0.001, univariable Cox regression analysis, see Table 24).

	cAS and bAS (n=146) HR (95%CI)	*p-value*	cAS only (n=112) HR (95%CI)	*p-value*
ATTR amyloid deposits	9.5 (2.5-35.8)	***0.001***	6.5 (1.7-24.7)	***0.006***
Age (years)	1.1 (1.02-1.23)	***0.02***	1.1 (1.0-1.2)	0.18
Gender	1.8 (0.5-6.9)	0.37	1.9 (0.5-7.2)	0.34
Aortic Valve				
Peak Velocity (m/sec)	0.5 (0.2-1.1)	0.09	0.5 (0.2-1.2)	0.11
Mean Gradient (mmHg)	0.96 (0.92-1.00)	0.06	0.96 (0.92-1.00)	0.07
Area, indexed (cm/m^2)	0.42 (0.01-23.2)	0.7	0.6 (0.01-39.7)	0.8
CMR parameters				
LVEF (%)	0.97 (0.94-1.00)	0.07	0.97 (0.94-1.01)	0.1
LV mass, indexed (g/m^2)	1.03 (1.00-1.52)	***0.05***	1.03 (1.01-1.06)	***0.02***
Myocardial Contraction Fraction (%)	0.04 (0.001-1.74)	0.1	0.07 (0.002-2.45)	0.14
Blood parameters				
NT-proBNP, pmol/L	2.1 (1.3-3.6)	***0.004***	2.2 (1.2-4.0)	***0.006***
eGFR, ml/min/1.73 m^2	0.99 (0.97-1.03)	0.8	1.0 (0.9-1.0)	0.7

Table 18: Univariate Predictors of Outcome.

At median follow-up of 2.3 years (0.02-4.7 years), 11 calcific aortic stenosis (cAS) patients had died whereas all of the bicuspid aortic stenosis (bAS) patients were alive. Of all parameters assessed, the presence of ATTR amyloid had the highest hazard ratio for death (HR 9.5 [2.5-35.8], p=0.001, univariable Cox regression analysis).

6.1.6 Discussion

In this single centre study of 146 severe AS undergoing surgery, to which 70% of all patients undergoing surgery were recruited, cardiac amyloid deposits were found at biopsy in 6 cases. All had wild-type ATTR (formerly senile systemic) amyloidosis. The youngest was 69, and all had calcific AS indicating a 6% prevalence of amyloid among this latter group. Comprehensive imaging was performed which showed a diagnostic hierarchy with non-contributory echocardiography, CMR detecting a third of cases, and cardiac DPD scintigraphy positive in all four patients who had this latter investigation. Biopsy showing wtATTR amyloid deposits was prognostic and its presence was the strongest predictor of adverse outcome after surgical aortic valve replacement – suggesting that the presence of cardiac amyloid is a disease modifier in AS. Two aspects of the coexistence of wtATTR and AS stand out: incorrect interpretation of the severity of AS, and modification of outcome. First, wtATTR amyloid in patients with moderate AS may cause severe hypertrophy and

LV impairment, which can be misdiagnosed as severe AS (as low-flow-low-gradient). This was highlighted by Rapezzi *et. al.* in a recent communication [248], who presented data on 43 elderly cAS patient with at least 1 "red flag" on echocardiography, performed DPD on 5 patients identified in this way (all positive) and confirmed diagnosis of wtATTR amyloid through biopsy and genotyping. Second, rather than leading to a misdiagnosis of severe AS, wtATTR amyloid may be a disease modifier, which exhibits a more severe phenotype with more heart failure and arrhythmias, and possibly amyloid involvement of other organ systems.

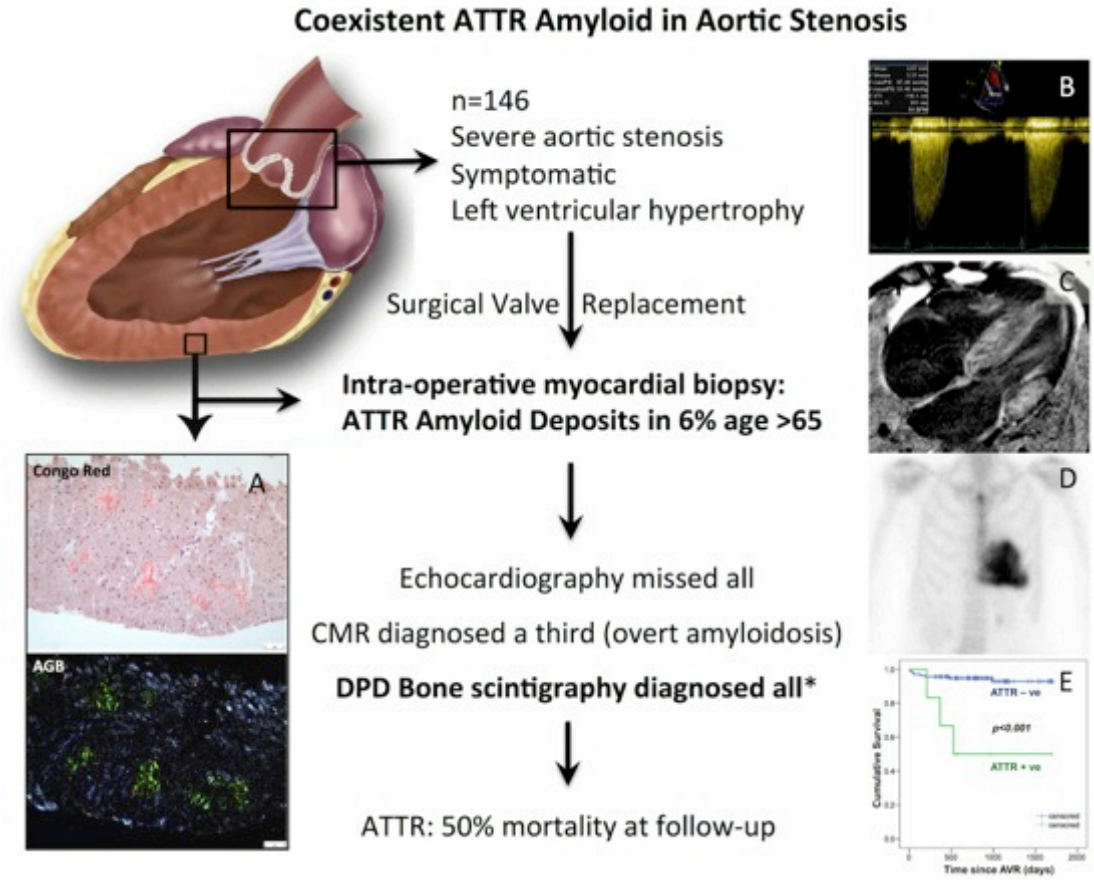

Figure 48: Coexistent ATTR amyloid in severe aortic stenosis.

*Wild-type transthyretin cardiac amyloid (wtATTR) is a disorder of ageing individuals, and therefore may coexist in elderly patient with aortic stenosis (AS). Invasive diagnosis (A) of wtATTR is made by cardiac biopsy (stained with Congo red showing typical apple green birefringence [AGB]). In this study of 146 patients with severe AS undergoing surgical aortic valve replacement, coexistent wtATTR amyloid was found in 6% of elderly (age >65). Although echocardiography (B) was key for diagnosis and grading of AS, it was non-contributory for the diagnosis of ATTR. Cardiac magnetic resonance (CMR) detected a third of cases (C), and cardiac scintigraphy with bone tracers (D) was diagnostic in all four patients studied (*two died prior). Dual pathology appeared to modify outcome (E) and may lead to incorrect interpretation of the severity of AS (Note: Cardiac figure adapted from Barone-Rochette JACC 2015 for illustration).*

6.1.6.1 Implications for management of Aortic Stenosis

Identification of cardiac amyloid is important for many reasons. The presentation of amyloid (LVH and diastolic then systolic function dysfunction) has substantial overlap with the changes of AS, particularly as systemic features are limited with only carpal tunnel syndrome as a common red flag [262]. Other traditional red flags (pericardial effusion, aortic valve thickening, concentric hypertrophy) are common in severe, symptomatic AS. Whilst it is possible that minor cardiac amyloid deposits might have no significant consequences in many individuals, the clinical syndromes caused by cardiac amyloid deposition of sufficient magnitude, i.e. overt cardiac amyloidosis of both ATTR and AL types, have a very poor prognosis from just months to a few years. Accurate typing of amyloid is essential since chemotherapy directed towards the plasma cell dyscrasias underlying AL amyloidosis can prolong life, and several specific therapies for ATTR amyloidosis are now at late stage of clinical development [254, 255]. The consequences of isolated sub-clinical cardiac wtATTR amyloid deposits are unknown; here we focus on wtATTR and severe AS. Possible changes in clinical management could include minimizing bypass time during open valve surgery (e.g. by using rapid deployment valves), switching to TAVI and influence the fundamental decision regarding medical management versus intervention [263]. Interestingly, perioperative mortality was not affected by the presence of wtATTR. In addition, although there are few systematic data, clinical experience has suggested avoiding calcium channel blockers and digoxin in the presence of cardiac amyloid.

6.1.6.2 ATTR amyloid and Heart Failure

Wild-type ATTR amyloid is emerging as an unrecognized, important bystander and potential disease modifier not only in AS but also in Hypertrophic Cardiomyopathy (HCM) and Heart Failure with preserved Ejection Fraction (HFpEF). Historically the requirement for histology has been a major obstacle to elucidating the significance of cardiac ATTR amyloid, but the remarkable diagnostic capability of non-invasive bone scintigraphy has lately yielded much new information. A large Italian non-selective endomyocardial biopsy study (n=4221 over 28 years) found amyloid 4% of cases [264]. More specific studies investigated autopsy specimens in a TAVI cohort in which amyloid was present in 5 out of 17 cases and thought to have contributed to progressive heart failure and the deaths of 3 patients [249], and examination of 95 specimens obtained at septal myectomy for LV outflow tract obstruction with

congenital or acquired aortic stenosis in which 7% contained ATTR amyloid deposits [265]. Cardiac amyloidosis is also a differential diagnosis for hypertrophic cardiomyopathy, especially in patients with predominantly basal involvement and outflow tract obstruction. Incidental deposits of amyloid have been reported in 1% of surgical septal myectomy specimens from patients with HCM [266, 267]. Mohammed *et. al.* reported 17% prevalence of ATTR amyloid in HFpEF patients on autopsy with a substantial (80%) male predominance [268]. In contrast to this series and the wider clinical impression, half of the patients with amyloid in our cohort were female; this was also a finding in a recent cohort of HFpEF patients who were studied with DPD scintigraphy [269], suggesting that the incidence may be underestimated in females generally, possibly due to a lower frequency of extreme hypertrophy that serves as the main red flag.

6.1.6.3 Relative strength of imaging modalities to identify amyloid

Comprehensive imaging here showed a diagnostic hierarchy comprising non-contributory echocardiography, CMR detecting a third of cases, and bone scintigraphy being diagnostic in all four patients studied. Bone scintigraphy (^{99m}Tc-DPD or ^{99m}Tc-PYP)[172, 270] is an attractive, low cost modality with high sensitivity and specificity for cardiac ATTR amyloid. It is more practicable than cardiac biopsy for exclusion of ATTR amyloid in HCM, HFpEF and AS, and its sensitivity for occult ATTR amyloid appears to be greater than CMR. Focal myocardial uptake of these tracers may occur transiently following myocardial infarction, and diffuse uptake does occur in a small proportion of patients with cardiac amyloid of AL type.

6.1.7 Limitations

Our study has limitations: patients were recruited from a single cardiothoracic centre. The entry criterion was surgical AVR with no CMR contraindications leading to some under-representation of older patients (undergoing TAVI instead of sAVR), renal impairment and pacemaker patients (though in reality only 18 patients were excluded due to pacemaker [n=8] or eGFR<30 [n=10]). With a recruitment rate of 76% of all sAVR performed for AS (81% had myocardial biopsy), the RELIEF-AS study was indeed representative of a surgical AVR cohort in a major UK cardiothoracic centre. DPD/PYP bone scintigraphy was not performed in all-comers due to limited availability at our centre at the start of the study, but should be part of any future studies. It is possible that other patients with wtATTR amyloid may have

died before their AS had been deemed severe enough to warrant intervention. Our echocardiographic analysis did not include strain rate imaging consistently (apically spared impaired longitudinal strain is characteristic of amyloid) – the markedly reduced GLS in two patients could have raised red flags at time of echocardiography. Finally, the study did not include a large proportion of Afro-Caribbean individuals, 3-4% of whom possess the transthyretin V122I variant [271] that causes hereditary cardiac ATTR amyloidosis and up to 10% of hospital admissions for heart failure in this ethnic group in South London [272].

6.1.8 Future outlook

The prevalence and adverse clinical outcomes here suggest that wtATTR amyloid is important in elderly individuals with AS. More work is needed. TAVI is mostly performed in older age, where there is greater risk, worse renal function and more heart failure (reflected by higher EuroScore II and STS score). Biopsy for amyloid is not practicable but bone tracer scintigraphy could be used. The data here suggests it could have a routine role in selected patients and influencing their management in terms of decisions surrounding intervention, procedure performance and specific amyloid therapies. Wider use of cardiac scintigraphy with bone tracers, by detecting early amyloid, is likely also to improve our understanding of conventional testing, such as echocardiography.

6.1.9 Conclusion

Six percent of patients over the age of 65 undergoing surgical AVR for cAS had wtATTR amyloid deposits on cardiac biopsy, which was associated with poor outcome. There appears to be a hierarchy of imaging diagnostic performance for identification of wtATTR amyloid, with DPD bone tracer scintigraphy superior to CMR, which was superior to echocardiography.

Chapter 7 Results 3: Myocardial Fibrosis by CMR and Histology

7.1.1 Preface

With the work described in this chapter I won the Early Career Award (Translation) at the 20th Annual Meeting of SCMR, Washington DC, 2017, and is based on the publication below:

**Thomas A. Treibel, *Begoña López, *Arantxa González, Katia Menacho, Rebecca S. Schofield, Susana Ravassa, Marianna Fontana, Steven K. White, Carmelo DiSalvo, Neil Roberts, Michael T. Ashworth, Javier Díez, James C. Moon; Reappraising myocardial fibrosis in severe aortic stenosis: an invasive and non-invasive study in 133 patients. Eur Heart J 2017 ehx353. doi: 10.1093/eurheartj/ehx353. *equal contribution.*

This work is the result of a collaboration with Prof Javier Diez, Dr Arantxa Gonzalez and Dr Begona Lopez, CIMA, Pamplona, Spain. I conceived this study, recruited and scanned all the patients, collected 90% of the myocardial biopsies in theatre, coordinated the image and histological analysis. Rebecca Kozor performed the LV volume and function analysis. Rebecca Schofield performed the LGE analysis. Together with Dr Arantxa González and Dr Begoña López, I performed the statistical analysis and wrote the manuscript. I also discovered the gradient of fibrosis and thickening of the endocardium during research visits to Pamplona, Spain. Dr Katia Menacho, María González and Sonia Martínez performed the collagen volume fraction analysis and measurement of the endocardial thickness.

7.1.2 Introduction

In aortic stenosis (AS), patient symptoms and outcome are determined by the severity of the valve stenosis, but also by the myocardial response, particularly myocardial fibrosis (MF). Pathophysiologically, the myocardium is assessed histologically on tissue samples. It is believed that a complex interplay of cellular changes (including hypertrophy and cell death by apoptosis or autophagy), microvascular ischaemia, and alterations of the extracellular matrix occurs with final common pathways leading to MF. Most of the evidence for this has been from a few small biopsy or autopsy studies. Whereas autopsy descriptions of MF can provide a global view, in *in-vivo* studies, sampling is limited by biopsy size, and fibrosis is typically described only by the quantity of collagen deposition (collagen volume fraction, CVF). However, histological analysis of heart tissue also allows differentiation of fibrosis subtypes based on location and morphological characteristics of collagen deposits (focal microscopic scars, diffuse interstitial and perivascular strands), with the functional impact of MF not only depending on the

amount of collagen tissue, but also on the characteristics of collagen deposits [273]. Although new insights are being generated by imaging tissue characterisation (the late gadolinium enhancement [LGE] technique permits quantification of focal interstitial expansion [33, 55, 58, 103, 274], and diffuse interstitial expansion can be measured by extracellular volume fraction [ECV][109, 110, 120, 121]) the histological basis of LGE and ECV in AS and their association with fibrosis subtypes are only partly understood.

7.1.3 Aims

We investigated myocardial fibrosis (MF) in a large series of severe aortic stenosis (AS) patients using invasive biopsy and non-invasive imaging. We simultaneously and at scale assessed cardiac status in severe symptomatic AS patients by measuring functional capacity and blood biomarkers (cardiomyocyte stress/damage markers), by imaging structure and function (echocardiography and CMR), and by performing non-invasive (ECV and LGE) and histological (fibrosis location, pattern and CVF) tissue characterisation.

7.1.4 Methods

7.1.4.1 Study Cohort

Details of AS patients are as described before. Control myocardial samples were obtained from autopsies of 10 subjects (7 male, 3 female; all Caucasian, age: 60±7 years) who died of non-cardiovascular causes with no macroscopic and microscopic cardiac lesions.

7.1.4.2 Cardiac Imaging

Details of imaging acquisition by echocardiography and CMR as well as the imaging analysis have been described previously.

7.1.4.3 Histomorphological Studies

Biopsies were harvested under direct vision from the basal anteroseptum when the native valve was removed by one of six surgeons using either a 14-gauge coaxial needle system (Temno evolution, Carefusion, USA) or a surgical scalpel, as per surgeon's choice (as per ethics) and fixed in 10% buffered formalin and embedded in paraffin. Histological analysis was performed blinded to clinical and imaging data. For MF, the fraction of myocardial volume with positive staining for collagen, CVF, was determined by quantitative morphometry (Cell^D, Olympus Soft imaging

Solutions GmbH, Münster, Germany) in sections stained with collagen-specific picrosirius red. All available myocardial tissue was analysed (average area was 5.21±3.62 mm^2/sample)[109]. Endocardial thickness was quantified as the mean value of 5 to 15 measurements.

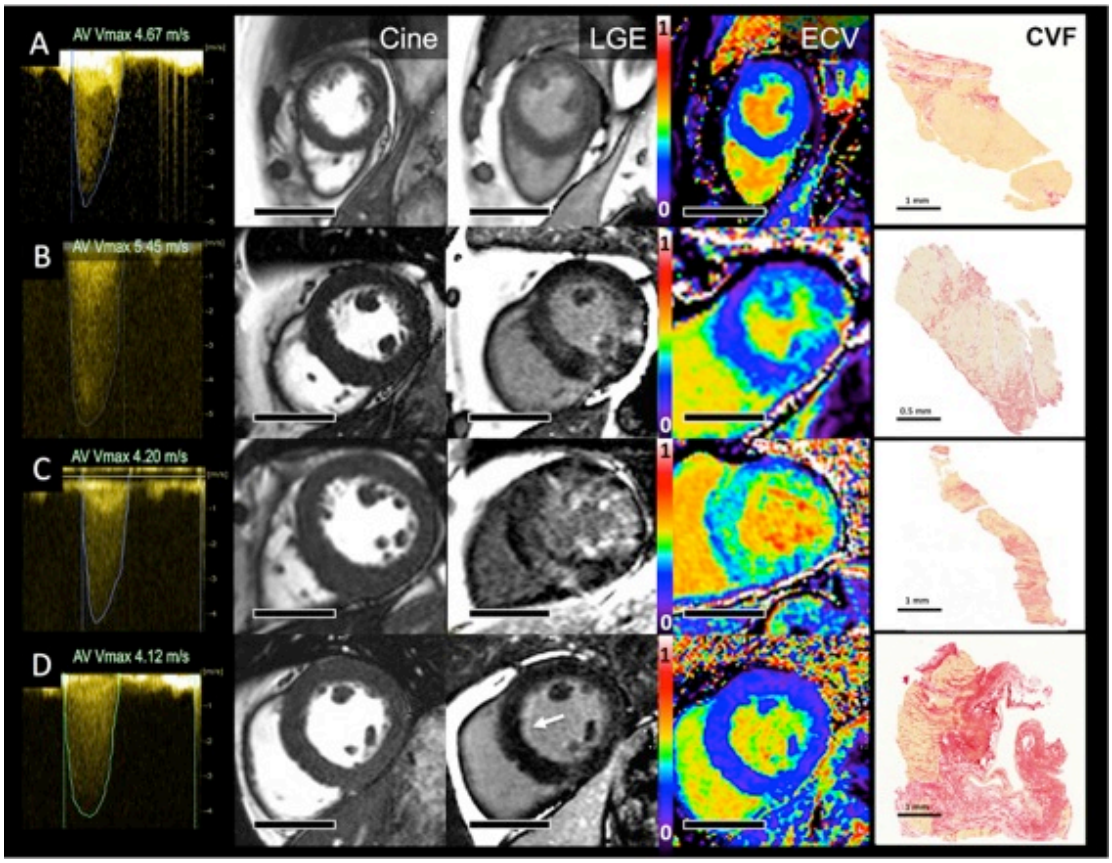

Figure 49: AS, myocardial hypertrophy and fibrosis by imaging and biopsy.

Four exemplar patients with symptomatic severe aortic stenosis (AS) showing continuous-wave Doppler echocardiography recordings through the aortic valve with maximum velocities >4m/s (AV Vmax, column 1), short axis SSFP cine stills in the left ventricular short axis demonstrating degrees of left ventricular hypertrophy (Cine; column 2), matching late gadolinium enhancement images (LGE, column 3), matching extracellular volume fraction images of the same short axis view (ECV, column 4), myocardial biopsy obtained during valve replacement and stained with picrosirus red (CVF, column 5). Patient A has minimal LVH, no LGE, an ECV of 28.4% and minimal subendocardial fibrosis on biopsy (CVF 4.6%). Patient B has concentric LVH, patchy non-ischemic LGE, an ECV of 29.9% and moderate fibrosis on biopsy (CVF 19.3%). Patient C has concentric LVH, widespread non-ischemic LGE, an ECV of 36.5%, and severe fibrosis on biopsy (CVF 24.5%). Patient D has mild concentric LVH, subtle subendocardial LGE (white arrow), an ECV of 24.5%, thickened endocardium and subendocardial scarring. Scale bars in the CMR imaging in columns 2-4 are equivalent to 5 cm; the scale bars in the histology column are indicated in the image.

7.1.4.4 Statistical Analysis

As described in the main methods section 3.8. Log transformation was applied to normalise NT-proBNP and hs-TnT. The influence of potential confounding factors

(age, gender, history of coronary artery disease) used multivariate linear regression analysis.

7.1.5 Results

7.1.5.1 Baseline Characteristics

The 133 patients with biopsy and no exclusion (cardiac amyloidosis n=6; Fabry Disease n=1) are shown in Table 14 [234].

7.1.5.2 Non-Invasive Assessment by CMR

Focal fibrosis, measured by LGE, was commonly seen, affecting 71% of men and 46% of women, with a similar split in ischemic vs non-ischemic split (males 19% vs 59%; females 13% vs 37% - some had both). The pattern of non-ischemic LGE was patchy mid-myocardial (18%), RV insertion point (60%), papillary muscle (19%) and/or patchy focal (26%). Mean enhanced LV myocardial mass was 14.3±11.2 g (median 10.5 g; IQR 6.0-20.3 g). Extracellular volume fraction was 28.4±2.9%.

7.1.5.3 Invasive Assessment by Biopsy

There were 53 myocardial biopsies with endocardium (60% from scalpel versus 29% from needle biopsies; $p<0.01$) and 80 samples with no identifiable endocardium. The endocardium was thickened due to collagen deposition in most biopsies, with a mean endocardial thickness of 228±129 microns versus 40±16 microns in the control samples ($p<0.001$; Figure 50A). Subendocardial fibrosis was caused predominantly by microscars, whereas midmyocardial fibrosis was due to interstitial bands preferentially located around cardiomyocytes (Figure 50B).

CVF was elevated in severe AS (11.5±8.6% vs 1.95±0.20% controls, $p<0.001$) and was higher in men than in women (12.9±8.8 vs 9.9±8.0%, $p<0.05$). Biopsies with endocardium showed higher CVF than biopsies without endocardium (15.0±12% vs 8.99±6.7% $p<0.001$*;* Figure 3). Segmental analysis of endocardium-containing biopsies (in those structurally feasible; n=40) revealed a decreasing gradient of fibrosis from the endocardium, (20.4±11.3% vs 15.2±8.7% vs 13.0±7.8%, $p<0.001$ and $p<0.05$ respectively*; p for trend*<0.01; Figure 51).

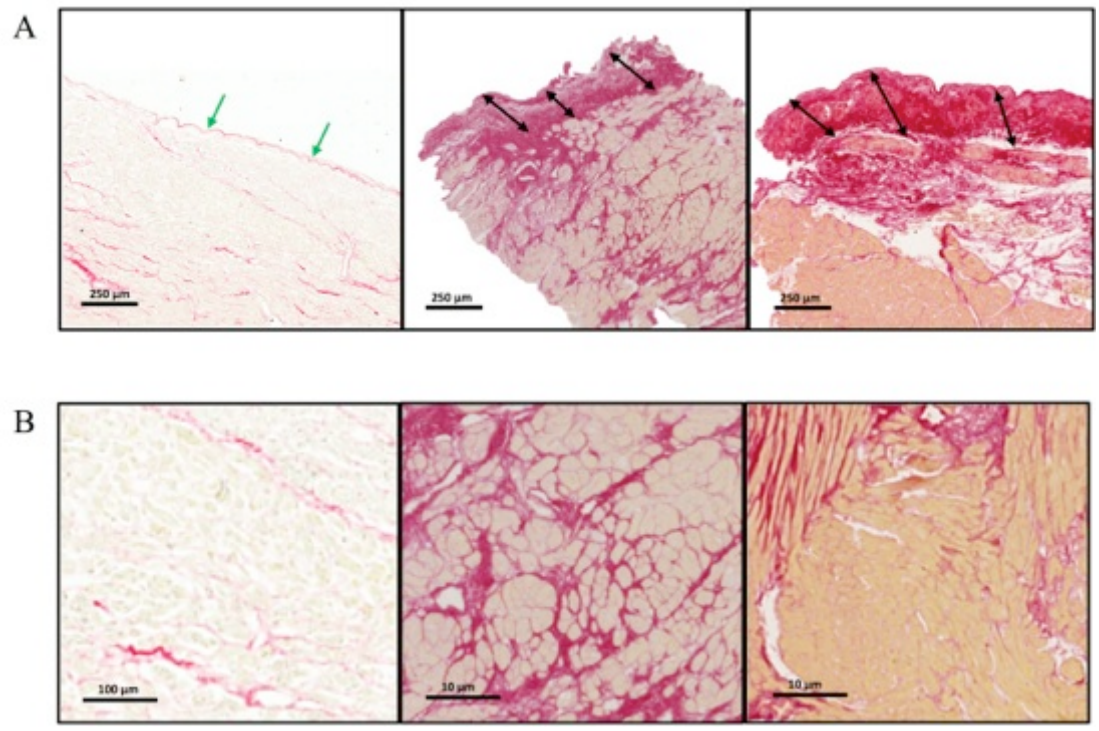

Figure 50: Patterns of fibrosis on histology

A- Representative images of endocardial thickness in one control subject (left panel) and in two aortic stenosis patients in picrosirius red-stained sections. The green arrows point to the endocardium in the control sample. The black arrows show the thickness of the endocardium in AS patients. B- Detail showing interstitial fibrosis in the subendocardial region of one control subject (left panel) and microscars and interstitial fibrosis in two aortic stenosis patients in picrosirius red-stained sections.

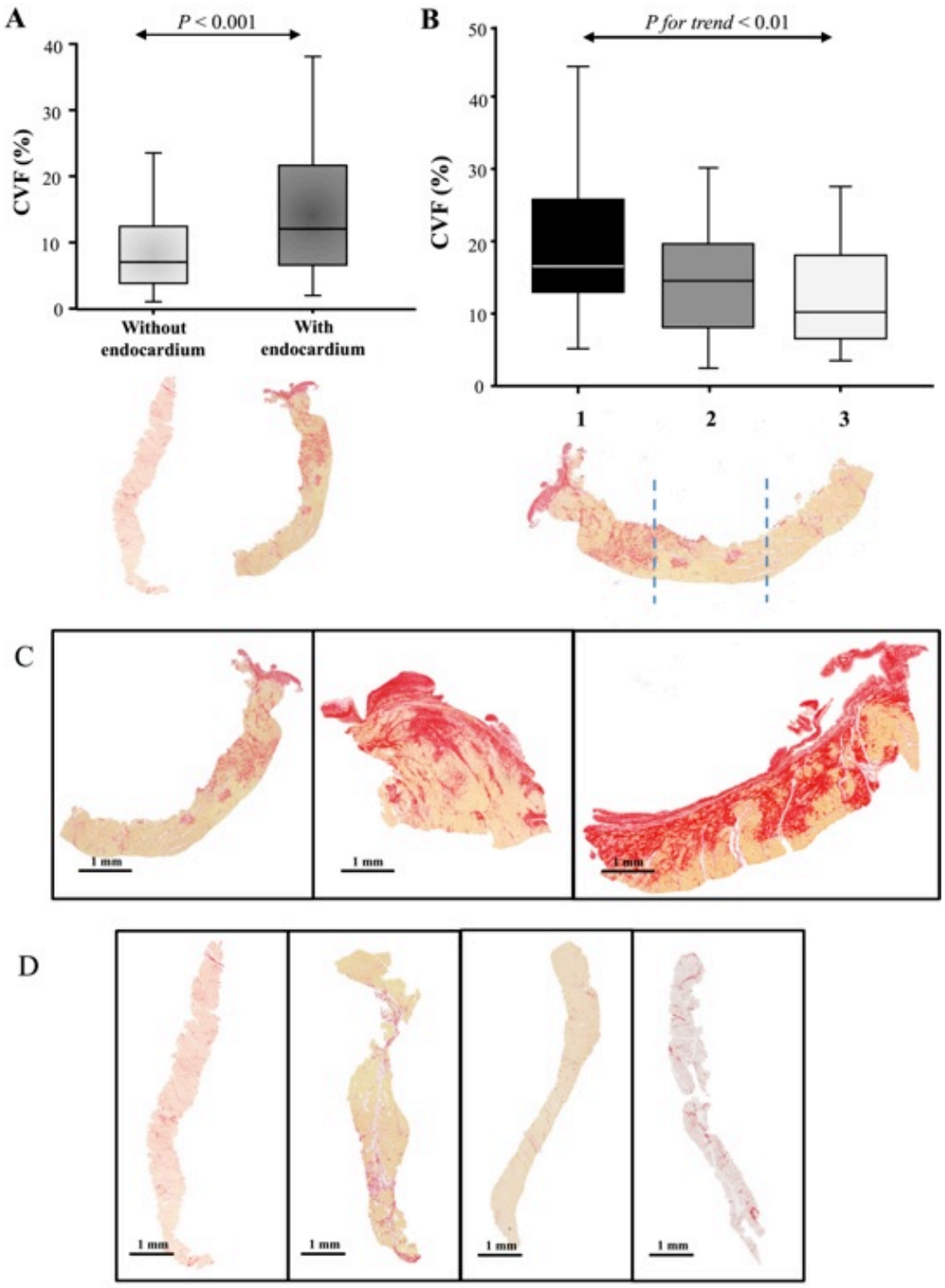

Figure 51: Biopsies with endocardium showing a gradient of fibrosis.

A- Collagen volume fraction in biopsies with and without endocardium. B- Collagen volume fraction in samples with endocardium divided in tertiles. Box plots show the 5th and 95th (vertical lines), 25th and 75th (boxes) and 50th (horizontal line) percentile values for collagen volume fraction. C- Representative images of 3 biopsies with endocardium (left panel needle and middle and right panel scalpel). D- Representative images of 4 biopsies without endocardium (needle).

7.1.5.4 Analysis of Associations

LGE quantification correlated with CVF in all samples (r=0.50, $p<0.001$), but this association was stronger in endocardial containing samples (r=0.71, $p<0.001$; Figure 52). These associations were independent of age, gender and history of coronary artery disease.

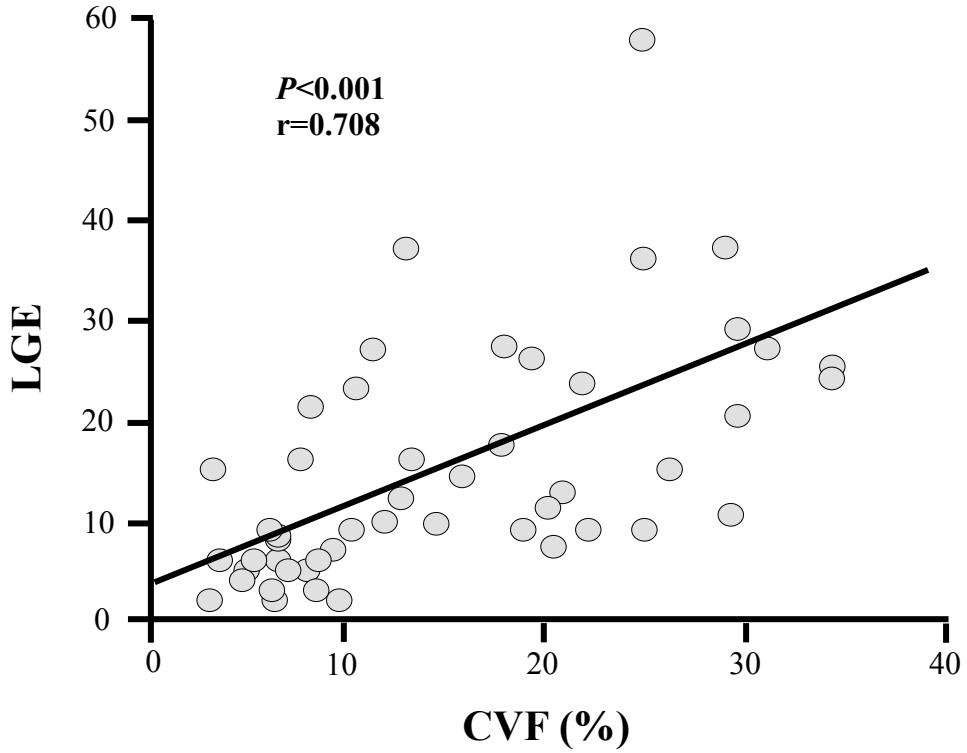

Figure 52: Association of LGE with collagen volume fraction.

Late gadolinium enhancement (LGE) quantified in grams by a three standard deviation method correlated strongest with collagen volume fraction (CVF) in endocardial containing samples (linear fit: y= 0.814x + 3.109).

CVF quantification was weakly associated with NT-proBNP (r=0.24, $p<0.05$) and hs-TnT (r=0.27, $p<0.01$) levels in all patients. The correlation between CVF and NT-proBNP improved slightly when we considered only the endocardial samples (r=0.35, $p<0.05$). These associations were lost when adjusting for confounding factors.

With regards to LV structure and function, both LGE and ECV correlated with LV end-diastolic volume index (LVEDVi; r=0.20, $p<0.05$ and r=0.26, $p<0.01$, respectively), LV end-systolic volume index (LVESVi; r=0.26, $p<0.01$ and r=0.34, $p<0.001$, respectively) and LVEF (r=-0.24, *p<0.01* and r=0.31, *p<0.01*, respectively);

but the associations were only independent of confounding factors for ECV. LGE was independently correlated with LVMi (r=0.30, p<0.01); ECV was not (p=0.06).

With regards to biomarkers, both LGE and ECV were independently correlated with NT-proBNP (r=0.46, p<0.001 and r=0.55, p<0.001, respectively; Figure 53 A-B) and hs-TnT (r=0.45, p<0.001 and r=0.36, p<0.001, respectively; Figure 53 C-D).

AS valve severity did not associate with CVF, endocardial thickness, LGE, ECV, NT-proBNP levels or the degree of LV remodelling. Of LGE, ECV and CVF, only ECV correlated weakly with the patient functional limitation (6-minute-walk test distance [6MWT]; r=-0.21, p<0.05), but this association was lost when adjusting for confounding factors.

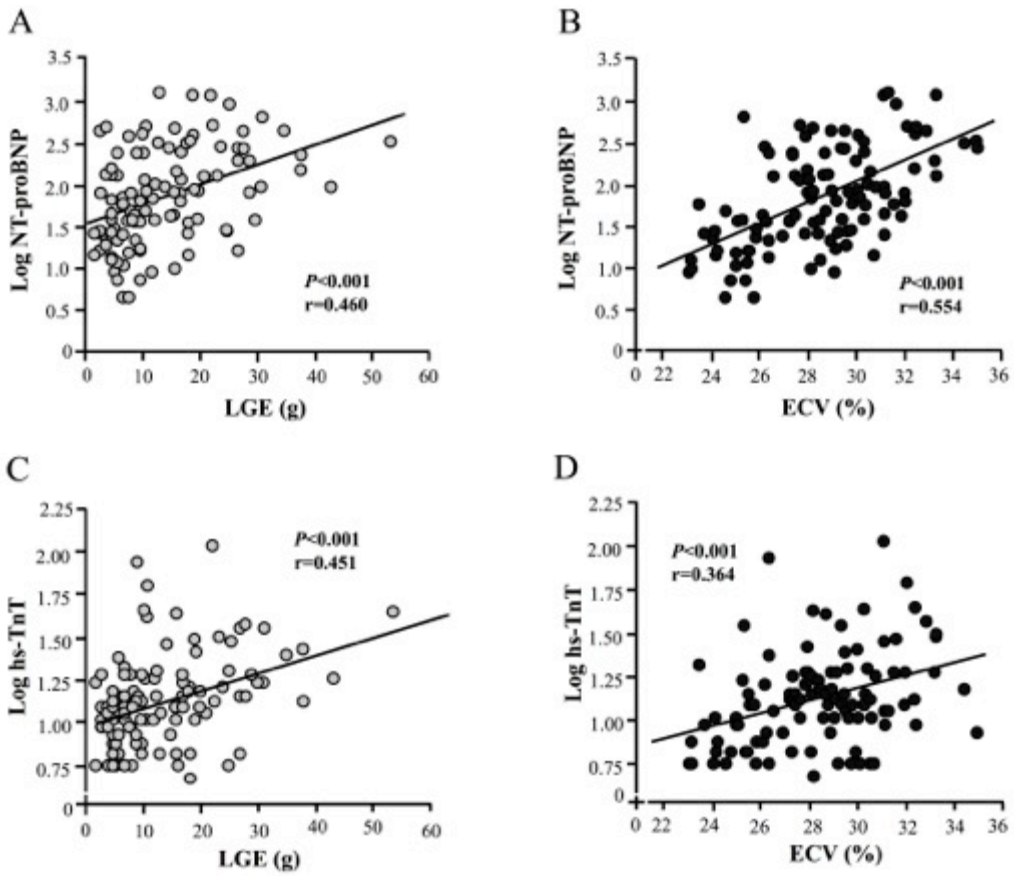

Figure 53: Associations of imaging and blood biomarkers.

Late gadolinium enhancement (LGE) and extracellular volume fraction (ECV) correlated with NT-proBNP (Panels A and B) and with hs-TnT (Panels C and D) (linear fit: A y= 0.119x – 1.498; B y= 0.037x + 0.103; C y= 0.025x + 1.567; D y= 0.110x + 1.008).

	LGE		ECV	
	<10.5 g	**>=10.5 g**	**<28.4%**	**>=28.4%**
	(n=65)	**(n=66)**	**(n=58)**	**(n=58)**
Age (years)	68.8±10.4	71.7±8.8	70.3±10.0	70.1±9.7
Gender (male/female)	28/37	45/21**	34/24	31/27
BMI (kg/m^2)	28.7±5.5	28.2±4.7	27.8±5.0	29.3±5.0
Comorbidities, n (%)				
HTN	44 (68%)	56 (89%)**	43 (75%)	49 (84%)
AF	6 (9%)	13 (20%)	7 (12%)	11 (19%)
CAD	13 (20.3%)	26 (40%)*	17 (29%)	20 (34%)
Symptom, n (%)				
Syncope	6 (9%)	4 (6%)	6 (10%)	4 (7%)
NYHA				
I	8 (12%)	9 (14%)	8 (14%)	5 (9%) *
II	33 (51%)	28 (42%)	34 (59%)	24 (41%)
III	17 (26%)	23 (35%)	13 (22%)	21 (36%)
IV	2 (3%)	2 (3%)	0 (0%)	4 (7%)
Chest pain				
0	41 (63%)	39 (59%)	35 (60%)	37 (64%)
1	3 (5%)	7 (11%)	5 (9%)	5 (9%)
2	15 (23%)	8 (12%)	12 (21%)	4 (7%)
3	4 (6%)	5 (8%)	4 (7%)	5 (9%)
Valve type, bi/tri (n)	20/45	18/48	16/42	17/41
AVAi (cm^2/m^2)	0.41±0.14	0.40±0.13	0.42±0.15	0.39±0.11
Mean gradient (mmHg)	44.8±11.9	47.8±14.7	47.1±14	44.8±13
Mitral regurgitation (%)	7.4±11.2	15.2±14.3*	9.1±12.7	11.5±12.9
EDVi (mL/m^2)	63.2±20.9	70.2±21.9*	61.0±19.1	71.4±24.7*
ESVi (mL/m^2)	19.0±15.6	25.6±20.7*	16.9±12.0	27.7±23.3**
LVMi (g/m^2)	83.9±27.5	90.7±20.7*	83.7±24.4	91.8±25.6
LVEF (%)	72.4±13.2	67.1±15.4*	73.9±11.4	65.6±17.0**
MAPSE (mm)	10.7±3.5	9.8±3.6	11.0±3.2	9.53±3.7*
LAAi (cm^2/m^2)	12.7±3.3	14.5±4.2**	12.8±3.3	14.4±4.6
E/A	0.91±0.42	1.08±0.58	0.87±0.38	1.10±0.59*
DT (ms)	245±69	227±82	236±72	237±81
E/e'	13.57±6.28	13.94±6.11	12.46±6.27	14.94±5.96*
6MWT (m)	468±190	412±187	488±145	393±210**
ECV (%)	27.5±2.6	29.5±2.8***	26.0±1.7	30.7±1.8***
LGE (g)	5.84±2.5	22.8±9.9	11.5±9.1	15.4±12.2
CVF (%)	7.3±4.7	15.7±9.8***	10.4±7.5	10.9±8.5
NT-proBNP (pg/mL)	96±139	277±341***	99±154	262±335***
hs-TnT (ng/L)	15±10	21±20**	15±13	21±18*

Table 19: Patients stratified according to LGE or ECV median value.

*LGE means late gadolinium enhancement; ECV, extracellular volume; BMI, body mass index; HTN, hypertension; AF, atrial fibrillation; CAD, coronary arterial disease; EDVi, end-diastolic volume index; ESVi, end-systolic volume index; LVMi, left ventricular mass index; LVEF, left ventricular ejection fraction; MAPSE, Mitral annular plane systolic excursion; LAAi, left atrial area index; E, peak early velocity of the transmitral flow; A, peak late velocity of the transmitral flow; DT, deceleration time; E´, peak early diastolic velocity of the mitral annulus displacement; 6MWT, 6-minute-walk test; bi, bicuspid; tri, tricuspid; AVAi, aortic valve area index; CVF, collagen volume fraction; NT-proBNP, N-terminal pro-brain natriuretic peptide; hs-TnT, high sensitivity troponin T. Values are given as mean ± SD or n (and percentage). *, P<0.05; **, P<0.01; ***, P<0.001 vs. patients with LGE<10.5 or ECV<28.4%, respectively.*

7.1.5.5 Clinical and Structural Impact of LGE and ECV Stratification

To compare LGE and ECV with clinical and structural parameters, we dichotomized the variables (above and below median: 10.5 g for LGE, 28.4% for ECV) with results shown in Table 19. Patients with high versus low LGE had more advanced LV

remodelling with higher LVESVi, LVEDVi, LV mass index, left atrial area index (LAAi), lower LVEF (all $p<0.01$) and more mitral regurgitation ($p<0.05$). High LGE patients had a higher prevalence of hypertension ($p<0.01$) and coronary artery disease ($p<0.05$). In accordance with the association analysis, these patients presented higher CVF values ($p<0.001$), NT-proBNP ($p<0.001$) and hs-TnT ($p<0.01$) levels.

Patients with high vs low ECV also had greater LV remodelling with increased LVEDVi ($p<0.05$), LVESVi ($p<0.01$) and lower LVEF ($p<0.01$). Although the LAAi was not significantly different (p=0.08), diastolic function was worse (E/A and E/e' ratio, $p<0.05$). Moreover they also had an impaired 6MWT and a higher NYHA functional class. In accordance with the association analysis these patients presented higher NT-proBNP ($p<0.001$) and hs-TnT ($p<0.05$) levels.

Combining LGE and ECV added value (Table 20). With increasing abnormality in these parameters, cavity dimensions (LVEDVi, LVESVi, LAAi) increase, LVEF decreases, NT-proBNP and hs-TnT levels increase, CVF increases, and patient functional capacity (6MWT) decreases ($p<0.05$).

	ECV-/LGE-	ECV-/LGE+ & ECV+/LGE-	ECV+/LGE+	*P* for trend
	(n=37)	(n=46)	(n=32)	
Age (years)	68.6±11.0	71.4±9.0	70.4±9.8	
Gender (male/female)	19/18	24/22	22-Oct	
BMI (kg/m^2)	28.3±5.3	28.4±5.4	29.0±4.5	
Comorbidities, n (%)				
HTN	24 (65%)	38 (83%)	29 (91%)	<0.05 c^2=6.41
AF	3 (8%)	7 (15%)	8 (25%)	
CAD	6 (16%)	17 (37%)	13 (41%)	0.063 c^2=5.53
Symptom, n (%)				
Syncope	5 (14%)	2 (4%)	3 (9.7%)	
NYHA				
I	5 (14%)	6 (13%)	2 (6%)	
II	24 (65%)	17 (37%)	16 (50%)	
III	16 (43%)	18 (39%)	10 (31%)	
IV	0 (0%)	2 (4%)	2 (6%)	
Chest pain				
0	23 (62%)	27 (59%)	21 (66%)	
1	2 (5%)	4 (9%)	4 (13%)	
2	9 (24%)	9 (20%)	5 (16%)	
3	1 (3%)	6 (13%)	2 (6%)	
Valve type, bi/tri (n)	Dec-25	Dec-34	Sep-23	
AVAi (cm^2/m^2)	0.42±0.16	0.40±0.12	0.39±0.13	
Mean gradient (mmHg)	45.2±14.1	46.7±11.2	45.8±16.6	
Mitral regurgitation (%)	6.8±12.3	10.3±11.4	15.1±15.2	<0.05
EDVi (mL/m^2)	59.5±20.8	66.8±18.7	73.9±27.2*	<0.01
ESVi (mL/m^2)	15.5±11.3	22.5±17.1	30.5±25.9**	<0.005
LVMi (g/m^2)	81.8±26.5	87.3±26.1	95.7±20.9*	<0.05
LVEF (%)	75.4±9.4	69.0±15.0	63.6±17.4**	<0.005
MAPSE (mm)	11.3±3.2	10.1±3.5	9.2±3.8*	<0.05
LAAi (cm^2/m^2)	12.4±3.3	13.3±3.1	15.6±5.2**	<0.005
E/A	0.84±0.26	0.97±0.54	1.24±0.63**	<0.005
DT (ms)	240±68	243±76	220±88	
E/e'	13.09±6.83	13.04±5.47	15.60±6.51	
6MWT (m)	512±136	420±207	391±188**	<0.05
ECV (%)	25.6±1.6	28.7±2.1	31.2±1.9***	<0.001
LGE (grams)	6.01±2.48	12.64±9.67	23.16±11.22***	<0.001
CVF (%)	7.84±5.01	10.26±8.03	14.45±9.45**	<0.005
NT-proBNP (pg/mL)	60±90	160±189	342±394***	<0.001
hs-TnT (ng/L)	13.5±14.5	17.5±12.2	23.6±20.4**	<0.01

Table 20: Patients stratified according to ECV and LGE combined.

*LGE means late gadolinium enhancement; ECV, extracellular volume; BMI, body mass index; HTN, hypertension; AF, atrial fibrillation; CAD, coronary arterial disease; EDVI, end-diastolic volume index; ESVI, end-systolic volume index; LVMI, left ventricular mass index; LVEF, left ventricular ejection fraction; MAPSE, Mitral annular plane systolic excursion; LAAi, left atrial area index; E, peak early velocity of the transmitral flow; A, peak late velocity of the transmitral flow; DT, deceleration time; E´, peak early diastolic velocity of the mitral annulus displacement; 6MWT, 6-minute-walk test; bi, bicuspid; tri, tricuspid; AVAi, aortic valve area index; CVF, collagen volume fraction; NT-proBNP, N-terminal of pro-brain natriuretic peptide; hs-TnT, high sensitivity troponin T. Values are given as mean ± SD or n (and percentage). *, P<0.05; **, P<0.01; ***, P<0.001 vs patients with ECV-/LGE-*

7.1.6 Discussion

In this, the largest prospective AS biopsy and multimodality imaging/biomarker study to date, the main findings are: (1) Histological assessment of the myocardium in severe AS revealed three patterns of fibrosis: thickened endocardium with a massive fibrotic layer; a fibrosis gradient in the subendomyocardium from superficial to deep regions with abundant microscopic scars; and diffuse interstitial fibrosis. (2) The main parameters here assessed captured different aspects of MF: CVF best captures the transmural gradient of fibrosis and microscars; LGE captures mainly microscars; and ECV appears to capture interstitial changes in the mid-myocardium. (3) The combination of LGE and ECV identified better those AS patients presenting with more adverse LV remodelling, more altered blood biomarkers and histological parameters, and a more reduced functional capacity than each parameter alone. These findings were independent of the presence of CAD.

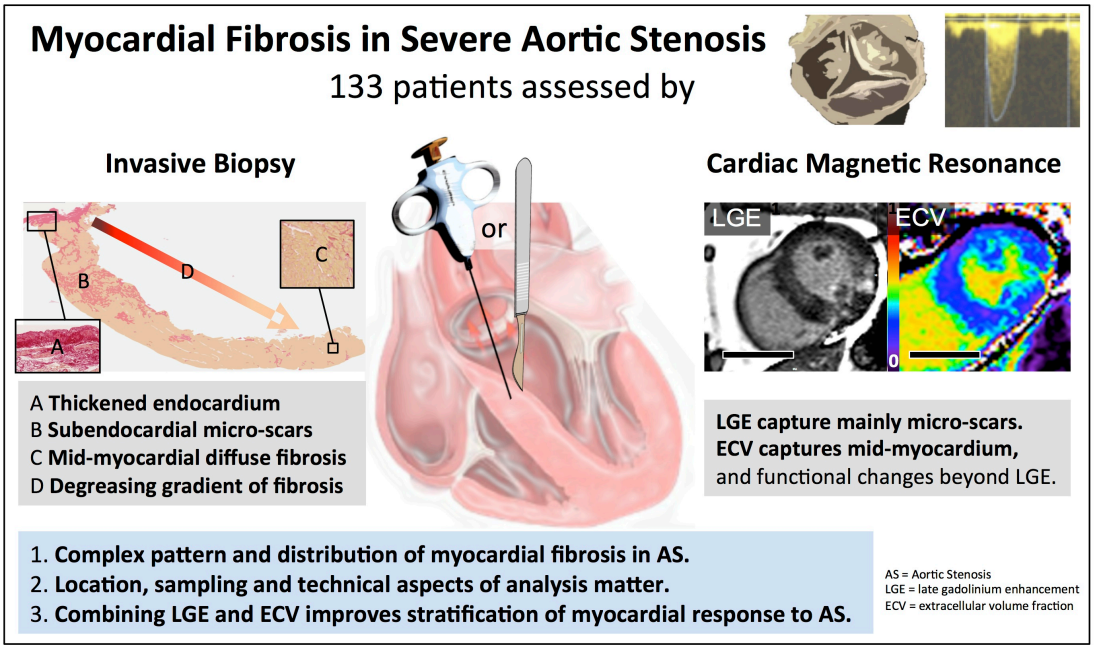

Figure 54: Myocardial fibrosis in AS.

7.1.6.1 Biopsy findings

In the last 40 years, several studies have described MF as histological hallmark of severe AS, documenting relevant clinical correlations and an important prognostic role [58, 273, 275-279]. However, detailed and systematic histological evaluation of the morphological characteristics of MF in severe AS are lacking.

We report the existence of a decreasing collagen gradient from endocardium to the mid-myocardium in severe AS, supporting prior studies [275, 276]. Importantly, the scalpel biopsies showed this better than needle biopsies as they have higher yield of endocardium (needed to orientate the sample).

The different patterns of collagen in severe AS may have different pathogenic mechanisms and possible consequences. Most collagen deposits exist as a thickened endocardial layer and subendocardial scattered microfoci and trabecular fibrosis. Mid-myocardial fibrosis appears as a diffuse network around cardiomyocytes and bundles. The fibrosis gradient may be related to low endocardial perfusion [276], thus reflecting a reparative response (i.e., replacement fibrosis) to ischemia and subsequent cell loss. This is supported by previous findings showing that reduced capillary density, in absolute terms as well as in relation to the number of cardiomyocytes, accompanies MF in patients with severe AS [280]. On the other hand, the diffuse MF located around cardiomyocytes may be reactive to pressure overload-induced mechanical stimulation of local fibroblasts, as well as to paracrine factors produced by mechanically-stressed (strain) cardiomyocytes that, in turn, stimulate fibroblasts (i.e., reactive fibrosis) [281].

7.1.6.2 CMR Findings

CMR tissue characterisation has developed over two decades, initially with the LGE technique for focal fibrosis [33, 55, 58, 103, 274], later with the ECV technique for diffuse fibrosis [109, 110, 119-121]. Combined biopsy and CMR study are rare and limited by small sample size. Instead, myocardial tissue characterisation in AS has been described by presence or absence and pattern of LGE (subendocardial infarct vs mid-wall non-infarct LGE). In the light of these histological findings of thickened endocardium and a gradient of myocardial fibrosis from endo- to epicardium suggest that these descriptive LGE pattern need to be revisited, possibly by utilizing the latest motion-correction or dark blood techniques [282].

Here, LGE correlated with CVF (although the biopsy was obtained from the basal anteroseptum which was not infarcted in any patient), especially on endocardial biopsies (r=0.7), which capture more of the subendocardial microscars. The ECV was only mildly elevated with broadly proportional increase in the cellular and extracellular components of the myocardium (as observed by Schwarz et al in 1978) [275], and, unlike other papers,' did not correlate with CVF. However, ECV is

capturing functionally important consequences, given that patients with high ECV showed worse NT-ProBNP, 6MWT and NYHA functional class [109, 110, 119-121]. There are a number of possible reasons for this discordance with other studies including the underestimation of subendocardial microscar and fibrosis gradient due to avoidance of the endo- and epicardium (for ECV we eroded 10% from the edge to avoid blood pool contamination); recruitment of a less severe (more representative) phenotypes with less extensive scarring (we recruited 50% of all AVR in our institution); reduced capillary density (lower ECV) or compensatory vasodilatation (higher ECV) may confound ECV measurements, which captures all extracellular space including the intravascular plasma [161, 165].

We suspect that LGE is a marker of the reparative fibrotic response to cardiomyocyte injury and loss. On the other hand, diffuse reactive interstitial fibrosis is intimately linked to its local environment and depends on cardiomyocyte function, strain and the cardiomyocyte-fibroblast interaction. ECV may therefore be more closely linked to the cardiomyocyte functional stress, and accordingly could be considered more a measure of cardiomyocyte-interstitial relationship than the current mainstream concept of ECV being a pure interstitial marker.

7.1.6.3 Clinical Impact

MF in severe AS has a characteristic pattern and distribution. When measuring by biopsy or CMR, location, sampling and technical aspects of analysis matter. Invasive biopsy is limited by size and sampling error, whereas LGE and ECV capture different regions of myocardium and provide complementary information. Both ECV and LGE track cardiomyocyte stress (NT-proBNP) and injury (hs-TnT). LGE is known to track troponin concentrations in AS which has been associated with advanced hypertrophy, replacement fibrosis and outcome [283]. Data on BNP vs ECV in AS is lacking. Blood biomarkers reflect “whole heart” cardiomyocyte stress and injury, but need to be interpreted in conjunction with structural and functional parameters from non-invasive imaging, as they can be elevated due to other causes. Imaging biomarkers LGE and ECV offer global but also regional insights. The combination of LGE and ECV – a multi-parametric approach – better identified worse adverse LV remodelling, altered biochemical and histological parameters, and functional capacity than each parameter alone. Timing of aortic

valve intervention is one of the challenges in AS, in particular in asymptomatic patients. Recent focus has turned towards the complex interplay between the degree of the valve stenosis, hemodynamic load and myocardial response. The combination of LGE and ECV may prove to help in a better understanding of this interplay.

7.1.6.4 Strengths and Limitations

This is the largest combined histology-multimodality imaging study in AS, with even sub-groups larger then previous small (n<20) validation studies. The analysis of the imaging and histological data was performed completely blinded by independent groups. To make this study as applicable as possible, we recruited all-comers (50% of all AVR for AS in our institution) rather then the severe end of the spectrum and thereby included patient with CAD, hypertension and diabetes. The effect of CAD was adjusted for as detailed in the methods. Furthermore, the location of the biopsy (basal anteroseptum) was never infarcted in this study. To achieve a standardized biopsy procedure, all biopsies were obtained under direct vision from the basal anteroseptum by a team of experienced surgeons using either a scalpel or needle technique.

7.1.7 Conclusion

In conclusion, this study supports that the combination of invasive and non-invasive techniques at scale is relevant to better characterize MF in severe AS patients. Whereas CVF best captures the transmural gradient of fibrosis and microscars, LGE appears to capture mainly microscars. ECV captures mid-myocardium-related functional changes beyond LGE. Importantly, the combination of LGE and ECV allows a better phenotyping of AS patients according to their myocardial structural and functional response to AS.

Chapter 8 Results 4: Fibrosis Regression after Valve Replacement

8.1.1 Preface

At time of printing of this thesis, a version of this section was under peer review.

***Thomas A Treibel**, Rebecca Kozor, Rebecca Schofield, Giulia Benedetti, Marianna Fontana, Amir Sheikh, Begoña Lopez, Arantxa Gonzalez, Charlotte Manisty, Guy Lloyd, Peter Kellman, Javier Díez, James C Moon. Reverse Myocardial Remodeling in Aortic Stenosis: Cellular Hypertrophy and Diffuse but not Focal Fibrosis Regress Following Aortic Valve Replacement*

My contribution was recruiting, consenting and performing the scans of all patients. I performed the T1 mapping analysis as first operator, performed quality control on LV volume and function as well as LGE analysis, I performed the statistical analysis and wrote the paper. RK performed the LV volume and function analysis. RS performed the LGE analysis.

8.1.2 Introduction

Following aortic valve replacement (AVR; surgical or transcatheter), LVH regresses by 20% to 30% by 1 year [37-41]. Whether this regression is cellular or interstitial has until recently been hard to differentiate because it requires paired biopsies for histology. ECV dichotomizes myocardium into cellular (myocytes, fibroblast, endothelial, red blood cells) and extracellular (extracellular matrix, blood plasma) compartments (see Figure 55) [109, 284, 285], and offers the opportunity to track dynamic changes in the cell and matrix compartments. In AS, outcome is predicted not only by LVH at baseline or its regression post AVR [26, 28, 29, 39], but also by focal (using LGE) [55, 58, 103], and diffuse fibrosis (using ECV) [286]. Histological studies show that myocardial fibrosis accompanies cellular hypertrophy,[275] and limited invasive studies suggest both may regress after AVR [45]. We hypothesised that human myocardial fibrosis is plastic and can regress, and that this regression can be measured non-invasively. We used patients pre and post AVR as a natural model of afterload reduction, measuring the valve gradient reduction by echocardiography, LVH by CMR cine imaging, focal fibrosis by LGE, DMF and cell hypertrophy by ECV, plus the functional consequences of AVR by NYHA functional class, 6-minute-walk test and blood biomarkers.

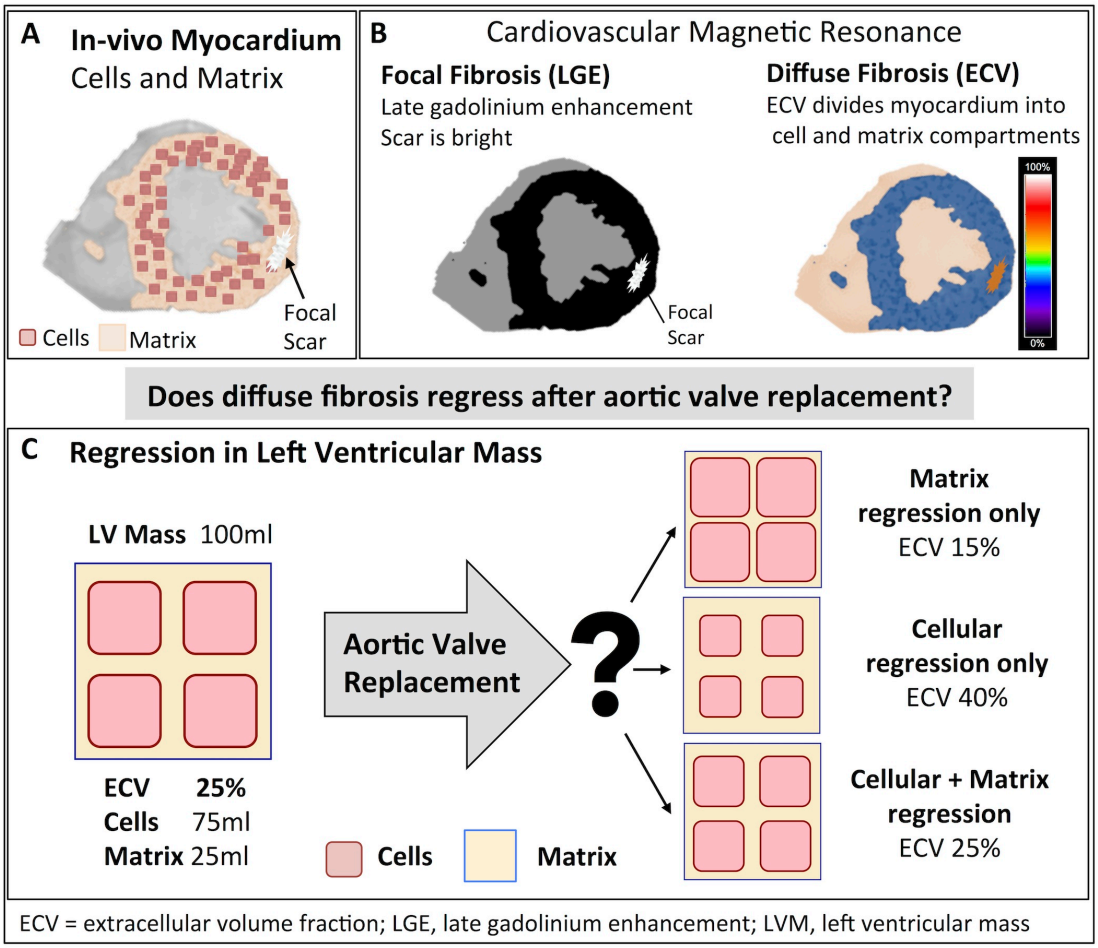

Figure 55: ECV dichotomizes the myocardium into cell and matrix.

A- *The in-vivo myocardium consists of cells and the surrounding extracellular matrix. Reactive fibrosis is characterized by expansion of the extracellular matrix, whereas replacement fibrosis follows cell death by focal scar.* ***B-*** *Cardiovascular magnetic resonance (CMR) measures both focal fibrosis (scar) by late gadolinium enhancement (LGE) imaging, where scar appears bright, and diffuse fibrosis by extracellular volume fraction (ECV) imaging. ECV divides the myocardium into cell and matrix compartments and allows calculation of cell and matrix volumes.* ***C-*** *A patient with a left ventricular volume of 100mL and an ECV of 25% would have a cell volume of 75mL and a matrix volume of 25mL. Regression of left ventricular mass following aortic valve replacement can either be driven by matrix regression alone, where the ECV reduces; by cellular regression alone, where the ECV increases; or by a proportional regression in cellular and matrix compartments, where the ECV is unchanged.*

8.1.3 Methods

Total LV matrix and cell volumes were calculated from the product of LV myocardial volume (LVM divided by the specific gravity of myocardium [1.05g/mL]) and ECV or (1- ECV), respectively – see Figure 55.

8.1.3.1 Statistics

As described before in Statistical Analysis 3.8. Changes between pre- and post AVR visits were compared using paired t-tests for continuous variables and using Wilcox signed rank test for categorical variables. Log transformation was applied to normalize the distribution of NT-proBNP and hsTnT. To identify predictors of matrix regression, all clinical parameters were proposed for inclusion in a univariate linear regression model and the most significant predictors per domain were then entered into a forward stepwise multivariable model to identify significant independent predictors. A two-sided p-value of <0.05 was considered significant.

8.1.4 Results

8.1.4.1 Study population

A total of 181 patients with severe, symptomatic AS (age 69±10, 56% male) were recruited. Overall 48% of patients undergoing surgical AVR for severe AS at our institution were recruited (Figure 56 for flowchart). Three patients did not undergo AVR and were treated medically. Following AVR, 14 patients were excluded (cardiac amyloid n=6 [234], claustrophobia n=4, severe mitral regurgitation n=2, pseudo-severe AS n=1, Fabry disease n=1). By one year, there were 11 deaths, 16 patients with pacemakers and 21 declined follow-up. A total of 116 patients underwent 1-year follow-up assessment and were included in the analysis (for Study Flowchart see Figure 2). There was no significant difference in baseline characteristics between patients that completed the follow-up and those that did not, in particular with regards to age, sex, aortic valve stenosis severity or surgical risk score (all *p>0.05*).

8.1.4.2 Baseline Findings

Baseline demographic, clinical, echocardiographic and CMR characteristics of the follow-up study cohort (n=116) are shown in Table 21 and Table 22, respectively.

Valve Stenosis Severity. All patients had severe AS by echocardiography (AVAi 0.40±0.13cm^2/m^2; mean gradient 48±14mmHg, peak velocity 4.4±0.6m/sec). The etiology of AS was determined as calcific AS (n=83, 72±8years; 52% male), bicuspid AS (n=32, 59±6years; 66% male) and unicuspid AS (n=1, 35-year-old female) by a combination of echocardiography, CMR and direct inspection during surgery.

Symptoms and functional capacity. All but seven patients were symptomatic (94%) with dyspnea (95%), chest pain (32%) and/or syncope (8%). Median 6MWT distance was 500m (IQR 390-600m).

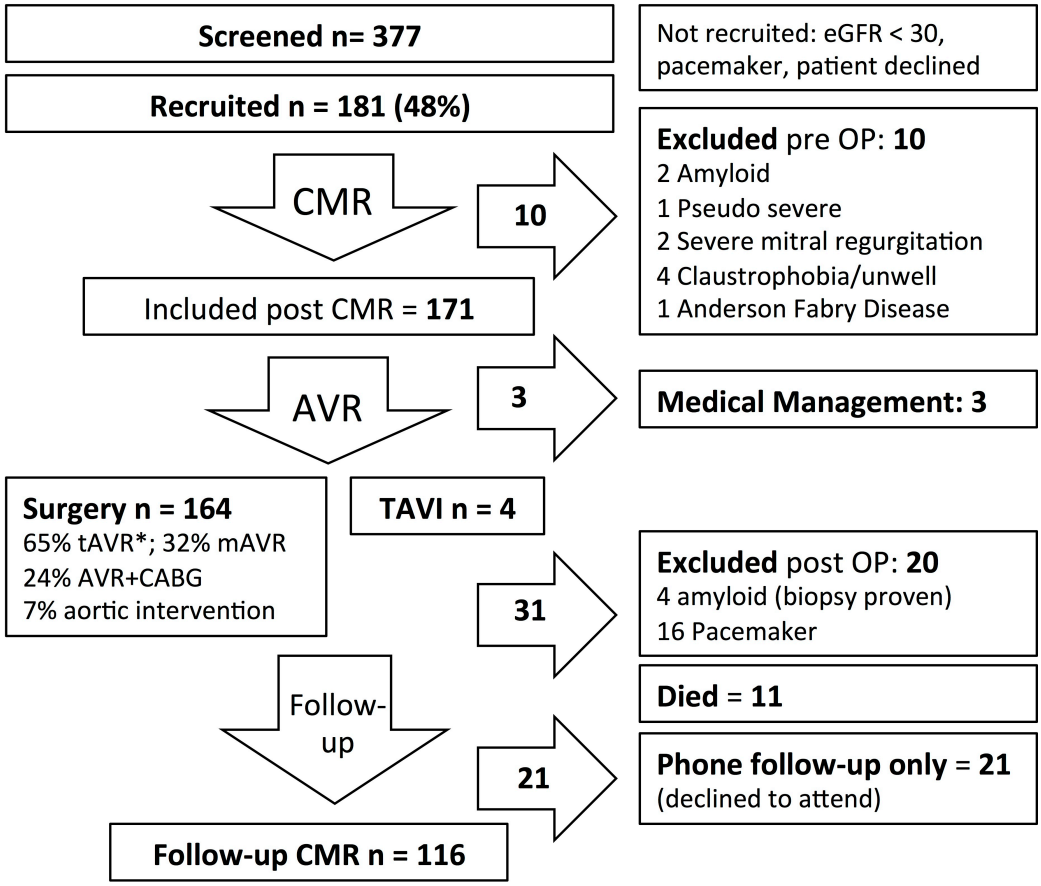

Figure 56: Study Flow Chart.

181 patients with severe, symptomatic aortic stenosis (AS) were recruited (48% of all surgical aortic valve replacements [AVR] at our institution [UCL]). Prior to AVR, 10 patients were excluded (claustrophobia n=4, cardiac amyloid n=2, severe mitral regurgitation n=2, pseudo-severe AS n=1, Fabry disease n=1), and three patients did not undergo AVR and were treated medically. Following AVR (164 surgical, 4 transcatheter), four further patients were excluded due to cardiac amyloid. By one year, there were 11 deaths, 16 patients with pacemakers and 21 declined follow-up. A total of 116 patients underwent 1-year follow-up assessment.

8.1.4.3 Intervention

The AVR was carried out using cardiopulmonary bypass with blood cardioplegia arrest. The valve received was a tissue (n=103, 61%), sutureless (n=7, 4%) or mechanical valve (n=54, 32%), with additional bypass grafting in 30 patients (24%) and intervention on the aorta in 11 (7%; interposition graft, reduction aortoplasty, replacement of the ascending aorta). Mean bypass and cross-clamp times were 91±26 and 72±25 minutes, respectively. Four patients initially referred for surgical

valve replacement underwent transcatheter AVR after review by the heart valve team, and were included in the final analysis.

	Total	Men	Women	p-value
n	116	63 (%)	53 (%)	
Age	70±10	68±11	71±8	0.1
Trileaflet*	83	40 (63%)	43 (81%)	
Bicuspid*	33	23 (37%)	10 (19%)	***0.04***
BSA (m^2)	1.90±0.22	2.00±0.20	1.77±0.16	***<0.001***
Six minute walk test (m)	500 (390-600)	540 (420-660)	435 (240-510)	***<0.001***
NYHA Functional Class	2.3±0.7	2.1±0.6	2.4±0.7	***0.02***
Co-morbidities				
Hypertension	75%	79%	71%	0.3
SBP (mmHg)	133±17	129±17	137±16	***0.005***
DBP (mmHg)	76±10	74±9	77±12	0.2
Diabetes	20%	21%	19%	0.8
Coronary artery disease	29%	35%	21%	0.09
Risk Scores				
STS, (%)	1.3 (1.0-2.1)	1.1 (0.8-1.9)	1.7 (1.1-2.4)	*0.02*
EuroScoreII (%)	1.4 (1.0-2.4)	1.1 (0.8-2.3)	1.7 (1.1-2.5)	*0.05*
Drug History				
ACE-I / ARB	44%	55%	31%	***0.01***
Beta-blocker	37%	37%	37%	0.9
Statin	64%	65%	63%	0.9
Aspirin	44%	50%	37%	0.2
Blood				
NT-proBNP (ng/L)	50 (26-173)	91 (31-266)	40 (25-105)	***0.01***
hs-Troponin T (pmol/L)	13 (9-19)	15 (11-22)	12 (7-17)	0.12
Creatinine (µmol/L)	85±26	95±27	73±18	***<0.001***
eGFR (mL/min/1.73m^2)	77±21	78±21	76±22	0.6
Hematocrit, %	40.4±4.5	41.7±4.6	38.8±3.7	***<0.001***

Table 21: Baseline Clinical Characteristics

**one patient had unicupid AS (female). Values are given as mean ± SD, median (and interquartile range) or n (and percentage).BSA means body surface area; SBP, systolic blood pressure; DBP, diastolic blood pressure; NYHA, New York Heart Association; IQR, interquartile range; STS, Society of Thoracic Surgeons' risk model score; EuroScoreII, European System for Cardiac Operative Risk Evaluation II score; ACE-I, angiotensin-converting-enzyme inhibitor; ARB, angiotensin-receptor blocker; LVH, left ventricular hypertrophy; NT-proBNP, N-terminal pro-brain natriuretic peptide; hs-TnT, high sensitivity troponin T; eGFR, estimated glomerular filtration rate.*

	Total	Men	Women	p-value
Echocardiography				
Vmax (m/s)	4.4±0.6	4.4±0.6	4.3±0.6	0.5
Peak gradient (mmHg)	77±20	78±21	76±19	0.7
Mean gradient (mmHg)	48±14	49±15	47±13	0.5
AVA (cm^2)	0.75±0.26	0.77±0.29	0.72±0.23	0.2
AVAi (cm^2/m^2)	0.40±0.13	0.38±0.13	0.41±0.13	0.4
LVOT:Aortic valve VTI ratio	0.23±0.08	0.21±0.09	0.24±0.09	0.07
E-wave (m/s)	0.83±0.29	0.80±0.29	0.87±0.29	0.2
E/A ratio	0.94±0.49	1.00±0.29	0.87±0.29	0.2
E deceleration time (ms)	234±72	228±74	240±69	0.4
Mean e' (m/s)	6.5±2.1	6.7±2.1	6.1±2.0	0.2
E/e' ratio	13.2±5.8	12.8±5.8	13.8±5.7	0.4
CMR parameters				
LVEDVi (mL/m^2)	66±23	72±24	59±20	***0.001***
LVESVi (mL/m^2)	22±21	27±23	16±17	***0.008***
LVEF (%)	71±16	67±17	75±13	***0.003***
LVMi (g/m^2)	88±26	101±25	73±20	***<0.001***
Septal wall thickness (mm)	14±3	15±3	13±2	***<0.001***
Left ventricular diameter (mm)	49±7	52±7	46±6	***<0.001***
Mass:Volume Ratio	1.42±0.37	1.50±0.42	1.33±0.29	***0.01***
LAAi_preop (cm^2/m^2)	13.2±3.0	13.4±3.2	12.9±2.6	0.4
CMR flow				
Aortic regurgitant fraction (%)	10 (3-29)	13 (4-46)	9.0 (2-23)	0.09
Mitral regurgitant fraction (%)	5 (0-20)	0 (0-21)	5.9 (0-20)	0.9
Tissue Characterization				
LGE 3SD method (g)	12.4±10.3	15.1±11.1	9.2±8.1	***0.002***
T1 myocardium (native; ms)	1039±40	1036±39	1043±40	0.4
ECV (%)	28.2±2.9	28.6±3.2	27.6±2.4	0.09
Cell volume (mL/m^2)	64±18	72±17	53±17	***<0.001***
Matrix Volume (mL/m^2)	25±9	29±9	20±7	***<0.001***

Table 22: Baseline Imaging Characteristics

Values are given as mean ± SD, median (and interquartile range) or n (and percentage). Vmax, peak velocity through the aortic valve; AVAi, aortic valve area index; LVOT, left ventricular outflow tract; VTI ratio, velocity-time-integral ratio; Zva, valvulo-arterial impedance; E, peak early velocity of the transmitral flow; DT, deceleration time; E´, peak early diastolic velocity of the mitral annulus displacement; EDVi, end-diastolic volume index; ESVi, end-systolic volume index; LVMi, left ventricular mass index; LVEF, left ventricular ejection fraction; SVi, stroke volume index, LAAi, left atrial area index; LGE, late gadolinium enhancement; 3SD, three standard deviations; ECV, extracellular volume.

8.1.4.4 Follow-up

At 1-year post-AVR, there was a marked afterload reduction (valve gradient reduction 48±16 to 12±6mmHg, *p<0.001*). Patients were less breathless (NYHA functional class improved by nearly one class [*p<0.001*]) and could walk further (6MWT improvement 90m; *p<0.001*). In addition, both left atrial pressure, reflected by a reduction in E/e' ratio (13±6 to 11±4 cm/s, *p=0.003*) and NT-proBNP levels reduced (50 (IQR 26-173) to 38 (IQR 23-99) ng/L; <0.001). The changes in pre- to post-operative parameters are summarized in

Table 23. There were no significance differences in these parameters in patients undergoing isolated AVR versus patient undergoing AVR+CABG.

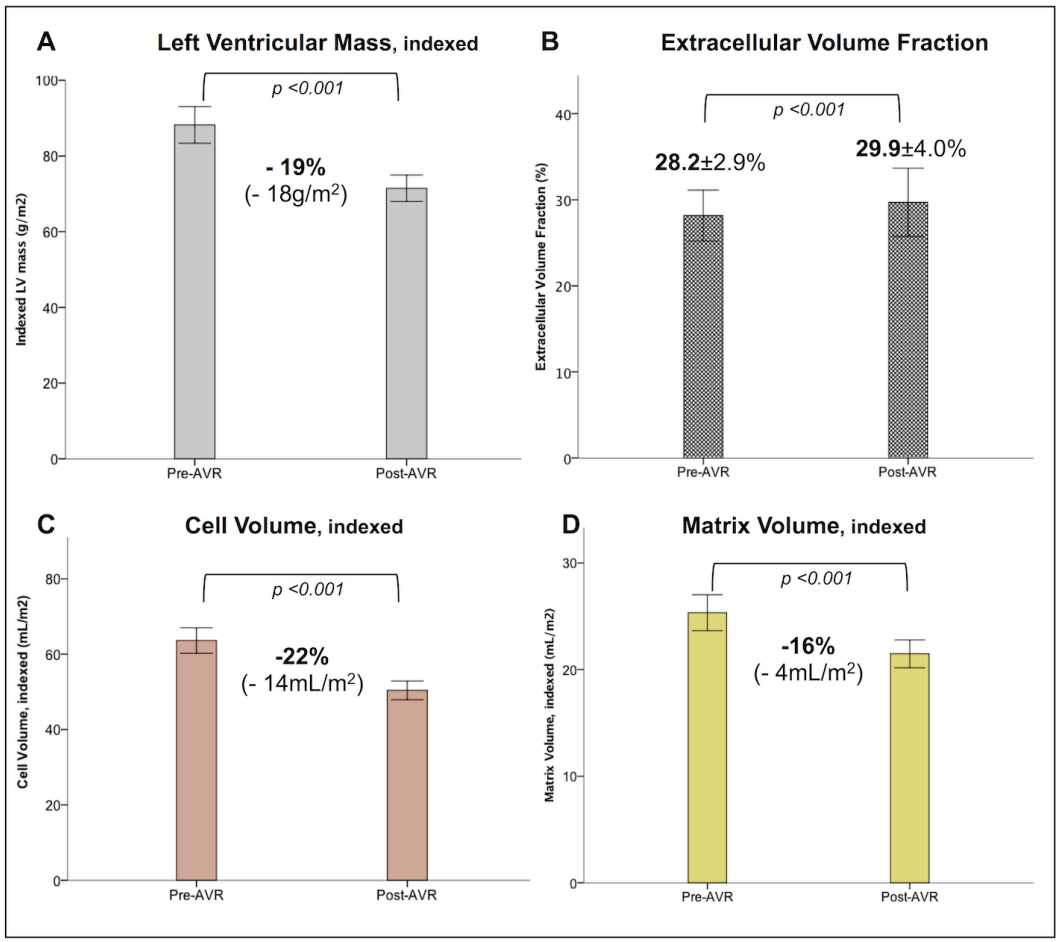

Figure 57: Left ventricular remodelling 1-year after aortic valve replacement.

At 1-year post aortic valve replacement (AVR), there was a 19% reduction in indexed left ventricular mass (88±26g/m^2 to 71±19g/m^2, p<0.001; panel A). Focal fibrosis (LGE) did not change at follow-up. Calculated ECV increased unexpectedly (28.2±2.9 to 29.9±4.0%, p<0.001; panel B). This was because the 16% reduction in matrix volume (25±9 to 21±7ml/m^2, p<0.001; panel D) was proportionately less than the 22% reduction in cell volume (64±18 to 50±13ml/m^2, p<0.001; panel C).

8.1.4.5 LV mass, cellular hypertrophy and myocardial fibrosis changes

There was a 19% reduction in indexed LV mass (88±26g/m^2 to 71±19g/m^2, *p<0.001*) as well as a reduction in LVEDVi and LVESVi, resulting in a reduction in the mass-volume-ratio. LVEF increased modestly (71±16 to 74±12%, *p<0.006*). LV mass regression occurred regardless of the baseline level of hypertrophy (i.e. also in patients with normal geometry), though both absolute and percentage LVMi regression were greatest in those patients with the highest LVMi at baseline.

Calculated ECV increased unexpectedly (28.2±2.9 to 29.9±4.0%, *p<0.001*). This was because the 16% (4.1±5.8ml/m^2) reduction in matrix volume (25±9 to 21±7ml/m^2, *p<0.001*) was proportionately less than the 22% (14.0±11.6ml/m^2) reduction in cell volume (64±18 to 50±13ml/m^2, *p<0.001*; see Figure 57). Native myocardial T1 was unchanged (1039±40 vs 1035±42ms, *p=0.3*). Focal fibrosis in absolute terms (LGE in grams) did not change at follow-up (12.4±10.3 vs 12.6±8.9g, p=0.9), but expressed as a percentage of the regressed LV mass, focal fibrosis (LGE as %) increased post-AVR (7.2±5.1 vs 8.9±4.9%, *p=0.001*). Therefore, both DMF and cardiomyocyte hypertrophy decreased after AVR, whereas focal fibrosis (LGE) remained comparable to findings at baseline. There were no differences in ECV, cell or matrix volume changes according to CAD status.

At univariate analysis, matrix regression was associated with baseline LV parameters (LV size, hypertrophy, systolic and diastolic function), baseline biomarkers (hs-TnT and NT-proBNP) and post-operative changes LV parameters, biomarkers as well as change in valve size and haemodynamics (Table 24). At multivariate analysis, matrix regression was only independently associated with baseline LVMi and ECV, as well as improvement in LVEF, hs-TnT level and indexed valve area (Table 25).

n=116	Pre-AVR	Post-AVR	p-value
NYHA functional class	2.3±0.7	1.4±0.6	***<0.001***
Six minute walk test (m)	477±177*	571±171	***<0.001***
NT-proBNP (ng/L)	50 (26-173)	38 (23-99)	***<0.001***
hs-Troponin T (pmol/L)	13 (9-20)	11 (7-17)	***0.002***
Echocardiography			
Vmax (m/s)	4.4±0.6	2.4±0.5	***<0.001***
Peak gradient (mmHg)	77±20	24±11	***<0.001***
Mean gradient (mmHg)	48±14	13±6	***<0.001***
EOAi (cm^2/m^2)	0.40±0.13	0.84±0.21	***<0.001***
LVOT:Aortic valve VTI ratio	0.23±0.08	0.51±0.12	***<0.001***
E-wave (m/s)	0.83±0.29	0.83±0.23	0.2
E/A ratio	0.94±0.49	0.91±0.26	0.6
E deceleration time (ms)	234±72	242±67	0.7
Mean E/e' ratio	13.2±5.8	10.8±4.2	***0.001***
Zva (mmHg/ml*m^2)	4.3±1.2	3.6±0.9	***<0.001***
CMR parameters			
LVEDVi (mL/m^2)	66±23	62±19	***0.03***
LVESVi (mL/m^2)	22±21	18±13	***0.003***
LVEF (%)	71±16	74±12	***0.006***
LVMi (g/m^2)	88±26	71±19	***<0.001***
Myocardial contraction fraction (%)	52±15	65±16	***<0.001***
Mass:Volume Ratio	1.42±0.37	1.19±0.27	***<0.001***
LAAi (cm^2/m^2)	13.2±3.0	12.1±2.2	0.09
Tissue characterization			
LGE 3SD method (g)	12.4±10.3	12.6±8.9	0.9
LGE 3SD method (%)	7.2±5.1	8.9±4.9	***0.001***
T1 myocardium (native, in ms)	1039±40	1035±42	0.3
ECV (%)	28.2±2.9	29.9±4.0	***<0.001***
Cell volume, indexed (mL/m^2)	64±18	50±13	***<0.001***
Matrix Volume, indexed (mL/m^2)	25±9	21±7	***<0.001***

Table 23: Changes in Baseline Characteristic after Aortic Valve Replacement.

**n=85; Values are given as mean ± SD, median (and interquartile range) or n (and percentage). Vmax, peak velocity through the aortic valve; AVAi, aortic valve area index; LVOT, left ventricular outflow tract; VTI ratio, velocity-time-integral ratio; Zva, valvulo-arterial impedance; E, peak early velocity of the transmitral flow; DT, deceleration time; E´, peak early diastolic velocity of the mitral annulus displacement; EDVi, end-diastolic volume index; ESVi, end-systolic volume index; LVMi, left ventricular mass index; LVEF, left ventricular ejection fraction; SVi, stroke volume index, LAAi, left atrial area index; LGE, late gadolinium enhancement; 3SD, three standard deviations; ECV, extracellular volume.*

Domain	Parameter	beta	95%CI	p-value
Baseline	Age	0.078	-0.034 - 0.191	0.2
	Sex	-2.229	-4.396 - -0.62	**0.04**
	Type of valve (bicuspid/tricuspid)	1.554	-0.844 - 3.953	0.2
	Six minute walk test distance	0.003	-0.003 - 0.01	0.3
	NYHA functional class	0.123	-1.543 - 1.79	0.9
	Hypertension	-2.103	-4.706 - 0.499	0.1
	SBP (mmHg)	0.043	-0.023 - 0.109	0.2
	DBP (mmHg)	0.014	-0.095 - 0.122	0.8
	Diabetes	-0.562	-3.318 - 2.195	0.7
	Coronary artery disease	-0.138	-2.618 - 2.342	0.9
	Atrial Fibrillation	-2.369	-5.446 - 0.707	0.1
	STS score	-0.157	-1.11 - 0.795	0.7
	EuroScore II	-0.438	-1.217 - 0.342	0.3
	ACE/ARB	-0.011	-2.243 - 2.22	0.9
	Beta-blocker	0.615	-1.683 - 2.912	0.6
	Statin	0.021	-2.28 - 2.321	0.9
	Aspirin	-2.005	-4.207 - 0.197	0.07
CMR	EDVi	-0.079	-0.124 - -0.034	**0.001**
	ESVi	-0.093	-0.143 - -0.044	**<0.001**
	LVMi	-0.117	-0.152 - -0.082	**<0.001**
	LVEF	0.136	0.069 - 0.204	**<0.001**
	SVi	-0.016	-0.118 - 0.086	0.8
	LAAi	-0.425	-0.791 - -0.059	**0.023**
	LGE	-0.116	-0.222 - -0.01	**0.032**
	Native T1	-0.053	-0.077 - -0.029	**<0.001**
	ECV	-0.872	-1.188 - -0.557	**<0.001**
Baseline AS severity	Vmax (m/s)	-1.297	-3.153 - 0.558	0.2
	Peak gradient (mmHg)	-0.035	-0.089 - 0.019	0.2
	Mean gradient (mmHg)	-0.054	-0.130 - 0.023	0.2
	AVAi (cm2/m2)	4.002	-4.345 - 12.349	0.3
	LVOT:Aortic valve VTI ratio	8.083	-5.108 - 21.274	0.2
	E-wave (m/s)	-3.19	-6.897 - 0.516	0.09
	E/A ratio	-3.988	-6.331 - -1.644	**0.001**
	E deceleration time (ms)	0.02	0.005 - 0.036	**0.008**
	E/e' ratio	-0.193	-0.391 - 0.005	**0.06**
	Zva (mmHg/ml*m2)	0.352	-0.540 - 1.244	0.4
Biomarkers	hs-TnT (ln)	-2.904	-4.465 - -1.343	**<0.001**
	NT-proBNP (ln)	-1.917	-2.666 - -1.167	**<0.001**
	Crea	-0.026	-0.068 - 0.016	0.2
	eGFR	-0.008	-0.061 - 0.045	0.8
	Hct	0.146	-0.11 - 0.40	0.3
Operation	CABG (y/n)	-0.627	-3.144 - 1.889	0.6
	Type of valve	-1.039	-3.406 - 1.329	0.4
	Size of valve	-0.547	-0.970 - -0.123	**0.012**
Post op	Time to follow-up	-0.009	-0.021 - 0.003	0.1
Change in	EDVi	0.162	0.110 - 0.215	**<0.001**
	ESVi	0.202	0.147 - 0.257	**<0.001**
	LVMi	0.27	0.227 - 0.313	**<0.001**
	LVEF	-0.48	-0.623 - -0.337	**<0.001**
	SVi	-0.005	-0.106 - 0.096	0.9
	LGE	-0.251	-0.554 - 0.52	0.1
	NYHA FC	-0.219	-3.048 - 2.610	0.9
	6MWT	-0.002	-0.010 - 0.005	0.5
	Vmax (m/s)	1.604	0.198 - 3.010	**0.026**
	Peak gradient (mmHg)	0.047	-0.002 - 0.096	0.06
	Mean gradient (mmHg)	0.071	0.002 - 0.139	**0.04**
	AVAi (cm2/m2)	-3.44	-5.668 - -1.211	**0.003**
	LVOT:Aortic valve VTI ratio	-5.629	-14.191 - 2.932	0.2
	E-wave (m/s)	5.094	1.188 - 9.000	**0.011**
	E/A ratio	3.386	1.272 - 5.501	**0.002**

	E deceleration time (ms)	0.019	0.006 - 0.032	**0.004**
	E/e' ratio	0.228	0.044 - 0.413	**0.016**
	Zva (mmHg/ml*m2)	-0.065	-1.072 - 0.941	0.9
	hs-TnT (ln)	3.643	1.496 - 5.789	**0.001**
	NT-proBNP (ln)	2.645	1.784 - 3.506	**<0.001**

Table 24: Univariate Predictors of Matrix Regression.

EDVi, end-diastolic volume index; ESVi, end-systolic volume index; LVMi, left ventricular mass index; LVEF, left ventricular ejection fraction; SVi, stroke volume index, LGE, late gadolinium enhancement; ECV, extracellular volume; Vmax, peak velocity through the aortic valve; AVAi, aortic valve area index; LVOT, left ventricular outflow tract; VTI ratio, velocity-time-integral ratio; Zva, valvulo-arterial impedance; E, peak early velocity of the transmitral flow; E/A ratio, early to late ventricular filling velocities; DT, deceleration time; E´, peak early diastolic velocity of the mitral annulus displacement; Zva, valvulo-arterial impedance; SBP, systolic blood pressure; DBP, diastolic blood pressure; NYHA, New York Heart Association; STS, Society of Thoracic Surgeons' risk model score; EuroScoreII, European System for Cardiac Operative Risk Evaluation II score; ACE-I, angiotensin-converting-enzyme inhibitor; ARB, angiotensin-receptor blocker; NT-proBNP, N-terminal pro-brain natriuretic peptide; hs-TnT, high sensitivity troponin T.

	Univariate				Multivariate		
Domain	**Parameter**	**beta**	**95%CI**	**p-value**	**beta**	**95%CI**	**p-**
Baseline	**Sex**	-2.229	-4.396 - -0.62	***0.044***			NS
CMR	**LVEF**	0.136	0.069 - 0.204	***<0.001***			NS
	LVMi	-0.117	-0.152 - -0.082	***<0.001***	-0.05	-0.083 - -0.017	**0.004**
	ECV	-0.872	-1.188 - -0.557	***<0.001***	-0.407	-0.756 - -0.058	**0.02**
Echo	**E/A ratio**	-3.988	-6.331 - -1.644	***0.001***			NS
Biomarkers	**hs-TnT (Ln)**	-2.904	-4.465 - -1.343	***<0.001***			NS
	NT-proBNP (Ln)	-1.917	-2.666 - -1.167	***<0.001***			NS
Operation	**Size of valve**	-0.547	-0.970 - -0.123	***0.012***			NS
Change in	**ΔLVEF**	-0.48	-0.623 - -0.337	***<0.001***	-0.118	-0.189 - -0.046	**0.002**
	ΔAVAi	-3.44	-5.668 - -1.211	***0.003***	-1.611	-3.184 - -0.039	**0.045**
	ΔE/A ratio	3.386	1.272 - 5.501	***0.002***			NS
	Δhs-TnT (ln)	3.643	1.496 - 5.789	***0.001***	2.591	0.429 - 4.753	**0.02**
	ΔNT-proBNP (ln)	2.645	1.784 - 3.506	***<0.001***			NS

Table 25: Multivariate Predictors of Matrix Regression.

LVMi, left ventricular mass index; LVEF, left ventricular ejection fraction; ECV, extracellular volume; E/A ratio, early to late ventricular filling velocities; AVAi, aortic valve area index; NT-proBNP, N-terminal pro-brain natriuretic peptide; hs-TnT, high sensitivity troponin T.

8.1.5 Discussion

In this study we sought to understand the dynamic nature of cellular and matrix components in myocardial hypertrophy by exploring reverse myocardial remodeling in AS at 1-year post-AVR. We show that myocardial cellular hypertrophy and extracellular matrix expansion (diffuse fibrosis) regress and is accompanied by structural, functional and biomarker improvement (Figure 58). Furthermore, it establishes that cardiomyocyte loss is irreversible as evidenced by the persistence of focal replacement fibrosis (LGE) after AVR. Moreover, these findings provide validation that CMR can be used to characterize and monitor the extent of cellular hypertrophy and myocardial fibrosis, differentiating between focal fibrosis (scar) and diffuse fibrosis due to accumulation of ECM, and importantly confirming myocardial fibrosis regression non-invasively similar to that reported more than 25-years ago requiring invasive myocardial biopsies [277, 278].

The concept of reverse myocardial remodeling after removal of a pathological insult has been studied both by echocardiography and CMR. LVH (i.e. combined cell and matrix compartments) is known to regress by 20% to 30% by 1-year post-AVR [37, 39, 41]. We now show that both cell and matrix regression contribute to the reduction in LVH over this period. Combined with our previous data showing that at 6 months post-AVR only cellular hypertrophy regresses [48], this suggests that the timeline for cardiomyocyte and extracellular matrix responses to afterload reduction are different, with remodeling of the extracellular matrix being slower. Diffuse fibrosis enhances myocardial tensile strength and three-dimensional force delivery but at the expense of reduced distensibility. Dense collagen meshwork within the subendocardium seen in AS can be considered pathological in that it entraps muscle fibers causing active stiffness to fall while impairing distensibility [287]. Previous data by Villari et al [45] suggested no change in interstitial fibrosis at 2 years post-AVR, but these data were from subendocardial samples rather than a global, “whole heart” measure as in our cohort. Location of the biopsy is crucial, as we have shown in previous work [288] where the subendocardial portion of the myocardium was predominated by replacement focal fibrosis with a decreasing superficial to deep such that reactive fibrosis predominates in the midmyocardium.

The ability to measure diffuse fibrosis regression non-invasively by CMR not only reflects a key biological response, but also has the potential to be used in drug development to validate proof-of-concept efficacy of drugs targeting myocardial fibrosis. The possibility of influencing myocardial (cellular and interstitial) remodeling with pharmacological interventions [67, 289, 290] requires a better understanding of the intricate interplay throughout all stages of disease. Non-invasive tracking of cellular and extracellular components may potentially establish the transition point between adaptive and maladaptive remodeling and provide a reliable method to monitor the response to matrix modulating therapies (anti-fibrotic, anti-amyloid) in the search for new individualized heart failure therapies [291].

Focal fibrosis identified by LGE is indicative of cardiomyocyte necrosis with replacement fibrosis (i.e., ranging from foci of necrosis to larger myocardial infarcts). Our data suggest that focal fibrosis, reflected by LGE, does not regress; this is consistent with previous findings reported post-AVR implying that AVR failed to reduce the degree of focal replacement fibrosis [33, 43]. In contrast, the reactive diffuse fibrosis did regress. These findings highlight the dynamic nature of the extracellular matrix in AS contributing to the pathobiology because changes in collagen turnover occur as a result of the reaction of cardiac fibroblasts to both mechanical and local humoral factors [292, 293]. Matrix volume and fraction (ECV) quantification may add more predictive information, particularly as our data clearly show that this method identifies measurable reversibility. This is also important from an outcome perspective, because recent data by Chin et al showed that both focal (LGE) and diffuse fibrosis (matrix volume) were univariate predictors of outcome [294].

Current management strategies for AS mainly rely on waiting until the onset of symptoms. However, it is recognized that for some this is too late; furthermore, there is a discrepancy between symptom development and markers of long-term outcome post AVR (e.g. LGE). While existing models of AS may be simplistic, our current understanding is that AS is a disease of both the valve and myocardium. Thus, treatment strategies need to assess both haemodynamic insult imposed by the valve lesion [286] and the extent of myocardial structural remodeling, particularly when seeking to quantify irreversible changes and predict outcome. Reduced LVEF, excessive LVH, abnormal response to exercise and critical AS (peak velocity >5m/sec)[23, 26], as well as LGE [55, 58, 103] are markers for this and have been

shown to predict adverse outcome. Whilst LVH regression occurs early post-AVR [295, 296], myocardial normalization is not always possible. We show that focal replacement fibrosis is not plastic but irreversible, which is not surprising, but may represent a point in the clinical progression of AS at which valve replacement should be recommended to prevent further irreversible damage. If this transition point to maladaptive remodeling could be anticipated then intervention could be performed before the emergence irreversible focal replacement scar – a combination of blood and imaging biomarkers may be able to identify these transition points in the future. Finally, drug therapies could be used post-AVR to augment or accelerate normalization of both cell hypertrophy and diffuse fibrosis.

There are limits to an exclusively non-invasive approach. The ECV technique is measuring extracellular water, which tracks fibrosis, but there are other explanations: vasodilatation, edema and amyloid. Compensatory capillary vasodilatation (hyperemia) would artifactually cause elevated native myocardial T1 and ECV [161]. However, AS is believed to have a reduced capillary density [165], and the changes found here are too large for blood volume – 16% of total myocardial volume. We also saw no predicted change in native T1. Edema could be a cause, which has been described in increased afterload [297]. However, these patients had normal baseline myocardial T2. Dual pathology with occult amyloid was specifically sought and excluded (n=6), so it was not present [234]. ECV quantification excluded infarct LGE but included non-ischemic LGE, as per guideline recommendation [196]. Although exclusion of all areas of LGE may appear theoretically attractive, it would be practically challenging to limit the ECV measurement area to exclude pixels of non-infarct LGE (highlighted by our thresholding method). Ultimately, the inclusion of areas of non-infarct LGE in the ECV measurement did not affect the overall regression trend, as the amount of LGE did not change at follow-up.

Other limitations of the present study include it being a single center and focused on surgical AVR by non-invasive CMR assessment without paired histology. Pressures were determined by non-invasive, echocardiography-derived values only**.** Renal failure and pacemaker patients are not represented (this excluded 7% of possible patients). Some patients declined follow-up – but there was no significant difference in baseline characteristics between patients that completed the follow-up and those that withdrew.

8.1.6 Conclusion

In aortic stenosis, cell hypertrophy but also of diffuse fibrosis are plastic and measurable non-invasively by CMR. Following AVR, both cellular hypertrophy and diffuse fibrosis regress, and are accompanied by structural, functional and biomarker improvement. Focal replacement fibrosis is irreversible. Together these suggest that therapeutic strategies should potentially aim for intervention before the emergence of irreversible focal scar, with the aim to normalize diffuse fibrosis, which is here seen to be plastic and measurable non-invasively.

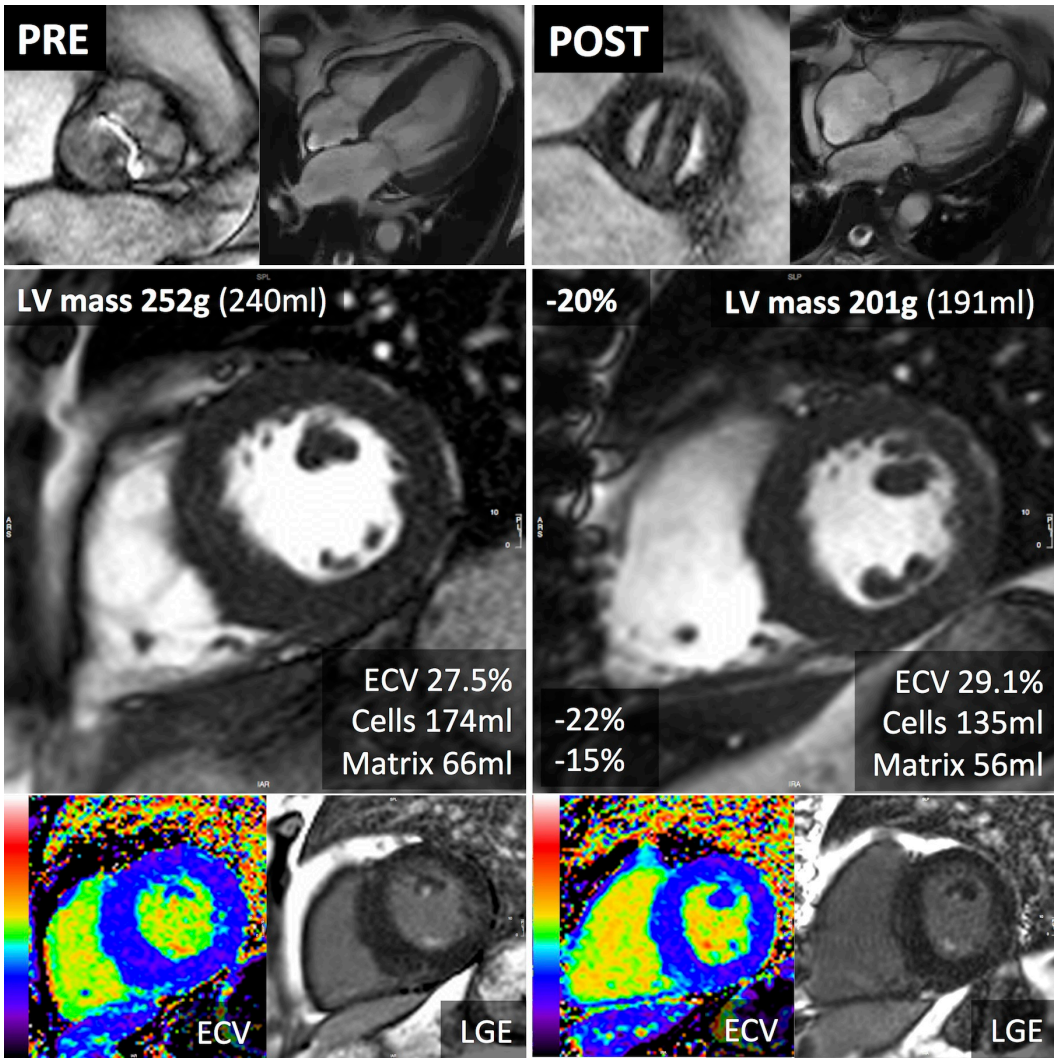

Figure 58: Myocardial Reverse Remodeling after Aortic Valve Replacement.

66-year-old male with severe aortic stenosis (peak velocity 4.66m/s, mean gradient 57mmHg, AVA 0.5cm^2). CMR prior to aortic valve replacement (AVR) showed concentric left ventricular hypertrophy (252g). Late gadolinium enhancement (LGE) demonstrated limited non-ischemic focal scar. Extracellular volume fraction (ECV) was 27.5%. 1-year after AVR (mechanical bileaflet valve), there was a 22% reduction in LV mass (to 201g). The LV mass regression was due to 22% reduction in cell and a 15% reduction in matrix volume, so the ECV rose to 29.1%. The focal fibrosis (LGE) was unchanged.

Chapter 9 Results 5: ECV as a Predictor of Outcome following AVR

9.1.1 Preface

In this section, the 1-year outcome data is presented. A more extensive analysis with longer follow-up will be pursued during post-doctoral work.

My contribution was recruiting, consenting and performing the scans of all patients. I performed the T1 mapping analysis as first operator, performed quality control on LV volume and function as well as LGE analysis, I performed the statistical analysis and wrote the manuscript. RK performed the LV volume and function analysis. RS performed the LGE analysis.

9.1.2 Hypotheses and Aims

We hypothesized that extracellular matrix expansion predicts outcomes post AVR. To be clinically useful, this would need to be measured non-invasively, so we aimed to assess whether non-invasive (CMR ECV) measurement predicts outcome (death) one year post-AVR for severe AS.

9.1.3 Methods

The cohort investigated is the same as in the baseline paper (section Chapter 5) and the methods have been detailed in section 5.1.4. Additional details below:

9.1.3.1 Samples size

As detailed in 2.1.9, we based our sample size calculation on a previous cohort in our institution [114], which was followed up at 6 months with a sample size of 63 patients, and showed a trend of higher mortality with severe DMF with 6 month mortality in mild and moderate fibrosis of 2.4% and in severe fibrosis of 19%. The requirements were an 80% power (binomial test) to show that patients with severe fibrosis (highest ECV tertile) have a higher event rate than patients with mild to moderate fibrosis (lowest and mid ECV tertile) at 1 year, and calculated a group size of 44 to achieve this, equalling a total sample size of 132. Furthermore, we decided to extend the follow-up to one year, and adjusting the sample size to allow for dropout (or implantation of non-MR compatible PPMs) of 10%. Therefore, a sample size of 150 patients was calculated to give adequate power our study, and is a realistic recruitment target for our institution (140 AVR/year, 50-60% participation).

9.1.3.2 Outcome measures

All deaths were identified through the NHS National Spine Database. We also assessed aortic stenosis–related mortality. This was established from the official death certificate and defined as any death in which AS was listed as either the primary cause or a contributing factor to that death by the clinical care team.

9.1.3.3 Statistical Analysis

As described before in Statistical Analysis 3.8. Survival was evaluated using Cox proportional hazards analysis, providing estimated hazard ratios (HR) with 95% confidence intervals (CI) and Kaplan Meier curves. Due to the low number of events (deaths), multivariable Cox regression models were not tested. A two-sided p-value of <0.05 was considered significant.

9.1.4 Results

9.1.4.1 Baseline characteristics

There were 181 patients with severe, symptomatic AS recruited (age 69±10, 56% male) representing 48% of all surgical AVRs at the study institution. Thirteen patients were excluded: claustrophobia (n=2), hemodynamic instability (n=1), pseudo-severe AS (n=1), severe mitral regurgitation (n=2), significant myocardial bystander disease (cardiac amyloidosis n=6; Fabry Disease n=1)[234]. Characteristics of the remaining 168 patients (age 70±10 years, 55% male; 70% trileaflet AS) are summarized in Table 14 and Table 15.

9.1.4.2 Details of surgery

The treatment received was tissue or mechanical valve in 64% and 29%, respectively, with additional bypass grafting in 25% and aortic intervention in 8% (interposition graft, reduction aortoplasty, replacement of the ascending aorta). Four patients underwent TAVI.

9.1.4.3 Mortality after AVR

A total of 8 deaths occurred at 1-year follow-up. This conferred an unadjusted all cause mortality rate of 49 deaths per 1000 patient years. There were no deaths in the low ECV tertile, 2 deaths in the middle ECV tertile and 6 deaths in the high ECV tertile. Mortality in lowest and mid ECV tertile (combined) was 1.8%, whereas in the highest ECV tertile it was 10.7%. The unadjusted all cause mortality rates were 34 and 116 deaths per 1000 patients years for middle and high ECV tertiles,

respectively. As described in 6.1.5.4, the six patient excluded with occult amyloid had a 50% mortality and all had ECV value that would have put them into the highest tertile; this would have resulted in the mortality of 16.1% for highest tertile had they been included as in previous studies.

9.1.4.4 Univariate predictors of mortality

As described in Table 26, univariate predictors of mortality were ECV (HR 6.2 [1.3-31.2], p=0.02), age (HR 1.1 [1.0-1.3], p=0.048), LVEF (HR 0.98 [0.93-0.99], p=0.023), indexed end-systolic volume (HR 1.02 [1.00-1.42], p=0.03), indexed left atrial area (HR 1.3 [1.1-1.4], p<0.001), LGE mass (HR 6.4 [1.3-31.7], p=0.023), hs-TnT (HR 2.5 [1.02-6.13], p=0.045) and NT-proBNP (HR 2.5 [1.3-4.8], p=0.023), but not sex, LV mass, native T1 or parameters of aortic valve stenosis severity. As shown in the Kaplan-Meier curves in Figure 59, patients with severe fibrosis (highest tertile ECV) had a higher event rates than patients with mild to moderate fibrosis (middle and lowest tertile ECV).

	HR	95%CI	Chi^2	p-value
Age	1.1	1.00-1.25	3.8	*0.048*
Sex	1.4	0.3-5.8	0.2	0.6
LVEF	0.98	0.93-0.99	5.6	*0.023*
EDVi	1.02	0.99-1.11	3.1	0.09
ESVi	1.02	1.00-1.05	5.3	*0.03*
LAAi	1.3	1.13-1.42	21.0	*<0.001*
LV mass index	1.0	0.98-1.03	0.2	0.6
ECV (Tertiles)	6.2	1.3-31.2	6.7	*0.024*
Native T1 (tertile)	1.9	0.5-7.9	0.9	*0.4*
LGE 3SD (tertile)	6.4	1.3-31.7	6.8	*0.023*
Trop (ln)	2.5	1.02-6.13	4.1	*0.045*
NT-proBNP (ln)	2.5	1.3-4.8	9.2	0.009

Table 26: Cox Regression.

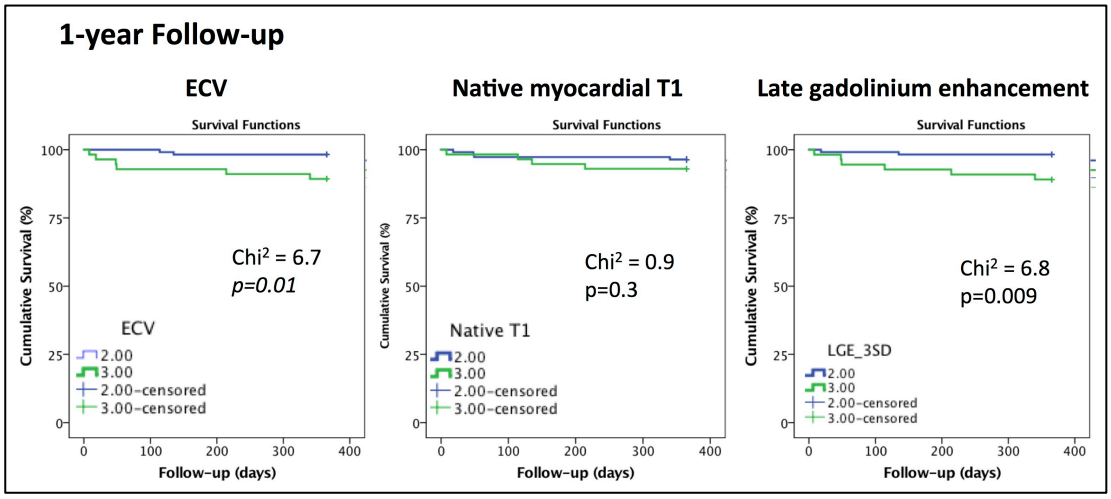

Figure 59: Kaplan-Meier Curves at 1-year.

At 1-year, patients with severe fibrosis (highest tertile ECV) have a higher event rates than patients with mild to moderate fibrosis (middle and lowest tertile ECV).

Variable	Lowest ECV Tertile	Mid ECV Tertile	Highest ECV Tertile	p-value
n	56	56	56	
Age (years)	69±9	71±11	69±9	0.4
Male (%)	61	48	55	0.2
Valve Type (Tricuspid, %)	64	75	55	0.9
Hypertension (%)	68	70	86	0.08
Diabetes (%)	11	18	32	0.3
Coronary artery disease (%)	32	27	38	0.7
CABG (%)	29	27	16	0.2
Bypass time (min)	102±35	92±24	89±27	0.1
EDVi (ml/m^2)	64±19	62±16	76±27	*<0.01*
ESVi (ml/m^2)	18±13	18±11	32±28	*<0.01*
LVEF (%)	73±12	73±12	63±18	*<0.01*
LVMi (g/m^2)	86±23	81±22	97±26	*<0.01*
LAAi (cm^2/m^2)	12.7±3.3	13.0±2.6	14.8±4.5	*<0.01*
Late enhancement (g)	12.9±9.1	11.4±7.8	17.2±13.3	*<0.01*
Native T1 (ms)	961±26	973±24	999±30	*<0.001*
ECV (%)	25.5±1.1	28.6±1.0	31.8±1.6	*<0.001*
Troponin T (pmol/L)	16±15	16±14	22±19	0.2
NT-proBNP (ng/L)	98±150	110±128	302±341	*<0.001*
SBP (mmHg)	134±16	133±21	131±18	0.7
DBP (mmHg)	75±10	76±13	75±11	0.8
6MWT (m)	497±158	468±192	412±204	0.1
AVAi (cm^2/m^2)	0.39±0.12	0.41±0.14	0.40±14	0.8
Vmax (m/s)	4.3±0.6	4.4±0.6	4.3±0.6	0.5
Mean Grad (mmHg)	47±13	49±14	46±15	0.5
VTI ratio	0.22±0.06	0.23±0.09	0.23±0.08	0.7
E-wave	0.74±0.24	0.81±0.27	0.98±0.32	*<0.001*
E/A ratio	0.86±0.37	0.93±0.43	1.11±0.63	*0.04*
E/e'	12±5	12±4	17±7	*0.001*

Table 27: Patient characteristics by ECV Tertile

9.1.4.5 Patient characteristics by ECV Tertile

As shown in **Error! Reference source not found.**, patients in the highest ECV tertile had worse LV remodeling, worse LVEF, more focal and diffuse fibrosis, larger left atrial area, high NT-proBNP and worse diastolic dysfunction. There were no significant differences in age, sex, valve type, aortic valve stenosis severity, co-morbidities in particular coronary artery disease (there was a trend towards higher prevalence of hypertension, but no difference in absolute blood pressure) or duration of surgery (bypass time).

9.1.4.6 Post-hoc Power calculation

On post-hoc power calculation, the actual event rates give a power of 75.5% to show a difference in mortality between the highest and lower ECV tertiles.

9.1.5 Discussion

Diffuse myocardial fibrosis assessed by ECV prior to AVR is a univariate predictor of all-cause mortality at 1-year follow-up. Patients with the highest fibrosis also have worse myocardial remodelling, systolic and diastolic function. The all-cause mortality in this cohort was 4.8%, and due to a low number of deaths, multivariate analysis was not performed.

This 1-year mortality was lower than expected from our sample size calculations (in a previous study in our institution, mortality overall and in the highest ECV tertile at 6 month were 7.9% and 19%). Therefore, although we over-recruited to our study, we missed the targeted power of 80%, achieving a power of 75.5%). Intensive recruitment for the RELIEF-AS study in our institution yielded the recruitment of nearly 50% of all patients undergoing AVR for severe AS into the study; this may have resulted in the recruitment of a less severe, though more representative phenotypes with lower mortality rates – overall the cohort had less fibrosis then the previous cohort in our institution [114]. Furthermore, in comparison to previous studies, we were able to detect patients with occult amyloid on myocardial biopsy and subsequently exclude these from our cohort. We believe this is correct as the high mortality in this group of patient in our study (50%) is suggestive that bystander TTR amyloid is an important disease modifier in elderly patients with severe AS. If we had included patients with occult cardiac amyloid, we would have had 50% more deaths in the high ECV tertile (i.e. an increase in mortality from 11.7% to 16.1%).

9.1.5.1 Limitations and Outlook

Neither cardiovascular mortality, nor major adverse cardiovascular events were available for analysis. Longer follow-up would have yielded in more events and a higher power – this will be pursued during post-doctoral work. Larger studies are required to confirm ECV as an independent predictor of cardiovascular mortality.

9.1.6 Conclusion

Diffuse myocardial fibrosis assessed by ECV prior to AVR predicts outcome (death) at 1-year follow-up. Patients with the highest fibrosis also have worse myocardial remodelling, systolic and diastolic function.

Chapter 10 Discussion and Conclusions

10.1 Background

In this thesis, I explored whether AS was a disease not just of the valve, but of the myocardium. I focused on myocardial remodelling in general and extracellular matrix – focal and diffuse fibrosis invasive and non-invasively (CMR with LGE, CMR with ECV and CT ECV) I applied ECV quantification to three key patient cohorts: Aortic Stenosis and hypertension (afterload-induced cell hypertrophy and matrix expansion), as well as cardiac amyloidosis (matrix expansion due to amyloid deposition in the myocardium).

10.2 Technical Development

As a by-product of the RELIEF-AS study, I developed the *synthetic* ECV methodology for CMR then CCT allowing instantaneous ECV quantification without the need of a venous haematocrit, and co-developed a simplified, bolus-only approach to quantify ECV by CCT and calibrated ECV_{CT} to diagnosis cardiac amyloidosis.

10.3 Key findings

10.3.1 Myocardial remodelling and fibrosis prior to AVR

In severe AS, CMR revealed sex dimorphism in myocardial remodelling way in excess of that recognised using conventional echocardiography. Given equal valve severity, and the associated biomarker and fibrosis changes, the myocardial response to AS appeared more maladaptive in men then previously reported.

10.3.2 Occult Amyloid in severe AS

I found that six percent of patients over the age of 65 years had wild-type transthyretin amyloid (wtATTR) deposits on cardiac biopsy, which was associated with poor outcome. There seemed to be a hierarchy of imaging diagnostic performance for identification of wtATTR amyloid, with DPD bone tracer scintigraphy superior to CMR, which was superior to echocardiography.

10.3.3 Combination of invasive and non-invasive tissue characterisation

Intra-operative myocardial biopsy revealed three patterns of fibrosis: endocardial fibrosis, microscars (mainly in the subendomyocardium), and diffuse interstitial fibrosis. CVF best captured the transmural gradient of fibrosis and microscars, whereas LGE appeared to capture mainly microscars, ECV likely captured mid-myocardium related functional changes beyond LGE. Combining LGE and ECV allowed better stratification of AS patients according to their myocardial response.

10.3.4 Diffuse Fibrosis regression after AVR

Following AVR, we show for the first time non-invasively that myocardial fibrosis regresses at 1-year – but less than cellular regression, so there is a small rise in ECV post-AVR. These data support the position that human diffuse fibrosis is dynamic and that this is measurable by CMR - a key biological result and proof-of-concept for drug development targeting myocardial fibrosis.

10.3.5 Outcome after AVR

Diffuse myocardial fibrosis assessed by ECV prior to AVR is a univariate predictor of all-cause mortality at 1-year follow-up (event rate was too low to perform multivariate analysis). Patients with the highest fibrosis also have worse myocardial remodelling, systolic and diastolic function. Studies with larger samples size are required.

10.4 Implication of Findings: Clinical Insights and Potentials

The findings presented in this body of work have important implications that I would like to address step by step:

1. The sex dimorphism in myocardial remodelling (more maladaptive myocardial response to AS in men) revealed by our study is way in excess of that recognised using conventional echocardiography and poses important questions: Firstly, given the stark differences in myocardial remodelling, how do these affect the interpretation of the haemodynamic severity of the valve stenosis? Secondly, these changes may be adaptive or maladaptive – can LVEF, NT-pro-BNP and hs-Troponin adequately highlight the transition into maladaptation, or are other biomarkers needed? And are blood biomarkers more informative than imaging? Finally, what are the mechanisms driving the sex differences in remodelling? Timing of aortic valve intervention is one of the greatest challenges in AS, in particular in

asymptomatic patients. Recent focus has turned towards the complex interplay between AoV stenosis, vascular load and myocardial response (inappropriate hypertrophy, myocardial stress [NT-proBNP], fibrosis [troponin, LGE, ECV], myocardial perfusion reserve). Our data supports the notion that we may need to treat men and women differently as they experience a different cardiac “milieu”, different combined (valve and vasculature) afterload and display a different myocardial response. Crucially, data showing reverse remodelling after valve replacement and its impact on outcome is required and pending.

2. Occult cardiac amyloid is a significant bystander in patients with severe aortic stenosis (six percent of patients > 65 years had wtATTR amyloid deposits on cardiac biopsy) and this was associated with poor outcome. The prevalence and adverse clinical outcomes suggest that wtATTR amyloid is important in elderly individuals with AS, but more work is needed. Prevalence in wtATTR increases with age. Future studies should focus on elderly patients (aged >75) who more and more undergo TAVI. In this setting, biopsy for amyloid is not practicable but bone tracer scintigraphy could be used. The data here suggests it could have a routine role in selected patients and influencing their management in terms of decisions surrounding intervention, procedure performance and specific amyloid therapies. Wider use of cardiac scintigraphy with bone tracers, by detecting early amyloid, is likely also to improve our understanding of conventional testing, such as echocardiography. We have therefore embarked on the ATTRact-AS study (see 10.5.2.2), a single centre, 250 patients, prospective observational cohort study with 1-year follow-up in patients aged >75 with severe AS referred to the Barts Heart Centre for consideration of intervention (surgical AVR or TAVI) using DPD scintigraphy.

3. Intra-operative myocardial biopsy revealed a characteristic pattern and distribution of fibrosis in AS (endocardial fibrosis, microscars [mainly in the subendomyocardium], and diffuse interstitial fibrosis). When measuring by biopsy or CMR, location, sampling and technical aspects of analysis matter. Invasive biopsy is limited by size and sampling error, whereas LGE and ECV capture different regions of myocardium and provide complementary information. The combination of LGE and ECV – a multi-parametric approach – better identified worse adverse LV remodelling, altered biochemical and histological parameters, and functional

capacity than each parameter alone. Further combined advanced histology and multi-modality non-invasive imaging studies will be required to elucidate other aspects of the pathophysiology of AS, with focus on the cellular and microcirculatory adaptations required.

4. Following AVR, we show for the first time non-invasively that myocardial fibrosis regresses at 1-year – but less than cellular regression, so there is a small rise in ECV post-AVR. These data support the position that human diffuse fibrosis is dynamic and that this is measurable by CMR - a key biological result and proof-of-concept for drug development targeting myocardial fibrosis. Whilst LVH regression occurs early post-AVR, myocardial normalization is not always possible. We show that focal replacement fibrosis is not plastic but irreversible, which is not surprising, but may represent a point in the clinical progression of AS at which valve replacement should be recommended to prevent further irreversible damage. If this transition point to maladaptive remodelling could be anticipated then intervention could be performed before the emergence irreversible focal replacement scar – a combination of blood and imaging biomarkers may be able to identify these transition points in the future. Furthermore, drug therapies could be used post-AVR to augment or accelerate normalization of both cell hypertrophy and diffuse fibrosis.

5. Diffuse myocardial fibrosis assessed by ECV prior to AVR is a univariate predictor of all-cause mortality at 1-year follow-up (event rate was too low to perform multivariate analysis). Patients with the highest fibrosis also have worse myocardial remodelling, systolic and diastolic function. Larger studies are required to confirm ECV as an independent predictor of cardiovascular mortality.

Current management strategies for AS mainly rely on waiting until the onset of symptoms. However, it is recognized that for some this is too late; furthermore, there is a discrepancy between symptom development and markers of long-term outcome post AVR (e.g. LGE). While existing models of AS may be simplistic, our current understanding is that AS is a disease of both the valve and myocardium. Thus, treatment strategies need to assess both haemodynamic insult imposed by the valve lesion and the extent of myocardial structural remodeling, particularly when seeking to quantify irreversible changes and predict outcome.

10.5 On-going / Future work:

10.5.1 Occult amyloid in AS: A sTudy invesTigating the Role of occult cardiac amyloid in the elderly with Aortic Stenosis (ATTRact AS).

This work is a direct product of my work on occult amyloid in AS detailed in Chapter 7.3. I supervised the successful funding application (British Heart Foundation CRTF FS/16/31/32185; Dr Paul Scully; £233,914) and continue to support Dr Paul Scully in his the on-going research.

Aim: To confirm the prevalence, clinical impact (procedural complications, symptom response to aortic valve replacement, 1-year mortality) and potential place of imaging (DPD scintigraphy, ECV by CT, CMR and echocardiography) in occult amyloid in severe AS. We hypothesize that in the elderly with severe AS being considered for intervention (TAVI, sAVR), ATTR is common, conveys a worse prognosis and can be reliably detected non-invasively.

Design: Single centre, 250 patients. Prospective observational cohort with 1-year follow-up in patients aged 75 or older with severe AS referred to the Barts Heart Centre for consideration of intervention (surgical AVR or TAVI).

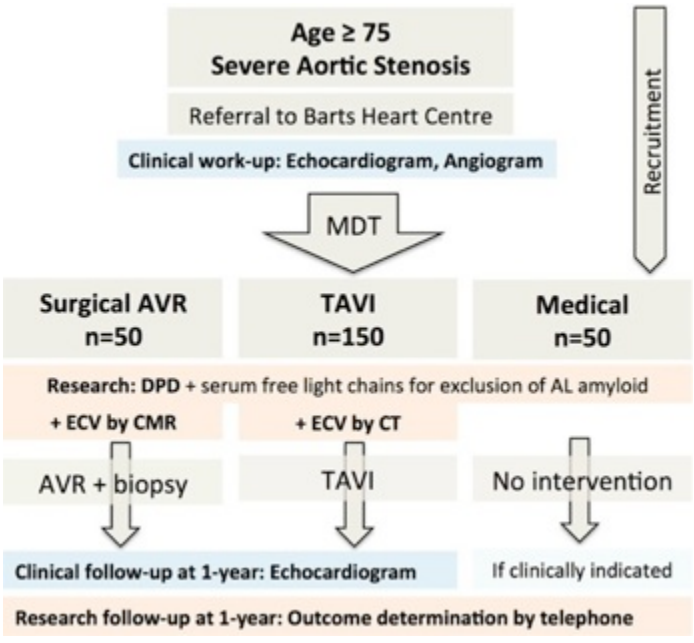

Figure 60: ATTRact-AS study scheme

10.5.2 ECV quantification by CCT

10.5.2.1 Amyloid cohort II - 3D volumes, co-registration, segmentation.

We have successfully recruited and scanned 50 patients with systemic amyloidosis at the National Amyloidosis Centre, Royal Free Hospital, in order to develop more advanced analysis processes and to thereby obtain a better understanding of the regional variation of amyloid deposition in the heart. Co-locating the test with the National Amyloidosis Centre has improved the patient experience and has also allowed us to take advantage of using the newest 3rd generation CT technology.

10.5.2.2 ATTRact-AS

ECV quantification by CCT is an integral part of the ATTRact-AS project; a cardiac CT is an integral part of pre-procedural planning prior to TAVI – adding ECV quantification is simple and safe.

10.5.3 Dark blood LGE for subendocardial scar in AS.

Dark blood PSIR late gadolinium enhancement imaging is an exciting new technique, that is particularly promising in revealing under-diagnosed subendocardial enhancement in AS [282].

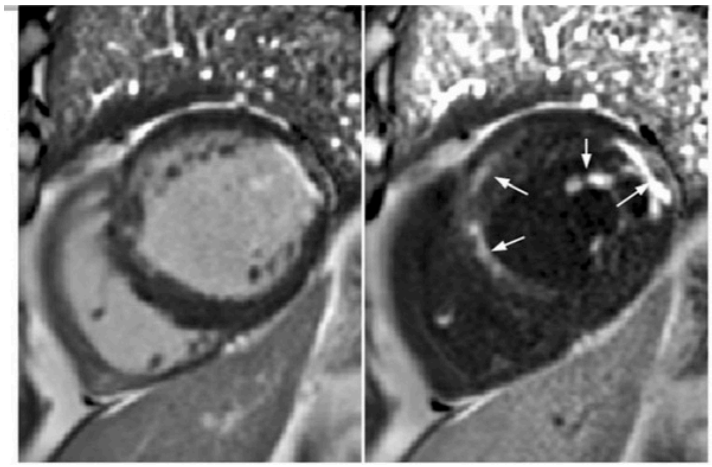

Figure 61: Dark blood PSIR LGE

Example of PSIR LGE dark and bright blood showing subtle subendocardial scar in the anteroseptum that is poorly visualised with bright blood imaging (Adapted from Kellman JCMR 2016 [282])

10.5.4 Basic science collaborations – ongoing work

10.5.4.1 Collagen Metabolism in Aortic Stenosis

Collaborator: Prof Javier Díez / Dr Begoña Lopez / Dr Arantxa Gonzalez, Center for Applied Medical Research, University of Navarra, Pamplona, Spain.

Aims: To evaluate the prognostic value of alterations in the extracellular matrix. To study the association between ECV and collagen quantity and quality.To analyse the potential incremental prognostic value of combining both.

10.5.4.2 ChipSeq

Collaborator: Prof Folkert Asselsberg / Dr Magdalena Harakalova, Department of Cardiology, Division Heart & Lungs, UMC Utrecht, the Netherlands.

Aim: To map the chromatin active regions in human myocardium with AS-induced myocardial remodelling to help identify key epigenetic pathways in disease aetiology using chromatin immuno-precipitation followed by read sequencing (ChIP-seq).

10.5.4.3 Proteomics

Collaborator: Dr Kevin Mills and Dr Anna Baud, Institute of Child Research, UCL.

Aim: To proteomic profiles in myocardial tissue from patients with different pattern of myocardial remodelling in AS and other forms of LVH.

10.5.4.4 Confocal Microscopy

Collaborator: Dr Patrizia Camelliti, University of Surrey, Guildford, UK.

Aim: Validation of ECV by CMR using confocal microscopy – insights into the constituents of the myocardium and their individual contribution to cellular and matrix volume.

10.5.4.5 Energy metabolism and stress response pathways in Aortic Stenosis

Collaborator: Prof Alun Hughes / Dr Anish Bhuva, ICS, UCL.

Aim: To explore the contribution of energy metabolism and stress response pathways to differential myocardial remodelling in AS.

10.6 Conclusion

In this thesis focussing on patient with severe aortic stenosis, I demonstrated the utility of invasive and non-invasive myocardial tissue characterisation, showing sex dimorphism in remodelling with worse remodelling in men, a significant prevalence of occult amyloid in AS associated with worse outcome, complex pattern of myocardial fibrosis on histology and CMR requiring combination of biopsy and imaging to broadening our understanding of AS pathophysiology, and finally a regression of diffuse fibrosis after aortic valve replacement. These insights support that AS is a disease of the myocardium as well as valve open up the potential for important further work to deepen our understanding of myocardial remodelling in aortic stenosis.

Chapter 11 References

1. *Fact sheet no 310:Global Burden of Disease update. In: Organization WH, (ed).* 2008.
2. Lindroos, M., et al., *Prevalence of aortic valve abnormalities in the elderly: an echocardiographic study of a random population sample.* Journal of the American College of Cardiology, 1993. **21**(5): p. 1220-5.
3. Fighali, S.F., et al., *Early and late mortality of patients undergoing aortic valve replacement after previous coronary artery bypass graft surgery.* Circulation, 1995. **92**(9 Suppl): p. II163-8.
4. Varadarajan, P., et al., *Clinical profile and natural history of 453 nonsurgically managed patients with severe aortic stenosis.* The Annals of thoracic surgery, 2006. **82**(6): p. 2111-5.
5. Kvidal, P., et al., *Observed and relative survival after aortic valve replacement.* Journal of the American College of Cardiology, 2000. **35**(3): p. 747-56.
6. Bonow, R.O., et al., *2008 focused update incorporated into the ACC/AHA 2006 guidelines for the management of patients with valvular heart disease: a report of the American College of Cardiology/American Heart Association Task Force on Practice Guidelines (Writing Committee to revise the 1998 guidelines for the management of patients with valvular heart disease). Endorsed by the Society of Cardiovascular Anesthesiologists, Society for Cardiovascular Angiography and Interventions, and Society of Thoracic Surgeons.* Journal of the American College of Cardiology, 2008. **52**(13): p. e1-142.
7. Taylor, J., *ESC/EACTS Guidelines on the management of valvular heart disease.* European heart journal, 2012. **33**(19): p. 2371-2.
8. Pellikka, P.A., et al., *Outcome of 622 adults with asymptomatic, hemodynamically significant aortic stenosis during prolonged follow-up.* Circulation, 2005. **111**(24): p. 3290-5.
9. Carabello, B.A., *Evaluation and management of patients with aortic stenosis.* Circulation, 2002. **105**(15): p. 1746-50.
10. Kelly, T.A., et al., *Comparison of outcome of asymptomatic to symptomatic patients older than 20 years of age with valvular aortic stenosis.* The American journal of cardiology, 1988. **61**(1): p. 123-30.
11. Otto, C.M., et al., *Prospective study of asymptomatic valvular aortic stenosis. Clinical, echocardiographic, and exercise predictors of outcome.* Circulation, 1997. **95**(9): p. 2262-70.
12. Walther, T., et al., *Contemporary management of aortic stenosis: surgical aortic valve replacement remains the gold standard.* Heart, 2012. **98 Suppl 4**: p. iv23-iv29.
13. McCann, G.P., et al., *Managing the asymptomatic patient with severe aortic stenosis: randomised controlled trials of early surgery are overdue.* Heart, 2011. **97**(14): p. 1119-21.

14. Rosenhek, R., et al., *Natural history of very severe aortic stenosis.* Circulation, 2010. **121**(1): p. 151-6.

15. Kang, D.H., et al., *Early surgery versus conventional treatment in asymptomatic very severe aortic stenosis.* Circulation, 2010. **121**(13): p. 1502-9.

16. Kitai, T., et al., *Clinical outcomes in non-surgically managed patients with very severe versus severe aortic stenosis.* Heart, 2011. **97**(24): p. 2029-32.

17. Vahanian, A., et al., *Guidelines on the management of valvular heart disease: The Task Force on the Management of Valvular Heart Disease of the European Society of Cardiology.* European heart journal, 2007. **28**(2): p. 230-68.

18. Davies, S.W., A.H. Gershlick, and R. Balcon, *Progression of valvar aortic stenosis: a long-term retrospective study.* European heart journal, 1991. **12**(1): p. 10-4.

19. Turina, J., et al., *Spontaneous course of aortic valve disease.* European heart journal, 1987. **8**(5): p. 471-83.

20. Members, A.T.F., et al., *Guidelines on the management of valvular heart disease (version 2012): The Joint Task Force on the Management of Valvular Heart Disease of the European Society of Cardiology (ESC) and the European Association for Cardio-Thoracic Surgery (EACTS).* European Heart Journal, 2012. **33**(19): p. 2451-2496.

21. Carabello, B.A., *Should severe aortic stenosis be operated on before symptom onset? Aortic valve replacement should be operated on before symptom onset.* Circulation, 2012. **126**(1): p. 112-7.

22. Ugander, M., et al., *Myocardial edema as detected by pre-contrast T1 and T2 CMR delineates area at risk associated with acute myocardial infarction.* JACC Cardiovasc Imaging, 2012. **5**(6): p. 596-603.

23. Nishimura, R.A., et al., *2014 AHA/ACC Guideline for the Management of Patients With Valvular Heart Disease: Executive Summary: A Report of the American College of Cardiology/American Heart Association Task Force on Practice Guidelines.* Journal of the American College of Cardiology, 2014. **63**(22): p. 2438-88.

24. Lorell, B.H. and B.A. Carabello, *Left ventricular hypertrophy: pathogenesis, detection, and prognosis.* Circulation, 2000. **102**(4): p. 470-9.

25. Dweck, M.R., et al., *Left ventricular remodeling and hypertrophy in patients with aortic stenosis: insights from cardiovascular magnetic resonance.* Journal of cardiovascular magnetic resonance : official journal of the Society for Cardiovascular Magnetic Resonance, 2012. **14**: p. 50.

26. Cioffi, G., et al., *Prognostic effect of inappropriately high left ventricular mass in asymptomatic severe aortic stenosis.* Heart, 2011. **97**(4): p. 301-7.

27. Greve, A.M., et al., *Differences in cardiovascular risk profile between electrocardiographic hypertrophy versus strain in asymptomatic patients with aortic stenosis (from SEAS data).* The American journal of cardiology, 2011. **108**(4): p. 541-7.

28. Mihaljevic, T., et al., *Survival after valve replacement for aortic stenosis: implications for decision making.* The Journal of Thoracic and Cardiovascular Surgery, 2008. **135**(6): p. 1270-8; discussion 1278-9.

29. Ali, A., et al., *Enhanced left ventricular mass regression after aortic valve replacement in patients with aortic stenosis is associated with improved long-term survival.* The Journal of Thoracic and Cardiovascular Surgery, 2011. **142**(2): p. 285-91.

30. Vahanian, A., et al., *Guidelines on the management of valvular heart disease (version 2012): the Joint Task Force on the Management of Valvular Heart Disease of the European Society of Cardiology (ESC) and the European Association for Cardio-Thoracic Surgery (EACTS).* European journal of cardio-thoracic surgery : official journal of the European Association for Cardio-thoracic Surgery, 2012. **42**(4): p. S1-44.

31. Casaclang-Verzosa, G., et al., *Does left atrial size predict mortality in asymptomatic patients with severe aortic stenosis?* Echocardiography, 2010. **27**(2): p. 105-9.

32. Greve, A.M., et al., *Prognostic importance of atrial fibrillation in asymptomatic aortic stenosis: the Simvastatin and Ezetimibe in Aortic Stenosis study.* International journal of cardiology, 2013. **166**(1): p. 72-6.

33. Weidemann, F., et al., *Impact of myocardial fibrosis in patients with symptomatic severe aortic stenosis.* Circulation, 2009. **120**(7): p. 577-84.

34. Aurigemma, G.P., et al., *Geometric changes allow normal ejection fraction despite depressed myocardial shortening in hypertensive left ventricular hypertrophy.* Journal of the American College of Cardiology, 1995. **26**(1): p. 195-202.

35. Delgado, V., et al., *Strain analysis in patients with severe aortic stenosis and preserved left ventricular ejection fraction undergoing surgical valve replacement.* European heart journal, 2009. **30**(24): p. 3037-47.

36. Lancellotti, P., et al., *Risk stratification in asymptomatic moderate to severe aortic stenosis: the importance of the valvular, arterial and ventricular interplay.* Heart, 2010. **96**(17): p. 1364-71.

37. Lim, E., et al., *Longitudinal study of the profile and predictors of left ventricular mass regression after stentless aortic valve replacement.* Ann Thorac Surg, 2008. **85**(6): p. 2026-9.

38. Repossini, A., et al., *Early clinical and haemodynamic results after aortic valve replacement with the Freedom SOLO bioprosthesis (experience of Italian multicenter study).* Eur J Cardiothorac Surg, 2012. **41**(5): p. 1104-10.

39. Beach, J.M., et al., *Ventricular hypertrophy and left atrial dilatation persist and are associated with reduced survival after valve replacement for aortic stenosis.* J Thorac Cardiovasc Surg, 2014. **147**(1): p. 362-369 e8.

40. Gotzmann, M., et al., *Hemodynamic results and changes in myocardial function after transcatheter aortic valve implantation.* Am Heart J, 2010. **159**(5): p. 926-32.

41. Lamb, H.J., et al., *Left ventricular remodeling early after aortic valve replacement: differential effects on diastolic function in aortic valve stenosis and aortic regurgitation.* J Am Coll Cardiol, 2002. **40**(12): p. 2182-8.

42. Dobson, L.E., et al., *Sex-related differences in left ventricular remodeling in severe aortic stenosis and reverse remodeling after aortic valve replacement: A cardiovascular magnetic resonance study.* Am Heart J, 2016. **175**: p. 101-11.

43. Fairbairn, T.A., et al., *Assessment of valve haemodynamics, reverse ventricular remodelling and myocardial fibrosis following transcatheter aortic valve implantation compared to surgical aortic valve replacement: a cardiovascular magnetic resonance study.* Heart, 2013. **99**(16): p. 1185-91.

44. La Manna, A., et al., *Left ventricular reverse remodeling after transcatheter aortic valve implantation: a cardiovascular magnetic resonance study.* J Cardiovasc Magn Reson, 2013. **15**: p. 39.

45. Villari, B., et al., *Normalization of diastolic dysfunction in aortic stenosis late after valve replacement.* Circulation, 1995. **91**(9): p. 2353-8.

46. Milano, A.D., et al., *Prognostic value of myocardial fibrosis in patients with severe aortic valve stenosis.* The Journal of Thoracic and Cardiovascular Surgery, 2012.

47. Shin, S., et al., *Mass reduction and functional improvement of the left ventricle after aortic valve replacement for degenerative aortic stenosis.* The Korean journal of thoracic and cardiovascular surgery, 2011. **44**(6): p. 399-405.

48. Flett, A.S., et al., *Diffuse myocardial fibrosis in severe aortic stenosis: an equilibrium contrast cardiovascular magnetic resonance study.* Eur Heart J Cardiovasc Imaging, 2012. **13**(10): p. 819-26.

49. Dweck, M.R., N.A. Boon, and D.E. Newby, *Calcific aortic stenosis: a disease of the valve and the myocardium.* Journal of the American College of Cardiology, 2012. **60**(19): p. 1854-63.

50. Yarbrough, W.M., et al., *Myocardial remodeling with aortic stenosis and after aortic valve replacement: mechanisms and future prognostic implications.* The Journal of Thoracic and Cardiovascular Surgery, 2012. **143**(3): p. 656-64.

51. Valencia F, L.B., Gómez Doblas JJ, Díez J, de Teresa E *Myocardial fibrosis in aortic stenosis: molecular mechanisms and an approach to its non-invasive assessment (Abstract).* J Am Coll Cardiol 2010. **55**: p. 148.

52. Kanzaki, Y., et al., *Images in cardiovascular medicine. Three-dimensional remodeling of cardiomyocytes in a patient with aortic stenosis: scanning electron microscopy.* Circulation, 2009. **119**(2): p. e10.

53. Ahmed, S.H. and M.L. Lindsey, *Titin phosphorylation: myocardial passive stiffness regulated by the intracellular giant.* Circ Res, 2009. **105**(7): p. 611-3.

54. Anderson, K.R., M.G. Sutton, and J.T. Lie, *Histopathological types of cardiac fibrosis in myocardial disease.* The Journal of pathology, 1979. **128**(2): p. 79-85.

55. Barone-Rochette, G., et al., *Prognostic Significance of LGE by CMR in Aortic Stenosis Patients Undergoing Valve Replacement.* Journal of the American College of Cardiology, 2014. **64**(2): p. 144-54.

56. Hein, S., et al., *Progression from compensated hypertrophy to failure in the pressure-overloaded human heart: structural deterioration and compensatory mechanisms.* Circulation, 2003. **107**(7): p. 984-91.

57. Schwarz, F., et al., *Correlation between myocardial structure and diastolic properties of the heart in chronic aortic valve disease: effects of corrective surgery.* The American journal of cardiology, 1978. **42**(6): p. 895-903.

58. Azevedo, C.F., et al., *Prognostic significance of myocardial fibrosis quantification by histopathology and magnetic resonance imaging in patients with severe aortic valve disease.* Journal of the American College of Cardiology, 2010. **56**(4): p. 278-87.

59. Becker, A.E., C.D. Heijmans, and C.E. Essed, *Chronic non-ischaemic congestive heart disease and endomyocardial biopsies. Worth the extra?* European heart journal, 1991. **12**(2): p. 218-23.

60. Carroll, J.D., et al., *Sex-associated differences in left ventricular function in aortic stenosis of the elderly.* Circulation, 1992. **86**(4): p. 1099-107.

61. Douglas, P.S., et al., *Gender differences in left ventricle geometry and function in patients undergoing balloon dilatation of the aortic valve for isolated aortic stenosis. NHLBI Balloon Valvuloplasty Registry.* Br Heart J, 1995. **73**(6): p. 548-54.

62. Aurigemma, G.P. and W.H. Gaasch, *Gender differences in older patients with pressure-overload hypertrophy of the left ventricle.* Cardiology, 1995. **86**(4): p. 310-7.

63. Villari, B., et al., *Sex-dependent differences in left ventricular function and structure in chronic pressure overload.* Eur Heart J, 1995. **16**(10): p. 1410-9.

64. Rossebo, A.B., et al., *Intensive lipid lowering with simvastatin and ezetimibe in aortic stenosis.* The New England journal of medicine, 2008. **359**(13): p. 1343-56.

65. Briand, M., et al., *Reduced systemic arterial compliance impacts significantly on left ventricular afterload and function in aortic stenosis: implications for diagnosis and treatment.* Journal of the American College of Cardiology, 2005. **46**(2): p. 291-8.

66. Diez, J., et al., *Losartan-dependent regression of myocardial fibrosis is associated with reduction of left ventricular chamber stiffness in hypertensive patients.* Circulation, 2002. **105**(21): p. 2512-7.

67. Bull, S., et al., *A prospective, double-blind, randomized controlled trial of the angiotensin-converting enzyme inhibitor Ramipril In Aortic Stenosis (RIAS trial).* Eur Heart J Cardiovasc Imaging, 2015. **16**(8): p. 834-41.

68. Nadir, M.A., et al., *Impact of renin-angiotensin system blockade therapy on outcome in aortic stenosis.* J Am Coll Cardiol, 2011. **58**(6): p. 570-6.

69. Banypersad, S.M., et al., *Updates in cardiac amyloidosis: a review.* Journal of the American Heart Association, 2012. **1**(2): p. e000364.

70. Falk, R.H., *Diagnosis and management of the cardiac amyloidoses.* Circulation, 2005. **112**(13): p. 2047-60.

71. Tanskanen, M., et al., *Senile systemic amyloidosis affects 25% of the very aged and associates with genetic variation in alpha2-macroglobulin and tau: a population-based autopsy study.* Ann Med, 2008. **40**(3): p. 232-9.

72. Gillmore, J.D., et al., *Non-Biopsy Diagnosis of Cardiac Transthyretin Amyloidosis.* Circulation, 2016.

73. Nietlispach, F., et al., *Pathology of transcatheter valve therapy.* JACC Cardiovasc Interv, 2012. **5**(5): p. 582-90.

74. Rossi, M.A., *Pathologic fibrosis and connective tissue matrix in left ventricular hypertrophy due to chronic arterial hypertension in humans.* Journal of hypertension, 1998. **16**(7): p. 1031-41.

75. Weber, K.T. and C.G. Brilla, *Myocardial fibrosis and the renin-angiotensin-aldosterone system.* Journal of cardiovascular pharmacology, 1992. **20 Suppl 1**: p. S48-54.

76. Beltrami, C.A., et al., *Structural basis of end-stage failure in ischemic cardiomyopathy in humans.* Circulation, 1994. **89**(1): p. 151-63.

77. Higgins, C.B., et al., *Nuclear magnetic resonance imaging of acute myocardial infarction in dogs: alterations in magnetic relaxation times.* The American journal of cardiology, 1983. **52**(1): p. 184-8.

78. Nair, V. and J. Butany, *Heart transplant biopsies: interpretation and significance.* Journal of clinical pathology, 2010. **63**(1): p. 12-20.

79. Kim, R.J., et al., *Myocardial Gd-DTPA kinetics determine MRI contrast enhancement and reflect the extent and severity of myocardial injury after acute reperfused infarction.* Circulation, 1996. **94**(12): p. 3318-26.

80. Flacke, S.J., S.E. Fischer, and C.H. Lorenz, *Measurement of the gadopentetate dimeglumine partition coefficient in human myocardium in vivo: normal distribution and elevation in acute and chronic infarction.* Radiology, 2001. **218**(3): p. 703-10.

81. Kim, R.J., D.J. Shah, and R.M. Judd, *How we perform delayed enhancement imaging.* Journal of cardiovascular magnetic resonance : official journal of the Society for Cardiovascular Magnetic Resonance, 2003. **5**(3): p. 505-14.

82. Schelbert, E.B., et al., *Late gadolinium-enhancement cardiac magnetic resonance identifies postinfarction myocardial fibrosis and the border zone at the near cellular level in ex vivo rat heart.* Circulation. Cardiovascular imaging, 2010. **3**(6): p. 743-52.

83. Flett, A.S., et al., *Evaluation of techniques for the quantification of myocardial scar of differing etiology using cardiac magnetic resonance.* JACC. Cardiovascular imaging, 2011. **4**(2): p. 150-6.

84. Jellis, C.L. and D.H. Kwon, *Myocardial T1 mapping: modalities and clinical applications.* Cardiovasc Diagn Ther, 2014. **4**(2): p. 126-37.

85. Goldman, M.R., et al., *Quantification of experimental myocardial infarction using nuclear magnetic resonance imaging and paramagnetic ion contrast enhancement in excised canine hearts.* Circulation, 1982. **66**(5): p. 1012-6.

86. Wesbey, G.E., et al., *Effect of gadolinium-DTPA on the magnetic relaxation times of normal and infarcted myocardium.* Radiology, 1984. **153**(1): p. 165-9.

87. Wesbey, G., et al., *Imaging and characterization of acute myocardial infarction in vivo by gated nuclear magnetic resonance.* Circulation, 1984. **69**(1): p. 125-30.

88. Simonetti, O.P., et al., *An improved MR imaging technique for the visualization of myocardial infarction.* Radiology, 2001. **218**(1): p. 215-23.

89. Kim, R.J., et al., *Relationship of MRI delayed contrast enhancement to irreversible injury, infarct age, and contractile function.* Circulation, 1999. **100**(19): p. 1992-2002.

90. Rehwald, W.G., et al., *Myocardial magnetic resonance imaging contrast agent concentrations after reversible and irreversible ischemic injury.* Circulation, 2002. **105**(2): p. 224-9.

91. Kim, R.J., et al., *The use of contrast-enhanced magnetic resonance imaging to identify reversible myocardial dysfunction.* The New England journal of medicine, 2000. **343**(20): p. 1445-53.

92. Selvanayagam, J.B., et al., *Value of delayed-enhancement cardiovascular magnetic resonance imaging in predicting myocardial viability after surgical revascularization.* Circulation, 2004. **110**(12): p. 1535-41.

93. Choi, K.M., et al., *Transmural extent of acute myocardial infarction predicts long-term improvement in contractile function.* Circulation, 2001. **104**(10): p. 1101-7.

94. Yan, A.T., et al., *Characterization of the peri-infarct zone by contrast-enhanced cardiac magnetic resonance imaging is a powerful predictor of post-myocardial infarction mortality.* Circulation, 2006. **114**(1): p. 32-9.

95. Kwong, R.Y., et al., *Impact of unrecognized myocardial scar detected by cardiac magnetic resonance imaging on event-free survival in patients presenting with signs or symptoms of coronary artery disease.* Circulation, 2006. **113**(23): p. 2733-43.

96. Wu, E., et al., *Infarct size by contrast enhanced cardiac magnetic resonance is a stronger predictor of outcomes than left ventricular ejection fraction or end-systolic volume index: prospective cohort study.* Heart, 2008. **94**(6): p. 730-6.

97. Klein, C., et al., *The influence of myocardial blood flow and volume of distribution on late Gd-DTPA kinetics in ischemic heart failure.* Journal of magnetic resonance imaging : JMRI, 2004. **20**(4): p. 588-93.

98. Wagner, A., et al., *Contrast-enhanced MRI and routine single photon emission computed tomography (SPECT) perfusion imaging for detection of subendocardial myocardial infarcts: an imaging study.* The Lancet, 2003. **361**(9355): p. 374-379.

99. Mahrholdt, H., et al., *Reproducibility of chronic infarct size measurement by contrast-enhanced magnetic resonance imaging.* Circulation, 2002. **106**(18): p. 2322-7.

100. Kim, R.J., et al., *Performance of delayed-enhancement magnetic resonance imaging with gadoversetamide contrast for the detection and assessment of myocardial infarction: an international, multicenter, double-blinded, randomized trial.* Circulation, 2008. **117**(5): p. 629-37.

101. Choudhury, L., et al., *Myocardial scarring in asymptomatic or mildly symptomatic patients with hypertrophic cardiomyopathy.* Journal of the American College of Cardiology, 2002. **40**(12): p. 2156-64.

102. Wagner, A., et al., *Long-term follow-up of patients paragraph sign with acute myocarditis by magnetic paragraph sign resonance imaging.* Magma, 2003. **16**(1): p. 17-20.

103. Dweck, M.R., et al., *Midwall fibrosis is an independent predictor of mortality in patients with aortic stenosis.* Journal of the American College of Cardiology, 2011. **58**(12): p. 1271-9.

104. Maceira, A.M., et al., *Cardiovascular magnetic resonance and prognosis in cardiac amyloidosis.* Journal of cardiovascular magnetic resonance : official journal of the Society for Cardiovascular Magnetic Resonance, 2008. **10**: p. 54.

105. Debl, K., et al., *Delayed hyperenhancement in magnetic resonance imaging of left ventricular hypertrophy caused by aortic stenosis and hypertrophic cardiomyopathy: visualisation of focal fibrosis.* Heart, 2006. **92**(10): p. 1447-51.

106. Lee, S.P., et al., *Early detection of subclinical ventricular deterioration in aortic stenosis with cardiovascular magnetic resonance and echocardiography.* J Cardiovasc Magn Reson, 2013. **15**: p. 72.

107. Rader, F., et al., *Left ventricular hypertrophy in valvular aortic stenosis: mechanisms and clinical implications.* Am J Med, 2015. **128**(4): p. 344-52.

108. Kehr, E., et al., *Gadolinium-enhanced magnetic resonance imaging for detection and quantification of fibrosis in human myocardium in vitro.* The international journal of cardiovascular imaging, 2008. **24**(1): p. 61-8.

109. Flett, A.S., et al., *Equilibrium contrast cardiovascular magnetic resonance for the measurement of diffuse myocardial fibrosis: preliminary validation in humans.* Circulation, 2010. **122**(2): p. 138-44.

110. White, S.K., et al., *T1 Mapping for Myocardial Extracellular Volume Measurement by CMR: Bolus Only Versus Primed Infusion Technique.* JACC. Cardiovascular imaging, 2013.

111. Miller, C.A., et al., *Comprehensive validation of cardiovascular magnetic resonance techniques for the assessment of myocardial extracellular volume.* Circulation. Cardiovascular imaging, 2013. **6**(3): p. 373-83.

112. Iles, L., et al., *Evaluation of diffuse myocardial fibrosis in heart failure with cardiac magnetic resonance contrast-enhanced T1 mapping.* Journal of the American College of Cardiology, 2008. **52**(19): p. 1574-80.

113. Iles, L., et al., *Evaluation of Diffuse Myocardial Fibrosis in Heart Failure With Cardiac Magnetic Resonance Contrast-Enhanced T1 Mapping.* Journal of the American College of Cardiology, 2008. **52**(19): p. 1574-1580.

114. Flett, A.S., et al., *Equilibrium contrast cardiovascular magnetic resonance for the measurement of diffuse myocardial fibrosis: preliminary validation in humans.* Circulation, 2010. **122**(2): p. 138-144.

115. Sibley, C.T., et al., *T1 Mapping in Cardiomyopathy at Cardiac MR: Comparison with Endomyocardial Biopsy.* Radiology, 2012. **265**(3): p. 724-732.

116. Mascherbauer, J., et al., *Cardiac magnetic resonance postcontrast T1 time is associated with outcome in patients with heart failure and preserved ejection fraction.* Circ Cardiovasc Imaging, 2013. **6**(6): p. 1056-65.

117. White, S.K., et al., *T1 mapping for myocardial extracellular volume measurement by CMR: bolus only versus primed infusion technique.* JACC Cardiovasc Imaging, 2013. **6**(9): p. 955-62.

118. Miller, C.A., et al., *Comprehensive Validation of Cardiovascular Magnetic Resonance Techniques for the Assessment of Myocardial Extracellular Volume.* Circulation. Cardiovascular imaging, 2013. **6**(3): p. 373-383.

119. Bull, S., et al., *Human non-contrast T1 values and correlation with histology in diffuse fibrosis.* Heart, 2013.

120. Lee, S.P., et al., *Assessment of diffuse myocardial fibrosis by using MR imaging in asymptomatic patients with aortic stenosis.* Radiology, 2015. **274**(2): p. 359-69.

121. de Meester de Ravenstein, C., et al., *Histological Validation of measurement of diffuse interstitial myocardial fibrosis by myocardial extravascular volume fraction from Modified Look-Locker imaging (MOLLI) T1 mapping at 3 T.* J Cardiovasc Magn Reson, 2015. **17**: p. 48.

122. Coelho-Filho, O.R., et al., *Quantification of cardiomyocyte hypertrophy by cardiac magnetic resonance: implications for early cardiac remodeling.* Circulation, 2013. **128**(11): p. 1225-33.

123. Ugander, M., et al., *Myocardial edema as detected by pre-contrast T1 and T2 CMR delineates area at risk associated with acute myocardial infarction.* JACC. Cardiovascular imaging, 2012. **5**(6): p. 596-603.

124. Karamitsos, T.D., et al., *Noncontrast T1 mapping for the diagnosis of cardiac amyloidosis.* JACC. Cardiovascular imaging, 2013. **6**(4): p. 488-97.

125. McDiarmid, A.K., et al., *Athletic Cardiac Adaptation in Males Is a Consequence of Elevated Myocyte Mass.* Circ Cardiovasc Imaging, 2016. **9**(4).

126. Sado, D.M., et al., *Noncontrast myocardial T mapping using cardiovascular magnetic resonance for iron overload.* Journal of magnetic resonance imaging : JMRI, 2014.

127. Sado, D.M., et al., *Identification and assessment of Anderson-Fabry disease by cardiovascular magnetic resonance noncontrast myocardial T1 mapping.* Circulation. Cardiovascular imaging, 2013. **6**(3): p. 392-8.

128. Dall'Armellina, E., et al., *Cardiovascular magnetic resonance by non contrast T1-mapping allows assessment of severity of injury in acute myocardial infarction.* J Cardiovasc Magn Reson, 2012. **14**: p. 15.

129. Raman, F.S., et al., *Modified look-locker inversion recovery T1 mapping indices: assessment of accuracy and reproducibility between magnetic resonance scanners.* J Cardiovasc Magn Reson, 2013. **15**: p. 64.

130. Kramer, C.M., et al., *Hypertrophic Cardiomyopathy Registry: The rationale and design of an international, observational study of hypertrophic cardiomyopathy.* Am Heart J, 2015. **170**(2): p. 223-30.

131. Captur, G., et al., *A T1 and ECV phantom for global T1 mapping quality assurance: The T1 mapping and ECV standardisation in CMR (T1MES) program.* Journal of Cardiovascular Magnetic Resonance, 2016. **18**(1): p. 1-3.

132. Ugander, M., et al., *Extracellular volume imaging by magnetic resonance imaging provides insights into overt and sub-clinical myocardial pathology.* European heart journal, 2012. **33**(10): p. 1268-78.

133. Wong, T.C., et al., *Association between extracellular matrix expansion quantified by cardiovascular magnetic resonance and short-term mortality.* Circulation, 2012. **126**(10): p. 1206-16.

134. Wong, T.C., et al., *Myocardial extracellular volume fraction quantified by cardiovascular magnetic resonance is increased in diabetes and associated with mortality and incident heart failure admission.* European heart journal, 2013.

135. Fontana, M., et al., *Differential Myocyte Responses in Patients with Cardiac Transthyretin Amyloidosis and Light-Chain Amyloidosis: A Cardiac MR Imaging Study.* Radiology, 2015. **277**(2): p. 388-97.

136. Messroghli, D.R., et al., *Modified Look-Locker inversion recovery (MOLLI) for high-resolution T1 mapping of the heart.* Magnetic resonance in medicine : official journal of the Society of Magnetic Resonance in Medicine / Society of Magnetic Resonance in Medicine, 2004. **52**(1): p. 141-6.

137. Piechnik, S.K., et al., *Shortened Modified Look-Locker Inversion recovery (ShMOLLI) for clinical myocardial T1-mapping at 1.5 and 3 T within a 9 heartbeat breathhold.* Journal of cardiovascular magnetic resonance : official journal of the Society for Cardiovascular Magnetic Resonance, 2010. **12**: p. 69.

138. Chow, K., et al., *Saturation recovery single-shot acquisition (SASHA) for myocardial T mapping.* Magnetic resonance in medicine : official journal of the Society of Magnetic Resonance in Medicine / Society of Magnetic Resonance in Medicine, 2013.

139. Roujol, S., et al., *Accuracy, precision, and reproducibility of four T1 mapping sequences: a head-to-head comparison of MOLLI, ShMOLLI, SASHA, and SAPPHIRE.* Radiology, 2014. **272**(3): p. 683-9.

140. Mehta, B.B., et al., *Accelerated and navigator-gated look-locker imaging for cardiac T1 estimation (ANGIE): Development and application to T1 mapping of the right ventricle.* Magn Reson Med, 2015. **73**(1): p. 150-60.

141. Kvernby, S., et al., *Simultaneous three-dimensional myocardial T1 and T2 mapping in one breath hold with 3D-QALAS.* J Cardiovasc Magn Reson, 2014. **16**: p. 102.

142. Xue, H., et al., *Phase-sensitive inversion recovery for myocardial T1 mapping with motion correction and parametric fitting.* Magnetic resonance in medicine : official journal of the Society of Magnetic Resonance in Medicine / Society of Magnetic Resonance in Medicine, 2013. **69**(5): p. 1408-20.

143. Kellman, P. and M.S. Hansen, *T1-mapping in the heart: accuracy and precision.* Journal of cardiovascular magnetic resonance : official journal of the Society for Cardiovascular Magnetic Resonance, 2014. **16**: p. 2.

144. Schelbert, E.B., et al., *Myocardial extravascular extracellular volume fraction measurement by gadolinium cardiovascular magnetic resonance in humans: slow infusion versus bolus.* J Cardiovasc Magn Reson, 2011. **13**: p. 16.

145. White, S.K., et al., *T1 mapping for myocardial extracellular volume measurement by CMR: bolus only versus primed infusion technique.* JACC. Cardiovascular imaging, 2013. **6**(9): p. 955-62.

146. McDiarmid, A.K., et al., *Single bolus versus split dose gadolinium administration in extra-cellular volume calculation at 3 Tesla.* J Cardiovasc Magn Reson, 2015. **17**(1): p. 6.

147. Kellman, P., et al., *Extracellular volume fraction mapping in the myocardium, part 1: evaluation of an automated method.* Journal of cardiovascular magnetic resonance : official journal of the Society for Cardiovascular Magnetic Resonance, 2012. **14**: p. 63.

148. Hamilton, J.I., et al., *MR fingerprinting for rapid quantification of myocardial T1 , T2 , and proton spin density.* Magn Reson Med, 2017. **77**(4): p. 1446-1458.

149. Moon, J.C., et al., *Myocardial T1 mapping and extracellular volume quantification: a Society for Cardiovascular Magnetic Resonance (SCMR) and CMR Working Group of the European Society of Cardiology consensus statement.* J Cardiovasc Magn Reson, 2013. **15**: p. 92.

150. Robson, M.D., et al., *T measurements in the human myocardium: The effects of magnetization transfer on the SASHA and MOLLI sequences.* Magnetic resonance in medicine : official journal of the Society of Magnetic Resonance in Medicine / Society of Magnetic Resonance in Medicine, 2013.

151. Coelho-Filho, O.R., et al., *Role of transcytolemmal water-exchange in magnetic resonance measurements of diffuse myocardial fibrosis in hypertensive heart disease.* Circulation. Cardiovascular imaging, 2013. **6**(1): p. 134-41.

152. Petersen, S.E., et al., *Imaging in population science: cardiovascular magnetic resonance in 100,000 participants of UK Biobank - rationale, challenges and approaches.* J Cardiovasc Magn Reson, 2013. **15**: p. 46.

153. Schelbert, E.B., et al., *Myocardial extravascular extracellular volume fraction measurement by gadolinium cardiovascular magnetic resonance in humans: slow infusion versus bolus.* Journal of cardiovascular magnetic resonance : official journal of the Society for Cardiovascular Magnetic Resonance, 2011. **13**: p. 16.

154. Bull, S., et al., *Human non-contrast T1 values and correlation with histology in diffuse fibrosis.* Heart, 2013. **99**(13): p. 932-7.

155. Chin, C.W., et al., *Optimization and comparison of myocardial T1 techniques at 3T in patients with aortic stenosis.* European heart journal cardiovascular Imaging, 2014. **15**(5): p. 556-65.

156. Singh, A., et al., *Rationale and design of the PRognostic Importance of MIcrovascular Dysfunction in asymptomatic patients with Aortic Stenosis (PRIMID-AS): a multicentre observational study with blinded investigations.* BMJ open, 2013. **3**(12): p. e004348.

157. Bull, S., et al., *Human non-contrast T1 values and correlation with histology in diffuse fibrosis.* Heart, 2013. **99**(13): p. 932-937.

158. Chin, C.W., et al., *Optimization and comparison of myocardial T1 techniques at 3T in patients with aortic stenosis.* Eur Heart J Cardiovasc Imaging, 2014. **15**(5): p. 556-65.

159. Chin, C.W., et al., *High-sensitivity troponin I concentrations are a marker of an advanced hypertrophic response and adverse outcomes in patients with aortic stenosis.* Eur Heart J, 2014. **35**(34): p. 2312-21.

160. Dusenbery, S.M., et al., *Left Ventricular Strain and Myocardial Fibrosis in Congenital Aortic Stenosis.* Am J Cardiol, 2015. **116**(8): p. 1257-62.

161. Mahmod, M., et al., *Adenosine stress native T1 mapping in severe aortic stenosis: evidence for a role of the intravascular compartment on myocardial T1 values.* J Cardiovasc Magn Reson, 2014. **16**: p. 92.

162. Singh, A., et al., *Myocardial T1 and extracellular volume fraction measurement in asymptomatic patients with aortic stenosis: reproducibility and comparison with age-matched controls.* Eur Heart J Cardiovasc Imaging, 2015. **16**(7): p. 763-70.

163. Kockova, R., et al., *Native T1 Relaxation Time and Extracellular Volume Fraction as Accurate Markers of Diffuse Myocardial Fibrosis in Heart Valve Disease- Comparison With Targeted Left Ventricular Myocardial Biopsy.* Circ J, 2016. **80**(5): p. 1202-9.

164. Nadjiri, J., et al., *Prognostic value of T1-mapping in TAVR patients: extra-cellular volume as a possible predictor for peri- and post-TAVR adverse events.* Int J Cardiovasc Imaging, 2016.

165. Rakusan, K., et al., *Morphometry of human coronary capillaries during normal growth and the effect of age in left ventricular pressure-overload hypertrophy.* Circulation, 1992. **86**(1): p. 38-46.

166. Schwarz, F., et al., *Myocardial structure and function in patients with aortic valve disease and their relation to postoperative results.* Am J Cardiol, 1978. **41**(4): p. 661-9.

167. Cheitlin, M.D., et al., *The distribution of fibrosis in the left ventricle in congenital aortic stenosis and coarctation of the aorta.* Circulation, 1980. **62**(4): p. 823-830.

168. Bandula, S., et al., *Measurement of myocardial extracellular volume fraction by using equilibrium contrast-enhanced CT: validation against histologic findings.* Radiology, 2013. **269**(2): p. 396-403.

169. Nacif, M.S., et al., *Interstitial myocardial fibrosis assessed as extracellular volume fraction with low-radiation-dose cardiac CT.* Radiology, 2012. **264**(3): p. 876-83.

170. Nacif, M.S., et al., *3D left ventricular extracellular volume fraction by low-radiation dose cardiac CT: assessment of interstitial myocardial fibrosis.* Journal of cardiovascular computed tomography, 2013. **7**(1): p. 51-7.

171. Willenheimer, R. and L.R. Erhardt, *Value of 6-min-walk test for assessment of severity and prognosis of heart failure.* Lancet, 2000. **355**(9203): p. 515-6.

172. Perugini, E., et al., *Noninvasive etiologic diagnosis of cardiac amyloidosis using 99mTc-3,3-diphosphono-1,2-propanodicarboxylic acid scintigraphy.* Journal of the American College of Cardiology, 2005. **46**(6): p. 1076-84.

173. Gertz, M.A., et al., *Definition of organ involvement and treatment response in immunoglobulin light chain amyloidosis (AL): a consensus opinion from the 10th International Symposium on Amyloid and Amyloidosis, Tours, France, 18-22 April 2004.* American journal of hematology, 2005. **79**(4): p. 319-28.

174. Fontana, M., et al., *Native T1 mapping in transthyretin amyloidosis.* JACC. Cardiovascular imaging, 2014. **7**(2): p. 157-65.

175. Maestrini, V., et al., *T1 Mapping for Characterization of Intracellular and Extracellular Myocardial Diseases in Heart Failure.* Curr Cardiovasc Imaging Rep, 2014. **7**: p. 9287.

176. Kellman, P., A.E. Arai, and H. Xue, *T1 and extracellular volume mapping in the heart: estimation of error maps and the influence of noise on precision.* Journal of cardiovascular magnetic resonance : official journal of the Society for Cardiovascular Magnetic Resonance, 2013. **15**: p. 56.

177. Xue, H., et al., *Motion correction for myocardial T1 mapping using image registration with synthetic image estimation.* Magnetic resonance in medicine : official journal of the Society of Magnetic Resonance in Medicine / Society of Magnetic Resonance in Medicine, 2012. **67**(6): p. 1644-55.

178. Hausleiter, J., et al., *Estimated radiation dose associated with cardiac CT angiography.* JAMA : the journal of the American Medical Association, 2009. **301**(5): p. 500-7.

179. Ganau, A., et al., *Patterns of left ventricular hypertrophy and geometric remodeling in essential hypertension.* J Am Coll Cardiol, 1992. **19**(7): p. 1550-8.

180. Maceira, A.M., et al., *Normalized left ventricular systolic and diastolic function by steady state free precession cardiovascular magnetic resonance.* Journal of cardiovascular magnetic resonance : official journal of the Society for Cardiovascular Magnetic Resonance, 2006. **8**(3): p. 417-26.

181. Clavel, M.A., et al., *B-type natriuretic peptide clinical activation in aortic stenosis: impact on long-term survival.* J Am Coll Cardiol, 2014. **63**(19): p. 2016-25.

182. Piechnik, S.K., et al., *Normal variation of magnetic resonance T1 relaxation times in the human population at 1.5 T using ShMOLLI.* Journal of cardiovascular magnetic resonance : official journal of the Society for Cardiovascular Magnetic Resonance, 2013. **15**: p. 13.

183. Fullerton, G.D., J.L. Potter, and N.C. Dornbluth, *NMR relaxation of protons in tissues and other macromolecular water solutions.* Magnetic resonance imaging, 1982. **1**(4): p. 209-26.

184. Braunschweiger, P.G., L. Schiffer, and P. Furmanski, *The measurement of extracellular water volumes in tissues by gadolinium modification of 1H-NMR spin lattice (T1) relaxation.* Magnetic resonance imaging, 1986. **4**(4): p. 285-91.

185. Martin, M.A., et al., *Determination of extracellular/intracellular fluid ratios from magnetic resonance images: accuracy, feasibility, and implementation.*

Magnetic resonance in medicine : official journal of the Society of Magnetic Resonance in Medicine / Society of Magnetic Resonance in Medicine, 1990. **15**(1): p. 58-69.

186. Lu, H., et al., *Determining the longitudinal relaxation time (T1) of blood at 3.0 Tesla.* Magnetic resonance in medicine : official journal of the Society of Magnetic Resonance in Medicine / Society of Magnetic Resonance in Medicine, 2004. **52**(3): p. 679-82.

187. Shimada, K., et al., *In vivo measurement of longitudinal relaxation time of human blood by inversion-recovery fast gradient-echo MR imaging at 3T.* Magnetic resonance in medical sciences : MRMS : an official journal of Japan Society of Magnetic Resonance in Medicine, 2012. **11**(4): p. 265-71.

188. Li, W., et al., *Quantitative theory for the longitudinal relaxation time of blood water.* Magn Reson Med, 2015.

189. Spees, W.M., et al., *Water proton MR properties of human blood at 1.5 Tesla: magnetic susceptibility, T(1), T(2), T*(2), and non-Lorentzian signal behavior.* Magn Reson Med, 2001. **45**(4): p. 533-42.

190. Elliott, P., et al., *Classification of the cardiomyopathies: a position statement from the European Society Of Cardiology Working Group on Myocardial and Pericardial Diseases.* European heart journal, 2008. **29**(2): p. 270-6.

191. Fontana, M., et al., *Native T1 Mapping in Transthyretin Amyloidosis.* JACC. Cardiovascular imaging, 2014.

192. Schelbert EB, P.K., Zareba KM, Moon JC, Ugander M, Messroghli DR, Valeti U, Chang C-CH, Shroff SG, Miller CA, Schmitt M, Kellman P, Butler J, Gheorghiade M, Wong TC., *Extracellular matric expansion in non-infarcted myocardium is associated with subsequent death, hospitalization for heart failure, or both across the ejection fraction spectrum (Abstract).* J Am Coll Cardiol, 2014. **63**: p. A1007.

193. Kellman, P., et al., *Extracellular volume fraction mapping in the myocardium, part 2: initial clinical experience.* Journal of cardiovascular magnetic resonance : official journal of the Society for Cardiovascular Magnetic Resonance, 2012. **14**: p. 64.

194. Kramer, C.M., et al., *Standardized cardiovascular magnetic resonance imaging (CMR) protocols, society for cardiovascular magnetic resonance: board of trustees task force on standardized protocols.* Journal of cardiovascular magnetic resonance : official journal of the Society for Cardiovascular Magnetic Resonance, 2008. **10**: p. 35.

195. White, S.K., T.A. Treibel, and J.C. Moon, *Reply: Effects of blood T1 on extracellular volume calculation.* JACC. Cardiovascular imaging, 2014. **7**(8): p. 849-50.

196. Moon, J.C., et al., *Myocardial T1 mapping and extracellular volume quantification: a Society for Cardiovascular Magnetic Resonance (SCMR) and CMR Working Group of the European Society of Cardiology consensus statement.* Journal of cardiovascular magnetic resonance : official journal of the Society for Cardiovascular Magnetic Resonance, 2013. **15**(1): p. 92.

197. Hill, V.L., et al., *Evaluation of the Performance of the Sysmex XT-2000i Hematology Analyzer With Whole Bloods Stored at Room Temperature.* Laboratory medicine, 2009. **40**(12): p. 709-718.

198. Schelbert, E.B., et al., *Therapeutic targets in heart failure: refocusing on the myocardial interstitium.* Journal of the American College of Cardiology, 2014. **63**(21): p. 2188-98.

199. Sado, D.M., et al., *Cardiovascular magnetic resonance measurement of myocardial extracellular volume in health and disease.* Heart, 2012. **98**(19): p. 1436-41.

200. Liu, C.Y., et al., *Evaluation of age-related interstitial myocardial fibrosis with cardiac magnetic resonance contrast-enhanced T1 mapping: MESA (Multi-Ethnic Study of Atherosclerosis).* Journal of the American College of Cardiology, 2013. **62**(14): p. 1280-7.

201. *00042871-200709010-00006.*

202. Banypersad, S.M., et al., *T1 mapping and survival in systemic light-chain amyloidosis.* European heart journal, 2015. **36**(4): p. 244-51.

203. Wong, T.C., et al., *Myocardial extracellular volume fraction quantified by cardiovascular magnetic resonance is increased in diabetes and associated with mortality and incident heart failure admission.* Eur Heart J, 2014. **35**(10): p. 657-64.

204. Thirup, P., *Haematocrit: within-subject and seasonal variation.* Sports medicine, 2003. **33**(3): p. 231-43.

205. Kramer, C.M., Y. Chandrashekhar, and J. Narula, *T1 mapping by CMR in cardiomyopathy: a noninvasive myocardial biopsy?* JACC. Cardiovascular imaging, 2013. **6**(4): p. 532-4.

206. Spottiswoode, B.S., M. Ugander, and P. Kellman, *Automated inline extracellular volume (ECV) mapping.* Journal of cardiovascular magnetic resonance : official journal of the Society for Cardiovascular Magnetic Resonance, 2015. **17(Suppl 1):W6**

207. Yilmaz, A., et al., *Determination of dependence of spin-lattice relaxation rate in serum upon concentration of added iron by magnetic resonance imaging.* Clinical physics and physiological measurement : an official journal of the Hospital Physicists' Association, Deutsche Gesellschaft fur Medizinische Physik and the European Federation of Organisations for Medical Physics, 1990. **11**(4): p. 343-9.

208. Wright, G.A., B.S. Hu, and A. Macovski, *1991 I.I. Rabi Award. Estimating oxygen saturation of blood in vivo with MR imaging at 1.5 T.* Journal of magnetic resonance imaging : JMRI, 1991. **1**(3): p. 275-83.

209. Silvennoinen, M.J., M.I. Kettunen, and R.A. Kauppinen, *Effects of hematocrit and oxygen saturation level on blood spin-lattice relaxation.* Magnetic resonance in medicine : official journal of the Society of Magnetic Resonance in Medicine / Society of Magnetic Resonance in Medicine, 2003. **49**(3): p. 568-71.

210. Liu, S., et al., *Diffuse myocardial fibrosis evaluation using cardiac magnetic resonance T1 mapping: sample size considerations for clinical trials.* Journal of cardiovascular magnetic resonance : official journal of the Society for Cardiovascular Magnetic Resonance, 2012. **14**: p. 90.

211. Banypersad, S.M., et al., *Quantification of myocardial extracellular volume fraction in systemic AL amyloidosis: an equilibrium contrast cardiovascular*

magnetic resonance study. Circulation. Cardiovascular imaging, 2013. **6**(1): p. 34-9.

212. New, P.F. and S. Aronow, *Attenuation measurements of whole blood and blood fractions in computed tomography.* Radiology, 1976. **121**(3 Pt. 1): p. 635-40.

213. Black, D.F., et al., *Cerebral venous sinus density on noncontrast CT correlates with hematocrit.* AJNR Am J Neuroradiol, 2011. **32**(7): p. 1354-7.

214. Collins, A.J., S. Gillespie, and B.E. Kelly, *Can computed tomography identify patients with anaemia?* Ulster Med J, 2001. **70**(2): p. 116-8.

215. Lan, H., S. Nishihara, and H. Nishitani, *Accuracy of computed tomography attenuation measurements for diagnosing anemia.* Jpn J Radiol, 2010. **28**(1): p. 53-7.

216. Jung, C., et al., *Assessment of anemia during CT pulmonary angiography.* Eur J Radiol, 2012. **81**(12): p. 4196-202.

217. Kamel, E.M., et al., *Radiological profile of anemia on unenhanced MDCT of the thorax.* Eur Radiol, 2008. **18**(9): p. 1863-8.

218. Wojtowicz, J., K. Rzymski, and R. Czarnecki, *Severe anaemia: its CT findings in the cardiovascular system.* Eur J Radiol, 1983. **3**(2): p. 108-11.

219. Doppman, J.L., R. Rienmuller, and J. Lissner, *The visualized interventricular septum on cardiac computed tomography: a clue to the presence of severe anemia.* J Comput Assist Tomogr, 1981. **5**(2): p. 157-60.

220. Treibel, T.A., et al., *Extracellular volume quantification by dynamic equilibrium cardiac computed tomography in cardiac amyloidosis.* J Cardiovasc Comput Tomogr, 2015.

221. Jalbert, F. and J.R. Paoli, *[Osirix: free and open-source software for medical imagery].* Rev Stomatol Chir Maxillofac, 2008. **109**(1): p. 53-5.

222. Nacif, M.S., et al., *3D left ventricular extracellular volume fraction by low-radiation dose cardiac CT: assessment of interstitial myocardial fibrosis.* J Cardiovasc Comput Tomogr, 2013. **7**(1): p. 51-7.

223. Rosmini, S., et al., *Cardiac computed tomography for the detection of cardiac amyloidosis.* J Cardiovasc Comput Tomogr, 2016.

224. Bydder, G.M. and L. Kreel, *The temperature dependence of computed tomography attenuation values.* J Comput Assist Tomogr, 1979. **3**(4): p. 506-10.

225. Cioffi, G. and C. Stefenelli, *Comparison of left ventricular geometry and left atrial size and function in patients with aortic stenosis versus those with pure aortic regurgitation.* Am J Cardiol, 2002. **90**(6): p. 601-6.

226. Baumgartner, H., et al., *Echocardiographic assessment of valve stenosis: EAE/ASE recommendations for clinical practice.* European journal of echocardiography : the journal of the Working Group on Echocardiography of the European Society of Cardiology, 2009. **10**(1): p. 1-25.

227. Garcia, D., et al., *Assessment of aortic valve stenosis severity: A new index based on the energy loss concept.* Circulation, 2000. **101**(7): p. 765-71.

228. Bahlmann, E., et al., *Prognostic value of energy loss index in asymptomatic aortic stenosis.* Circulation, 2013. **127**(10): p. 1149-56.

229. Hachicha, Z., J.G. Dumesnil, and P. Pibarot, *Usefulness of the valvuloarterial impedance to predict adverse outcome in asymptomatic aortic stenosis.* J Am Coll Cardiol, 2009. **54**(11): p. 1003-11.

230. Sprigings, D.C., et al., *Ventricular stroke work loss: validation of a method of quantifying the severity of aortic stenosis and derivation of an orifice formula.* J Am Coll Cardiol, 1990. **16**(7): p. 1608-14.

231. Devereux, R.B., et al., *Echocardiographic assessment of left ventricular hypertrophy: comparison to necropsy findings.* Am J Cardiol, 1986. **57**(6): p. 450-8.

232. Schulz-Menger, J., et al., *Standardized image interpretation and post processing in cardiovascular magnetic resonance: Society for Cardiovascular Magnetic Resonance (SCMR) board of trustees task force on standardized post processing.* J Cardiovasc Magn Reson, 2013. **15**: p. 35.

233. Maceira, A.M., et al., *Reference left atrial dimensions and volumes by steady state free precession cardiovascular magnetic resonance.* Journal of Cardiovascular Magnetic Resonance, 2010. **12**: p. 65.

234. Treibel, T.A., et al., *Occult Transthyretin Cardiac Amyloid in Severe Calcific Aortic Stenosis: Prevalence and Prognosis in Patients Undergoing Surgical Aortic Valve Replacement.* Circ Cardiovasc Imaging, 2016. **9**(8).

235. de Simone, G., et al., *Normalization for body size and population-attributable risk of left ventricular hypertrophy: the Strong Heart Study.* Am J Hypertens, 2005. **18**(2 Pt 1): p. 191-6.

236. Enright, P.L. and D.L. Sherrill, *Reference equations for the six-minute walk in healthy adults.* Am J Respir Crit Care Med, 1998. **158**(5 Pt 1): p. 1384-7.

237. Kostkiewicz, M., et al., *Left ventricular geometry and function in patients with aortic stenosis: gender differences.* Int J Cardiol, 1999. **71**(1): p. 57-61.

238. Legget, M.E., et al., *Gender differences in left ventricular function at rest and with exercise in asymptomatic aortic stenosis.* Am Heart J, 1996. **131**(1): p. 94-100.

239. Piro, M., et al., *Sex-related differences in myocardial remodeling.* J Am Coll Cardiol, 2010. **55**(11): p. 1057-65.

240. Deschepper, C.F. and B. Llamas, *Hypertensive cardiac remodeling in males and females: from the bench to the bedside.* Hypertension, 2007. **49**(3): p. 401-7.

241. Petrov, G., et al., *Regression of myocardial hypertrophy after aortic valve replacement: faster in women?* Circulation, 2010. **122**(11 Suppl): p. S23-8.

242. Kararigas, G., et al., *Sex-dependent regulation of fibrosis and inflammation in human left ventricular remodelling under pressure overload.* Eur J Heart Fail, 2014. **16**(11): p. 1160-7.

243. Marsh, J.D., et al., *Androgen receptors mediate hypertrophy in cardiac myocytes.* Circulation, 1998. **98**(3): p. 256-61.

244. Orlowska-Baranowska, E., et al., *Influence of ACE I/D genotypes on left ventricular hypertrophy in aortic stenosis: gender-related differences.* J Heart Valve Dis, 2004. **13**(4): p. 574-81.

245. Mitchell, G.F., et al., *Hemodynamics of increased pulse pressure in older women in the community-based Age, Gene/Environment Susceptibility-Reykjavik Study.* Hypertension, 2008. **51**(4): p. 1123-8.

246. Dahl, J.S., et al., *Effect of left ventricular ejection fraction on postoperative outcome in patients with severe aortic stenosis undergoing aortic valve replacement.* Circ Cardiovasc Imaging, 2015. **8**(4).

247. Omran, H., et al., *Silent and apparent cerebral embolism after retrograde catheterisation of the aortic valve in valvular stenosis: a prospective, randomised study.* Lancet, 2003. **361**(9365): p. 1241-6.

248. Longhi, S., et al., *Coexistence of Degenerative Aortic Stenosis and Wild-Type Transthyretin-Related Cardiac Amyloidosis.* JACC Cardiovasc Imaging, 2016. **9**(3): p. 325-7.

249. Nietlispach, F., et al., *Pathology of transcatheter valve therapy.* JACC. Cardiovascular interventions, 2012. **5**(5): p. 582-90.

250. Castano, A., S. Bokhari, and M.S. Maurer, *Could late enhancement and need for permanent pacemaker implantation in patients undergoing TAVR be explained by undiagnosed transthyretin cardiac amyloidosis?* Journal of the American College of Cardiology, 2015. **65**(3): p. 311-2.

251. Fontana, M., et al., *Native T1 mapping in transthyretin amyloidosis.* JACC Cardiovasc Imaging, 2014. **7**(2): p. 157-65.

252. Fontana, M., et al., *Prognostic Value of Late Gadolinium Enhancement Cardiovascular Magnetic Resonance in Cardiac Amyloidosis.* Circulation, 2015. **132**(16): p. 1570-9.

253. Hutt, D.F., et al., *Utility and limitations of 3,3-diphosphono-1,2-propanodicarboxylic acid scintigraphy in systemic amyloidosis.* Eur Heart J Cardiovasc Imaging, 2014. **15**(11): p. 1289-98.

254. Pinney, J.H., et al., *Senile systemic amyloidosis: clinical features at presentation and outcome.* Journal of the American Heart Association, 2013. **2**(2): p. e000098.

255. Benson, M.D., et al., *Antisense oligonucleotide therapy for TTR amyloidosis.* Amyloid, 2011. **18 Suppl 1**: p. 60.

256. Sun, J.P., et al., *Differentiation of hypertrophic cardiomyopathy and cardiac amyloidosis from other causes of ventricular wall thickening by two-dimensional strain imaging echocardiography.* Am J Cardiol, 2009. **103**(3): p. 411-5.

257. King, D.L., L. El-Khoury Coffin, and M.S. Maurer, *Myocardial contraction fraction: a volumetric index of myocardial shortening by freehand three-dimensional echocardiography.* J Am Coll Cardiol, 2002. **40**(2): p. 325-9.

258. Carroll, J.D., W.H. Gaasch, and K.P. McAdam, *Amyloid cardiomyopathy: characterization by a distinctive voltage/mass relation.* Am J Cardiol, 1982. **49**(1): p. 9-13.

259. Puchtler, H. and F. Sweat, *Amidoblack as a stain for hemoglobin.* Arch Pathol, 1962. **73**: p. 245-9.

260. Gilbertson, J.A., et al., *A comparison of immunohistochemistry and mass spectrometry for determining the amyloid fibril protein from formalin-fixed biopsy tissue.* J Clin Pathol, 2015. **68**(4): p. 314-7.

261. Vrana, J.A., et al., *Classification of amyloidosis by laser microdissection and mass spectrometry-based proteomic analysis in clinical biopsy specimens.* Blood, 2009. **114**(24): p. 4957-9.

262. Kyle, R.A., M.A. Gertz, and R.P. Linke, *Amyloid localized to tenosynovium at carpal tunnel release. Immunohistochemical identification of amyloid type.* Am J Clin Pathol, 1992. **97**(2): p. 250-3.

263. Monticelli, F.C., et al., *Cardiac amyloidosis as a potential risk factor for transapical transcatheter aortic valve implantation.* J Card Surg, 2014. **29**(5): p. 623-4.

264. Chimenti, C. and A. Frustaci, *Contribution and risks of left ventricular endomyocardial biopsy in patients with cardiomyopathies: a retrospective study over a 28-year period.* Circulation, 2013. **128**(14): p. 1531-41.

265. Allen, R.D., et al., *Surgical pathology of subaortic septal myectomy not associated with hypertrophic cardiomyopathy: a study of 98 cases (1996-2000).* Cardiovascular pathology : the official journal of the Society for Cardiovascular Pathology, 2003. **12**(4): p. 207-15.

266. Lamke, G.T., et al., *Surgical pathology of subaortic septal myectomy associated with hypertrophic cardiomyopathy. A study of 204 cases (1996-2000).* Cardiovascular pathology : the official journal of the Society for Cardiovascular Pathology, 2003. **12**(3): p. 149-58.

267. Helder, M.R., et al., *Impact of incidental amyloidosis on the prognosis of patients with hypertrophic cardiomyopathy undergoing septal myectomy for left ventricular outflow tract obstruction.* The American journal of cardiology, 2014. **114**(9): p. 1396-9.

268. Mohammed, S.F., et al., *Left ventricular amyloid deposition in patients with heart failure and preserved ejection fraction.* JACC Heart Fail, 2014. **2**(2): p. 113-22.

269. Gonzalez-Lopez, E., et al., *Wild-type transthyretin amyloidosis as a cause of heart failure with preserved ejection fraction.* Eur Heart J, 2015. **36**(38): p. 2585-94.

270. Bokhari, S., et al., *(99m)Tc-pyrophosphate scintigraphy for differentiating light-chain cardiac amyloidosis from the transthyretin-related familial and senile cardiac amyloidoses.* Circ Cardiovasc Imaging, 2013. **6**(2): p. 195-201.

271. Yamashita, T., et al., *A prospective evaluation of the transthyretin Ile122 allele frequency in an African-American population.* Amyloid, 2005. **12**(2): p. 127-30.

272. Buxbaum, J., et al., *Transthyretin V122I in African Americans with congestive heart failure.* J Am Coll Cardiol, 2006. **47**(8): p. 1724-5.

273. Villari, B., et al., *Influence of collagen network on left ventricular systolic and diastolic function in aortic valve disease.* J Am Coll Cardiol, 1993. **22**(5): p. 1477-84.

274. Herrmann, S., et al., *Low-gradient aortic valve stenosis myocardial fibrosis and its influence on function and outcome.* Journal of the American College of Cardiology, 2011. **58**(4): p. 402-12.

275. Schwarz, F., et al., *Myocardial structure and function in patients with aortic valve disease and their relation to postoperative results.* The American journal of cardiology, 1978. **41**(4): p. 661-9.

276. Cheitlin, M.D., et al., *The distribution of fibrosis in the left ventricle in congenital aortic stenosis and coarctation of the aorta.* Circulation, 1980. **62**(4): p. 823-30.

277. Hess, O.M., et al., *Diastolic stiffness and myocardial structure in aortic valve disease before and after valve replacement.* Circulation, 1984. **69**(5): p. 855-65.

278. Krayenbuehl, H.P., et al., *Left ventricular myocardial structure in aortic valve disease before, intermediate, and late after aortic valve replacement.* Circulation, 1989. **79**(4): p. 744-55.

279. Fielitz, J., et al., *Activation of the cardiac renin-angiotensin system and increased myocardial collagen expression in human aortic valve disease.* J Am Coll Cardiol, 2001. **37**(5): p. 1443-9.

280. Moreno, M.U., et al., *Decreased Nox4 levels in the myocardium of patients with aortic valve stenosis.* Clin Sci (Lond), 2013. **125**(6): p. 291-300.

281. Pellman, J., J. Zhang, and F. Sheikh, *Myocyte-fibroblast communication in cardiac fibrosis and arrhythmias: Mechanisms and model systems.* J Mol Cell Cardiol, 2016. **94**: p. 22-31.

282. Kellman, P., et al., *Dark blood late enhancement imaging.* J Cardiovasc Magn Reson, 2016. **18**(1): p. 77.

283. Chin, C.W., et al., *High-sensitivity troponin I concentrations are a marker of an advanced hypertrophic response and adverse outcomes in patients with aortic stenosis.* European heart journal, 2014.

284. Pinto, A.R., et al., *Revisiting Cardiac Cellular Composition.* Circ Res, 2016. **118**(3): p. 400-9.

285. Maestrini, V., et al., *T1 Mapping for Characterization of Intracellular and Extracellular Myocardial Diseases in Heart Failure.* Current cardiovascular imaging reports, 2014. **7**: p. 9287.

286. Chin, C.W.L., et al., *Myocardial Fibrosis and Cardiac Decompensation in Aortic Stenosis.* JACC: Cardiovascular Imaging, 2016.

287. Jalil, J.E., et al., *Fibrillar collagen and myocardial stiffness in the intact hypertrophied rat left ventricle.* Circ Res, 1989. **64**(6): p. 1041-50.

288. Treibel, T.A.L., B; González, A; Menacho, K; Schofield, R S; Ravassa, S; Fontana, M; White, S K; DiSalvo, C; Roberts, N; Ashworth, M T; Díez, J; Moon, J C, *Reappraising myocardial fibrosis in severe aortic stenosis: an invasive and non-invasive study in 133 patients.* Eur Heart J 2017, 2017.

289. Devereux, R.B., et al., *Regression of hypertensive left ventricular hypertrophy by losartan compared with atenolol: the Losartan Intervention for Endpoint Reduction in Hypertension (LIFE) trial.* Circulation, 2004. **110**(11): p. 1456-1462.

290. Dahl, J.S., et al., *Effect of candesartan treatment on left ventricular remodeling after aortic valve replacement for aortic stenosis.* The American journal of cardiology, 2010. **106**(5): p. 713-719.

291. Butler, J., G.C. Fonarow, and M. Gheorghiade, *Strategies and opportunities for drug development in heart failure.* JAMA, 2013. **309**(15): p. 1593-4.

292. Swynghedauw, B., *Molecular mechanisms of myocardial remodeling.* Physiol Rev, 1999. **79**(1): p. 215-62.

293. Weber, K.T., et al., *Myofibroblast-mediated mechanisms of pathological remodelling of the heart.* Nat Rev Cardiol, 2013. **10**(1): p. 15-26.

294. Chin, C.W., et al., *Myocardial Fibrosis and Cardiac Decompensation in Aortic Stenosis.* JACC Cardiovasc Imaging, 2016.

295. Lindman, B.R., et al., *Early regression of severe left ventricular hypertrophy after transcatheter aortic valve replacement is associated with decreased hospitalizations.* JACC Cardiovasc Interv, 2014. **7**(6): p. 662-73.

296. Monrad, E.S., et al., *Time course of regression of left ventricular hypertrophy after aortic valve replacement.* Circulation, 1988. **77**(6): p. 1345-1355.

297. Laine, G.A. and S.J. Allen, *Left ventricular myocardial edema. Lymph flow, interstitial fibrosis, and cardiac function.* Circ Res, 1991. **68**(6): p. 1713-21.

Chapter 12 Appendix

12.1 Location of research

Clinical Research was carried out at the Heart Hospital (part of UCLH NHS trust), University College Hospital and the Royal Free Hospital. Histological analysis was carried out at Great Ormond Street Hospital for Children NHS Trust, National Amyloidosis Centre, Royal Free Hospital, and the Center for Applied Medical Research, University of Navarra, Pamplona, Spain.

12.2 Personal contributions

I performed all CMR scans, coordinated the image analysis, performed data analysis and statistical analysis presented in this thesis except chapters 4.2 (ECV quantification by CCT), which I jointly performed with Dr Steve Bandula).

I would like to acknowledge the following further contributions:

Rebecca Kozor (volume and function analysis) and Rebecca Schofield (late gadolinium enhancement quantification) analysed CMR images as primary observers; I performed the T1 mapping analysis as primary observer and was secondary observer in all other analyses. Patrizia Reant, Maria Espinoza, James Malcolmson and Rebecca McCrae supported me in performing and analysing the echocardiographic scans.

Martin Hayward, Jon Yap, Shyam Kolvekar, David Lawrence, Giulio Bognolo, Carmelo diSalvo, and Prof Christopher McGregor performed the intraoperative biopsies in aortic stenosis patients.

Histological preparation and analysis of biopsy specimen were performed by Dr. Michael Ashworth and his team, Janet Gilbertson (National Amyloidosis Centre) and Prof Javier Díez and his team (University of Navarra, Pamplona, Spain).

12.3 Supervision

Primary project supervisor: **Prof. James Moon**

Secondary supervisor: **Prof. Stuart Taylor**

12.4 Funding

Doctoral Research Fellowship – National Institute for Health Research

3 years funding (£301,619; Ref. DRF-2013-06-102) for project entitled "The Role of Diffuse Myocardial Fibrosis in Aortic Stenosis: Translation of Non- Invasive Quantification into Clinical Practice".

12.5 Collaborators

12.5.1 Application of new T1 mapping sequences for ECV quantification:

- Dr S Piechnik, Prof S Neubauer, Oxford, UK.
- Dr Peter Kellman, National Institute of Health, NHLBI, Bethesda,USA.
- Dr Bruce Spottiswoode, Siemens Health Care, Chicago, USA.

12.5.2 Development of Extracellular Volume Fraction Quantification by CT

- S Bandula, S Punwani, S Taylor, Centre of Medical Imaging, UCLH.
- Toshiba Medical Visualisation Systems, Edinburgh, UK.

12.5.3 Advanced Histology and Collagen Biomarkers

- Prof C McGregor and team, Department of Academic Surgery, UCLH.
- Dr Michael Ashworth, Histopathology, Institute of Child Health, UCL.
- Prof Javier Diez, Dr Begona Lopez, CIMA, Pamplona/Spain.
- Patrizia Camelliti, University of Surrey, Guildford, UK.

12.5.4 Occult amyloid in the myocardium and valves in Aortic Stenosis

- Prof Philip Hawkins and team, National Amyloid Centre, Royal Free Hospital.

12.5.5 Proteonomics and genetics of cardiac remodelling and fibrosis in AS

- Dr Kevin Mills, Institute of Cardiovascular Science, UCL.
- Prof Hugh Montgommery, Cardiovascular Genetics Group, UCL.
- Prof Folkert Asselsberg, University of Utrecht, The Netherlands.

12.6 Prizes/Awards related to research activity

12.6.1 National

- **Young Investigator Award. Winner.** British Society of CMR AGM 2015.
- **Young Investigator Award. Runner-up.** British Heart Valve Society AGM 2014.
- **Doctoral Research Fellowship.** National Institute for Health Research, UK 2013.
- **Clinical Research Training Fellowship.** British Heart Foundation, UK, 2013, turned down in favour of NIHR DRF.

12.6.2 International

- **Early Career Award, Translational Research. Winner.** Society for CMR Annual Meeting, Washington DC, 2017.
- **SCMR Travel Award** ($400) to attend SCMR Washington DC 2017.
- **Early Career Award, Clinical Research. Short-listed x2. Runner-up.** Society for CMR Annual Meeting, Los Angeles, 2016.
- **SCMR Travel Award** ($1000) to attend SCMR Los Angeles 2016.
- **Young Investigator Award. Short-Listed.** European Society for Cardiovascular Magnetic Resonance Annual Meeting, Florence, May 2016.
- **Young Investigator Award. Short-Listed.** Society of Cardiovascular Computed Tomography, July 2016.

12.7 Publications arising from research activities

In total, there are 36 papers published so far from this thesis. This includes papers in Circulation, European Heart Journal, JACC, Circulation Research, Radiology, JACC imaging, Circulation imaging and others. There are 2 more first author manuscripts under review and multiple more middle author papers pending.

12.7.1 1st Author original papers

10. **Treibel TA**, Rebecca Kozor, Fontana M, Tolasco T, Reant P, Badiani S, Espinoza M, Yap J, Diez J, Hughes A, Lloyd G, Moon JC. Sex Dimorphism in Myocardial Remodelling. **JACC Cardiovasc Imaging.** 2017 (in press).

9. **Treibel TA*,** López B, González A, Menacho K, Schofield RS, Ravassa S, Fontana M, White SK, DiSalvo C, Roberts N, Ashworth MT, Díez J, Moon JC; Reappraising myocardial fibrosis in severe aortic stenosis: an invasive and non-

invasive study in 133 patients. **Eur Heart J** 2017. doi: 10.1093/eurheartj/ehx353. *equal contribution.

8. **Treibel TA**, Fontana M, Steeden JA, Nasis A, Yeung J, White SK, Sivarajan S, Punwani S, Pugliese F, Taylor SA, Moon JC, Bandula S. Automatic Quantification of the Myocardial Extracellular Volume by Cardiac Computed Tomography: Synthetic ECV by CT. **J Cardiovasc Comput Tomogr.** 2017.

7. **Treibel TA**, Gilbertson JA, Taylor GW, Rendell NB, Fontana M, Gillmore JD, Hawkins PN, Moon JC. Sex Dimorphism in Aortic Valve Calcification - Amyloid Deposition is associated with Calcium and Male Sex. **Circulation Research.** Circ Res. 2017 Mar 3;120(5):e24-e25.

6. **Treibel TA**, Moon JC. T1 and T2 mapping and ECV in Cardiomyopathy. *Cardiovascular Magnetic Resonance, 3rd Edition*. Elsevier Publishing. Edited by Prof. DJ Pennell and WJ Manning. Book Chapter. In Press.

5. **Treibel TA***, Rosmini S*, Bandula S, Stroud T, Fontana M, Hawkins PN, Moon JC. Cardiac computed tomography for the detection of cardiac amyloidosis. **J Cardiovasc Comput Tomogr.** 2016 Sep 15. pii: S1934-5925(16)30220-9.

4. **Treibel TA**, Fontana M, Gilbertson JA, Castelletti S, White SK, Scully PR, Roberts N, Hutt DF, Rowczenio DM, Whelan CJ, Ashworth MA, Gillmore JD, Hawkins PN, Moon JC. Occult Transthyretin Cardiac Amyloid in Severe Calcific Aortic Stenosis: Prevalence and Prognosis in Patients Undergoing Surgical Aortic Valve Replacement. **Circ Cardiovasc Imaging.** 2016 Aug;9(8).

3. **Treibel TA,** Fontana M, Maestrini V, Castelletti S, Rosmini S Simpson J, Nasis A, Bulluck H, Abdel-Gadir A, White SK, Manisty C, Spottiswoode BS, Robson MD, Wong TC, Piechnik SK, Kellman P, Schelbert EB, Moon JC. Automatic Measurement Of The Myocardial Interstitium: Synthetic Extracellular Volume Quantification without Haematocrit Sampling. **JACC Cardiovasc Imaging.** 2016 Jan;9(1):54-63.

2. **Treibel TA**, Bandula S, Fontana M, White SK, Gilbertson JA, Gillmore JD, Punwani S, Hawkins PN, Taylor SA, Moon JC. Quantification and diagnosis of cardiac amyloid by cardiac computed tomography: Clinical Development And Application Of Extracellular Volume Quantification By Dynamic Equilibrium Computed Tomography (DynEQ-CT). **J Cardiovasc Comput Tomogr.** 2015 Jul 10.

1. **Thomas A Treibel***, Filip Zemrak*, Daniel M Sado, Sanjay Banypersad, Steven K White, Viviana Maestrini, Andrea Barison, Vimal Patel, Anna S Herrey, Ceri Davies, Mark J Caulfield, Steffen E Petersen, James C Moon. Myocardial Fibrosis In Well-Controlled Systemic Hypertension. **J Cardiovasc Magn Reson. 2015**, 17:74. DOI: 10.1186/s12968-015-0176-3

12.7.2 1st Author manuscripts under review

1. Reverse Myocardial Remodeling in Aortic Stenosis: Cellular Hypertrophy and Diffuse but not Focal Fibrosis Regress Following Aortic Valve Replacement. **Thomas A Treibel**, Rebecca Kozor, Rebecca Schofield, Giulia Benedetti,

Marianna Fontana, Amir Sheikh, Begoña Lopez, Arantxa Gonzalez, Charlotte Manisty, Guy Lloyd, Peter Kellman, Javier Díez, James C Moon.

12.7.3 Co-Author publications related to the topic

20. Martinez-Naharro A, **Treibel TA**, Abdel-Gadir A, Bulluck H, Zumbo G, Knight DS, Kotecha T, Francis R, Hutt DF, Rezk T, Rosmini S, Quarta CC, Whelan CJ, Kellman P, Gillmore JD, Moon JC, Hawkins PN, Fontana M. Magnetic Resonance in Transthyretin Cardiac Amyloidosis. **J Am Coll Cardiol.** 2017 Jul 25;70(4):466-477. doi: 10.1016/j.jacc.2017.05.053.

19. Fent GJ, Garg P, Foley JR, Swoboda PP, Dobson LE, Erhayiem B, Greenwood JP, Plein S, **Treibel TA,** Moon JC. Synthetic Myocardial Extracellular Volume Fraction. **JACC Cardiovasc Imaging.** 2017 Feb 9.

18. Bulluck H, Rosmini S, Abdel-Gadir A, Bhuva AN, **Treibel TA**, Fontana M, Gonzalez-Lopez E, Ramlall M, Hamarneh A, Sirker A, Herrey AS, Manisty C, Yellon DM, Moon JC, Hausenloy DJ. Diagnostic Performance of T1 and T2 Mapping to Detect Intramyocardial Hemorrhage in Reperfused ST-Segment Elevation Myocardial Infarction (STEMI) Patients. **J Magn Reson Imaging.** 2017 Feb 15.

17. Fontana M, **Treibel TA**, Martinez-Naharro A, Rosmini S, Kwong RY, Gillmore JD, Hawkins PN, Moon JC. A case report in cardiovascular magnetic resonance: the contrast agent matters in amyloid. **BMC Med Imaging.** 2017 Jan 7;17(1):3.

16. Bulluck H, Rosmini S, Abdel-Gadir A, White SK, Bhuva AN, **Treibel TA**, Fontana M, Ramlall M, Hamarneh A, Sirker A, Herrey AS, Manisty C, Yellon DM, Kellman P, Moon JC, Hausenloy DJ. Residual Myocardial Iron Following Intramyocardial Hemorrhage During the Convalescent Phase of Reperfused ST-Segment-Elevation Myocardial Infarction and Adverse Left Ventricular Remodeling. **Circ Cardiovasc Imaging.** 2016 Oct;9(10). pii: e004940.

15. Bulluck H, Rosmini S, Abdel-Gadir A, Bhuva AN, **Treibel TA**, Fontana M, Weinmann S, Sirker A, Herrey AS, Manisty C, Moon JC, Hausenloy DJ. Impact of microvascular obstruction on semiautomated techniques for quantifying acute and chronic myocardial infarction by cardiovascular magnetic resonance. **Open Heart.** 2016 Dec 12;3(2):e000535.

14. Kozor R, Nordin S, **Treibel TA**, Rosmini S, Castelletti S, Fontana M, Captur G, Baig S, Steeds RP, Hughes D, Manisty C, Grieve SM, Figtree GA, Moon JC. Insight into hypertrophied hearts: a cardiovascular magnetic resonance study of papillary muscle mass and T1 mapping. **Eur Heart J Cardiovasc Imaging.** 2016 Sep 2.

13. Bulluck H, Rosmini S, Abdel-Gadir A, White SK, Bhuva AN, **Treibel TA**, Fontana M, Gonzalez-Lopez E, Reant P, Ramlall M, Hamarneh A, Sirker A, Herrey AS, Manisty C, Yellon DM, Kellman P, Moon JC, Hausenloy DJ. Automated Extracellular Volume Fraction Mapping Provides Insights Into the Pathophysiology of Left Ventricular Remodelling Post-Reperfused ST-Elevation Myocardial Infarction. **J Am Heart Assoc.** 2016 Jul 11;5(7).

12. Moon JC, **Treibel TA**, Schelbert EB. Myocardial Fibrosis in Hypertensive Heart Failure: Does Quality Rather Than Quantity Matter? Moon JC, Treibel TA, Schelbert EB. **J Am Coll Cardiol**. 2016 Jan 26;67(3):261-3.

11. Fontana M, Pica S, Reant P, Abdel-Gadir A, **Treibel TA**, Banypersad SM, Maestrini V, Barcella W, Rosmini S, Bulluck H, Sayed RH, Patel K, Mahmood S, Bucciarelli-Ducci C, Whelan CJ, Herrey AS, Lachmann HJ, Wechalekar AD, Manisty CH, Schelbert EB, Kellman P, Gillmore JD, Hawkins PN, Moon JC. Prognostic Value of Late Gadolinium Enhancement Cardiovascular Magnetic Resonance in Cardiac Amyloidosis. **Circulation.** 2015 Sep 11.

10. Fontana M, Banypersad SM, **Treibel TA**, Abdel-Gadir A, Maestrini V, Lane T, Gilbertson JA, Hutt DF, Lachmann HJ, Whelan CJ, Wechalekar AD, Herrey AS, Gillmore JD, Hawkins PN, Moon JC. Differential Myocyte Responses in Patients with Cardiac Transthyretin Amyloidosis and Light-Chain Amyloidosis: A Cardiac MR Imaging Study. **Radiology.** 2015 May 21:141744.

9. Bulluck H, White SK Rosmini S, Bhuva A, **Treibel TA**, Fontana M, Abdel-Gadir A; Herrey AS, Manisty C, Wan SMY; Groves A, Menezes L, Moon JC, Hausenloy DJ. T1 mapping and T2 mapping at 3T for quantifying area-at-risk in reperfused STEMI patients. **J Cardiovasc Magn Reson** 17:73.

8. Flett AS, Maestrini V, Milliken D, Fontana M, **Treibel TA**, Harb R, Sado DM, Quarta G, Herrey A, Sneddon J, Elliott P, McKenna W, Moon JC. Diagnosis of apical hypertrophic cardiomyopathy: T-wave inversion and relative but not absolute apical left ventricular hypertrophy. **Int J Cardiol.** 2015 Jan 27;183C:143-148.

7. Kellman P, Xue H, Spottiswoode BS, Sandino CM, Hansen MS, Abdel-Gadir A, **Treibel TA**, Rosmini S, Mancini C, Bandettini WP, McGill LA, Gatehouse P, Moon JC, Pennell DJ, Arai AE. Free-breathing T2* mapping using respiratory motion corrected averaging. **J Cardiovasc Magn Reson**. 2015 Jan 24;17(1):3.

6. Pica S, Sado DM, Maestrini V, Fontana M, White SK, **Treibel T**, Captur G, Anderson S, Piechnik SK, Robson MD, Lachmann RH, Murphy E, Mehta A, Hughes D, Kellman P, Elliott PM, Herrey AS, Moon JC. Reproducibility of native myocardial T1 mapping in the assessment of Fabry disease and its role in early detection of cardiac involvement by cardiovascular magnetic resonance. **J Cardiovasc Magn Reson.** 2014 Dec 5;16:99.

5. White SK, Frohlich GM, Sado DM, Maestrini V, Fontana M, **Treibel** TA, Tehrani S, Flett AS, Meier P, Ariti C, Davies JR, Moon JC, Yellon DM, Hausenloy DJ. Remote Ischemic Conditioning Reduces Myocardial Infarct Size and Edema in Patients With ST-Segment Elevation Myocardial Infarction. **JACC Cardiovasc Interv.** 2014 Sep 9. pii: S1936-8798(14)01073-5.

4. Fontana M, Banypersad SM, **Treibel TA**, Maestrini V, Sado DM, White SK, Pica S, Castelletti S, Piechnik SK, Robson MD, Gilbertson JA, Rowczenio D, Hutt DF, Lachmann HJ, Wechalekar AD, Whelan CJ, Gillmore JD, Hawkins PN, Moon JC. Native T1 Mapping in Transthyretin Amyloidosis. **JACC Cardiovasc Imaging.** 2014 Feb;7(2):157-65.

3. White SK, **Treibel TA**, Moon JC. Reply: Effects of blood T1 on extracellular volume calculation. **JACC Cardiovasc Imaging**. 2014 Aug;7(8):849-50.

2. Moon JC, **Treibel TA**, Schelbert EB. T1 mapping for diffuse myocardial fibrosis - a key biomarker in cardiac disease? **J Am Coll Cardiol.** 2013 Jul 3.

1. Sado DM, White SK, Piechnik SK, Banypersad SM, **Treibel TA,** Captur G, Fontana M, Maestrini V, Robson MD, Lachman R, Murphy E, Mehta A, Hughes D, Neubauer S, Elliott PM, Moon JC. The identification and assessment of Anderson Fabry disease by cardiovascular magnetic resonance non-contrast myocardial T1 mapping. **Circulation Imaging.** April 5 2013.

12.7.4 Reviews relevant to this thesis

6. **Treibel TA**, White SK, Moon JC. Myocardial Tissue Characterization: Histological and Pathophysiological Correlation. **Current Cardiovascular Imaging Reports,** 7 (3), 1-9, 2014.

5. Badiani S, van Zalen J, **Treibel TA**, Bhattacharyya S, Moon JC, Lloyd G. Aortic Stenosis, a Left Ventricular Disease: Insights from Advanced Imaging. **Curr Cardiol Rep.** 2016 Aug;18(8):80.

4. Bulluck H, Maestrini V, Rosmini S, Abdel-Gadir A, **Treibel TA**, Castelletti S, Bucciarelli-Ducci C, Manisty C, Moon JC. Myocardial T1 mapping. **Circ J.** 2015;79(3):487-94.

3. Abdel-Gadir A, **Treibel TA**, Moon JC. Myocardial T1 mapping: where are we now and where are we going? **Research Reports in Clinical Cardiology**. Volume 2014:5 Pages 339—347.

2. Bhuva AN, **Treibel TA**, Fontana M, Herrey AS, Manisty CH, Moon JC. T1 mapping: non-invasive evaluation of myocardial tissue composition by cardiovascular magnetic resonance. **Expert Rev Cardiovasc Ther.** 2014 Dec;12(12):1455-64.

1. Maestrini V, **Treibel TA**, White SK, Fontana M, Moon JC. T1 Mapping for Characterization of Intracellular and Extracellular Myocardial Diseases in Heart Failure. **Curr Cardiovasc Imaging Rep.** 2014;7:9287.

12.7.5 Abstract Presentations

Only first author presentations listed.

12.7.5.1 Oral presentations:

Thomas A Treibel, Begoña López, Arantxa González, Katia Menacho, Rebecca S Schofield, Susana Ravassa, Marianna Fontana, Steven K White, Carmelo DiSalvo, Neil Roberts, Michael T Ashworth, Javier Díez, James C Moon. Building Understanding Of The

Myocardial Phenotype: ECV, LGE And Biopsy Measure Complementary But Overlapping Aspects. A 133 Biopsy Severe Aortic Stenosis Study. **Oral Presentation (Early Career Award).** Society of Cardiovascular Magnetic Resonance, Washington DC, January 2017.

Thomas A Treibel, Rebecca Kozor, Katia Menacho, Silvia Castelletti, Heerajnarain Bulluck, Stefania Rosmini, Sabrina Nordin, Viviana Maestrini, Marianna Fontana, James C Moon. ECV Measurement In Left Ventricular Hypertrophy: Cell And Matrix Expansion Have Disease-Specific Relationships. **Oral Presentation.** Society of Cardiovascular Magnetic Resonance, Washington DC, January 2017.

Thomas A Treibel, Yaron Fridman, Brianne Hackman, MAjay Kadakkal, Aatif Sayeed, Maren Maanja, Hussein Abu Daya, James C. Moon, Timothy C. Wong, Erik B. Schelbert. ECV associates with outcomes more strongly than native or post-contrast myocardial T1. **Oral Presentation (Early Career Award).** EuroCMR, Florence/Italy, May 2016.

Thomas A Treibel, Marianna Fontana, Rebecca Kozor, Patricia Reant, Maria A Espinosa, Silvia Castelletti, Heerajnarain Bulluck, Anish N Bhuva, Steven K White, Anna S Herrey, Charlotte Manisty and James C Moon. Diffuse myocardial fibrosis - a therapeutic target? Proof of regression at 1-year following aortic valve replacement: the RELIEF-AS study. **Oral Presentation (Early Career Award).** Society of Cardiovascular Magnetic Resonance, Los Angeles, January 2016. JCMR 18(Suppl 1):O37.

Thomas A Treibel, Marianna Fontana, Janet A Gilbertson, Karen A Boniface, Steven K White, Amna Abdel-Gadir, Stefania Rosmini, David F Hutt, Carol J Whelan, Julian D Gillmore, Ashutosh Wechalekar, Martin P Hayward, Michael A Ashworth, Philip N Hawkins and James C Moon. Occult senile cardiac amyloid in severe calcific aortic stenosis is not rare and has a poor prognosis: a 146 patient CMR biopsy study. **Oral Presentation (Early Career Award).** Society of Cardiovascular Magnetic Resonance, Los Angeles, January 2016. JCMR 2016 18(Suppl 1):O40

Thomas A Treibel, Marianna Fontana, Patricia Reant, Maria A Espinosa, Silvia Castelletti, Anna S Herrey, Charlotte Manisty, Neil Roberts, John Yap and James Moon. T1 mapping in severe aortic stenosis: insights into LV remodelling. Oral Presentation. Society of Cardiovascular Magnetic Resonance, Nice, France, January 2015. JCMR 2015 17(Suppl 1):O89.

Thomas A Treibel, Arthur Nasis, Marianna Fontana, Viviana Maestrini, Silvia Castelletti, Anish N Bhuva, Stefania Rosmini, Amna Abdel-Gadir, Heerajnarain Bulluck, Peter Kellman, Stefan K Piechnik, Matthew D Robson and James Moon. Synthetic ECV: ECV with no blood sampling. **Oral Presentation (Young Investigator Award).** British Society of CMR Annual

Meeting, London, 2015.

Thomas A Treibel, Marianna Fontana, Filip Zemrak, Patricia Reant, Charlotte Manisty, Anna Herrey, Martin Hayward, Shyam Kolvekar, James Moon. Novel Insights into Myocardial Remodelling in Aortic Stenosis using Extracellular Volume Imaging by Cardiovascular Magnetic Resonance. **Oral Presentation (Young Investigator Award).** British Heart Valve Society Annual Meeting, London, 2014.

Treibel TA, White SK, Zemrak F, Sado D, Banypersad S, Flett AS, Caulfield M, Petersen SE, Moon JC. Interstitial expansion in pressure overload left ventricular hypertrophy. Oral Abstract Presentation, SCMR, San Francisco/USA, February 2013.

Treibel TA, Flett AS, Sado D, Hardman SM, Moon JC. Asymptomatic Isolated Hypoplastic Left Ventricular Apex Syndrome (Abstract). Oral Abstract Presentation, SCMR, San Francisco/USA, February 2013.

Treibel TA, White S, Sado D, Hasleton J, Flett A, Herrey A, Hausenloy D, Moon J. Not All LGE Is The Same. Scar Contrast Volume Of Distribution Is Lower In HCM Than In Infarction. Oral Abstract Presentation, SCMR, Orlando/USA, February 2012.

12.7.5.2 Poster Presentations:

Thomas A Treibel, Marianna Fontana**,** Janet A Gilbertson, Karen B Boniface, Steven K White, Theodora Bampouri, Louise Warren, Michael T Ashworth, Philip N Hawkins, James C Moon. Unexpected senile cardiac amyloid in 5% of severe aortic stenosis patients undergoing surgery. European Society of Cardiology Congress, London, August 2015.

Thomas A Treibel, Steve Bandula, Marianna Fontana, Steven White, Janet Gilbertson, Julian D Gillmore, Shonit Punwani, Philip Hawkins, Stuart Taylor, James Moon. Quantification of Cardiac Amyloid by Cardiac Computed Tomography. ICNC12, Madrid, March, 2015.

Thomas A Treibel, Arthur Nasis, Marianna Fontana, Viviana Maestrini, Silvia Castelletti, Anish N Bhuva, Stefania Rosmini, Amna Abdel-Gadir, Heerajnarain Bulluck, Peter Kellman, Stefan K Piechnik, Matthew D Robson and James Moon. An instantaneous ECV with no blood sampling: using native blood T1 for hematocrit is as good as standard ECV. Society of Cardiovascular Magnetic Resonance, Nice, January 2015. JCMR 2015 17(Suppl 1):Q129.

Treibel TA, White SK, Zemrak F, Sado D, Banypersad S, Flett AS, Caulfield M, Petersen

SE, Moon JC. Interstitial expansion in pressure overload left ventricular hypertrophy (Abstract). Journal of Cardiovascular Magnetic Resonance 2013, 15(Suppl 1):P251.

12.8 Book Chapters

Treibel TA, Moon JC. T1 and T2 mapping and ECV in Cardiomyopathy. *Cardiovascular Magnetic Resonance, 3rd Edition*. Elsevier Publishing. Edited by Prof. DJ Pennell and WJ Manning.

12.9 Invited Talks

- Assessment of Valvular Heart Disease, London Core Medical Training Day, Barts Heart Centre, 16th March 2017.
- Aortic Stenosis beyond Echocardiography. Royal Society of Medicine. Cardiology Training Day, 13th April 2016.
- Assessment of Valvular Heart Disease, Advanced CMR course for Radiographers, Barts Heart Centre, 22nd October 2016.
- Case Presentation, British Society of CMR AGM, Exeter, March 2016.